# The optimisation of web-tapered portal frame buildings

by

Herman Aucamp

*Thesis presented in fulfilment of the requirements for the degree of Master of Engineering in Structural Engineering in the Faculty of Engineering at Stellenbosch University*

Department of Structural Engineering,
University of Stellenbosch,
Private Bag X1, Matieland 7602, South Africa.

Supervisor: Mr E. van der Klashorst

Co-supervisor: Dr H. de Clercq

March 2017

# Declaration

By submitting this thesis electronically, I declare that the entirety of the work contained therein is my own, original work, that I am the owner of the copyright thereof (unless to the extent explicitly otherwise stated), that reproduction and publication thereof by Stellenbosch University will not infringe any third party rights and that I have not previously in its entirety or in part submitted it for obtaining any qualification.

Name: Herman Aucamp

_____

Signature

_____

Date

# Synopsis

Web-tapered members are widely advocated as a cost-effective alternative to conventional structural sections for portal frames. These non-prismatic members improve the distribution of internal stresses throughout a frame, which leads to substantial weight savings and increases the clear spans achievable. Web-tapered portal frames constitute a well-established practice in many countries. However, this construction technique is rarely seen in South Africa, despite its potential.

Some software developers have developed automated design packages for structures with web-tapered members that produce cost-effective buildings and expedite the design process. However, the principles that govern the design of web-tapered members are unclear as none of the major international steel design specifications have adequate provisions for non-prismatic steel members. Design Guide 25 for the design of portal frames using web-tapered members was published by the Metal Building Manufacturers Association and the American Institute of Steel Construction. This guide utilises the concept of an equivalent prismatic member to allow the design to be done using AISC 360.

In this study, a new approach is developed for the design of web-tapered members, based on SANS 10162-1 but utilising the equivalent prismatic member concept from Design Guide 25. This new approach was validated against the results of full non-linear analyses, with imperfections taken into account, in the finite element software Abaqus and found to yield safe results. The proposed design approach was subsequently incorporated into a structural optimisation procedure specifically developed to obtain the lightest possible structure for multiple load combinations. The optimisation procedure uses a genetic algorithm in search of an optimum solution when using doubly symmetric, welded sections that are either prismatic or web-tapered. The results show a weight reduction of up to 17% for span lengths of 50 m when comparing web-tapered portal frames with prismatic ones. These results were also compared to designs produced by a commercial software package for web-tapered frames that reduced frame weights by 38% from what can be achieved with prismatic sections.

# Samevatting

Elemente met tapse webbe word wyd gepropageer as 'n ekonomiese alternatief vir konvensionele struktuurelemente in portaalrame. Die gebruik van hierdie varieërende struktuurdele verbeter die verspreiding van interne spanning regdeur 'n raam. Hierdie proses lei tot 'n aansienlike gewigsbesparing en langer moontlike spanwydtes. Tapse web portaalrame is 'n gevestigde bedryf in baie lande; tog word hierdie konstruksietegniek selde in Suid-Afrika gesien, ten spyte van die voordele wat dit bied.

Sommige sagteware-ontwikkelaars bemark geoutomatiseerde ontwerppakkette vir die ontwerp van kostedoeltreffende, tapse web strukture. Die beginsels wat die ontwerp van elemente met tapse webbe bepaal is egter nie duidelik omskryf nie, aangesien geen van die internasionale staalontwerpspesifikasies voldoende voorsiening maak vir tapse web strukture nie. DG25, vir die ontwerp van portaalrame met tapse webbe, is onlangs gesamentlik deur MBMA en AISC gepubliseer. Hierdie gids maak gebruik van die konsep van 'n ekwivalente prismatiese stuktuurdeel vir die ontwerp van tapse web elemente, met behulp van AISC 360.

Tydens hierdie studie is 'n nuwe benadering ontwikkel vir die ontwerp van tapse web strukture. Dit word baseer op SANS 10162-1, maar gebruik die ekwivalente prismatiese element konsep uit DG25. Die akkuraatheid van hierdie nuwe benadering is bevestig deur 'n reeks eindige element analises in die sagteware Abaqus, met inagneming van nie-lineêre materiaal en geometriese gedrag, asook imperfeksies. Daar is bevind dat die voorgestelde ontwerpmetode 'n veilige oplossing bied vir tapse web elemente. 'n Strukturele optimaliseringprogram is ook ontwikkel, gebaseer op die voorgestelde ontwerpmetode, om die ligste moontlike portaaalraam te verkry onder die invloed van verskeie laskombinasies. Die optimale oplossing word gevind deur die gebruik van 'n genetiese algoritme, en is in staat om dubbele simmetriese, gesweisde struktuurdele in beide prismatiese óf tapse web portaalrame te ontwerp. Die resultate dui op 'n vermindering van tot 17% vir 50 m spanwydtes. Hierdie resultate is ook vergelyk met ontwerpe met 'n kommersiële sagtewarepakket, doelgemaak vir tapse web portaalrame. 'n Totale gewigsbesparing van 38% staal is gevind in vergelyking met die konvensionele portaalrame.

# Acknowledgements

It is a pleasure to express my gratitude to a number of people who have helped me in many ways over the course of my postgraduate studies. Without their support and guidance, this dissertation would not have been possible.

My supervisor, Mr Etienne van der Klashorst, who presented me with the opportunity for further studies. His patience, encouragement and willingness to assist in all matters related to engineering were always exceptional.

I am fortunate to have been introduced to Dr Hennie de Clercq during my studies. The completion of this thesis was greatly aided by his wise advice and guidance. I am thankful for his assistance and the motivation he provided.

Clotan Steel (Pty) Ltd., for their generous contribution towards this research. In particular, Mr Danie Joubert and Mr Hertzog Badenhorst for expressing their interest in the research subject and their willingness to pursue new innovative techniques; and Mr Frederik du Toit Oosthuizen, for his aid with the commercial design software, developing new ideas and his positive outlook.

My dear parents, Deon and Ronelle Aucamp, for their continued love. Thank you for the supportive environment you created for us children to prosper in all our endeavours.

To my loving and supportive wife, Su-anrie. Thank you for believing in me and encouraging me to pursue further studies. Your cheerful nature can brighten any day.

*Ecclesiastes 4:12*

# Contents

# List of Figures

# List of Tables

# Nomenclature

In this paper all large number systems are indicated using short scale notation (i.e. billion = $10^9$, trillion = $10^{12}$).

The strong and weak axes are denoted respectively by x and y throughout this paper, unless indicated otherwise (i.e. when working with Eurocode 3).

### Abbreviations

| | |
|---|---|
| AASHTO | American Association of State Highway and Transportation Officials |
| AISC | American Institute of Steel Construction |
| AISI | American Iron and Steel Institute |
| AWS | American Welding Society |
| CEN | Comité Européen de Normalisation |
| CSA | Canadian Standards Association |
| DG25 | Design Guide 25 |
| DL | Dead Load |
| EC3 | Eurocode 3 – Design of steel structures |
| ECCS | European Convention of Constructional Steelwork |
| FEA | Finite Element Analysis |
| FEM | Finite Element Methods |
| GA | Genetic Algorithm |
| LL | Live Load |
| LPF | Load Proportionality Factor |
| LRFD | Load and Resistance Factor Design |
| LTB | Lateral-Torsional Buckling |
| MBMA | Metal Building Manufacturers Association |
| MBS | Metal Building Systems |
| SABS | South African Bureau of Standards |
| SANS | South African National Standards |
| SLS | Serviceability Limit State |
| SSRC | Structural Stability Research Council |
| ULS | Ultimate Limit State |
| WL | Wind Load |

### General

| | |
|---|---|
| $A$ | Cross-sectional area |
| $A'$ | Area above the inspected level for shear stress |
| $A_{crit}$ | Critical cross-sectional area |
| $A_{eff}$ | Effective cross-sectional area |
| $A_f$ | Flange area |
| $A_g$ | Gross cross-sectional area |
| $A_w$ | Web area |
| $b$ | Flange width |
| $C_b$ | Equivalent moment or stress gradient factor |
| $C_e$ | Elastic flexural buckling load |
| $C_u$ | Ultimate applied axial load |
| $C_w$ | Warping constant |
| $C_y$ | Axial yield load |
| $d$ | Depth of beam |
| $E$ | Material elasticity modulus |
| $f_{axial}$ | Stress due to axial forces |
| $f_{bending}$ | Stress due to bending forces |
| $f_{c,flange}$ | Compression flange stress due to bending |
| $f_{cr}$ | Critical elastic lateral-torsional buckling stress in the flange |
| $f_e$ | Elastic buckling stress |
| $f_{max}$ | Maximum stress brought on by combined axial and bending forces |
| $f_r$ | Permissible compression flange resistance stress in bending |
| $f_{rw}$ | Shear stress carried by the web |
| $f_s$ | Ultimate shear stress |
| $f_t$ | Tension-field stress |
| $f_y$ | Yield stress of the material |
| $G$ | Shear modulus of the material |
| $h$ | Section height |
| $h_w$ | Web height |
| $h_0$ | Distance between flange centroids |
| $I$ | Moment of inertia |
| $I'$ | Modified moment of inertia |
| $I_{large}$ | Moment of inertia at the small end |
| $I_{small}$ | Moment of inertia at the large end |
| $I_y$ | Moment of inertia about the weak-axis |
| $J$ | Sectional torsional constant |
| $k_v$ | Shear buckling coefficient |
| $L$ | Physical length of the member |
| $M$ | Bending moment |
| $M_A$ | Bending moment at the first quarter position |
| $M_B$ | Bending moment at the centre position |
| $M_C$ | Bending moment at the third quarter position |
| $M_{cr}$ | Critical elastic lateral-torsional buckling moment |
| $M_{max}$ | Maximum bending moment occurring in a beam |
| $M_{larger}$ | Larger end moment applied to a beam |
| $M_{n,cross}$ | Nominal cross-sectional resistance moment |

| | |
|---|---|
| $M_p$ | Plastic moment of resistance |
| $M_{pr}$ | Reduced full plastic resistance moment |
| $M_{smaller}$ | Smaller end moment applied to a beam |
| $M_u$ | Ultimate bending moment |
| $M_y$ | Elastic moment of resistance |
| $P$ | Concentrated force |
| $P_{cr}$ | Elastic buckling force |
| $P_{pr}$ | Reduced axial yielding force |
| $P_u$ | Ultimate applied force |
| $Q$ | Static moment of area |
| $r$ | Radius of gyration ($r^2 = I/A$) |
| $r_{ts}$ | Effective radius of gyration |
| $s$ | Transverse stiffener spacing |
| $t_f$ | Flange thickness |
| $T_r$ | Factored tensile resistance load |
| $T_u$ | Ultimate tensile load |
| $t_w$ | Web thickness |
| $V_{mod}$ | Modified shear force |
| $V_u$ | Ultimate shear force |
| $y_n$ | Distance below the centroid to the neutral axis |
| $\overline{y}'$ | Distance between the neutral axis and the centroid of the $A'$ |
| $Z_e$ | Elastic section modulus |
| $Z_{pl}$ | Plastic section modulus |
| $\alpha$ | Angle of taper (defined in Figure 4.3) |
| $\Delta$ | Lateral sway deflection |
| $\delta$ | Mid-span deflection |
| $\lambda$ | Non-dimensional slenderness parameter |
| $\lambda_{LTB}$ | Non-dimensional slenderness parameter for lateral-torsional buckling |
| $\kappa$ | End moment ratio |
| $\nu$ | Poisson's ratio |

**CSA S16**

| | |
|---|---|
| $C_f$ | Factored applied axial load |
| $C_r$ | Factored axial resistance load |
| $M_f$ | Factored applied bending moment |
| $M_u$ | Critical elastic lateral-torsional buckling moment |
| $M_r$ | Factored moment of resistance |
| $n$ | Flexural buckling curve exponent |
| $U_1$ | Amplification factor for $P - \delta$ and moment gradients |
| $\beta$ | Weak-axis moment amplification factor |
| $\lambda_y$ | Weak-axis non-dimensional slenderness parameter |
| $\omega_1$ | Equivalent uniform beam-column coefficient |
| $\omega_2$ | Equivalent moment or stress gradient factor |
| $\phi$ | Steel resistance factor ($= 0.9$) |

### AISC 360

| | |
|---|---|
| $L_p$ | Limiting length for yielding |
| $L_r$ | Limiting length for inelastic lateral-torsional buckling |
| $M_c$ | Available bending moment resistance |
| $M_r$ | Factored bending moment to be resisted |
| $P_c$ | Available axial resistance |
| $P_r$ | Factored axial force to be resisted |
| $\phi_c$ | LRFD column resistance factor ($= 0.9$) |
| $\phi_b$ | LRFD beam resistance factor ($= 0.9$) |

### DG25

| | |
|---|---|
| $f_{cr,mid}$ | Critical elastic lateral-torsional buckling stress using the mid-span properties |
| $f_L$ | Upper limit flexural compression flange stress ($= 0.7f_y$) |
| $f_r$ | Compression flange stress due to bending |
| $f_{r,max}$ | Maximum compression flange stress due to bending |
| $M_n$ | Nominal moment of resistance |
| $R_{pg}$ | Bending strength reduction factor |
| $R_{pc}$ | Web plastification factor |
| $\gamma_{eLTB}$ | Nominal buckling strength multiplier |

### AASHTO

| | |
|---|---|
| $f_{mid}$ | Stress at the middle of an unbraced length |
| $f_0$ | Compression flanges stress at the opposite end of $f_2$ |
| $f_1$ | Calculated compression flange stress to determine $C_b$ |
| $f_2$ | Maximum compression flange stress |

### EC3

| | |
|---|---|
| $x - x$ | Denotes the axis along a member |
| $y - y$ | Denotes the strong-axis of a cross-section |
| $z - z$ | Denotes the weak-axis of a cross-section |
| $C_m$ | Bending moment shape modification factor |
| $I_T$ | Sectional torsional constant |
| $I_w$ | Warping constant |
| $I_z$ | Moment of inertia about the weak-axis |
| $k_{ij}$ | Interaction factor |
| $L_{cr}$ | Buckling length of a beam |

| | |
|---|---|
| $M_{b,Rd}$ | Design buckling resistance moment |
| $M_{c,Rd}$ | Design cross-sectional bending resistance |
| $M_{Ed}$ | Design bending moment |
| $\Delta M_{Ed}$ | Additional moment from shift of the centroid of the effective area |
| $M_{y,Ed}$ | Applied bending moment about the strong-axis |
| $M_{y,Rk}$ | Characteristic resistance moment about the strong-axis |
| $N_{b,Rd}$ | Design compression buckling resistance |
| $N_{c,Rd}$ | Design cross-sectional axial resistance |
| $N_{Ed}$ | Design axial force |
| $W_{eff,y}$ | Strong-axis effective section modulus |
| $W_{el,y}$ | Strong-axis elastic section modulus |
| $W_{pl,y}$ | Strong-axis plastic section modulus |
| $W_y$ | Strong-axis section modulus depending on the section classification |
| $\alpha$ | Imperfection factor for flexural buckling |
| $\alpha_{LT}$ | Imperfection factor for lateral-torsional buckling |
| $\gamma_{M1}$ | Partial steel resistance factor for member instability checks (= 1.0) |
| $\overline{\lambda}$ | Non-dimensional slenderness parameter |
| $\overline{\lambda}_{LT}$ | Non-dimensional slenderness parameter for lateral-torsional buckling |
| $\Phi$ | Intermediate value for determining the reduction factor $\mathcal{X}$ |
| $\Phi_{LT}$ | Intermediate value for determining the reduction factor $\mathcal{X}_{LT}$ |
| $\mathcal{X}$ | Axial slenderness reduction factor |
| $\mathcal{X}_{LT}$ | Lateral-torsional buckling slenderness reduction factor |

**Research by Marques, et al. (2014)**

| | |
|---|---|
| $x_c^I$ | Critical cross-section without imperfections |
| $x_{c,lim}^{II}$ | Critical cross-section with imperfections |
| $\alpha_{ult,k}$ | Resistance load multiplier |
| $\alpha_{cr}$ | Critical load amplifier |
| $\beta$ | Imperfection parameter for increased stability |
| $\gamma$ | Tapering ratio ($= h_{max}/h_{min}$) |
| $\epsilon$ | Utilisation ratio |
| $\eta$ | Generalised imperfections |
| $\overline{\lambda}_z$ | Non-dimensional slenderness parameter about the weak-axis |
| $\phi$ | Over-strength factor |

**Structural analysis**

| | |
|---|---|
| $\{\mathbf{D}\}$ | Displacement vector |
| $\delta\{\mathbf{D}\}$ | Infinitesimal small displacement vector |
| $E_k$ | Kinetic energy |
| $[\mathbf{k}_e]$ | Element stiffness matrix |
| $[\mathbf{K}_e]$ | Constant elastic stiffness matrix |
| $[\mathbf{K}_g]$ | Geometric stiffness matrix |
| $k$ | Shear correction factor |

| | |
|---|---|
| $P_{ref}$ | Reference force |
| $\{\mathbf{P}\}$ | Force vector |
| $P_e$ | Elastic buckling force |
| $U$ | Potential energy |
| $u$ | Displacement degree of freedom |
| $v$ | Displacement degree of freedom |
| $\gamma_e$ | Elastic buckling multiplier |
| $\kappa$ | Element curvature |

**Structural optimisation**

| | |
|---|---|
| $c$ | Dynamic penalty constant |
| $\mathbb{D}$ | Feasible search space |
| $f(s)$ | Objective function |
| $f'(s)$ | Adjusted objective function |
| $g$ | Number of generations completed |
| $m$ | Number of constraints |
| $p_c$ | Crossover proportion |
| $p_m$ | Mutation proportion |
| $p_s$ | Static penalty parameter |
| $v_i(s)$ | Number of violations |
| $\alpha$ | Dynamic penalty exponent |

# Chapter 1

# Introduction

## 1.1 Background

The use of web-tapered members in portal frames as an alternative to prismatic sections is rarely seen in South Africa (Rudman, 2009). This concept has become increasingly popular worldwide and is the basis of an established industry in the USA. However, the principles that govern the design of web-tapered members are vague. The following can be said about the matter when consulting the most important design specifications:

a) Design by analysis using a Finite Element Method (FEM) is recommended by the EC3 specification to determine the load-carrying capacities of non-uniform members, without any formal guidance on the implementation thereof (Marques, 2012).

b) Previous editions of the AISC 360 specification (1978 - 1999) considered simple web-tapered members in an appendix, when using the allowable stress design approach. However, this appendix has been removed in later editions of AISC 360.

c) No provisions are made for the design of web-tapered members in the CSA S16 and SANS 10162-1 design specifications.

Software packages by Metal Building Software Incorporated, Butler Manufacturing, and others, have become popular in the industry and are available commercially for the design of web-tapered portal frames. These software packages provide automated design and manufacturing capabilities to fabricators that are claimed to be more economical than conventional portal frames by producing lightweight structures with increased clear span potential. Manufacturers completely rely on these software packages whose inner workings and underlying theory are unknown, while no design procedure for web-tapered frames is generally accepted internationally.

The Metal Building Manufacturers Association (MBMA) in collaboration with the American Institute of Steel Construction (AISC), recently published Design Guide 25 (Kaehler et al., 2011) for the design of web-tapered portal frame structures, commonly referred to as Metal Building

Systems (MBS). The guideline utilises the concept of an equivalent prismatic member to represent a non-uniform member. In doing so, the AISC 360 design specifications for conventional steel design can be implemented. Similarly, European researchers have proposed the use of an equivalent prismatic member to allow web-tapered members to be designed using the EC3 steel design specification. The use of web-tapered portal frames in an aircraft hangar is shown in Figure 1.1.

Figure 1.1: Aircraft hangar constructed with web-tapered portal frames by R & M Steel Company

## 1.2 Relevance of web-tapered portal frames to industry

It has been widely reported that the use of web-tapered members leads to improved material efficiency in portal frames. This efficiency is achieved by distributing steel towards areas that experience high bending moments while reducing the self-weight of the frame at other strategic positions. The following advantages are noted for using web-tapered members as an alternative to hot-rolled sections and conventional plate-girders in portal frames:

a) Different researchers have reported a material savings potential of between 10% and 40% when using web-tapered portal frames (Hayalioglu and Saka, 1992; Müller et al., 1999; Meera, 2013; Zende et al., 2013; Roa and Vishwanath, 2014; Mckinstray et al., 2015).

b) Newman (2004) observed over an extended period that web-tapered portal frames are typically 10% to 20% less expensive than conventional portal frames, while other researchers have found the cost of web-tapered portal frames to be up to 30% lower (Meera, 2013; Roa and Vishwanath, 2014).

c) Web-tapered portal frames are typically fabricated by a specialised manufacturer, thus leading to more predictable construction times (Newman, 2004). This is of particular importance to clients who cannot afford to be non-operational during critical periods of the year, e.g. major holidays for retailers, or harvesting seasons in agriculture.

d) Web-tapered members are most effective for long-span applications, where only trusses are regarded as economically viable alternatives. However, trusses require more effort during design, fabrication and erection (Firoz et al., 2012).

e) Unlike hot-rolled sections, a large variety of dimensions can be produced by welding together plates cut from either standard sheets, flat bars, or coiled sheets (Ziemian, 2010).

f) While hot-rolled plates are still readily available in South Africa, the supply of hot-rolled structural sections has become unpredictable. South Africa's isolation from any nearby steel-producing countries further aggravates the challenges posed by importing. This is compounded by long shipping times and unpredictable quality.

g) The cross-sections in web-tapered frames may be adjusted to resist external loads optimally. In doing so, clear span distances have been recorded of up to 100 m (Davison et al., 2011; Zoad, 2012; Zende et al., 2013), which is ideal for warehouses, fitness centres and aircraft hangars. The limiting factor in most cases is the depth of the cross-section that can be accommodated within the automated welding machines.

Despite the many positives, there remains scepticism towards the use of web-tapered structural members. Newman (2004) points out that these members may suffer from a lack of reserve strength so that any future additions to the building's roof structure or overhead services could theoretically lead to an overstressed situation. Additionally, structural steel designers might be hesitant to adopt web-tapered members into their practice as the current guidelines available are limited and makes commercial software difficult to validate.

To remain competitive, some manufacturers and designers have embraced the use of web-tapered members, as the manufacturing process is similar to that used in plate-girder fabrication. More than 50% of all new single-storey, non-residential construction in the USA utilises MBS techniques; and in 2014 it represented a $2.45 billion industry (MBMA, 2016), with some manufacturers having more than 50 years' experience in the design, fabrication and erection of MBS structures.

## 1.3 Purpose and objectives of the study

A need was identified to introduce web-tapered portal frames to South African conditions and practices, due to the apparent financial advantages and the unstable supply of hot-rolled mem-

bers locally. This study will bring together various aspects that need to be considered for the design of web-tapered portal frames and review if this method of construction is safe and worth pursuing as an alternative to conventional building techniques.

To address these issues the following objectives were set:

1. Determine what principles and procedures are currently employed internationally for the design of web-tapered members.
2. Select or develop an adequate methodology for designing web-tapered portal frames in South Africa.
3. Review how the methodology from objective 2 performs by comparing the findings to full non-linear finite element analysis in Abaqus.
4. Create a structural optimisation algorithm capable of finding the lightest possible frame, when subjected to various load combinations and design constraints.
5. Confirm the reported material savings potential of web-tapered portal frames designed with the method in objective 2 against conventional portal frames with prismatic plate-girders designed according to SANS 10162-1.
6. Evaluate the optimal portal frames produced in this study against portal frames generated by the automated design software by Metal Building Software Incorporated.

## 1.4 Scope and limitations

The scope of the research is restricted to web-tapered portal frames under typical South African loading conditions. The study is mainly focused on the in-plane strength and lateral-torsional behaviour of web-tapered members under combined bending and compression forces.

The design provisions in EC3 for non-uniform members are presented in Chapter 2, but excluded from the rest of the study as it was found to be inconsistent and vague to implement. Ultimately, the equivalent prismatic member concept, as used by Design Guide 25, was selected and combined with SANS 10162-1 to form a new design approach that can be applied to web-tapered members.

Physical testing was ruled out on account of a larger need to establish the principles required for design verification and to establish an understanding of the behaviour of web-tapered members. The scope of the study, however, allowed for a series of full non-linear analyses, using shell elements with imperfections of the geometry, to evaluate the adequacy of the proposed design method.

The following limitations apply to the proposed design method:

a) Only linearly varying web heights were used.

b) Only doubly symmetric I-beam sections were considered, thus restricting torsional-flexural interaction.

c) Constrained-axis torsional buckling, caused by lateral supports without sufficient torsional twisting restraints, were assumed to be negligible.

d) Out-of-plane forces and biaxial bending was excluded.

e) The position of load application was not considered that may lead to a destabilising/stabilising effect about the longitudinal axis.

f) Plate elements were all assumed to be oxy-flame cut from hot-rolled S355JR steel plates before fabrication of the welded I-beams.

g) The tapering angles ($\alpha$) of webs were limited to the range between $0^{o}$ and $5^{o}$.

h) Cross-sections with flanges prone to local buckling were excluded, while slender webs were permissible.

i) Unstiffened webs were assumed. Thus, the post-buckling capacity that arises from tension field action was ignored.

j) The vertical component of force in sloped flanges was also ignored due to a general lack of research to validate this mechanism.

k) Structural analysis using the plastic design method for portal frames were excluded.

Optimisation was limited to the mass of the portal frame, i.e. its flange and web plates. The assumption was made that a reduction in steel weight directly correlates with the financial gain that can be achieved by taking all cost into account. The scope excluded the cost implications of web-stiffeners, welding material, connections, labour and overheads.

## 1.5 Research outline

In the current chapter (Chapter 1) the background and relevance of web-tapered portal frames were introduced. The purpose and objectives of the research were defined, and the scope and limitations were stipulated.

Chapter 2 provides a historical context for the use of web-tapered members. This is followed by a presentation of theory for web-tapered member design, structural analysis and optimisation required during this study.

Chapter 3 establishes a full non-linear analysis technique that incorporates material and geometric non-linearity with imperfections into the modelling of thin-walled structural members using shell elements in Abaqus. The non-linear procedure is then verified against international design specifications for prismatic structural members.

In Chapter 4 a new design approach is proposed to obtain the in-plane axial and lateral-torsional buckling resistance of columns and beams, respectively. This design approach is based on the provisions of SANS 10162-1 and employs the equivalent prismatic member concept adapted from Design Guide 25. The predicted resistances for web-tapered elements are then evaluated using the full non-linear modelling techniques in Chapter 3. To conclude, the use of the SANS 10162-1 interaction equation for combined axial and bending forces is clarified.

Chapter 5 describes the development of the optimisation algorithm in Matlab. The algorithm is first verified against a mathematical test function before being expanded to include problems of a structural engineering nature. The proposed design approach is incorporated into the program as a means to evaluate member capacity, thus imposing constraints on the algorithm when searching for the optimal and feasible web-tapered portal frame structure.

In Chapter 6, several structural configurations are considered as case studies. Each case study is optimised using either prismatic or web-tapered plate-girders to evaluate the material savings potential of web-tapered portal frames. The results are then compared to designs produced when using automated design software for MBS buildings that are available commercially to manufacturers.

Chapter 7 provides a summary and draws conclusions derived from this study with various recommendations that are presented for web-tapered member design and possible future investigations. Ultimately, the study achieved all the research objectives successfully.

# Chapter 2

# Review of literature and theories

## 2.1 Introduction

This chapter reports on a range of topics that are relevant to the research project. This will serve to provide background to the MBS industry and current design approaches, while also forming a basis for the structural analysis and optimisation methodologies used in subsequent chapters. Furthermore, concerns about manufacturing and welding are investigated in this chapter.

## 2.2 Historical progression of metal building systems

One of the earliest investigations into the behaviour of non-prismatic elements was done by Leonard Euler in the latter half of the $18^{th}$ century. The major building materials of the time, timber and masonry, tended to be stocky due to unpredictable material characteristics and would yield before the onset of elastic instability (Nelson and Murray, 1979). Thus, Euler's line of study remained dormant until the introduction of wrought iron and structural steel, which renewed interest in his theories. His work on differential equations for elastic deflection of columns with varying cross-sections are available in German translation by Ostwald (1910) in the series titled: *Klassiker der exakten Wissenschaften*, meaning the classics of the exact sciences.

The roots of MBS buildings can be traced back to the prefabricated buildings industry in the USA at the start of the $20^{th}$ century. It filled a gap in the market for structures less prone to fire than that offered by the lumber industry, which was well established at the time. Due to their record for being poorly built and the uninspiring aesthetics of prefabricated buildings, it was soon viewed in a negative light by many (Newman, 2004). By the mid $20^{th}$ century, manufacturers had to improve their products to achieve less stale and utilitarian-looking buildings. Buildings were marketed under the name pre-engineered buildings, in a bid to differentiate them from their predecessors. Although prospective clients were still restricted to catalogue designs, the manufacturers managed to modernise the industry by providing new cladding solu-

tions to address the long-regarded lacklustre aesthetic appeal. Steel trusses were popular for a long time, but they required considerable design time and were cumbersome to assemble. Rigid frames became a popular alternative solution, with clear span capabilities reaching 30 m by the late 1950s (Newman, 2004). This is around the time when the first use of web-tapered members in primary framing was observed (Kaehler et al., 2011). An illustration of a typical MBS building and its components is provided in Figure 2.1. Due to various issues at the time relating specifically to the buildings industry, ranging from business administration to the use of building codes, Butler Manufacturing Company and other leading manufacturers formed the MBMA in 1956 with the mandate to conduct research, and advance building codes and standards. Since its inception, the MBMA has been responsible for a wide range of developments ranging from engineering standards, wind-tunnel research on low-rise buildings, snow loading, thermal loadings and fire-rating research (Newman, 2004), to name a few. As access to computers increased during the 1960s, so did the use of automated design. Designers were able to create custom designs while remaining competitive in the market. This signalled a true departure from catalogue designs. The industry adopted and marketed these buildings under the name metal building systems, which is still the most used terminology today, although other synonymous terms such as pre-engineered metal buildings or engineered metal buildings are sometimes used (Firoz et al., 2012).

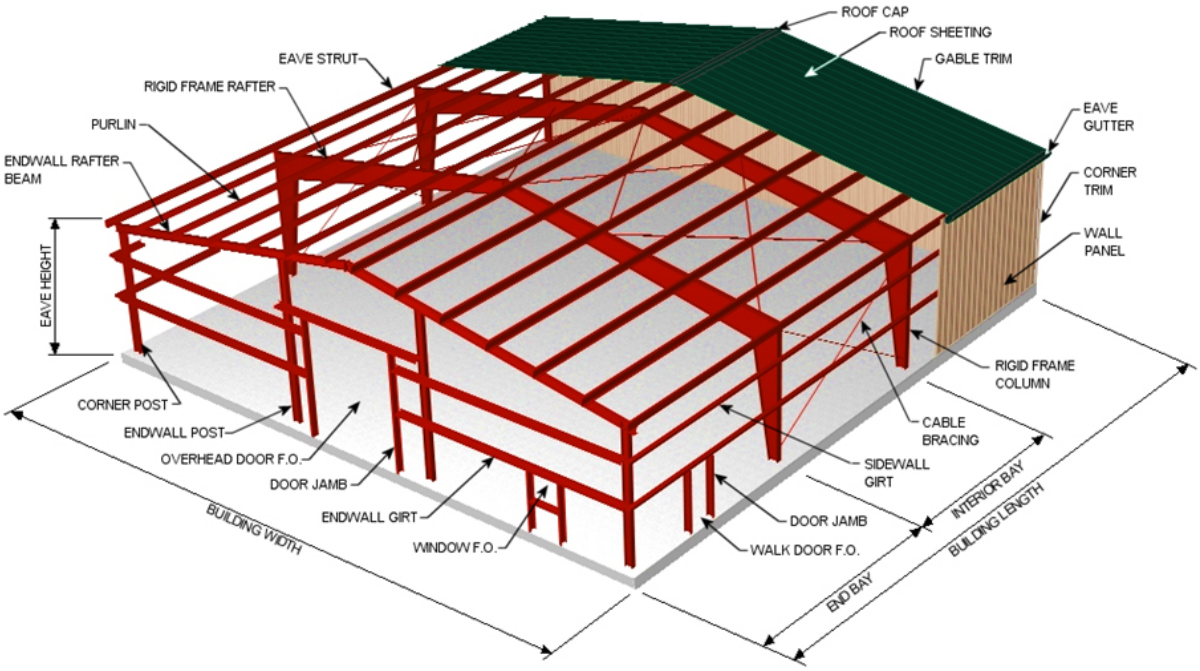


Figure 2.1: Typical layout of MBS structure by Kirby Building Systems

Design Guide 25 was published by MBMA, in partnership with AISC, in 2011. It is based on the research by Kim and White (2006a), Kim and White (2006b), White and Kim (2006), White (2006), Guney and White (2007), Kim and White (2007a), Kim and White (2007b), Ozgur

et al. (2007), White and Chang (2007), and Kim (2010) into the behaviour of web-tapered members and the stability effects in rigid frames. Design Guide 25 retained the concept of an equivalent prismatic member used in the old AISC provisions, which was originally proposed by Timoshenko and Gere (1961) and refined by Lee and others (Lee, Morell, et al., 1972; Lee and Morrell, 1975). The equivalent prismatic member approach is used to map the theoretical elastic buckling strength of a tapered member to a conventional section that allows a design to be performed with AISC 360. With regard to the advantages of Design Guide 25, Ziemian (2010) made the following statement:

> *"Furthermore, by focusing on the elastic buckling load level along with the flange stress ratio, designers can use any applicable design standard for calculating the design strength of tapered members based on the above concept in the MBMA/AISC design guide."*

From this, it can be concluded that the principles in Design Guide 25 (DG25) may be used with any of the design specifications considered in this study (see Section 1.1). However, from the literature, it is not clear how DG25 should be implemented in combination with international steel specifications other than AISC 360 and what the resulting reliability would be.

## 2.3 Design of structural members that are subject to axial and bending forces

Sections 2.3.1 to 2.3.3 are presented next to establish the theory used to design prismatic members according to different design specifications. At the end of each section a presentation of popular theories for the design of web-tapered members is then presented.

### 2.3.1 In-plane flexural resistance of columns

#### 2.3.1.1 Prismatic column design approaches

The theoretical load capacity of a column is governed by its physical dimensions, material properties and support conditions. Short steel columns are prone to plastic failure, where the full cross-section reaches the material yield stress at an axial load called $C_y$. As the length increases, a column becomes increasingly unstable and prone to buckling before $C_y$ is reached. This is known as the elastic buckling load ($C_e$) and is characterised by a cross-section still within the material's elastic range and the onset of the elastic instability phenomenon, called bifurcation (Craig, 1999). Bifurcation is a mathematical instability in the system of equilibrium, where a small change in the parameters leads to an abrupt qualitative change in the system's behaviour. At bifurcation, more than one load-deflection path is mathematically feasible under

the same conditions (Ziemian, 2010). The elastic buckling load for prismatic members can be determined by Euler's closed-form solution in Equation 2.1.

$$C_e = \frac{\pi^2 \cdot E \cdot I}{L^2} \tag{2.1}$$

In reality, the flexural buckling resistance of steel columns exhibits behaviour different from the theoretical buckling resistance. Imperfections due to the manufacturing and construction process may significantly influence the resistance of columns and should be considered in the design. Galambos and Surovek (2008) summarised these imperfections as:

a) Variations in the material model assumed from the actual material behaviour.

b) Residual stresses that arise during the fabrication and cooling process.

c) Variation in the geometry of the cross-section.

d) The initial out-of-straightness.

e) The eccentricity of loading.

$C_y$ and $C_e$ merely provide an upper bound solution to the maximum attainable loads, due to the imperfections above. It is thus useful to categorise column behaviour into regions exhibiting either plastic, inelastic or elastic behaviours, depending on the column's slenderness. The non-dimensional slenderness parameter ($\lambda$) is typically used to represent the degree of slenderness.

$$\lambda = \sqrt{\frac{C_y}{C_e}} \tag{2.2}$$

Some columns are especially prone to inelastic behaviour, which is characterised by partial yielding of the cross-section and displays a non-linear relationship between displacement and any applied load (Ziemian, 2010). Considering the number of variables that influence a column's true behaviour and the probability distribution of each variable, it becomes difficult to accurately determine a specific column's behaviour analytically, which has led to numerous studies on the flexural buckling resistance of columns (Galambos and Surovek, 2008). Probabilistic formulae were derived based on experiments on various sections by Bjorhovde in the 1970s at Lehigh University (Bjorhovde and Tall, 1971; Bjorhovde, 1972; Bjorhovde, 1978). The samples were documented according to the manufacturing and erection imperfections mentioned above. By analysing the test results, Bjorhovde found definite groupings and was able to predict column behaviour according to the manufacturing process, cross-section and material yield stress (Galambos and Surovek, 2008). This resulted in the Structural Stability Research Council (SSRC) column strength curves designated as SSRC curves No.1 to 3 on which AISC 360, CSA S16 and SANS 10162-1 are based. During the same time Beer and Schultz (1970), Sfintesco (1970) and Jacquet (1970) conducted similar experiments on steel columns under the authority

of the European Convention of Constructional Steelwork (ECCS, 1976). Their research findings subsequently led to the adoption of multiple probabilistic-based column strength curves by the ECCS, which were slightly modified to become the column curves used today in the EC3 (Ziemian, 2010).

An overview of the flexural buckling curves employed by the design specifications considered for this study is presented next.

#### 2.3.1.1.1 AISC 360-10

The AISC column curve consists of the two-part formula in Equation 2.3. It is based on the SSRC curve No.2 from Bjorhovde's findings (AISC, 2010).

$$P_c = \begin{cases} \phi_c \cdot A_g \cdot f_y \left(0.658^{\lambda^2}\right), & \text{for } \lambda \leq 1.5 \\ \phi_c \cdot A_g \cdot f_y \left(\frac{0.877}{\lambda^2}\right), & \text{for } \lambda > 1.5 \end{cases} \tag{2.3}$$

The column's available axial strength is designated as $P_c$, with $\phi_c = 0.9$ when using the Load and Resistance Factor Design (LRFD) approach. The components indicated in brackets in Equation 2.3 have the function of reducing the column's axial resistance as a function of the slenderness.

#### 2.3.1.1.2 CSA S16-14

Equation 2.4 shows the double-exponential formula utilised in CSA S16 to determine the factored axial resistance load, indicated as $C_r$.

$$C_r = \phi \cdot f_y \cdot \left(1 + \lambda^{2n}\right)^{\frac{-1}{n}} \tag{2.4}$$

The background to the development of the double-exponential curve was presented by Loov (1996) and has the benefit of representing multiple curves by only varying the exponent $n$. This formula, when applied with a steel resistance factor equal to unity, provides results generally accurate to within 3% to the SSRC column curves. The SSRC's curve No.1 ($n = 2.24$) is employed for welded wide-flange columns made from flame-cut plate, while curve No.2 ($n = 1.34$) is used as the basic column strength curve (Galambos, 1998). A limit states design methodology with a steel resistance factor is utilised by CSA, where $\phi = 0.9$. The latter part of Equation 2.4, $(1+\lambda^{2n})^{-1/n}$, has the function of reducing the column's axial resistance according to the column's slenderness and varies between unity and a value asymptotically equal to zero.

#### 2.3.1.1.3 SANS 10162-1:2011

South Africa adopted and subsequently adapted the Canadian design specification (CSA S16), in SANS 10162-1 for hot-rolled steelwork (Walls and Viljoen, 2016). As a result, the same column strength curves are found in CSA S16-14 and SANS 10162-1:2011, with both steel specifications using a structural steel resistance factor of 0.9.

#### 2.3.1.1.4 EN 1993-1-1:2005

As mentioned during the background discussion of column design in Section 2.3.1, EN 1993-1-1:2005 (EC3) incorporates slightly modified ECCS column curves. Similar to the reduction techniques used by the previous design specifications considered, the design compression buckling resistance ($N_{b,Rd}$) is obtained using the slenderness reduction factor, $\mathcal{X}$ in Equation 2.5.

$$N_{b,Rd} = \frac{\mathcal{X} \cdot A \cdot f_y}{\gamma_{M1}} \tag{2.5}$$

with

$$\mathcal{X} = \frac{1}{\Phi + \sqrt{\Phi^2 - \overline{\lambda}^2}} \leq 1.0$$

$$\Phi = 0.5\left(1 + \alpha(\overline{\lambda} - 0.2) + \overline{\lambda}^2\right)$$

This slenderness reduction factor is determined using an Ayrton–Perry model (Badari and Papp, 2015), based on an analytically determined first yield curve allowing for geometric imperfections (Trahair et al., 2008). The original geometric imperfection term has subsequently been replaced by $\alpha(\overline{\lambda} - 0.2)$, where $\overline{\lambda}$ is used as the non-dimensional slenderness parameter and $\alpha$ is an imperfection factor as listed in Table 2.1. The values for $\alpha$ were calibrated to include the effects of all imperfections based on the physical test results by ECCS (Ziemian, 2010). The appropriate buckling curve is selected according to the steel type, cross-sectional properties, method of manufacturing and axis of buckling from EC3. The factor $\Phi$ is then used to calculate the slenderness reduction factor ($\mathcal{X}$) and in turn the design axial resistance load. It is noteworthy that the partial steel resistance factor ($\gamma_{M1}$) in EC3 is equal to unity. This is partly due to the refined column curve model employed by the specification, but can be superseded by national annexes.

Table 2.1: EC3 imperfection factors for flexural buckling

| Buckling curve | $a_0$ | a | b | c | d |
|---|---|---|---|---|---|
| $\alpha$ | 0.13 | 0.21 | 0.34 | 0.49 | 0.76 |

#### 2.3.1.2 Web-tapered column behaviour

Web-tapered members exhibit the same characteristics and modes of failure as that of prismatic members, but their design is more elaborate. Local failures due to material yielding or plate instability remain the same on a cross-sectional basis, but global member instability becomes complex with the variation in the cross-sectional area. Ziemian (2010) discusses the difficulty surrounding the stability analysis of web-tapered columns, with specific reference to the non-uniform distribution of stress and stiffness throughout the length. This renders the Euler buckling formula in Equation 2.1 no longer applicable. No exact closed-form solution that can be applied to all web-tapered configurations exists for $C_e$. In addition, the critical cross-section needs to be identified, based on the cross-section with the highest internal stress after any area reduction due to slender plates (Kaehler et al., 2011). Sections 2.3.1.2.1 and 2.3.1.2.2 are considered below for recommended design approaches for web-tapered columns found in the literature.

##### 2.3.1.2.1 DG25:2011

The development of appendices for web-tapered member design in the older AISC specifications (1978 to 1999) was mentioned in the historical overview of the MBS industry in Section 2.2. This was based on the allowable stress method and has since been omitted after the adoption of LRFD by AISC. Instead, DG25 was published, in which the elastic flexural buckling load of a web-tapered column is used to determine the non-dimensional slenderness parameter in Equation 2.2. This uses an equivalent prismatic member to allow web-tapered members to be designed using the AISC 360 provisions for prismatic members.

Equation 2.6 presents an empirical formula from DG25 that resembles Euler's formula for the approximate elastic buckling load. This provides a means for calculating the elastic flexural buckling load for linearly web-tapered columns with constant plate thickness and flange width members, and pinned end conditions about the strong-axis.

$$C_e = \frac{\pi^2 \cdot E \cdot I'}{L^2} \tag{2.6}$$

The modified moment of inertia ($I'$) is measured at a distance of $0.5L(I_{small}/I_{large})^{0.0732}$ from the small end. The moment of inertia at the small and large ends are denoted as $I_{small}$ and $I_{large}$, respectively. Marques, Taras, et al. (2012) provide an overview of other empirical expressions found in the literature, in addition to the above approximation. When the elastic flexural buckling load is required about the weak-axis, DG25 recommends that Euler's formula be used based on the mid-height section properties. This is justified based on the insignificant variation of the weak-axis moment of inertia in web-tapered columns. As an alternative to approximate

methods, DG25 suggests the calculation of $C_e$ using the numerical techniques presented later in Sections 2.5.3.1 and 2.5.3.2.

By obtaining the theoretical buckling load of a web-tapered column, the equivalent prismatic slenderness can be combined with the area at the most stressed cross-section to calculate the axial resistance. DG25 determines the critical cross-section through inspection of the columns at various locations, namely at the top, bottom and mid-height. Finally, the AISC 360 column buckling formulae can be incorporated to account for inelastic column behaviour and to derive the axial resistance load. This same principle of using an equivalent prismatic member is employed by other researchers, i.e. Baptista and Muzeau (1998) and Trahair et al. (2008), when designing a web-tapered member.

#### 2.3.1.2.2 EN 1993-1-1:2005

Any one of the following methods is recommended in EC3:

a) An eigenvalue buckling analysis combined with the general method (section 6.3.4 in EC3).

b) A three-dimensional second-order analysis (section 5.2.2 in EC3).

c) Full geometric and material non-linear analysis.

Marques, Taras, et al. (2012) considered the implementation and accuracy of these methods for the design of web-tapered columns. They noted that the first two methods were vague and questioned the effectiveness of performing a complex structural analysis that accounts for local and global geometrical imperfections, and then combining the results with oversimplified design procedures in EC3. They found the existing buckling curves (see Table 2.1) to be conservative and did not account for the added stability of web-tapered members in a particular plane. In addition, the current provisions require a tedious structural analysis to identify the critical cross-section, based on the location of the highest internal stress. This led to designers resorting to the most conservative assumption and to base the cross-sectional area on the smaller end of the column.

They concluded that a full non-linear analysis would require slightly more effort than the previous two methods, but would provide more accurate results. Here, the slenderness reduction factor ($\mathcal{X}$) in Equation 2.5 is obtained as the buckling load multiplier in a full geometric and material non-linear (with imperfections) analysis, henceforth referred to in this dissertation as a full non-linear analysis. In doing so, Marques, Taras, et al. (2012) were able to accurately represent the physical model, thus rendering the use of probabilistic column curves unnecessary as the intermediate value ($\Phi$) is not required (see Equation 2.5).

Marques, Taras, et al. (2012) also proposed a stability verification procedure for web-tapered columns, with some additional parameters to those in EC3 that were calibrated using the test

results from over 350 full non-linear analyses in Abaqus, based on shell elements. Here, the critical cross-section of a column is determined as a function of the tapering ratio ($\gamma = h_{max}/h_{min}$) and the non-dimensional slenderness parameter ($\overline{\lambda}$). They proposed an additional imperfection parameter $\beta$ to account for the increased stability of web-tapered members relative to uniform members. In Equation 2.5, $(\alpha \cdot \beta)$ replaces the imperfection parameter $\alpha$ for prismatic columns in Table 2.1 when calculating $\Phi$. The resistance of a web-tapered column is then calculated using the remaining formulae in Equation 2.5 and the critical cross-section's properties.

#### 2.3.1.3 Review of in-plane flexural column resistances

It was found that all the steel design specification considered in this study use probabilistic-based column strength curves to determine the maximum strength of prismatic columns. The provisions in each design specification may appear different, but the main principles remain the same. The principles to determine the flexural buckling resistance are:

a) Identify the non-dimensional slenderness parameter, which provides information on the mathematical instability of the column without imperfections and with an infinite yield stress.

b) Select an appropriate probabilistic-based design curve to address the presence of imperfections in columns and describe the inelastic behaviour.

DG25 uses the same principles, but requires additional consideration for calculating the non-dimensional slenderness parameter ($\lambda$) and the selection of the critical cross-section. No closed-form solution exists for the elastic flexural buckling load of non-prismatic members, but empirical and numerical methods could be used in this regard. An equivalent slenderness parameter can then be derived using the elastic flexural buckling load. This forms the basis of DG25, which allows web-tapered members to be designed using the provisions for prismatic members. Similar methods were also found to be used in web-tapered column design as published by Baptista and Muzeau (1998) and Trahair et al. (2008). Despite the original intention that DG25 be used in combination with AISC 360, Ziemian (2010) stated that it could be used with other design specifications.

Marques, Taras, et al. (2012) found the recommended methods in EC3 (see Section 2.3.1.2.2) to be vague or impractical to implement routinely. The same authors suggested that a new design procedure be used by modifying the existing EC3 design specifications, based upon an extensive array of full non-linear analyses.

### 2.3.2 Bending resistance of laterally unsupported beams

#### 2.3.2.1 Prismatic beam design approaches

The cross-sectional bending resistance of sufficiently short or continuous laterally supported members is governed by the section's capacity to redistribute bending moments and the ability of localised plate elements to remain stable during loading (SANS 10162-1, 2011). However, slender beams with long spans between lateral restraints are subject to elastic lateral-torsional buckling as the mode of failure at loads smaller than the in-plane cross-sectional capacity (Ziemian, 2010). As the bending moment increases about a beam's strong-axis plane, the beam deflects in-plane until a critical elastic lateral-torsional buckling moment ($M_{cr}$) is reached where bifurcation of the equilibrium conditions takes place (Galambos and Surovek, 2008). As in the case of columns, this would cause a compression flange plate to buckle about its weak-axis. However, through the restraint provided by the web, the compression flange is forced to buckle laterally. This results in a cross-section displaced in the plane of the strong-axis, coupled with torsional deformation. Beams bent about their weak-axis do not fail due to elastic lateral-torsional buckling, as the weak-axis describes the plane of least flexural resistance (Ziemian, 2010).

The analytical solution of the governing differential equation for the critical bending moment ($M_{cr}$) only exists for the simple beam cases, i.e. prismatic doubly symmetric sections with simply supported end restraints that are subject to uniform strong-axis moment applied at the centroid of the cross-section (Ziemian, 2010). The solution to the differential equation is presented below as published by Timoshenko and Gere (1961). It is assumed in the derivation of Equation 2.7 that restraint is provided to both end supports against lateral displacement and rotation, while being free to warp and rotate about the weak-axis (Wong and Driver, 2010).

$$M_{cr} = \frac{\pi}{L}\sqrt{E \cdot I_y \cdot G \cdot J + \left(\frac{\pi \cdot E}{L}\right)^2 I_y \cdot C_w} \tag{2.7}$$

The weak-axis moment of inertia ($I_y$) in the equation above is utilised in combination with $J$ and $C_w$, which are the section's torsional and warping constants, respectively. The other terms commonly encountered in structural engineering are clarified in the nomenclature on page xiv. The loading conditions as described in Equation 2.7 represent the most detrimental case of the critical bending moment, i.e. uniform bending moments between supports (Galambos and Surovek, 2008). An equivalent moment factor is used in order to relate Equation 2.7 to other loading configurations. This factor applies to all design specifications considered in this study, although the name and designated symbol may vary as discussed in the respective design specifications.

The steel design specifications considered in this study may define the moment of resistance either as a function of stable lengths, the critical elastic lateral-torsional buckling load, or a

modified non-dimensional slenderness parameter. The modified non-dimensional slenderness parameter for lateral-torsional buckling ($\lambda_{LTB}$) is defined in terms of bending moments below as the square root of the ratio between the nominal cross-sectional resistance and the elastic lateral-torsional buckling resistance.

$$\lambda_{LTB} = \sqrt{\frac{M_{n,cross}}{M_{cr}}} \tag{2.8}$$

This provides a convenient means to define beam slenderness similar to what is used for columns. All the design specifications base their formulae for beam resistance on this interaction, although it is not always apparent as only EC3 explicitly uses this convention. This will prove useful later when discussing web-tapered beams in Section 2.3.2.2. Next, an overview of the design approaches to laterally unsupported prismatic beams by several prominent design specifications is considered.

#### 2.3.2.1.1 AISC 360-10

AISC 360 classifies cross-sections into three classes, i.e. compact, non-compact and slender. This corresponds to the cross-section's ability to redistribute bending moment and the stability of plate elements. The classification is based on the width-to-thickness ratios of plate elements with limits available in AISC (2010). The flexural design provisions in AISC (2010) (sections F2 to F5) are arranged for optimal ease of use when designing beams with specific cross-sectional classifications, by removing irrelevant terms to calculate the moment of resistance.

In the AISC 360 design specifications, $M_{cr}$ may be calculated directly from Equation 2.9, which is based on the derivation by Timoshenko and Gere (1961).

$$M_{cr} = \frac{C_b \cdot \pi}{L} \sqrt{E \cdot I_y \cdot G \cdot J + \left(\frac{\pi \cdot E}{L}\right)^2 I_y \cdot C_w} \tag{2.9}$$

The equivalent moment factor ($C_b$) exploits the increased stability that manifests in beams subject to non-uniform bending moment distributions by increasing the critical elastic lateral-torsional buckling moment (see Figure 2.2). This can be determined using the quarter-point method in Equation 2.10, with adjusted constants based on the work of Kirby and Nethercot (1979).

$$C_b = \frac{12.5 M_{max}}{2.5 M_{max} + 3 M_A + 4 M_B + 3 M_C} \leq 3.0 \tag{2.10}$$

$M_A$, $M_B$ and $M_C$ corresponds to the bending moments at the first quarter-, centre- and third quarter positions in the beam, while $M_{max}$ is the maximum bending moment occurring throughout the beam. All moments introduced in Equation 2.10 are in terms of their absolute values. This form of the quarter-point method was found to give greater accuracy in general and may be applied to a broad spectrum of loading configurations (AISC, 2010).

AISC 360 also provides the stress-based equivalent as presented in Equation 2.11. This represents the critical elastic lateral-torsional buckling stress ($f_{cr}$) that is present in the compression flange. This was introduced in an effort to establish uniformity between the AISC 360 design procedures for singly and doubly symmetric sections.

$$f_{cr} = \frac{C_b \cdot \pi^2 \cdot E}{(L/r_{ts})^2} \sqrt{1 + 0.078 \frac{J}{Z_{ex} \cdot h_o} \left(\frac{L}{r_{ts}}\right)^2} \tag{2.11}$$

The derivation of the stress-based form is available in Galambos and Surovek (2008). Here, the effective radius of gyration is $r_{ts}$, with $r_{ts} = \sqrt{I_y \cdot h_0 / 2Z_{ex}}$ and $h_0$ being the distance between the flange centroids. Figure 2.2 represents the available flexural strength ($M_c$) using the provisions in section F2 in AISC 360 for compact cross-sections that are based on their plastic moment of resistance ($M_p$).

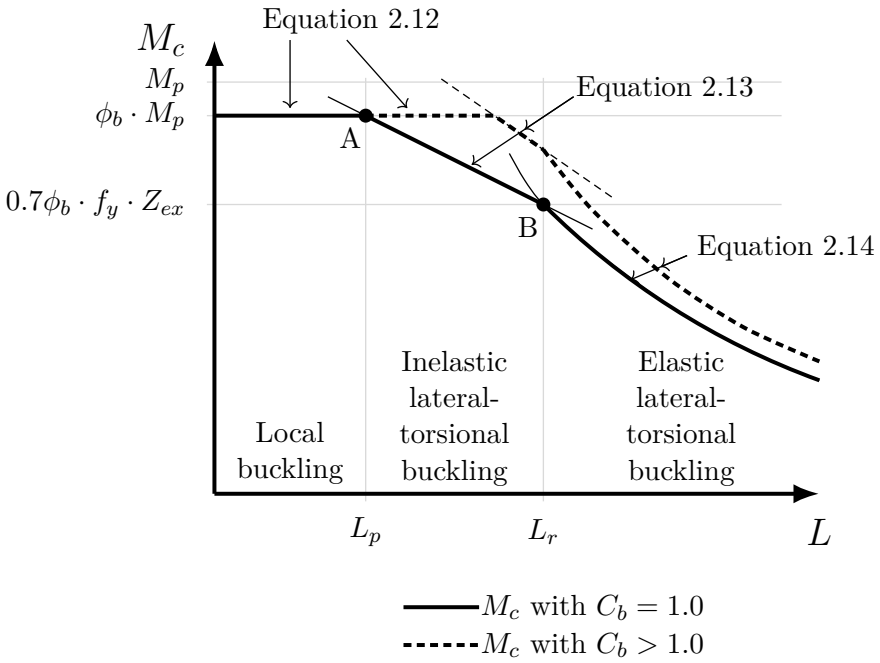


Figure 2.2: The nominal flexural strength in AISC 360, as a function of the unbraced length and moment gradient

$$M_c = \phi_b \cdot M_p = \phi_b \cdot f_y \cdot Z_{plx}, \qquad \text{if L} \leq \text{L}_\text{p} \tag{2.12}$$

$$M_c = \phi_b \cdot C_b \left[ M_p - (M_p - 0.7 f_y \cdot Z_{ex}) \left( \frac{L - L_p}{L_r - L_p} \right) \right] \leq \phi_b \cdot M_p, \qquad \text{if } \text{L}_\text{p} \leq \text{L} \leq L_\text{r} \tag{2.13}$$

$$M_c = \phi_b \cdot M_{cr} = \phi_b \cdot f_{cr} \cdot Z_{ex} \leq \phi_b \cdot M_p, \qquad \text{if } \text{L}_\text{r} \leq \text{L} \tag{2.14}$$

$L_p$ and $L_r$ are defined as functions of the material and cross-sectional properties of a beam and form the limiting lengths for the states of yielding and inelastic lateral-torsional buckling, respectively. AISC 360 may be consulted in this regard. The mode of failure for beams with unbraced lengths shorter than $L_p$ is subject to the cross-section's ability to redistribute bending

moment, without plate members becoming unstable locally. This is described by Equation 2.12 and illustrated in Figure 2.2. Here, the full cross-section is considered to reach the material's yield stress ($f_y$). The plastic moment ($M_p$) is determined as the product of the material's yield stress ($f_y$) and the plastic section modulus of the section about the strong-axis ($Z_{plx}$). On the other hand, slender beams have unbraced lengths exceeding $L_r$ and are subject to elastic lateral-torsional buckling as defined in Equation 2.14. Here, the beam becomes unstable when the outermost fibre on the cross-section reaches the critical elastic lateral-torsional buckling stress ($f_{cr}$), as found in Equation 2.11. For intermediate lengths, beams are subject to inelastic buckling, using the interpolation formula in Equation 2.13. AISC 360 assumes strengths to vary linearly between the interpolation points A and B, indicated in Figure 2.2 (Kim, 2010). Similar to columns, a flexural resistance factor of $\phi_b = 0.9$ is used by AISC 360.

#### 2.3.2.1.2 CSA S16-14

Cross-sections in CSA S16-14 subject to bending are classified into four categories, based on their respective width-to-thickness ratios. The categories are described in Table 2.2.

Table 2.2: Description of CSA S16 beam cross-section classifications

| Classification | Description of behaviour |
|---|---|
| Class 1 | The plastic moment may be reached, with further moment redistribution. |
| Class 2 | The plastic moment may be reached, without any further moment redistribution. |
| Class 3 | Only the yield moment may be reached. |
| Class 4 | Local buckling is reached before the yield moment and governs member resistance. |

The provisions for doubly symmetric I-beam sections in CSA S16 are discussed below. It should, however, be noted that CSA S16 does not apply in the case of beams where the flanges and web are both considered class 4. The North American specification for the design of cold-formed steel structural members (CSA S136) should be consulted in this regard (AISI-CSA, 2007).

In CSA S16 the critical elastic lateral-torsional buckling formula by Timoshenko and Gere (1961) (see Equation 2.7) is modified to become Equation 2.15.

$$M_{cr} = \frac{\omega_2 \cdot \pi}{L} \sqrt{E \cdot I_y \cdot G \cdot J + \left(\frac{\pi \cdot E}{L}\right)^2 \cdot I_y \cdot C_w} \tag{2.15}$$

Here, the critical elastic moment is designated as $M_{cr}$ and the notation for the equivalent moment factor is replaced by the symbol $\omega_2$. The equivalent moment factor may then be calculated using either of the two following methods:

$$\omega_2 = 1.75 + 1.05\kappa + 0.3\kappa^2 \leq 2.5 \tag{2.16}$$

$$\omega_2 = \frac{4M_{max}}{\sqrt{M_{max}^2 + 4M_A^2 + 7M_B^2 + 4M_C^2}} \tag{2.17}$$

Equation 2.16 applies when the bending moment distribution is considered to be linear, based on the findings by Salvadori (1955). This quadratic equation is based on the end moment ratio $\kappa = M_{smaller}/M_{larger}$. Equation 2.17 by Wong and Driver (2010), may be used as a general method that also allows for non-linear bending moment distributions and is based on a modified form of the quarter-point method first proposed by Kirby and Nethercot (1979).

In CSA S16, the moment of resistance ($M_r$) for class 1 and 2 beams, subject to strong-axis bending moments and without sufficient lateral supports, are shown in Figure 2.3 and defined below.

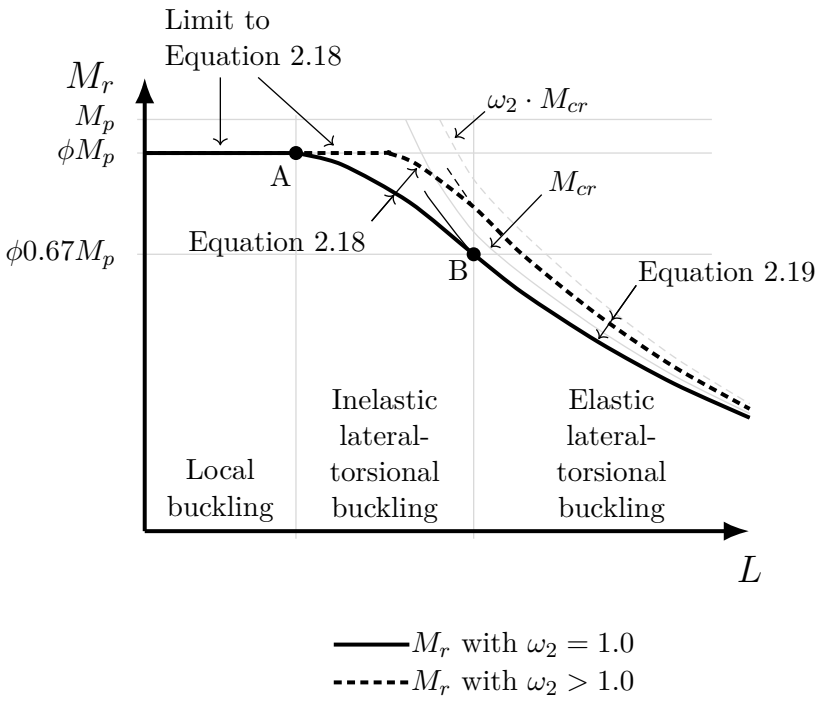


Figure 2.3: The factored moment of resistance in CSA S16, as a function of the unbraced length and moment gradient

$$M_r = 1.15\phi \cdot M_p \left(1 - \frac{0.28 M_p}{M_{cr}}\right) \leq \phi \cdot M_p, \qquad \text{if } M_{cr} > 0.67 M_p \tag{2.18}$$

$$M_r = \phi \cdot M_{cr}, \qquad \text{if } M_{cr} \leq 0.67 M_p \tag{2.19}$$

Equations 2.18 describes a non-linear transitions between the points A and B for the inelastic region (see Figure 2.3). The curve resulting from Equations 2.18 and 2.19 is based on statistical analysis performed by Baker and Kennedy (1984) on test results obtained by Dibley (1969) on rolled I-section beams. In the case of beams that are classified as either class 3 or 4 cross-sections, the plastic sectional properties are replaced by the elastic sectional properties for Figure 2.3 and, Equations 2.18 and 2.19.

#### 2.3.2.1.3 SANS 10162-1:2011

As discussed in Section 2.3.1.1.3, SANS 10162-1 was adapted from the CSA S16 steel design specifications. These specifications are essentially the same for beams with the only notable differences as follows:

a) The calculation of the equivalent moment factor ($\omega_2$), according to Equation 2.17 has not been introduced into SANS 10162-1.

b) Beams that are classified as having flanges and webs that are both class 4 elements have to be designed in terms of SANS 10162-2 for cold-formed steelwork.

#### 2.3.2.1.4 EN 1993-1-1:2005

In EC3 cross-sections in bending are grouped using the same classification as CSA S16 and SANS 10162-1 in Table 2.2. The formula in Equation 2.20, which is based on Timoshenko and Gere (1961), may be used, although no explicit provisions are made in EC3 for calculating $M_{cr}$. Other formulae for $M_{cr}$ may also be found in literature as alternatives in respect to the solution below (Walls and Viljoen, 2016).

$$M_{cr} = C_m \frac{\pi}{L_{cr}} \sqrt{E \cdot I_z \cdot G \cdot I_T + \left(\frac{\pi \cdot E}{L_{cr}}\right)^2 \cdot I_z \cdot I_w} \tag{2.20}$$

Here, $L_{cr}$ is the buckling length in the plane considered and $I_z$ denotes the moment of inertia around the weak-axis. The torsional constant ($I_T$) and warping constant ($I_w$) is synonymous with $J$ and $C_w$, respectively, as used by the other design specifications. The shape of the bending moment diagram is taken into account through the use of the $C_m$ modification factor, available in annexure A or B of EC3.

The EC3 provisions for lateral-torsional buckling design are applied using the Ayrton–Perry model developed for flexural buckling in Section 2.3.1.1.4 (Badari and Papp, 2015). The general case as per section 6.3.2.2 in EC3 is presented below for the design buckling resistance moment ($M_{b,Rd}$), which makes use of a slenderness reduction factor for lateral-torsional buckling, $\mathcal{X}_{LT}$.

$$M_{b,Rd} = \mathcal{X}_{LT} \cdot W_y \frac{f_y}{\gamma_{M1}} \tag{2.21}$$

with

$$\mathcal{X}_{LT} = \frac{1}{\Phi_{LT} + \sqrt{\Phi_{LT}^2 - \overline{\lambda}_{LT}^2}} \leq 1.0$$

$$\Phi_{LT} = 0.5\left(1 + \alpha_{LT}(\overline{\lambda}_{LT} - 0.2) + \overline{\lambda}_{LT}^2\right)$$

$$\overline{\lambda}_{LT} = \sqrt{\frac{W_y \cdot f_y}{M_{cr}}}$$

The same buckling curves used for columns are used for the design of beams, with the exception of curve $a_0$ (see Table 2.3). EC3 may be consulted for the appropriate lateral-torsional buckling imperfection factors ($\alpha_{LT}$), according to the cross-sectional properties and the method of manufacturing. The non-dimensional slenderness parameter for lateral-torsional buckling ($\overline{\lambda}_{LT}$) is described above in terms of the strong-axis section modulus ($W_y$) determined according to Table 2.4.

Table 2.3: EC3 imperfection factors for lateral-torsional buckling

| Buckling curve | a | b | c | d |
|---|---|---|---|---|
| $\alpha_{LT}$ | 0.21 | 0.34 | 0.49 | 0.76 |

Table 2.4: Section modulus for beam design, according to EC3

| Class 1 or 2 | Class 3 | Class 4 |
|---|---|---|
| $W_y = W_{pl,y}$ | $W_y = W_{el,y}$ | $W_y = W_{eff,y}$ |

Depending on the classification of the section, the weak-axis section modulus may either be based on a plastic, elastic or effective section modulus, denoted as $W_{pl,y}$, $W_{el,y}$ or $W_{eff,y}$, respectively. The intermediate value for lateral-torsional buckling is then used to calculate the lateral-torsional buckling slenderness reduction factor and, in turn, the design buckling resistance moment. Here, a partial steel resistance factor ($\gamma_{M1}$) equal to unity still applies.

#### 2.3.2.2 Web-tapered beam behaviour

Web-tapered beams are subject to the same limit states as prismatic beams (Kaehler et al., 2011). As for web-tapered columns, the local instability checks of plate members are performed on a cross-sectional basis. However, global member instability requires additional consideration, as it is influenced by the varying cross-sectional properties and factors that include the moment gradient and end conditions (Ziemian, 2010). As a result the closed-form solution for the critical elastic lateral-torsional buckling load cannot be applied to non-uniform beams. Sections 2.3.2.2.1 and 2.3.2.2.2 are considered next for the design of web-tapered beams by referring to findings from the literature.

##### 2.3.2.2.1 DG25:2011

In DG25, the critical cross-section is determined based on the cross-section utilisation ratio, defined as the ratio between the applied bending moment and the resistance moment about the strong-axis. Identifying the critical cross-section becomes troublesome for web-tapered members, as both the distribution of bending moment and the section modulus that define the utilisation

ratio varies throughout the length of the beam. A more useful description of the utilisation ratio would be in terms of the compression flange stress, which is the cause of lateral-torsional instability (described in Section 2.3.2.1). However, the cross-sectional classification can also vary, adding additional complexity to identifying the critical cross-section. Due to these matters, web-tapered members typically require the utilisation ratio to be checked at several locations (Kaehler et al., 2011).

The use of compression flange stress distributions is central to the methodology employed by DG25. This is a departure from the use of bending moments used in AISC 360 for prismatic beams. Furthermore, beam design in DG25 is conducted using a generalised AISC 360 procedure developed by White and Kim (2006) and has the advantage of applying to any I-beam cross-section classifications. Subsequent research was completed by the same researchers to refine the generalised procedure to apply to prismatic and web-tapered I-shape members (Kaehler et al., 2011). A series of full non-linear analyses using Abaqus was conducted to model web-tapered beams that were previously studied by Prawel et al. (1974), Salter et al. (1980), and Shiomi et al. (1983), by accounting for residual stress patterns and geometric imperfections (Kim and White, 2006b; Kim and White, 2007b; Kim, 2010). A close resemblance was observed between the proposed procedure and the behaviour of test specimens that failed due to lateral-torsional buckling.

DG25 states that the elastic lateral-torsional buckling load may be determined using a numerical technique that can adequately determine the out-of-plane buckling behaviour of beams. These numerical techniques will be considered in more detail in Section 2.5.4. However, to routinely determine the critical elastic lateral-torsional buckling load, DG25 makes use of the method purposed by Yura and Helwig (1996) for determining the critical elastic lateral-torsional buckling load. This approach is based on the cross-sectional properties at mid-span on the unbraced length, using the AISC 360 stress-based formulation for $f_{cr}$ as presented in Equation 2.11. In the case of doubly symmetric I-beams, close agreement was obtained with the numerical studies by Kim (2010), with improved accuracy observed when using the AASHTO (2007) method to account for stress gradient effects. On the other hand, very conservative results were noted by the same researcher when applying the proposed method with singly symmetric I-beams subject to double curvature bending.

In DG25, the moment gradient factor (defined in Section 2.3.2.1.1) is replaced by a stress gradient factor, which also increases the beam's elastic buckling resistance in the presence of non-uniform compression flange stress. The AASHTO method for determining the stress gradient factor is based on the formulation by Salvadori (1955), but accounts for non-linear compression flange stress as discussed by White (2006), Kim and White (2007a), and Wong and Driver (2010). The stress gradient factor ($C_b$) is determined in Equation 2.22, using the compression stress values as depicted in Figure 2.4.

$$C_b = \begin{cases} \text{If } \frac{f_{mid}}{f_2} \leq 1.0 \text{ or } f_2 = 0 \text{ or for cantilevers:} \\ 1.0 \\ \text{Otherwise:} \\ 1.75 - 1.05\left(\frac{f_1}{f_2}\right) + 0.3\left(\frac{f_1}{f_2}\right)^2 \leq 2.3 \end{cases} \tag{2.22}$$

with

$$f_1 = \begin{cases} f_0, & \text{if } |f_{mid}| < \left|\frac{f_0+f_2}{2}\right| \\ 2f_{mid} - f_2 \geq f_0, & \text{if } |f_{mid}| \geq \left|\frac{f_0+f_2}{2}\right| \end{cases}$$

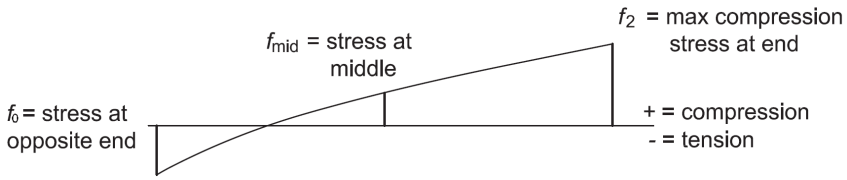


Figure 2.4: Stress definitions to the AASHTO (2007) stress gradient formula

Similar to AISC 360, the stress gradient factor is used to modify the elastic buckling lateral-torsional buckling stress before mapping it to a real beam with inelastic properties (Kaehler et al., 2011). The flexural design provisions in sections F2 to F5 in AISC (2010) are arranged for optimal ease of use when designing beams, by removing irrelevant factors to the calculation of available strength. In DG25 a single set of formulae is used, based on slightly modified AISC provisions, which is more convenient in dealing with a variety of different plate classifications and buckling limits within a specific beam. The resistance moment is then accounted for by using the nominal buckling strength multiplier ($\gamma_{eLTB}$), which is defined as the ratio between mid-span critical elastic lateral-torsional buckling stress ($f_{cr,mid}$) that may be determined using Equation 2.11, and the maximum factored compression flange stress ($f_{r,max}$).

$$\gamma_{eLTB} = \frac{f_{cr,mid}}{f_{r,max}} \tag{2.23}$$

Kim (2010) discusses the derivation of the DG25 general design procedure, and found that for all practical applications, the same results are provided by the single formulae set in DG25 when compared to AISC 360. The general procedure in DG25 for designing web-tapered members is presented below.

$$M_n = R_{pg} \cdot R_{pc} \cdot M_y = R_{pg} \cdot R_{pc} \cdot f_y \cdot Z_{ex}, \qquad \text{if } \sqrt{\frac{f_y}{\gamma_{eLTB} \cdot f_r}} \leq \frac{1.1}{\pi} \tag{2.24}$$

$$M_n = R_{pg} \cdot R_{pc} \cdot M_y \Big[1 - \left(1 - \frac{f_L}{R_{pc} \cdot f_y}\right) \times \left(\frac{\pi\sqrt{f_y \;/\; \gamma_{eLTB} \cdot f_r} - 1.1}{\pi\sqrt{f_y \;/\; f_L} - 1.1}\right)\Big] \leq R_{pg} \cdot R_{pc} \cdot M_y, \qquad \text{if } \frac{1.1}{\pi} < \sqrt{\frac{f_y}{\gamma_{eLTB} \cdot f_r}} < \frac{f_y}{f_L} \tag{2.25}$$

$$M_n = \begin{cases} \gamma_{eLTB} \cdot f_r \cdot Z_{ex} \cdot R_{pg}, & \text{for slender webs} \\ \gamma_{eLTB} \cdot f_r \cdot Z_{ex}, & \text{for all other} \end{cases} \qquad \text{if } \frac{f_y}{f_L} \leq \sqrt{\frac{f_y}{\gamma_{eLTB} \cdot f_r}} \tag{2.26}$$

The general procedure in Equations 2.24 to 2.26 is derived from equations F4–1 to F4–3 in AISC 360, which are based on the elastic moment ($M_y$), but includes additional terms when dealing with sections of various cross-section classifications (Kim, 2010). Here, $R_{pg}$ and $R_{pc}$ are respectively the bending strength reduction factor and web plastification factors available from AISC 360. In DG25, the beam behaviour regions are defined in terms of stress, whereas AISC 360 (in Section 2.3.2.1.1) uses the unbraced length. The value $f_L$ is the upper limit for the flexural stress in the compression flange when lateral-torsional buckling is influenced by partial yielding (AISC, 2010). A recommended value of $f_L = 0.7f_y$ is used for doubly symmetric I-shaped members in AISC 360.

The slenderness is now represented by the factor $\sqrt{f_y \;/\; \gamma_{eLTB} \cdot f_r}$, with $f_r$ being the compression flange stress. Here, the denominator may be rewritten using Equation 2.23 as $f_{cr,mid}(f_r/f_{r,max})$. This form demonstrates how $f_{cr,mid}$ is effectively scaled, according to the compression flange stress utilisation ratio at any arbitrary position. Thus, a similar convention is obtained to that in Equations 2.2 and 2.8 to describe a non-dimensional slenderness parameter as the square root of the ratio between yield stress ($f_y$) and critical buckling stress (now represented by $\gamma_{eLTB} \cdot f_r$).

#### 2.3.2.2.2 EN 1993-1-1:2005

EC3 considers web-tapered beams to a limited extent, with annexure BB3.2 in EC3 suitable for calculating a beam's stable length between points of restraint. Lateral-torsional buckling may then be ignored for haunches and web-tapered I-sections of unbraced lengths shorter than this length. Marques, da Silva, Greiner, et al. (2013) noted that no explicit code-based provisions are available in EC3 for the design of tapered members, and the methods outlined earlier in Section 2.3.1.2.2 should rather be used.

Similar to their previous study on web-tapered columns, they determined that the recommended procedures in EC3 for web-tapered beams were inconsistent and described vaguely. The general

method (section 6.3.2.2 in EC3) makes use of the prismatic imperfection factors for lateral-torsional buckling given in Table 2.3. Marques (2012) found that this provides results that are conservative in most cases when compared to the numerically obtained results from full non-linear analysis. A summary of the aforementioned results is presented as Figure 2.5 concerning the slenderness reduction factor at the critical position. Each dot represents a numerical result with its value from the general method in EC3 on the ordinate and that from a full non-linear analysis on the abscissa.

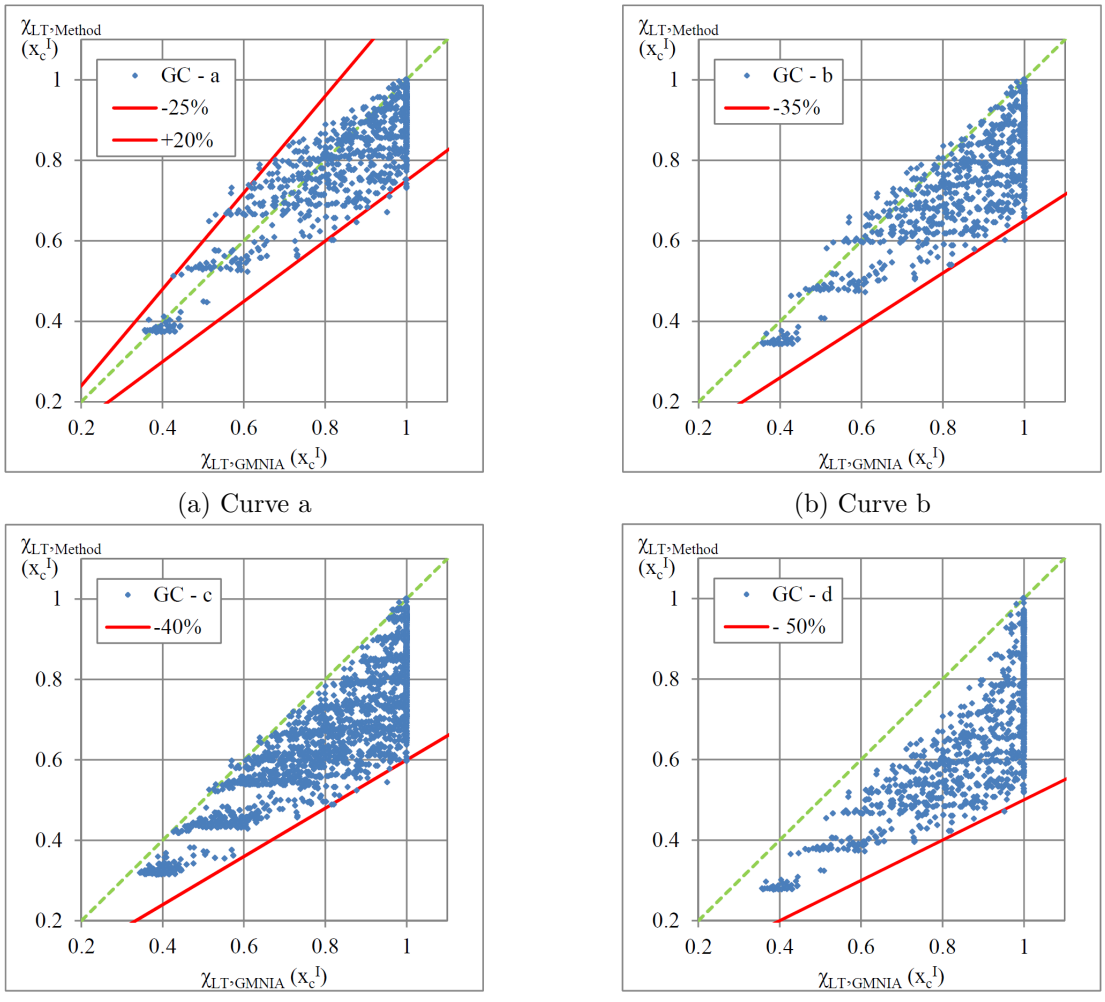


(a) Curve a

(b) Curve b

(c) Curve c

(d) Curve d

Figure 2.5: Statistical error when using the EC3 $\alpha_{LT}$ curves for web-tapered members by Marques (2012)

It is apparent from the results that the prismatic imperfection factors provide widely varying results when applied to web-tapered members, but these tend towards a conservative to very conservative estimate of member resistance, except when using curve $a$.

In an effort to address the inconsistent results produced by the general method in EC3 and to make optimal use of web-tapered beam capacities, Marques, da Silva, Greiner, et al. (2013)

proposed a stability verification of their own. The procedure is based on the Ayrton–Perry model and derived analytically for lateral-torsional buckling with geometrical imperfections to be consistent with EC3. Over 3000 full non-linear analyses were conducted in Abaqus, using shell elements. The method proposed by Marques, da Silva, Greiner, et al. (2013) utilises new imperfection factors that were calibrated according to the test results obtained during full non-linear analyses. Their proposal can be summarised into the following steps:

1. The position of the critical cross-section without imperfections ($x_c^I$) must be determined through inspection of the beam at several locations (e.g. 10 positions), by evaluating the utilisation ratio, defined as $\epsilon = M_{y,Ed}/M_{y,Rk}$. This represents the ratio of applied bending moment to characteristic moment of resistance about the strong-axis. The resistance load multiplier at the critical cross-section is then found as $\alpha_{ult,k}(x_c^I) = 1/\epsilon(x_c^I)$.

2. The critical load amplifier ($\alpha_{cr}$) may be determined using any adequate manner, such as a finite element analysis.

3. A modified form that incorporates an over-strength factor ($\phi$) is proposed for the slenderness reduction factor for lateral-torsional buckling at the critical cross-section ($\mathcal{X}_{LT}(x_c^I)$).

$$\mathcal{X}_{LT}(x_c^I) = \frac{\phi}{\Phi_{LT} + \sqrt{\Phi_{LT}^2 - \phi \cdot \overline{\lambda}_{LT}^2(x_c^I)}} \leq 1.0 \tag{2.27}$$

4. The formula for the intermediate value of lateral-torsional buckling ($\Phi_{LT}$) is also modified to account for the effects of a web-tapered geometry, as follows.

$$\Phi_{LT} = 0.5\left(1 + \phi \cdot \eta \frac{\overline{\lambda}_{LT}^2(x_c^I)}{\overline{\lambda}_z^2(x_{c,lim}^{II})} + \phi \cdot \overline{\lambda}_{LT}^2(x_c^I)\right) \tag{2.28}$$

5. The non-dimensional slenderness parameter at the critical cross-section is determined as the square root of the ratio between the resistance load multiplier ($\alpha_{ult,k}(x_c^I)$) and critical load amplifier ($\alpha_{cr}$). This is synonymous with the term $\sqrt{f_y \ / \ \gamma_{eLTB} \cdot f_r}$ used in DG25, discussed under Section 2.3.2.2.1.

$$\overline{\lambda}_{LT}(x_c^I) = \sqrt{\frac{\alpha_{ult,k}(x_c^I)}{\alpha_{cr}}} \tag{2.29}$$

6. Lastly, the over-strength factor ($\phi$), the position of the critical cross-section with imperfections ($x_{c,lim}^{II}$), and generalised imperfections ($\eta$) are given in Marques, da Silva, Greiner, et al. (2013). These parameters were calibrated based on the numerical test results by the same authors.

By using their proposed method, an improved correlation was observed between the calculated slenderness reduction factor (on the ordinate) and that found from full non-linear analysis (on the abscissa). The results from their findings are presented in Figure 2.6.

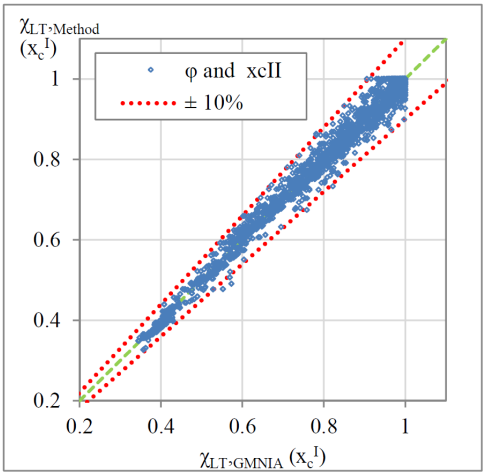


Figure 2.6: Statistical error when using the proposed procedure for web-tapered members by Marques (2012)

#### 2.3.2.3 Review of laterally unsupported beam resistances

In this section, it was shown that the underlying mechanisms for prismatic beams in the different design specifications considered for this study are fundamentally the same. The principles can again be summarised as follows:

a) A beam may be classified according to its lateral-torsional stability, e.g. the ratio between the nominal cross-sectional resistance moment and the critical elastic lateral-torsional buckling moment. The latter can be represented conveniently as a modified non-dimensional slenderness parameter for lateral-torsional buckling as in Equation 2.8.

b) The bending capacity is then determined based on the cross-section's ability to remain stable from local failures when a beam is sufficiently braced against lateral deflection or short enough. On the other hand, the critical elastic lateral-torsional buckling moment may be used to describe the moment of resistance for slender beams. The design specifications found in this study use different methods to account for the inelastic region. The North American-based design specifications make use of an interpolation scheme between the plastic and elastic regions, while EC3 is based on the Ayrton–Perry model initially developed for flexural buckling.

For web-tapered members, the identification of the critical cross-section is hampered by the unclear location of maximum utilisation. Thus, it is often required that the cross-section is inspected at various locations along the unbraced length (Kaehler et al., 2011; Marques, da Silva, Greiner, et al., 2013).

DG25 uses a general procedure based on the AISC 360 beam design equations, which include all cross-section factors and is presented in terms of stress rather than limiting lengths ($L_p$ and $L_r$).

This aids in dealing with the variable cross-sections along the length of web-tapered beams. The formula recommended in DG25 is again ordered into regions of plastic, inelastic or elastic behaviour by considering the compression flange stress.

In a separate study, Marques, da Silva, Greiner, et al. (2013) determined that the use of the prismatic EC3 imperfection factors on web-tapered beams is typically inconsistent or conservative. Consequently, they proposed a refined method that may be applied using a modified form of the EC3 provisions.

### 2.3.3 Resistance of beam-columns to combined axial and bending forces

#### 2.3.3.1 Prismatic beam-column design approaches

For the simultaneous action of axial and bending forces in beam-columns, the resistance is determined using interaction formulae. The effects of the forces that were studied until now, are considered next for the simply supported beam-column subject to in-plane flexure, with sufficient cross-sectional capacity to attain the plastic moment. This behaviour is illustrated in Figure 2.7.

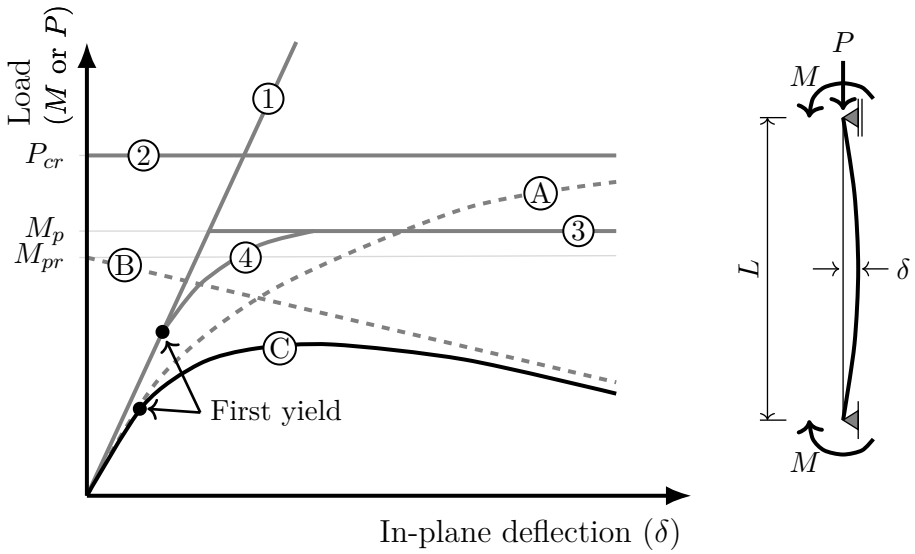


Figure 2.7: In-plane behaviour of a beam-column, adapted from Trahair et al. (2008)

In the figure above, line 1 represents the in-plane deflection as measured at mid-span due to the applied moment ($M$) when only the linear elastic beam behaviour in considered, without axial loads ($P$). Line 2 applies when only elastic axial load capacity ($P_{cr}$) is considered, with $M = 0$. During the elastic interaction of these forces, secondary moments arise due to the deflected shape under axial loading to form line A.

However, the maximum attainable resistance moment for class 1 and 2 beams is the section's plastic moment ($M_p$) when $P = 0$, indicated by line 3. In reality, beams start to undergo partial yielding within the cross-section at the point of first yield. Line 4 demonstrates the realistic transition between elastic-perfectly plastic behaviour and includes the effects of initial imperfections. In the presence of axial loads the section's plastic neutral axis shifts and a reduced full plastic resistance moment, $M_{pr}$, is reached and indicated by line B, which includes the effect of secondary moments. This forms the upper bound solution of the resistance of a beam-column. The actual behaviour is shown as line C, which is a transition from the elastic behaviour to the full plastic behaviour of a structural element (Trahair et al., 2008).

For a theoretical beam-column of zero length, line B, known as the point of first yield (Trahair et al., 2008), can be calculated from:

$$\begin{aligned} f_{max} &= f_{axial} + f_{bending,x} + f_{bending,y} \\ &= \frac{P_u}{A} + \frac{M_{u,x}}{Z_{e,x}} + \frac{M_{u,y}}{Z_{e,y}} \end{aligned} \tag{2.30}$$

Equation 2.30 describes the maximum stress ($f_{max}$) due to axial loads ($f_{axial}$) and bending moments ($f_{bending}$) at the furthest location from the respective neutral axes. The axial stress is determined from the ultimate axial load ($P_u$) acting over the cross-sectional area ($A$), while the stress arising from the bending moment is determined from the ultimate bending moment ($M_u$) over the elastic section modulus ($Z_e$). Here, the subscripts $x$ and $y$ are used to denote the strong and weak-axes, respectively.

Assuming a perfectly straight beam-column with no residual stresses, the maximum stress attainable is equal to the material yield stress ($f_y$) (Trahair et al., 2008). By rearranging the above formula the point of first yielding can be defined as Equation 2.31.

$$\begin{aligned} \frac{P_u}{A \cdot f_y} + \frac{M_{u,x}}{f_y \cdot Z_{e,x}} + \frac{M_{u,y}}{f_y \cdot Z_{e,y}} &\leq 1.0 \\ \frac{P_u}{P_y} + \frac{M_{u,x}}{M_{y,x}} + \frac{M_{y,y}}{M_{e,y}} &\leq 1.0 \end{aligned} \tag{2.31}$$

The numerators and denominators in this equation refer to the ultimate applied loads and the elastic section resistances, respectively.

Similarly, an interaction relationship between axial and flexural forces may be found as the point where the cross-section attains full plasticity. Due to the presence of both forces, the plastic neutral axis is shifted to balance the tension and compression forces. For I-shaped beam-columns, the reduced plastic moment capacity ($M_{pr}$) and reduced axial yielding capacity ($P_{yr}$) can be found analytically depending on the location of the in-plane plastic neutral axis (see Figure 2.8).

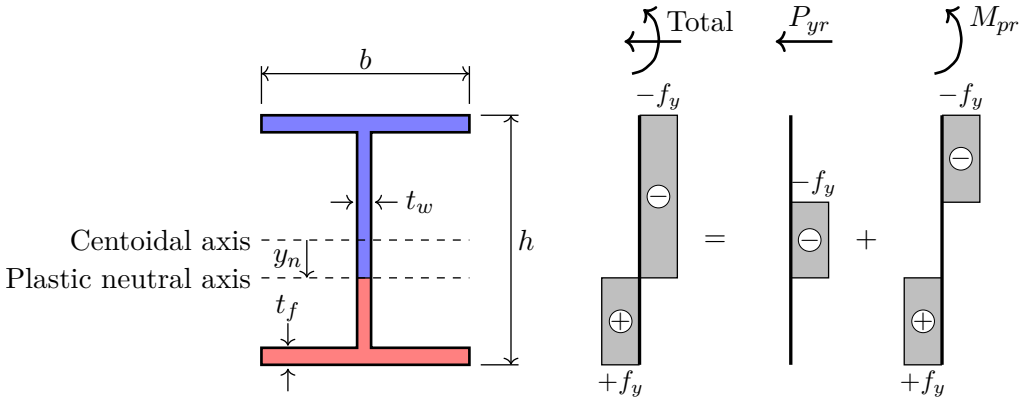


Figure 2.8: Plastic section subjected to combined axial forces and bending moments, adapted from Trahair et al. (2008)

When the plastic neutral axis lies within the web, $0 \leq y_n < (h - 2t_f)/2$:

$$P_{yr} = 2f_y \cdot y_n \cdot t_w$$
$$M_{pr} = f_y \cdot b \cdot t_f(h - t_f) + f_y \cdot t_w \left[ \left( \frac{h - 2t_f}{2} \right)^2 - y_n^2 \right] \tag{2.32}$$

When the plastic neutral axis lies within the flange, $((h - 2t_f)/2 \leq y_n \leq h/2)$:

$$P_{yr} = f_y(h - 2t_f)t_w + 2f_y \cdot b \left[ y_n - \frac{h - 2t_f}{2} \right]$$
$$M_{pr} = f_y \cdot b \left[ \left( \frac{h}{2} \right)^2 - y_n^2 \right] \tag{2.33}$$

The analytical solution above, may be approximated by the formulae in Equations 2.34 and 2.35, and is illustrated visually in Figure 2.9 (Kulak and Grondin, 2002).

$$M_{pr,x} = 1.18 M_{p,x} \left( 1 - \frac{P_{yr}}{P_y} \right) \leq M_{p,x}, \qquad \text{for strong-axis bending} \tag{2.34}$$

$$M_{pr,y} = 1.67 M_{p,y} \left( 1 - \frac{P_{yr}}{P_y} \right) \leq M_{p,y}, \qquad \text{for weak-axis bending} \tag{2.35}$$

Figure 2.9 (a) shows the approximation for strong-axis bending that generally conforms to the analytical solutions for various ratios of flange area ($A_f$) to web area ($A_w$), with the highest error of 5% occurring at high bending moment ratios (Trahair et al., 2008). A larger error is noticeable for the weak-axis approximation in Equation 2.35 and it is visibly conservative, as can be seen in Figure 2.9 (b).

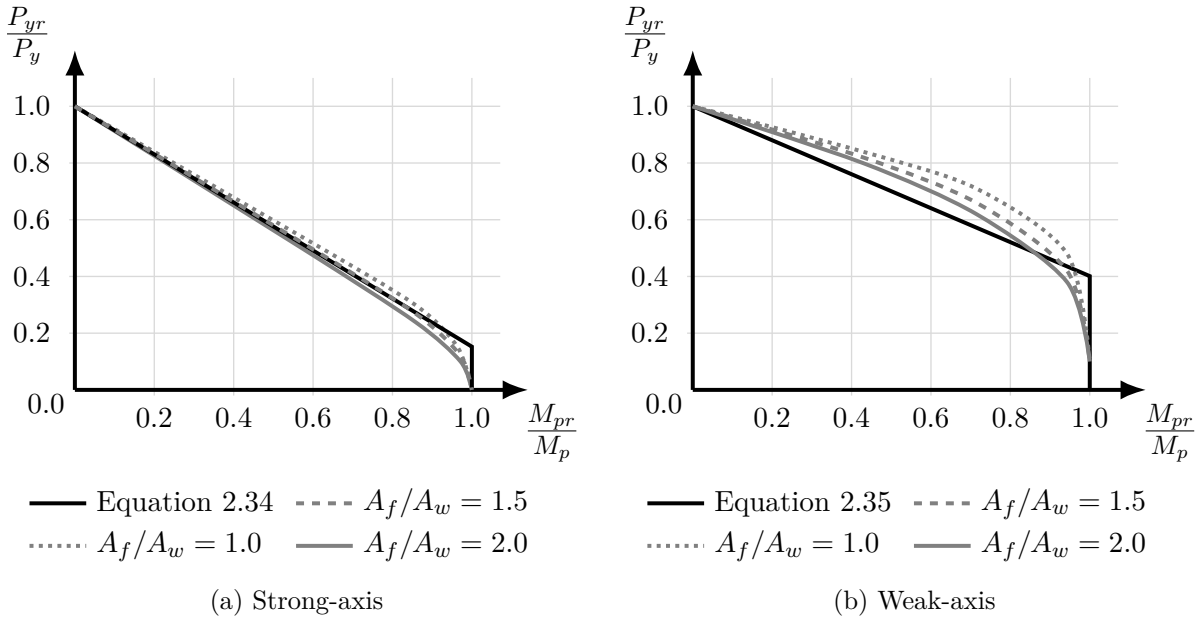


(a) Strong-axis

(b) Weak-axis

Figure 2.9: Theoretical plastic interaction diagrams, adapted from Kulak and Grondin (2002)

By rearranging Equations 2.34 and 2.35 the approximate interaction equation for short beam-columns under plastic axial and bending forces, can be obtained as shown by Ziemian (2010).

$$\frac{P_{yr}}{P_y} + \frac{0.85M_{pr,x}}{M_{p,x}} + \frac{0.6M_{pr,y}}{M_{p,y}} \leq 1.0 \tag{2.36}$$

Each design specification's approach to interaction equations is discussed in the sections that follow. White and Clarke (1997) concluded that the different approaches employed by various steel design specifications make it difficult to draw comparisons over several different cross-sections, but determined that the interaction formulae were generally within an acceptable range from each other.

#### 2.3.3.1.1 AISC 360-10

A bi-linear set of interaction equations is used in AISC 360 for combined axial and flexural forces, based the strong-axis approximation in Equation 2.34. However, the behaviour of real beam-columns, i.e. with actual length, different cross-sections and residual stress profiles are addressed by the normalisation of applied forces to the respective factorised strengths as determined in sections E and F of AISC (2010). In doing so, the modes of failure namely, local buckling, in-plane yielding and lateral-torsional buckling can be considered by using the two linear interaction equations below (AISC, 2010).

$$\frac{P_r}{P_c} + \frac{8}{9}\left(\frac{M_{r,x}}{M_{c,x}} + \frac{M_{r,y}}{M_{c,y}}\right) \leq 1.0, \qquad \text{if } \frac{P_r}{P_c} \geq 0.2 \tag{2.37}$$

$$\frac{P_r}{2P_c} + \left(\frac{M_{r,x}}{M_{c,x}} + \frac{M_{r,y}}{M_{c,y}}\right) \leq 1.0, \qquad \text{if } \frac{P_r}{P_c} < 0.2 \tag{2.38}$$

In Equations 2.37 and 2.38 the respective force capacities act as denominators, while the required forces to be withstood are placed as the numerators. AISC 360 accepts that all secondary moments arising from both $P-\Delta$ and $P-\delta$ effects are included in the required forces to be resisted (Kaehler et al., 2011). Furthermore, the subscripts $x$ and $y$ are used for the strong and weak axes, respectively.

A good correlation exists between Equation 2.37 and the approximated interaction produced by Equation 2.34. This is attributed to the fraction 8/9, which is approximately equal to the reciprocal of the strong-axis constant 1.18 in Equation 2.34. Ziemian (2010) noted that the set of equations above provides conservative results for doubly symmetric I-beams bent about their major-axis when the lateral-torsional buckling limit state is evaluated. An optional, less conservative check is provided in section H1.3 of AISC (2010) to compensate for this.

#### 2.3.3.1.2 CSA S16-14

The Canadian steel design specification distinguishes between class 1 and 2 members, which are able to attain the plastic moment of resistance and class 3 and 4 members that become unstable prematurely. The CSA S16 interaction formula is based on Equation 2.36 and presented below when dealing with class 1 and 2 I-shaped members.

$$\frac{C_f}{C_r} + \frac{0.85U_{1,x} \cdot M_{f,x}}{M_{r,x}} + \frac{\beta \cdot U_{1,y} \cdot M_{f,y}}{M_{r,y}} \leq 1.0 \tag{2.39}$$

The forces are normalised according to the relevant resistance strengths for the limit states, i.e. cross-sectional strength, overall member strength and lateral-torsional buckling strength. The same axis convention is used as above, while the denominators indicate the respective member capacities and the numerators contain the maximum factored loads. Although the interaction equation is based on the strong-axis approximation for full plasticity, the constant 0.6 for weak-axis bending (inverse of the constant 1.67 in Equation 2.35) was found to be non-conservative for large bending moments with intermediate slenderness and was modified by a factor $\beta$, which is a function of the non-dimensional weak-axis slenderness parameter ($\lambda_y$) (Driver, 2014) and brings distributed plasticity into account.

$$\beta = \begin{cases} 0.6, & \text{for cross-sectional strength} \\ 0.6 + 0.4\lambda_y \leq 0.85, & \text{for all other modes of failure} \end{cases} \tag{2.40}$$

CSA S16 requires a structural analysis to be conducted, which considers the amplified forces that result from $P-\Delta$ sway-effects (CSA, 2013). CSA S16 have included provisions for this in the form of an amplification factor, $U_1$, unless is has been specifically included in a structural analysis. This amplification factor simultaneously addresses the effects of $P-\delta$ (detrimental) and moment gradient (beneficial) on the member stability (Driver, 2014).

$$U_1 = \frac{\omega_1}{1 - C_f/C_e} \tag{2.41}$$

with

$$\omega_1 = \begin{cases} 0.6 - 0.4\kappa \geq 0.4, & \text{if no transverse loads are applied} \\ 1.0, & \text{if a near uniform distribution of load(s) apply} \\ 0.85, & \text{if only a single point load or moment is applied} \end{cases}$$

The benefit of moment gradient on a steel member's stability is described by the equivalent uniform beam-column coefficient ($\omega_1$). The $\omega_1$ factor is determined as a function of the smaller to larger ultimate end moment ratio ($\kappa$), when no transverse loads are applied between the lateral brace points. However, two exceptions are made with regard to unbraced frames. Firstly, the $U_1$ factor can be considered equal to 1.0. The rational is that unbraced frames are moment resisting and the maximum moment would tend to lie at the end of an unbraced length, and will thus not be influenced by $P-\delta$ effects (Driver, 2014). Secondly, the cross-sectional limit state may be ignored as it is undermined by the overall member strength limit state.

Class 3 and 4 cross-sections are treated in a parallel manner as above, with the exception that the moment multipliers (0.85 and $\beta$) are discarded in Equation 2.39, which would otherwise account for post-yielding capacity (Driver, 2014).

#### 2.3.3.1.3 SANS 10162-1:2011

Due to the adoption of the CSA S16 design specification by SANS 10162-1, the design of doubly symmetric I-shaped sections acting as beam-columns is identical in the two specifications.

#### 2.3.3.1.4 EN 1993-1-1:2005

In the European steel design specifications a distinction is made between four classes of beam-columns, similar to CSA S16 and SANS 10162-1. The limit states of cross-sectional strength, overall member strength and lateral-torsional buckling strength are also considered in EC3. The cross-sectional capacity is evaluated in terms of the EC3 axes notation based on a modification of the first yield interaction in Equation 2.31 (Trahair et al., 2008).

$$\frac{N_{Ed}}{N_{c,Rd}} + \frac{M_{y,Ed}}{M_{c,y,Rd}} + \frac{M_{z,Ed}}{M_{c,z,Rd}} \leq 1.0 \tag{2.42}$$

In the equation above, the ratios of axial and bending moment design forces ($N_{Ed}$ and $M_{Ed}$, respectively) are related to the cross-section's capacity to withstand the factored design resistance under uniform compression ($N_{c,Rd}$) or uniaxial bending ($M_{c,Rd}$) (Trahair et al., 2008). A more economical alternative is provided in section 6.2.9.1 of EC3 for evaluating class 1 and 2 sections.

EC3 uses different formulae for the design of beam-columns that buckle in-plane and those that buckle out-of-plane to evaluate beam-columns for overall member strength and lateral-torsional buckling strength, respectively.

$$\frac{N_{Ed}}{N_{b,y,Rd}} + k_{yy}\frac{M_{y,Ed} + \Delta M_{y,Ed}}{M_{b,y,Rd}} + k_{yz}\frac{M_{z,Ed} + \Delta M_{z,Ed}}{M_{z,Rd}} \leq 1.0 \tag{2.43}$$

$$\frac{N_{Ed}}{N_{b,z,Rd}} + k_{zy}\frac{M_{y,Ed} + \Delta M_{y,Ed}}{M_{b,y,Rd}} + k_{zz}\frac{M_{z,Ed} + \Delta M_{z,Ed}}{M_{z,Rd}} \leq 1.0 \tag{2.44}$$

Here, the axial and bending moment design forces are as defined above, with provision for an additional moment that may arise due to the shift in the plastic neutral axis, included as the $\Delta M$ terms. The denominators once again refer to the member's resistance regarding either axial force or bending moment. Member resistance, referred to by the subscript $b$, is based on values that include the slenderness reduction factor ($\mathcal{X}_y$, $\mathcal{X}_z$ or $\mathcal{X}_{LT}$). No reduction applies to the weak-axis resistance moment as it is not susceptible to lateral-torsional buckling. The interaction factors ($k_{ij}$) are available in the annexures A or B of EC3 for the respective limit states, member classifications, moment gradient and secondary moments caused by $P - \delta$ effects (CEN, 2005).

The additional moments that arise from sway-effects ($P - \Delta$) are required by EC3 to be determined using either a second-order analysis. This allows resistance capacities to be determined for an unbraced length considered in isolation (CEN, 2005).

#### 2.3.3.2 Web-tapered beam-column behaviour

None of the design specifications discussed in this study explicitly cover the design of web-tapered beam-columns. Only EC3 has some provisions in place but requires a design-by-analysis with limited guidance on the implementation thereof (Marques, Taras, et al., 2012). Two approaches from the literature are discussed next in Sections 2.3.3.2.1 and 2.3.3.2.2 for the design of web-tapered beam-columns.

##### 2.3.3.2.1 DG25:2011

The recommended design procedure in DG25 uses the AISC 360 prismatic beam-column interaction formulae (see Section 2.3.3.1.1). These interaction formulae remain applicable when normalised to account for web-tapered member strength in the absence of other forces (Kaehler et al., 2011). This normalisation effectively leads to interaction formulae that combines the

different allowable utilisation ratios, similar to the design approach for web-tapered members in previous AISC appendices (Lee and Morrell, 1975). The application of the AISC 360 prismatic interaction formulae to web-tapered members was verified by Kim (2010) by comparing the calculated resistances with full non-linear analysis using shell elements in Abaqus.

#### 2.3.3.2.2 EN 1993-1-1:2005

Marques (2012) studied the use of the recommended general method (section 6.3.4 in EC3) and the validity of implementing the EC3 prismatic beam-column interaction formulae by comparing these approaches with numerically obtained resistances of web-tapered members, using full non-linear analyses. The study concluded that:

a) The EC3 general method produced highly variable and unreliable results, from 80% (safe) to 120% (unsafe) of the full non-linear member resistance. This was attributed to a lack of guidance on implementing the EC3 provisions. Uncertainties were noted regarding the modelling of imperfections, the selection of appropriate buckling curve and the interpolation scheme employed between the slenderness reduction factors, $\mathcal{X}$ and $\mathcal{X}_{LT}$. In the latter case, an over conservative method is permitted by EC3, based on the minimum value of the slenderness reduction factor for either flexural buckling or lateral-torsional buckling, but this was found to be mechanically inconsistent with the physical behaviour.

b) Marques, da Silva, Rebelo, et al. (2014) noted improved results when using the EC3 interaction formulae with web-tapered members instead of the general method, even though the interaction formulae were developed for use in prismatic members. Their study found that the results were improved to between 80% (safe) and 103% (unsafe), with an average resistance of 93% (safe) of the full non-linear member resistance, when using the EC3 interaction formulae in combination with their procedures for columns and beams.

When using the EC3 interaction formulae with web-tapered members, the equivalent moment factor ($C_m$) is determined based on the distribution of the utilisation of the applied bending moment to the resistance moment. This approach for considering the moment gradient corresponds to the method in DG25 for determining the stress profile in the compression flange of a web-tapered member.

### 2.3.3.3 Review of beam-column resistances to axial and bending forces

All the international design specifications rely on the same principles, where an interaction equation is used to predict member resistance under the influence of combined axial and flexural forces. In deriving the interaction for imperfect beam-columns with actual lengths, normalisation is performed in terms of the relevant limit state strengths and interaction factors to account for

moment gradient and $P-\delta$ effects. AISC 360 assumes that $P-\delta$ secondary moments are included in the factorised applied loads (Kaehler et al., 2011), while the CSA S16, SANS 10162-1 and EC3 include provisions if these secondary moments were not included during a structural analysis (Ziemian, 2010).

Marques, da Silva, Rebelo, et al. (2014) found the interaction formulae in EC3 when used for web-tapered members to yield safe results, but never by more than 20%. This accounted for their proposed methods for designing columns and beams with a strong emphasis on numerical modelling during design. In doing so, they produced less conservative member resistance estimates and reduced the amount of variance observed when using the EC3 general method. DG25 uses a less onerous procedure, as it is less reliant on numerical methods during the design process. As the principles and use of interaction formulae are similar to the design specifications considered in this study, it is reasoned that DG25 may be adapted to other steel design specifications (Ziemian, 2010).

## 2.4 Shear and manufacturing considerations

The variation in the web depth of web-tapered members causes secondary shear stresses to form. The effect of this secondary stress becomes more pronounced with increasing tapering angles ($\alpha$). In prismatic members the normal stresses would develop perpendicular to the cross-sectional plane, as indicated by the blue line in Figure 2.10. However, when viewing a web-tapered member, the line now takes the form of the curved red line in Figure 2.10, each end of which is perpendicular to an inclined flange. Additional shear stresses are then required to maintain vertical equilibrium of the section (Marques, 2012).

Bleich (1932) found that this bowed normal stress surface may be sufficiently represented using a bilinear surface for the practical evaluation of the elastic shear capacity, as indicated by the green line in Figure 2.10. A simple method was proposed by Blodgett (1966), for the modified shear by assuming the entire resistance moment is produced in the flanges. The vertical components of forces in the flanges are either added or subtracted to or from the ultimate shear resistance of the web to determine the modified shear resistance. In the configuration shown in Figure 2.10, a portion of the shear force is counteracted by a vertical component of the force in the flanges. In this case, a reduced shear force has to be withstood by the web, i.e. $V_{mod} = V_u - (P_{tf,t} + P_{cf,t})$. Conversely, for $\alpha < 0$ in the figure below, the vertical flange force components would act in the same direction as the applied load and $V_{mod} = V_u + (P_{tf,t} + P_{cf,t})$.

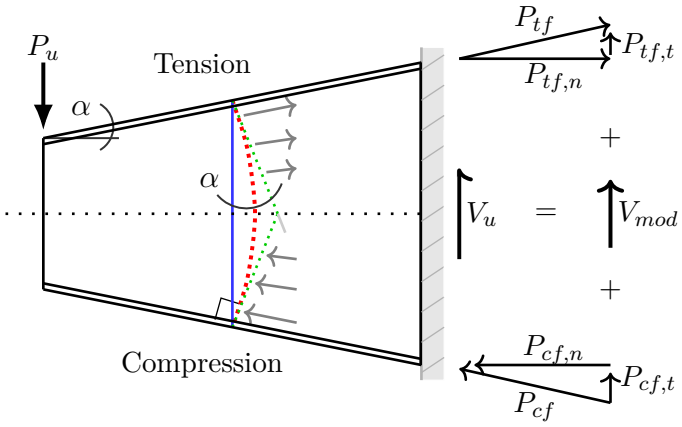


Figure 2.10: Directional force equilibrium in web-tapered members

Analytically determined solutions, as published in Timoshenko and Goodier (1970), are available in the literature. As the greatest portion of the in-plane shear resistance is attributed to the web, Galambos (1988) proposed that the additional effects arising from the inclined flanges are for practical purposes negligible when $\alpha \leq 15^o$ and the prismatic formulae for shear design may be applied to tapering members. This is supported by White, Barker, et al. (2008), who found the interaction between bending moment and shear resistance to be insignificant when using adequate flange sizes and the normal AISC 360 shear interaction formulae to be valid for members investigated with tapering angles up to $15^o$ (Kaehler et al., 2011). Thus, the web height to thickness ratio ($h_w/t_w$) and the ratio of transverse stiffener spacing to web height ($s/h_w$) govern the shear resistance of a member. Due to the variance in web height in web-tapered members, DG25 recommends that the shear strength of unstiffened webs be checked at several places along a member.

### 2.4.1 Welding and manufacturing

Web-tapered beams are manufactured as welded plate members, typically with an automated submerged arc welding process, which aids in the handling of beam members and reduces manufacturing cost (Murthy, 2013). Most automated welding equipment available is restricted to manufacturing beams with equal top and bottom flange widths. As a result, MBS buildings are commonly constructed with equal flange widths, although different widths may be used for the flanges (Kaehler et al., 2011). The manufacturing process resembles the techniques employed in conventional plate-girder fabrication. As for prismatic girders, the height to thickness ratios of web and flange plates are sometimes limited to avoid distortion of plate members during the welding process. Beams may be produced either from flat bars, coils or hot-rolled sheets. Common methods for cutting plates include shear cutting with a guillotine and flame cutting using plasma or oxygen. Substantial research has been conducted by Prawel et al. (1974) on the cutting of web-tapered members. In their study, the residual stress formations were measured

and recorded for beam specimens produced from shear and flame-cut plates. For the latter they noted that locked-in tension stresses formed, while shearing of the plate caused compression at the edges, which led to a loss of inelastic stability and lowered the bending and buckling resistance of the specimens.

Single-sided fillet welds at the junction between the web and flange plates of web-tapered members have become widely used in low rise metal buildings (Chen et al., 2001). This significantly reduces the amount of handling as there is no need to rotate the beam to gain access to the other side (Murthy, 2013). The behaviour of web-tapered beam-columns with single-sided continuous fillet welds was studied by Prawel et al. (1974). They found that unsymmetrical residual stresses formed about the weak-axis of the built-up I-sections, which caused the specimens in the study to bow laterally in the direction opposite of the weld. The degree of curvature was found to be unpredictable and it was noted that the last flange to be welded was prone to cause larger lateral deflection. This initial imperfection resulted in no clearly-defined buckling load being identified, as out-of-plane deflection was detected from the onset of loading. Specimens were tested to the point of destruction and failed by lateral-torsional buckling, local flange buckling, or a combination of the two. Their study concluded that single-sided welding did not influence the static strength of beam-columns with lateral supports, when members complied with local buckling requirements. Similar studies using slender webs with single-sided fillet welds have been performed, where, in addition to the above modes of failure, web buckling was noted (MBMA, 2012). In none of the specimens did any of the single-sided fillet welds fail and weld integrity was maintained even at the point of failure when flange plates and webs remained perpendicular (MBMA, 2012). With regard to the performance of single-sided welds in doubly symmetric I-beams under lateral-torsional buckling, a general lack of international publications was noted by Younes et al. (2009).

Chen et al. (2001) studied the ability of single-sided fillet welds, prepared in accordance with AWS (1998), to transfer shear and resist tensile and compressive forces produced by webs up to 8 mm thick. The following findings were made:

a) With regard to shear, they concluded that no noticeable difference was observed in the static capacity of single-sided fillet welds and double-sided fillet welds.

b) In the presence of tensile force acting perpendicular to a flange, an eccentricity arises because of the single-sided weld, causing a localised bending moment to form (see Figure 2.11). This adverse effect was noted, but no signs of failure were observed in the weld specimens. Furthermore, tensile forces are generally not applied to the flange of portal frame structures, thus diminishing concern about the use of single-sided welds.

c) The web buckling capacity was determined when using a single-sided fillet weld, causing the boundary conditions at the junction between web and flange to be altered and no longer

symmetrical. From the experimental results it was found that only a minor reduction in shear buckling capacity resulted when using single-sided welds.

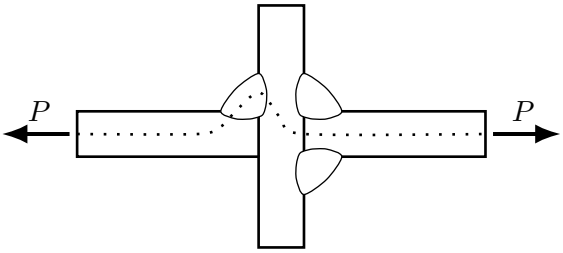


Figure 2.11: Eccentricity of shear flow path under tensile load

The provisions in DG25 state that single-sided welds may be used, unless the shear resistance of the web is exceeded, in which case double-sided welds are required (Kaehler et al., 2011). Shear resistance is usually not a concern in portal frame structures. Intermittent single-sided fillet welds at discrete intervals could be justified if the weld is able to transfer the shear flow and any concentrated forces from the web to the flange (Craig, 1999). In DG25, the shear stress to be carried by the weld ($f_{rw}$) is determined using the prismatic beam shear-stress formula.

$$f_{rw} = \frac{V_u \cdot Q}{I_x \cdot t_w} = \frac{V_u \cdot A' \cdot \overline{y}'}{I_x \cdot t_w}, \tag{2.45}$$

Here, the ultimate shear force ($V_u$) at any cross-section is found during a structural analysis and $I_x$ and $t_w$ are the respective strong-axis moment of inertia and web thickness. The static moment of area ($Q$) is determined as the product of the area ($A'$) and distance ($\overline{y}'$) between the neutral axis and the centroid of the area above the inspected level. In DG25 the weld capacity should not be lower than the maximum shear stress in the web, which lies at the neutral axis, times the web thickness.

Single-sided welds are, however, not suitable for structural members that are subjected to regular cyclic loading or intended for seismic applications. In this case, double-sided fillet or complete joint penetration groove welds to AWS D1.1 are recommended (MBMA, 2012; Kaehler et al., 2011).

## 2.5 Structural Analysis

### 2.5.1 Design specification requirements

To design structural elements, the member forces and displacements must be determined by means of a structural analysis. All of the design specifications considered in this study require a second-order structural analysis to be performed. Structural effects may either be considered by rigorous second-order elastic analysis, or by code specific amplification factors applied to the

results of a linear elastic analysis to account for sway and secondary moments (Ziemian, 2010). Another similarity between the design specifications discussed in this study is the use of notional loads, or equivalent horizontal loads in the case of EC3. Due to the complex nature of structural analysis and modelling, the use of these fictional lateral loads allows the following:

a) The sway-moments caused by out-of-plumb columns ($P - \Delta$) can be taken into account.

b) A small amount of lateral sway is induced to avoid situations where columns and vertical forces directly oppose each other, without resulting in lateral deflections. Thus, additional bending moments are generated that are realistic to the physical structure.

c) The partial yielding and redistribution of moment in sections, when only a linear elastic analysis is used.

d) It bases the resistance of a beam-column on its actual length, rather than an effective length.

e) The moments in beam members are also increased rather than only increasing the moments in columns, through equilibrium (Driver, 2014).

Second-order effects are mainly associated with axial forces and thus a linear elastic analysis may be justified when axial forces are small. As axial loads are typically very low in portal frame structures in regions where snow loads are generally disregarded (e.g. South Africa), the second-order effects may become insignificant.

### 2.5.2 Basic web-tapered frame analysis with stepped-representation

A simple method accepted by DG25 for the analysis of web-tapered members is using stepped-representation (see Figure 2.12). This involves the discretisation of tapered members into piece-wise prismatic finite beam elements to represent the distribution of stiffness and mass. Although this method is simple in implementation, it is well known to be lowly efficient, as large, sparse system stiffness matrices are formed (G. Li and J. Li, 2002). Sparsely populated matrices are matrices that contain mostly zero values as entries. Even if a good arrangement of elements is defined in the structure, it may lead to unnecessary use of computing resources due to the storage and manipulation of many degrees of freedom. Many software products for multi-variable calculus use specialised storage algorithms for faster processing to avoid the unnecessary storing and manipulation of excessive zero entries (Cook et al., 2001).

The direct stiffness method may be employed to construct the stiffness matrix of each discretised element. Euler-Bernoulli beam elements are adequate for slender finite elements, where deformation is governed by bending. These elements, however, only apply to large $L/d$ ratios. Due to the discretisation procedure for stepped-representation, the finite elements tend to become short and stocky. This leads to ill-conditioned stiffness matrices and the occurrence of shear

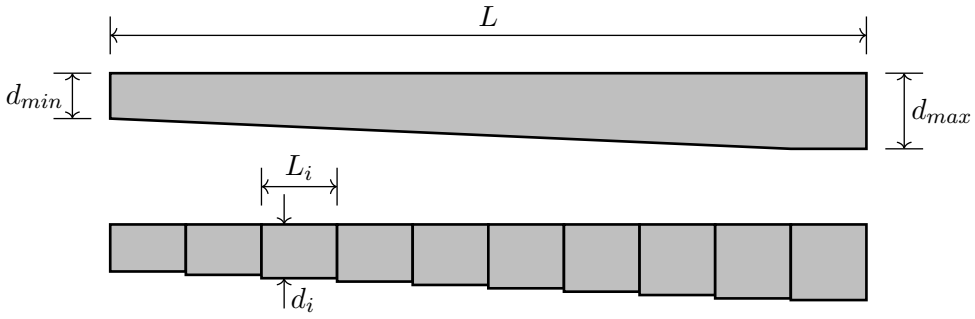


Figure 2.12: Stepped-representation

locking (Cook et al., 2001). Timoshenko beam elements may be applied to all $L/d$ ratios to deal with these issues. The element stiffness matrix for a Timoshenko beam with axial stiffness is presented in Equation 2.46.

$$[\mathbf{k}_e] = \begin{bmatrix} A \cdot E/L & & & -A \cdot E/L & & \\ & \psi/L & \psi/2 & & -\psi/L & \psi/2 \\ & \psi/2 & \psi(4+\phi)L/12 & & -\psi/2 & \psi(2-\phi)L/12 \\ -A \cdot E/L & & & A \cdot E/L & & \\ & -\psi/L & -\psi/2 & & \psi/L & -\psi/2 \\ & \psi/2 & \psi(2-\phi)L/12 & & -\psi/2 & \psi(4+\phi)L/12 \end{bmatrix} \tag{2.46}$$

with

$$\psi = \frac{12E \cdot I_x}{(1+\phi)L^2}$$
$$\phi = \frac{12E \cdot I_x \cdot k}{A \cdot G \cdot L^2}$$

Dong et al. (2010) explain that several shear correction factors ($k$) have been proposed in the past, but still lack general consensus among peers. An often-used means of establishing $k$ was proposed by Cowper (1966) and is described below.

$$k = \frac{10(1+\nu)(1+3\beta)^2}{\alpha} \tag{2.47}$$

with

$$\begin{aligned} \alpha = {} & 12 + 72\beta + 150\beta^2 + 90\beta^3 \\ & + \nu(11 + 66\beta + 135\beta^2 + 90\beta^3) \\ & + 30\eta^2 \cdot \beta(1+\beta) + 5\nu \cdot \eta^2 \cdot \beta(8+9\beta) \end{aligned}$$

$$\beta = \frac{2b \cdot t_f}{h \cdot t_w}$$
$$\eta = \frac{b}{h}$$
$$\nu = \text{Poisson's ratio}$$

Not all deformation modes are, however, included in standard beam elements (Cook et al., 2001). As an example, thin-walled open sections bent around their strong-axis may undergo significant out-of-plane deformations as a result of lateral-torsional deformation. The preceding analysis technique using simple beam finite elements is only adequate for design when used in conjunction with code-based design specifications. In this regard, design specifications not only provide guidelines for the design and construction of safe buildings, but account for modes of failure - such as local yielding, out-of-plane behaviour and inelasticity - that are not captured during the simple frame analysis.

### 2.5.3 Numerical techniques for deriving the elastic buckling load

The lack of a closed-form solution to the elastic buckling load of web-tapered members was discussed in Sections 2.3.1.2 and 2.3.2.2. Empirical approaches were presented in those sections that approximate the buckling loads characterised by in-plane flexural or lateral-torsional deformations. As an alternative, more accurate elastic buckling loads can be found with the use of numerical and energy-based methods, in computer techniques and Finite Element Analysis (FEA). This also provides a general method for handling the elastic buckling for arbitrary column shapes, i.e. singly or doubly symmetric cross-sections (Ziemian, 2010). A buckling analysis then readily provides an elastic buckling multiplier ($\gamma_e$) as the ratio of the elastic buckling load to an arbitrarily chosen reference load required for numerical purposes. This ratio is shown using Equation 2.48.

$$P_e = \gamma_e \cdot P_{ref} \tag{2.48}$$

#### 2.5.3.1 Method of successive approximations

The method of successive approximations as originally published and applied by Newmark (1943) is considered herein as a solution for in-plane elastic flexural buckling load. Successive approximation is a calculus method used for solving complicated polynomial and differential equations, by means of a recursive technique based on an initial approximation or previously obtained solution. Where energy-based methods provide an upper bound solution, the method of successive approximation provides a lower- and upper bound solution at each recursion. The desired level of accuracy can be obtained as the solution converges to a narrower band of solutions (Timoshenko and Gere, 1961). This method also has the advantage of being easy to implement into any spreadsheet software.

Newmark (1943) applied the method of successive approximation with finite difference expressions for accurately determining the elastic buckling load of prismatic and stepped columns, although similar procedures have been developed before by Vianello (1898), Engesser (1909), Atkinson et al. (1937), and Bradfield and Southwell (1937) and Niles and Newell (1938). The method by Newmark is discussed by Timoshenko and Gere (1961), Ghali et al. (2009) and Kaehler et al. (2011). The latter two sources discuss Newmark's method when expanded to tapering beams.

To determine the elastic buckling load of a column, the member is subdivided into several nodal stations along its length. An initial deflected shape is assumed along with a reference axial load. The eccentricity resulting from the initial deflected curve coupled with the reference load creates an internal moment due to $P - \delta$ effects (Figure 2.13). Next, the conjugate beam method is employed to account for the variation in stiffness along the length of the column by dividing the internal moment by the stiffness. This makes for convenient representation of the internal force as an external (lateral) shear force, known as the elastic load (Ghali et al., 2009). From static beam theory the elastic load is equivalent to the curvature of the element ($\kappa$), as seen in Equation 2.49.

$$\frac{P \cdot \delta(x)}{E \cdot I(x)} = \frac{M(x)}{E \cdot I(x)} \approx \frac{d^2 v(x)}{dx^2} = \kappa(x) \tag{2.49}$$

In Equation 2.49, two terms exist which both refer to the deflected eccentricity at each station, namely $\delta(x)$ and $v(x)$. The first was initialised by defining a deflection value, $\delta(x)$, at each station according to the expected mode shape. For the equation the hold true the resulting deflection $v(x)$ should be the same at each station.

To calculate the deflection $v(x)$, a beam deflection analysis is performed. Any analysis capable of accurately finding the deformed shape caused by the distributed load may be utilised. Newmark performed integration by simplifying the distributed load into fictitious concentrated forces (or "stinger loads") at each station (Kaehler et al., 2011). Newmark's method utilises parabolic load expressions to easily integrate numerically the effects of the shear force to find the slope between each station. From the slope information and position of each station the displacement ($v$) can be computed. As the initial deflection $\delta(x)$ was chosen arbitrarily and on the intuition of the user it is unlikely that $v$ will equal $\delta(x)$ after the first iteration, but the displacement $v$ would be closer to the true form of the deflected shape at the elastic buckling load (see Figure 2.13). This displacement may then be used as the new initial displacement, yielding new moments and the process of balancing Equation 2.49 can recommence. The process can be repeated until a set convergence limit has been reached.

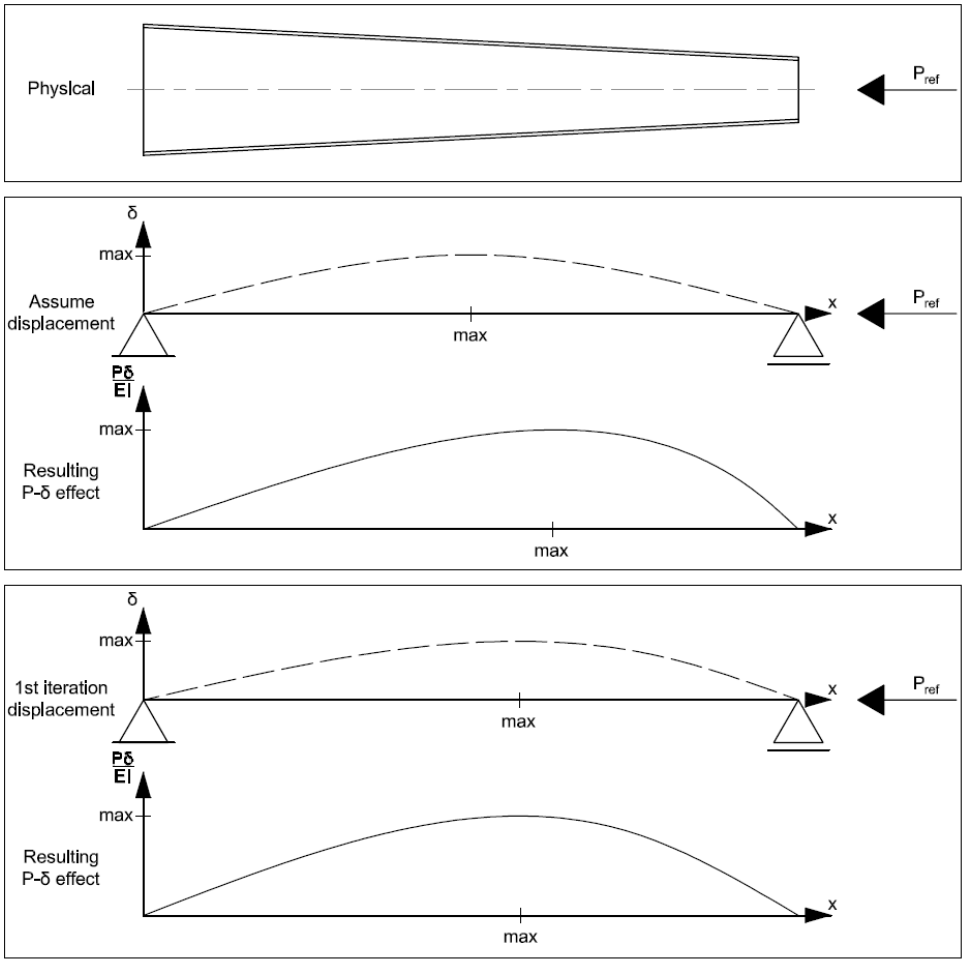


Figure 2.13: Curvature resulting from assumed $P-\delta$ effects in Newmark's method

#### 2.5.3.2 Eigenvalue buckling analysis

Another numerical procedure to determine the elastic buckling multiplier is by using an eigenvalue buckling analysis (also referred to as a linear buckling analysis). This is a finite element formulation, based on the energy method, used for determining the elastic buckling strength of a perfectly straight column with no imperfections and can be implemented using finite element analysis. When considering linear elastic analysis the relationships of the displacements $\{\mathbf{D}\}$ to the forces $\{\mathbf{P}\}$ are calculated based on a constant elastic stiffness matrix $[\mathbf{K}_e]$ (Cook et al., 2001).

$$[\mathbf{K}_e] \cdot \{\mathbf{D}\} = \{\mathbf{P}\} \tag{2.50}$$

At the elastic buckling load the potential energy stored as membrane strain ($U$) is transferred into kinetic energy as large bending strains ($E_k$), without any additional applied load. In order to account for the non-linear stiffness the elastic stiffness matrix, $[\mathbf{K}_e]$, has to be amended depending on the magnitude of the applied load. This is done by using a geometric stiffness

matrix, $[\mathbf{K}_g]$, owing its name to the fact that it considers the effect of applied load and the resulting membrane strains, without considering any material properties (Cook et al., 2001).

When considering a scalar increase ($\gamma_e$) in the reference load (see Equation 2.48), it can be deduced from the above paragraph, that no change will take place to $[\mathbf{K}_e]$, as only $[\mathbf{K}_g]$ is a function of the applied loading. The result when $[\mathbf{K}_g]$ and the scalar multiplier $\gamma_e$ is considered, is as follows:

$$\Big([\mathbf{K}_e] + \gamma_e \cdot [\mathbf{K}_g]_{ref}\Big) \cdot \{\mathbf{D}\}_{ref} = \gamma_e \cdot \{\mathbf{P}\}_{ref} \tag{2.51}$$

At the moment when bifurcation takes place, the column is still straight, but on the verge of buckling without the need of additional load. At this stage the addition of an infinitesimal small virtual displacement will cause buckling to take place.

$$\Big([\mathbf{K}_e] + \gamma_e \cdot [\mathbf{K}_g]_{ref}\Big) \cdot \{\mathbf{D}_{ref} + \delta\mathbf{D}\} = \gamma_e \cdot \{\mathbf{P}\}_{ref} \tag{2.52}$$

The difference in Equations 2.51 and 2.52 may then be expressed as a mathematical eigenvalue problem.

$$\Big([\mathbf{K}_e] + \gamma_e \cdot [\mathbf{K}_g]_{ref}\Big) \cdot \{\delta\mathbf{D}\} = \{\mathbf{0}\} \tag{2.53}$$

The following remains if the arbitrary case is ignored, namely $\{\delta\mathbf{D}\} = \{\mathbf{0}\}$

$$\Big([\mathbf{K}_e] + \gamma_e \cdot [\mathbf{K}_g]_{ref}\Big) = \{\mathbf{0}\} \tag{2.54}$$

To obtain the elastic buckling multiplier the smallest positive root ($\gamma_e$), known as an eigenvalue, will define the magnitude the reference load should be scaled to reach the elastic buckling load (Equation 2.48). In turn, the eigenvector $\{\delta\mathbf{D}\}$ corresponding with the specific eigenvalue, is used to describe the absolute shape of the fundamental buckling mode.

Kaehler et al. (2011) pointed out that although this technique is powerful in evaluating various configurations, it may be time consuming to model and thus not be practical for design unless it can be implemented with an automated analysis program. In addition, by using energy-based techniques with virtual displacement an upper bound solution is obtained, which marginally overestimates the true elastic buckling load (Timoshenko and Gere, 1961).

### 2.5.4 Numerical techniques to evaluate out-of-plane behaviour

Finite element analysis using stepped prismatic beam elements to represent the variation of a beam's cross-section are regularly used in practice (Kaehler et al., 2011). However, Andrade and Camotim (2005a) and Boissonnade and Maquoi (2005) found this method to give inaccurate results when evaluating elastic lateral-torsional buckling, as the inclination of the flanges is not

accounted for adequately (Marques, da Silva, Greiner, et al., 2013). The development of advanced beam elements capable of accurately modelling lateral-torsional buckling has attracted much research interest. Some of the most recent research in this regard was performed by Andrade and Camotim (2005a), Andrade and Camotim (2005b), Boissonnade and Maquoi (2005), Chang (2006), Andrade, Camotim, and Dinis (2007), Andrade, Providência, et al. (2010), and Jeong (2014). All these studies confirmed that 3D stepped-representation does not accurately predict the lateral-torsional buckling failure mode, even when using finely discretised models.

Alternatively, the critical lateral-torsional buckling moment of a member could be determined using an eigenvalue buckling analysis with shell finite elements, available in most structural analysis software. Models with shell elements are able to incorporate the effects of shear lag, warping and torsional effects, which would otherwise be excluded in the case of finite beam elements. Shell elements are defined as bodies of which the thickness is significantly smaller than the other dimensions (Cook et al., 2001). They are typically used in modelling thin-walled sections as these elements have both translational and rotational degrees of freedom.

### 2.5.5 Non-linear structural analysis for deriving member capacity

The structural analysis techniques considered until now assumed a linear relationship between the applied force and resulting deformation of structural elements. In reality, structures can exhibit a non-linear response due to actual geometric and material behaviour. The member capacity can be determined using a non-linear structural analysis, without having to resort to code-based design specifications.

The arc-length method allows for non-linear response by incrementally adjusting the external load and tracking the load-deflection path iteratively. At each interval, the method simultaneously solves both the loads and displacements. This process is depicted in Figure 2.14 below.

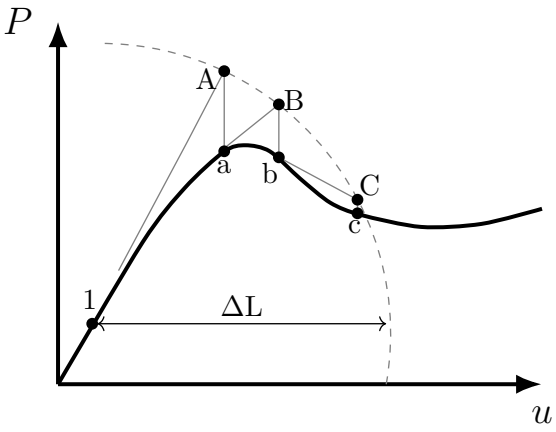


Figure 2.14: Successive iterations performed during the arc-length method

During each increment of the analysis, external loads at a distance of $\Delta L$ from the origin (point 1) are applied, thus forming a radius that defines the points A, B and C (Cook et al., 2001). In doing so, complex non-linear stiffness trajectories can be followed on a deformation path that includes loopbacks and descending branches. The tangent stiffness found during each iteration is approximated by linearised load-displacement equations until static equilibrium is established. If the residual found in the equilibrium equations resulting from the load (A, B or C) and displacement (a, b or c) is adequately small, the solution is accepted and the next increment initiated. Otherwise, a next iteration is undertaken in search of convergence (Bhatti, 2006).

## 2.6 Structural Optimisation

### 2.6.1 Introduction

One of the objectives of the study is to determine the material savings benefit of web-tapered members. A wide variance in the savings has been reported in the literature (see Section 1.2), which might be attributed to a lack in uniformity when comparing different frame designs. It would be ideal to compare the material savings when considering an optimised structure using web-tapered members against an equally optimal (or near optimal) solution based on conventional plate-girder construction.

An optimal structure depends on the objective function that defines what is to be optimised, e.g. weight minimum or profit maximum. In structural optimisation, an optimisation algorithm is typically coupled with a finite element analysis. The general concepts can be expressed in the following example:

1. Minimise $f(x)$.
2. Subject to $g(x) \leq 0$ and $h(x) = 0$.
3. For the domain $x \in \mathbb{D}$.

Here, the expression $f(x)$ is the objective function to be minimised, subject to the other conditions ($g(x)$ and $h(x)$) being true. The design variable $x$ may be varied to occupy any position within the domain $\mathbb{D}$. Structural optimisation involves geometry optimisation and optimisation algorithms (Saitou et al., 2005).

Geometry optimisation is the process of selecting and defining the characteristics of a geometric object. Three basic geometry optimisation techniques are presented in Figure 2.15 in order of increasing degree of freedom and sophistication. These optimisation techniques are:

a) Size optimisation: The process of finding the optimal solution to a given structural configuration by selecting sizes of the members from a defined set of solutions.

b) Shape optimisation: The constraints of a structural domain are reduced to allow for variation in the geometric boundaries. The connectivity remains unaltered and no new boundaries are formed.

c) Topology optimisation: As an extension of the shape optimisation, topology optimisation allows the structure to be altered within the predefined domain.

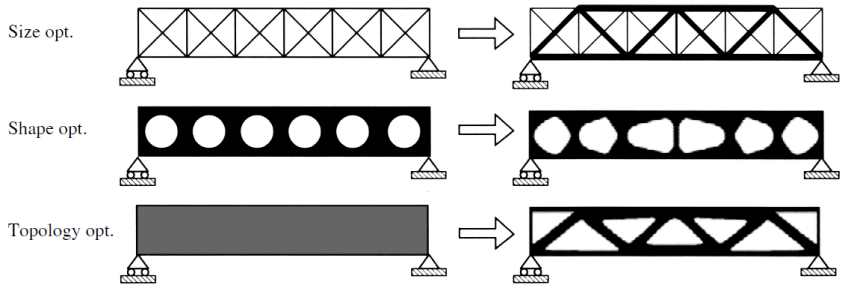


Figure 2.15: Types of geometry optimisation techniques by Tsavdaridis et al. (2015)

New or updated optimisation algorithms that apply to a variety of different research fields are constantly emerging (Haftka and Gürdal, 1992). Table 2.5 categorises the most utilised methods into broad fields of use.

Table 2.5: Summary of popular optimisation techniques by Rao (2009)

| Mathematical techniques | | Non-traditional techniques |
|---|---|---|
| Calculus methods | Integer programming | Genetic algorithms |
| Calculus of variations | Stochastic programming | Simulated annealing |
| Linear programming | Separable programming | Ant colony optimisation |
| Non-linear programming | Multi-objective programming | Particle swarm optimisation |
| Geometric programming | Network methods | Neural networks |
| Quadratic programming | Game theory | Fuzzy optimisation |
| Dynamic programming | | |

A smooth and continuous function as represented by the surface in Figure 2.16 is a good candidate for finding the optimum using calculus-based techniques. According to Goldberg (1989), the methods may be divided into indirect and direct methods. The former proceed by identifying positions of local optima by equating the derivatives of non-linear sets of equations to zero. The latter group of methods sample positions on the surface and trace the steepest route, until a local optimum is reached. Calculus-based methods, however, require procedures to force re-sampling or to restart at different locations as they tend to identify only local optima. Another drawback is that they rely on a well-defined mathematical space to derive the gradients needed to identify local optima. Most structural engineering problems have multiple variables with discrete values

that create a search space that is discontinuous and disjointed. These are best dealt with using other adequate techniques (Haftka and Gürdal, 1992; Rajeev and Krishnamoorthy, 1992).

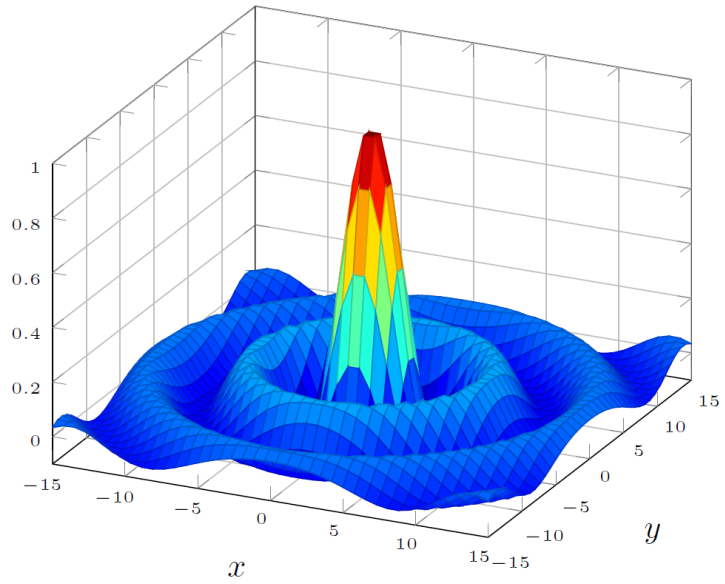


Figure 2.16: Drop-wave trigonometric function for $\sin(\sqrt{x^2+y^2})/\sqrt{x^2+y^2}$

The non-traditional techniques listed in Table 2.5 can provide solutions when the objective function is discontinuous, non-differentiable, stochastic or highly non-linear. When the search space is ill-defined due to discrete variables and not differentiable, these methods may be used to identify global optima (or near optima) using random sampling techniques combined with probabilistic decision making (Haftka and Gürdal, 1992). These methods tend to possess characteristics observed in nature, e.g. genetics, molecular properties, insect behaviour and neurobiological systems. For structural optimisation, genetic algorithms are regularly used as a technique for solving global optimal solutions. Discrete or continuous (or mixed) design variables can be dealt with and it applies to both constrained and unconstrained problems (Rao, 2009). Mckinstray et al. (2015) recently studied the use of genetic algorithms for optimising portal frames according to EC3 using a discrete list of British universal beam sections and provided references to prior studies of a similar nature.

### 2.6.2 Genetic algorithms

The Genetic Algorithm (GA) is modelled on analogue principles of biological evolution and natural selection. GAs may be described as a heuristic method where a population of possible solutions is created and traits are reproduced in successive generations that retain or gain superior properties depending on constraint conditions. As explained by Mitchell (1998), exact definitions for GAs vary in the science community, but all GAs consist of common aspects,

namely populations of chromosomes, fitness-based selection and reproduction of the fittest, resulting in crossover and mutation.

#### 2.6.2.1 Population

Each chromosome defines a point within the search space of possible solutions and consists of a sequence of "genes" representing each variable of the problem simulated (see Figure 2.17). Instead of sampling a single point within the search space, the GA initialises a trial population of multiple sampling points. The population size is typically defined as twice to four times the number of variables in the problem (Roa and Vishwanath, 2014). The population is then evaluated based on a predefined objective function. New generations are created with the properties from the fittest "chromosomes", using selection and reproduction operators. This is commonly known as the natural selection process and it ensures that the traits of weaker chromosomes are inherently removed from the population.

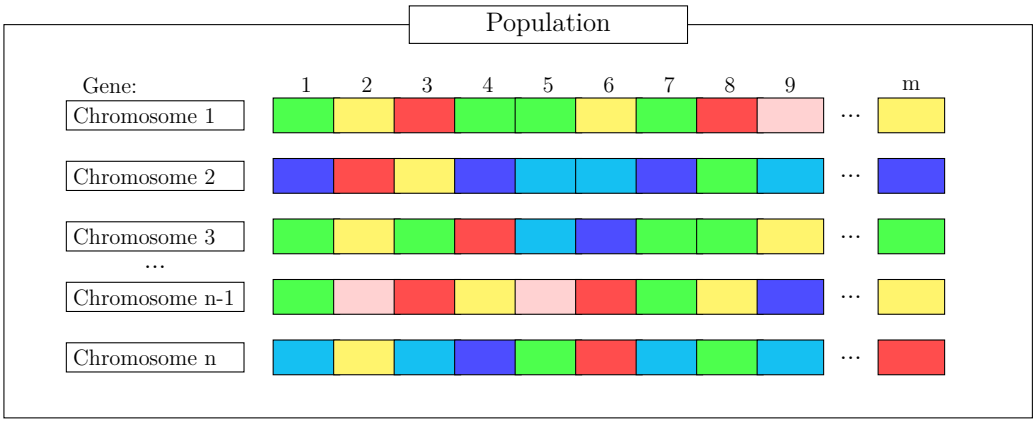


Figure 2.17: Chromosome population with gene sequence

#### 2.6.2.2 Selection

The selection method dictates which chromosomes will survive to reproduce traits in the next generation, based on their fitness in the current population. Choosing the fitter chromosomes for reproduction increases the likelihood of offspring being produced with a higher measure of fitness. The selection method is responsible for maintaining a balance between exploiting the fittest solutions for reproduction and ensuring a degree of exploration of the search space for peripheral solutions. For the latter, the operators called crossover and mutation are employed to ensure that new solutions are introduced into the population, as will be discussed in Sections 2.6.2.3 and 2.6.2.4. Various methods have been developed to synthesise the selection operation, of which the most common are discussed below (Mitchell, 1998):

a) Fitness proportional selection:

The fitness proportional selection method is based on stochastic processes, where the probability that an individual would reproduce into a following generation is based on the individual's fitness in proportion to the population fitness. This is commonly explained using a roulette wheel analogy, where the proportion of the individual's fitness is represented by the size of the sector on a circular disc. The disc is "spun" $n$ times, where $n$ is the size of the population and the likelihood that a chromosome will reproduce is in proportion to its sector size on the wheel. As this method is based on probability, populations may experience a possible loss of highly ranked individuals or disproportional representation of weak individuals.

b) Rank selection:

Rank selection identifies fit individuals, based only on their relative rank within the population. Instead of focussing on the proportion of the fitness that is attributed to an individual, the rank selection method ignores the fitness value in determining which individuals will reproduce. This avoids large formations of offspring from a small number of highly fit chromosomes, thus ensuring that diverse solutions remain within the population.

#### 2.6.2.3 Crossover

After the selection operation has established the fittest individuals, crossover may take place. During this operation, the chromosomes selected for reproduction exchange characteristic traits by crossing gene sequences to create a new set of solutions into the population. This results in exploration of the search space as discussed in Section 2.6.2.2. The offspring may be either an improvement or a weaker solution than previous generations. In the latter case, the GA will simply not carry weaker solutions over to the next generation, due to the selection operator.

A portion of the population of the fittest solution is reserved into the next generation to avoid destroying the fittest chromosomes, as will be discussed in Section 2.6.2.5. The crossover proportion, $p_c$, is therefore used to determine the portion of the population to be replaced in the reproduction process. Thus, $100p_c\%$ of the population will reproduce, while $100(1-p_c)\%$ of the fittest solutions will be carried over to the next generation. It is important to note that when crossover takes place, the parent chromosomes are chosen at random from the list selected to reproduce. When the parent chromosomes are crossed two offspring chromosomes will result, thus keeping the population size constant. The process of randomly selecting parent chromosomes may result in the possibility of a single chromosome being reproduced multiple times (Mitchell, 1998). Many techniques are available to implement the crossover operation. The most notable are discussed below.

a) One-point crossover:

The simplest form is the one-point crossover technique. A single position on the gene sequence is selected, where information is cut and exchanged between the parent chromosomes (see Figure 2.18). This method is generally considered adequate for short (low-order) chromosomes, but positional bias may take place where the ends of the chromosome are not crossed (Mitchell, 1998).

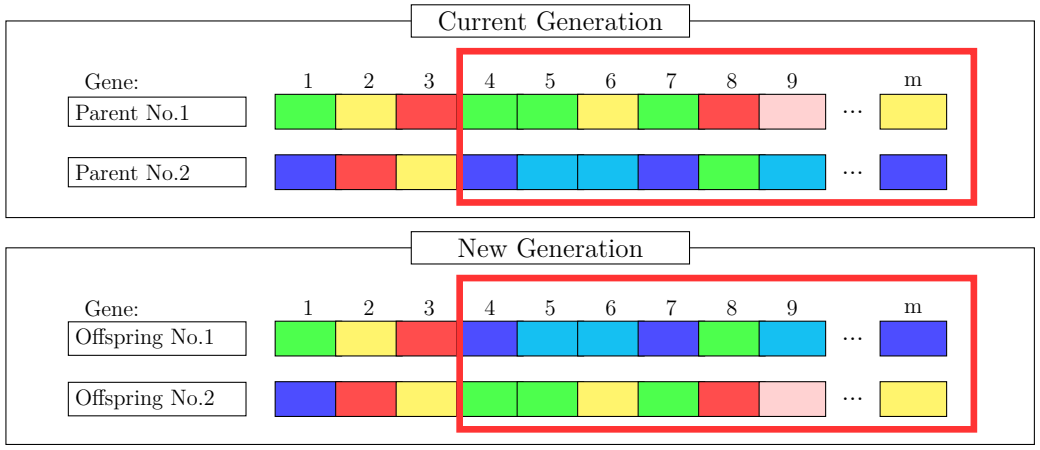


Figure 2.18: One-point crossover of genes

b) Two-point crossover:

Two-point crossover reduces the positional bias observed when using the first method. Here, two positions are chosen at random where information from the parent chromosomes are cut and exchanged (see Figure 2.19).

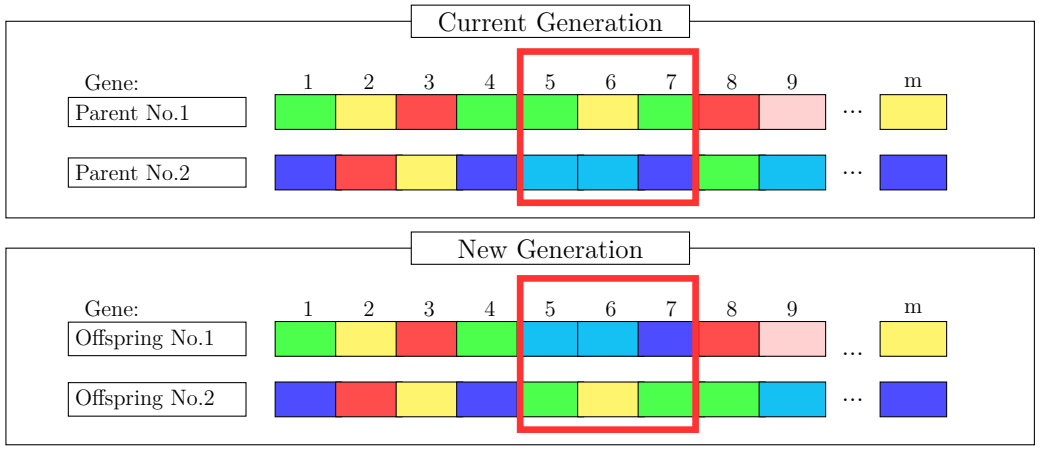


Figure 2.19: Two-point crossover of genes

c) Parameterised uniform crossover:

This method contains no positional bias and exchanges information between potentially every position on the gene sequence as determined by a predefined probability (see Figure 2.20). Mitchell (1998) noted that this method is highly disruptive and could prevent the advantageous formation of complementary gene groups.

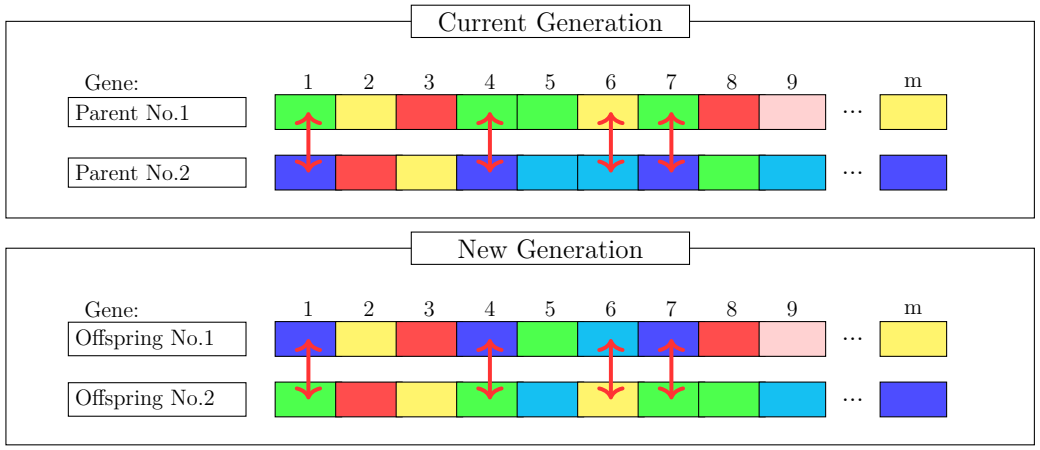


Figure 2.20: Parameterised uniform crossover of genes

#### 2.6.2.4 Mutation

Until now the population can be regarded as a closed system, circulating the same genes that originated from the randomly generated initial population. In this regard random gene mutations are permitted in the offspring chromosomes. Mutation prevents saturation of the same genes and ensure a diversity of genes, either lost during previous generations or never seen in the population (Rao, 2009). This results in a localised exploration of the search space by using the mutation proportion $p_m$. In this case $100p_m\%$ is the proportion of the genes to mutate during each reproduction cycle, unlike $p_c$ which is a measure of the proportion of the chromosomes to reproduce. The uniform mutation method selects a random gene from a random chromosome. The gene is then switched with a random value from the predefined vector of design variables.

#### 2.6.2.5 Elitism

In order not to destroy the best solutions in a population, elitism bypasses the crossover and mutation operations. Thus, the portion $100(1 - p_c)\%$ of the best solutions are able to proceed to the next generation, as discussed in Section 2.6.2.3. It has been established that elitism drastically improves the performance of GAs (Mitchell, 1998).

#### 2.6.2.6 Fitness evaluation

To evaluate the adequacy of each individual in the population, its fitness is required. The fitness is measured against an objective function either to maximise or minimise a specific attribute of the solutions. However, structural optimisation problems are constrained so that not all solutions within the search space are viable, due to deflection or stress limits, for example. Conventional GAs may readily be applied to unconstrained problems (Nanakorn and Meesomklin, 2001; Rao, 2009), but emulate the effects of constraints by adapting the fitness value through penalty functions to limit the search space.

#### 2.6.2.7 Penalty function

Instead of totally discarding infeasible solutions, penalty functions typically reduce the fitness of solutions outside the bounds of the viable search space, making them less likely to reproduce into the next generation. The result is a focused search, while still considering solutions that exist on the periphery of the feasible search space (Coley, 1999). Many penalty functions are available in the literature, e.g. death penalties, annealing penalties, adaptive penalties. As borderline solutions may arise during early generations with good potential, the ideal would be to consider the solutions on the periphery and narrow the search for the fittest solutions with each passing generation (Cazacu and Grama, 2014). In this regard, the following penalty methods are discussed:

a) Static penalties:

The static penalties method augments the objective function ($f(s)$), using the product of the static penalty parameter ($p_s$) and the number of violations ($v_i(s)$) until all the constraints ($m$) have been evaluated. The objective function is used in maximisation problems to decrease the fitness of invalid solutions, while the opposite can be said for minimisation problems. The values used for $p_s$ should be carefully considered, as too large a value would restrict exploration of the search space, while too small a value would be unable to form a distinctive boundary between feasible and infeasible solutions (Coley, 1999).

$$f'(s) = \begin{cases} f(s), & \text{if } s \in \mathbb{D} \\ f(s) + \sum_{i=1}^{m} p_s \cdot v_i(s), & \text{if } s \notin \mathbb{D} \end{cases} \tag{2.55}$$

In the equation above, the objective function is augmented if the solution falls outside of the feasible search space ($\mathbb{D}$) to cause the fitness level to be perceived as less favourable ($f'(s)$).

b) Dynamic penalties:

To vary the degree of manipulation, a dynamic penalty may be used, which considers the number of design variables and the number of generations completed ($g$). The penalty value for this method is determined in two steps. Firstly, the product of the dynamic penalty constant ($c$) and the number of constraint violations is found. Secondly, a non-linear increase may be defined by using a dynamic penalty exponent ($\alpha$).

$$f'(s,g) = \begin{cases} f(s), & \text{if } s \in \mathbb{D} \\ f(s) + \sum_{i=1}^{m} (c \cdot g)^{\alpha} \cdot v_i(s), & \text{if } s \notin \mathbb{D} \end{cases} \tag{2.56}$$

A value for $c$ ranging between 0.5 and 2.0, and $\alpha$ between 1 and 2 have been proposed as reasonable by Lagaros et al. (2002). The parameters in Equation 2.56 should be chosen based on the number of generations, as the penalty term may become unreasonably severe for a large number of generations, which would penalise even a small number of violations for a particular solution to such an extent that only a local optimum would be reached (Lagaros et al., 2002).

#### 2.6.2.8 Genetic algorithm performance

The operations that take place during the GA allow for a robust search algorithm that is both efficient and effective in finding global optima by directing the search procedure using probabilistic operators. Goldberg and Samtani (1986) illustrated the power of this method by their 10-bar benchmarking problem. Their conclusion on the GA performance was described to be equivalent to searching for the "fittest" person in the world's population (at the time 4.5 billion) by only interviewing 26 people.

### 2.6.3 Summary of genetic algorithms

GAs provide an easy-to-implement method to effectively search a large search space even when the search space is discontinuous. Constraints may be applied to the search algorithm by penalising solutions that fall outside the allowable criteria.

## 2.7 Overview and conclusions of literature and theories

Many aspects relevant to the use of web-tapered members in portal frame structures were considered during the literature and theory review. The most relevant of these aspects apply to design, structural analysis and optimisation.

### 2.7.1 Design

During the review of literature and theory, it was found that none of the design specifications considered in this study makes provision for the design of web-tapered members, and other sources had to be consulted in this regard. Several studies are available that address particular issues relating to the design of web-tapered members, but the most topical and comprehensive literature on the matter was found by Kaehler et al. (2011) and Marques, da Silva, Rebelo, et al. (2014). These publications form the pinnacle of separate studies that investigated the use of web-tapered members, based either on the AISC 360 or EC3 steel design specifications. These respective groups of researchers use similar concepts, namely:

a) The critical cross-section that governs member strength for a particular set of forces is to be determined. Both methods determine the critical cross-section through inspection. DG25 requires 3 locations to be checked, i.e. the ends and middle of an unbraced length, while Marques, da Silva, Rebelo, et al. (2014) is not specific in this regard, but suggests 10 locations to be sufficient.

b) The stability of a web-tapered member must be quantified through appropriate methods that predict buckling behaviour. This may be done either through numerical or empirical methods. Typically, the non-dimensional slenderness parameter is used in this regard.

c) Lastly, the prismatic design formulae in the respective design specifications may be applied to web-tapered members, using the properties at the critical cross-section and by considering the overall buckling stability of the member.

Marques, da Silva, Rebelo, et al. (2014) proposed amending the EC3 design formula to apply to web-tapered members, by including additional terms derived through the Ayrton–Perry model and calibrated during an extensive study using full non-linear models to predict member resistance. Marques, da Silva, Rebelo, et al. (2014) demonstrated a good level of correlation between their proposed method and the results obtained through full non-linear analysis. This method, however, is still reliant on advanced buckling analysis to account for out-of-plane behaviour.

The alternative method proposed in DG25 is less cumbersome to use on a routine basis as only simple numerical and empirical methods are employed to quantify buckling stability. The method in DG25 is referred to as the equivalent prismatic member approach, as initially proposed by Timoshenko and Gere (1961) and later refined by Lee, Morell, et al. (1972). DG25 was developed to be used in conjunction with the AISC 360 steel specifications, but has the advantage that it can be used with other design specifications as well (Ziemian, 2010). This is also evident from the publications by Baptista and Muzeau (1998), Trahair et al. (2008) and Marques (2012), who found a similar approach as the equivalent prismatic member method to apply with the EC3 steel specifications. Although the consequences of implementing DG25 with other design

specifications remain unclear, it is believed to provide conservative results based on the following findings:

a) DG25 uses an empirical method to determine the critical elastic lateral-torsional buckling moment, as initially proposed by Yura and Helwig (1996) and investigated by Kim (2010). The latter found it to provide accurate to conservative estimates across a wide range of configurations (see Section 2.3.2.2.1).

b) The same buckling curves are used for web-tapered members as for their prismatic counterparts. Marques, da Silva, Greiner, et al. (2013) found that using the prismatic buckling curves was conservative in most cases and do not include the beneficial increase of member stability (see Section 2.3.2.2.2).

In order to establish the suitability of DG25 when used with other design specifications, a survey was done of some other major design specifications to understand their underlying mechanisms. It was found that these design specifications are fundamentally similar for prismatic steel members, and based on a mixture of analytical and probabilistic derivations. Furthermore, each specification has its own system of cross-section classification, to account for the loss of resistance when individual plate members are prone to local instability.

### 2.7.2 Structural Analysis

All the steel specifications considered in the study require second-order effects to be included. As second-order effects are mostly influenced by the presence of axial force, it was hypothesised that a linear elastic analysis may be sufficient for portal frames under loading conditions in South Africa. A finite beam analysis may be used to obtain the forces and displacements. The distribution of mass and stiffness throughout a web-tapered member can be simulated by discretising the beam into small prismatic beams, through a process referred to as stepped-representation (see Section 2.5.2). The discretisation process tends to produce finite beam elements that are short and stocky and suffer from ill-conditioned stiffness matrices and shear locking effects. The use of Timoshenko beam elements was considered to alleviate the loss of accuracy experienced during the discretisation process.

Numerical techniques were also presented for obtaining the elastic buckling loads of structural members. The drawbacks of using conventional finite beam elements for modelling out-of-plane behaviour in web-tapered members were highlighted. Either advanced finite beam elements were recommended by several researchers in this regard or the use of finite shell elements. The background to the arc-length method was also provided for use in non-linear structural analysis techniques to determine member capacity, without having to resort to code-based design specifications.

### 2.7.3 Optimisation

The optimisation of structures was discussed by considering the different categories of geometry optimisation. The optimal dimensions of each member are required for the web-tapered portal frames to be studied in this text, which would lead to the least amount of steel. This would conventionally be classified as a size optimisation problem. However, web-tapered structures are typically built with vertical walls. As the beam is tapered, a shift in the centroidal axis occurs, causing the nodes used during the finite beam analysis to shift during each step. This shift of the node positions induces minor additional moments, but is advantageous as the spans of the rafter beams are reduced in a portal frame. This leads to a shape optimisation problem.

As structural optimisation problems tend to form discrete search spaces, it was found that traditional mathematical techniques were not feasible and non-traditional techniques were considered. The genetic algorithm was found to be well suited, as it is relatively easy to implement and well established in structural engineering.

# Chapter 3

# Numerical techniques for studying thin-walled structural members

## 3.1 Introduction

A suitable means is required to study the behaviour and capacity of web-tapered members, as physical experimentation was not included within the scope of the research. A numerical technique is established in this chapter for modelling thin-walled structural members, using full non-linear finite element analysis with imperfections. Shell elements were selected as they are well suited and efficient for the analysis of thin-walled sections as discussed in Section 2.5.4.

A shortage of past published results was noted to validate the numerical techniques for web-tapered members directly. For this reason, finite elements methods are established in this chapter by considering prismatic I-sections and validated against the design specifications found in this study. This numerical procedure will then be used in later chapters to verify web-tapered member and frame resistances.

## 3.2 Modelling and analysis

Abaqus was selected for modelling of the members and frames for finite element analysis, as it is capable of considering material and geometric non-linearities as well as imperfections. The procedure includes material and geometric non-linearity and the physical phenomena associated with local and out-of-plane actions, i.e. shear lag, warping and torsional effects. The input parameters utilised in this study are discussed in the following sections.

### 3.2.1 Geometric and finite element representation

The thin-walled members were modelled in Abaqus using a solid extrusion process, which allows the user to remove "open" surfaces to reveal the general shell surface arrangement. The web-to-flange junction was simplified by excluding the fillet weld from the model. This is viewed as acceptable, based on the findings by Serna et al. (2006).

The finite element selected for the study is a quad node shell with doubly curved edges. It is well suited to general-purpose modelling as it is robust for a variety of applications. This element is designated as the S4R shell in Abaqus. It supports thick to thin shells, without any loss of accuracy due to the transverse shear deformations witnessed when modelling thin plates. The S4R shell element avoids the numerical problem of shear locking normally attributed to lower order elements by utilising reduced integration. This results in improved computation time when compared to fully integrated elements, but may lead to hourglassing unless a sufficiently small element size is selected (Dassault Systems, 2013). In this regard, an element size of 25 mm was used throughout this study. A quad-dominated meshing procedure was employed due to the sloping flange angles brought on by a tapered web plate.

### 3.2.2 Material properties

As mentioned, the finite element software allows for non-linear material properties to be incorporated into the model. The stress-strain curve recommended in CEN (1995) was imported into the finite element analysis package based on S355JR steel with a nominal yield stress of 355 MPa. This is illustrated in Figure 3.1 along with the material test results obtained by Outinen (2007) on S355 steel as a means of comparison.

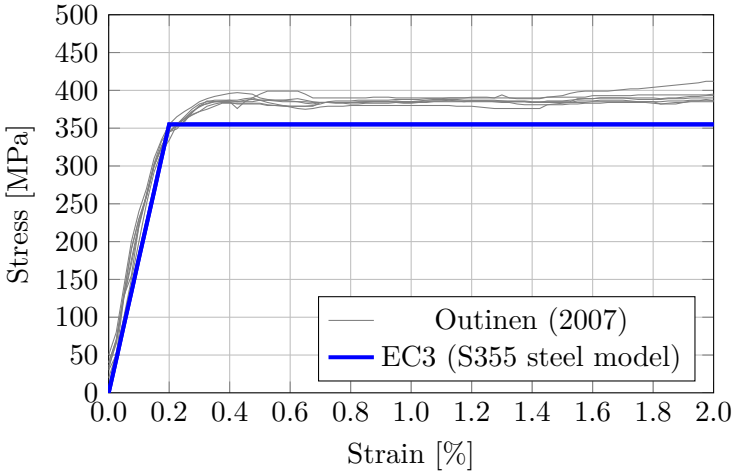


Figure 3.1: EC3 stress-strain material model for S355JR steel

The material model depicted above illustrates the elastic-perfectly plastic behaviour of the material for strains below 2%, whereafter significant strain hardening occurs and the plastic curve increases non-linearly up to the ultimate material stress. This region of material behaviour was excluded, as the study is mainly concerned with identifying the member capacity up to the point of first yield, without accounting for increased post-yield member strength.

### 3.2.3 Imperfections

The presence of imperfections is known to contribute significantly to a decrease in ultimate load capacity of structural members and frames. These imperfections can be classified into two broad groups.

a) Geometric imperfections:

A geometric imperfection may be defined as any deviation of the actual structure from its perfect form. These imperfections are typically caused by the processes used during fabrication, transport and erection. The tolerance applicable to any imperfection is governed by local manufacturing and construction standards. The tolerable deviations from the specified dimensions for plate-girders in South Africa can be found in table 5 of SANS 2001-CS1 (2005).

Global geometric imperfections, which include out-of-straightness of the centreline of the member or individual flanges, or twisting of the section, have a maximum tolerance of $L/1000$. This is internationally regarded as the acceptable geometric imperfection and formed the basis of the ECCS and SSRC buckling curves (Beer and Schultz, 1970; Bjorhovde, 1972). As an indication of the conservatism of this assumption, Bjorhovde (1972) measured the average out-of-straightness of all the test samples used in deriving the SSRC buckling curves, to be only $L/1470$. Similarly, the tolerance of local imperfections (i.e. included web distortion, the squareness of section and flange flatness) is also included in SANS 2001-CS1 (2005) with tolerable imperfection typically in the range of one hundredth of the relevant plate dimension.

b) Material imperfections:

Imperfections of the material properties may be attributed to variations in material composition or to the process followed during manufacturing. In the latter case, the differential cooling of structural members after manufacturing and welding causes an uneven distribution of residual stresses over the cross-section, as illustrated in Figure 3.2, with areas that are either in tension or compression. This leads to early yielding of certain parts of the cross-section, which significantly influences the member capacity.

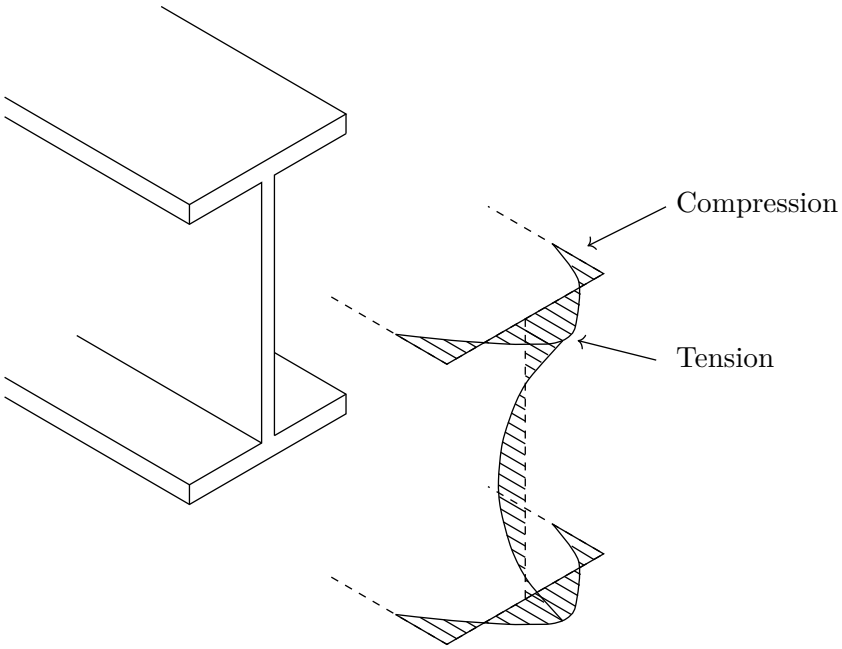


Figure 3.2: Typical distribution of residual stresses

Hendy and Johnson (2006) have noted that the effects of residual stress can successfully be modelled using equivalent geometric imperfections in addition to the actual geometric imperfections. In this regard, section 5.3 of EC3 provides guidelines for introducing initial member imperfections for each of the respective EC3 design curves with bow-like shapes. The equivalent imperfections to be used during plastic analysis are listed in Table 3.1. These equivalent imperfections are noticeably larger than the geometric eccentricity of $L/1000$ assumed in both the ECCS and SSRC buckling curves discussed on the previous page.

Table 3.1: EC3 equivalent geometric imperfections for modelling initial member imperfections

| EC3 buckling curve | $a_0$ | a | b | c | d |
|---|---|---|---|---|---|
| Eccentricity | $L/300$ | $L/250$ | $L/200$ | $L/150$ | $L/100$ |

### 3.2.4 Boundary conditions and constraints

Member boundary conditions that describe an idealised simply supported system allowing for minor-axis rotation and warping of the flanges are required. In the study of in-plane column resistance, an additional boundary condition was imposed to ensure strong-axis flexure under axial loads, without torsional-flexural and out-of-plane flexure. The constrained degrees of freedom describing the boundary conditions are presented in Figure 3.3.

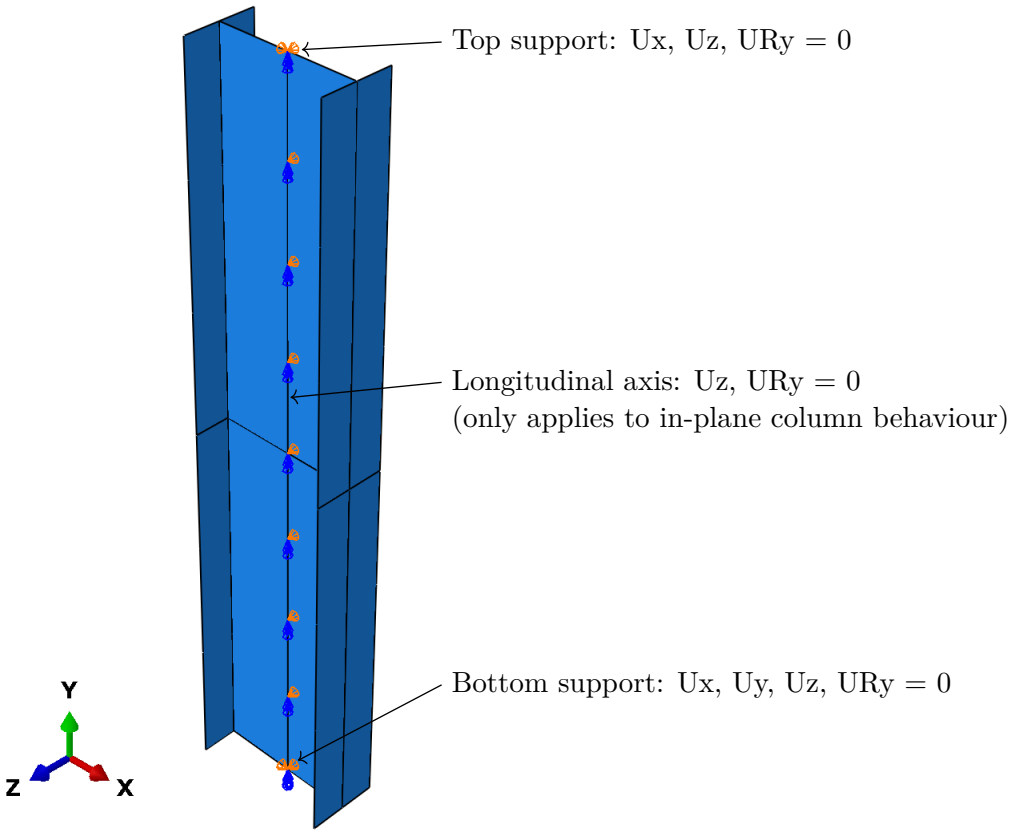


Figure 3.3: Idealised simply supported boundary conditions

The supports and points of external load application are modelled based on the centre node at each end of the member. The reference node was constrained so as not to cause local plate failure, while allowing plates to rotate and displace with a uniform distribution of forces at the member ends. This was specifically required as restricting a member's ends against minor-axis rotation and warping may lead to an increase in the member's load carrying capacity (Trahair, 1993). In this regard, a structural coupling was applied over the entire cross-section, which enforces rotational degrees of freedom to remain relative to each other. In addition, a kinematic coupling served to ensure rigid body movement of the unsupported flange edges to overcome local buckling by tying the rotational and displacement degrees of freedom together for each flange, as presented in Figure 3.4.

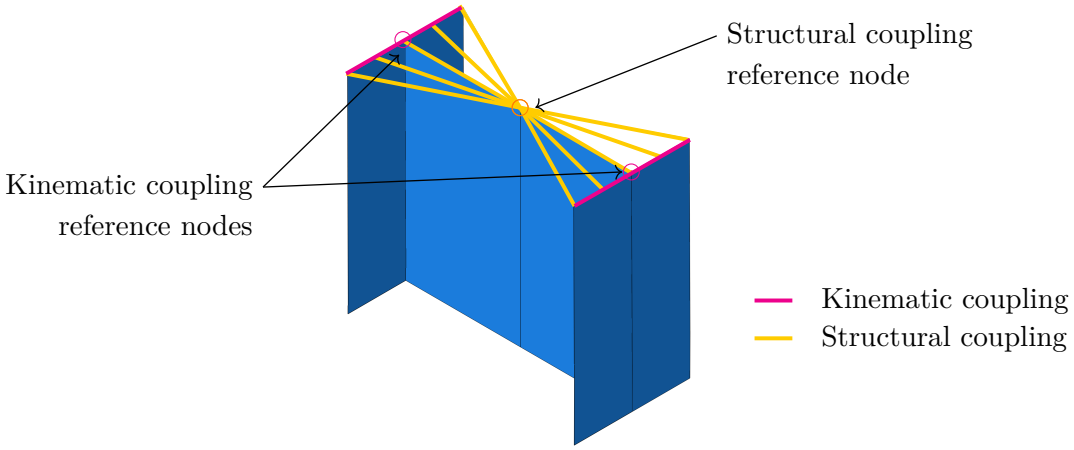


Figure 3.4: Plate end couplings

This arrangement provided satisfactory results for most members investigated, but members that tended towards being stocky experienced local plate buckling at the point of load application. In these cases, a constraint configuration that forced rigid body movement of the entire cross-section was used. In this regard, a kinematic coupling was again made use of in the finite element analysis software.

### 3.2.5 Full non-linear finite element analysis

The individual member capacity was evaluated using the Riks method, which allows for the study of post-buckling response in complex and unstable structural systems. It is regularly used to predict geometrically non-linear collapse brought on by all $P - \Delta$ and $P - \delta$ effects and may include non-linear material and boundary conditions. The Riks analysis method is often preceded by a linear eigenvalue buckling analysis to investigate the imperfection sensitivity of a given structure (Dassault Systems, 2013).

#### 3.2.5.1 Eigenvalue buckling analysis

A linear eigenvalue buckling analysis is an effective means for the study of critical modes that lead to structural failure. These may be found by subjecting the "perfect" structure to specific load mechanisms as described during the review of literature and theories (see Section 2.5.3.2).

In addition to describing the critical mode shapes, the eigenvalue buckling analysis has the benefit of readily providing the nodal data for each mode shape. It would otherwise be laborious to describe each model with the desired geometric imperfections for full non-linear analysis. The buckling mode shapes represent normalised vectors of deformation due to specific loads and are scaled according to the maximum displacement component during different modes of failure. The perturbations of geometry are introduced into the Riks analysis to mimic the "worst" local

and global member deformities that can arise from manufacturing and erection inaccuracies. Figure 3.5 illustrates some of the mode shapes experienced by a prismatic beam under uniform bending moment in their order of probability.

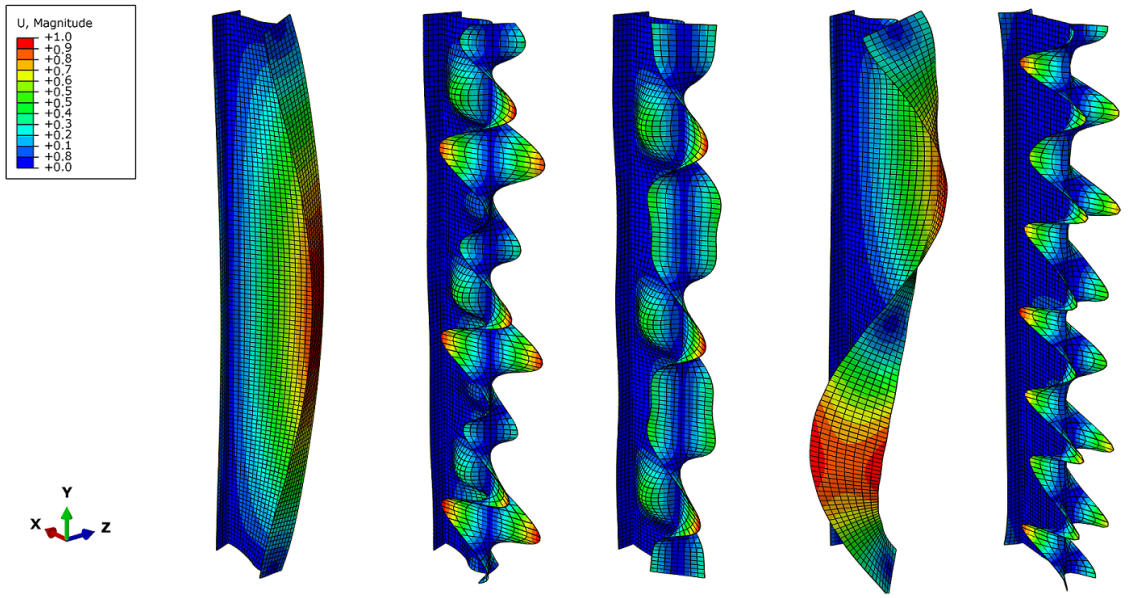


(a) Mode A (b) Mode B (c) Mode C (d) Mode D (e) Mode E

Figure 3.5: Typical compression flange buckling modes for a prismatic beam under uniform bending moment

The mode shape described on the left side of the figure above is synonymous with lateral-torsional buckling and forms the fundamental mode of failure for the particular case. Although the other mode shapes are not critical to the study of elastic member instability, they provide additional nodal information for modelling local imperfections of the web and flange plates. In members and frames that are slender, the early mode shapes tend to correspond to global buckling mechanisms, while higher order mode shapes correspond to local instabilities. In this case, only the first few mode shapes are of real concern to the designer. However, the global buckling modes may be difficult to obtain for members that fall within the plastic or inelastic range and tend to be found in the higher order range of eigenvalue solutions, as the probability of a member becoming unstable globally decreases. This drawback is exacerbated when using a more refined mesh as it gives rise to a larger number of mode shapes that correspond to the increased number of degrees of freedom within the system. Relating to members characterised by plastic and inelastic behaviour, the global buckling load contributes less towards member capacity and is mostly of concern when comparing it to theoretical elastic loads, as will be considered later in Sections 4.2 and 4.3.

The nodal data for the buckling modes are used as the basis for the initial imperfections in the non-linear model to follow. This is done by adding the following instruction to the linear model's field output in Abaqus:

```
*NODE FILE, global = yes
u,
```

This generates the ".fil"-files with nodal data describing the translation degrees of freedom to be used in the non-linear analysis considered next. The files are automatically stored with the "job" name as the filename in Abaqus.

#### 3.2.5.2 Riks analysis

The Riks analysis method in Abaqus utilises the arc-length method as presented earlier in Section 2.5.5. This allows the structural analysis to track any non-linear response of the load-deflection path iteratively. The non-linear model was set up based on the linear eigenvalue buckling model, by first replacing the buckling analysis with a Riks analysis step and removing all edits from the keywords editor. The following code was then added to account for the initial geometric imperfections by referring to the nodal data results created in Section 3.2.5.1. As an example, the following was added to the non-linear model's keyword editor:

```
*IMPERFECTION, FILE = nodaldata , STEP =1
1, 0.001
5, 0.0001
```

Typically, the magnitudes of the imperfections are tiny compared to the relevant structural dimension. In structures that are not imperfection sensitive, the early buckling modes tend to influence load capacity the greatest (Dassault Systems, 2013). In the example presented above, the translational degrees of freedom in the Riks model are modified by superimposing the first and fifth modal vectors with a maximum eccentricity of $L/1000$ and $L/10000$ of the model's overall length, respectively. Global lateral-torsional buckling imperfections are introduced by the fundamental mode shape nodal data, while imperfections of the compression flange are acquired from the fifth mode shape (see Figure 3.5).

## 3.3 Implementation of the numerical techniques

Having established the procedures and assumptions that were used in the study, this section is presented to shed light on the implementation of the full non-linear analysis. Figure 3.6 shows a flowchart for the modelling of structural elements in Abaqus.

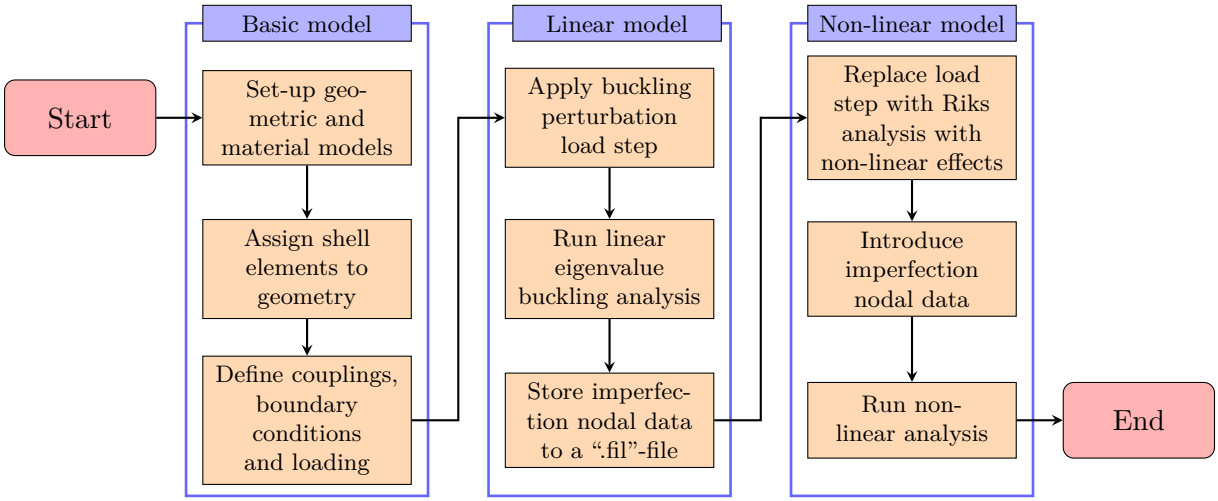


Figure 3.6: Abaqus procedural implementation

A prismatic welded I-beam subjected to a uniform bending moment was selected for illustrating the results obtained during full non-linear analysis. The beam has a total length of 3 m and an initially bowed imperfection describing pure lateral-torsional imperfection with a maximum eccentricity of $L/150$, which corresponds to the buckling curve c in Table 3.1. All other boundary conditions, loading mechanisms and constraints are as described under Section 3.2. The beam is defined by the cross-sectional properties below.

Table 3.2: Section properties of steel member 400x200 (8W, 10F)

| b [m] | $t_f$ [m] | h [m] | $h_w$ [m] | $t_w$ [m] | A [$m^2$] | $r_x$ [m] | $r_y$ [m] |
|---|---|---|---|---|---|---|---|
| 0.200 | 0.010 | 0.400 | 0.380 | 0.008 | 7.04E-03 | 0.164 | 0.044 |

| $I_x$ [$m^4$] | $I_y$ [$m^4$] | $Z_{e,x}$ [$m^3$] | $Z_{pl,x}$ [$m^3$] | $M_{y,x}$ [N.m] | $M_{p,x}$ [N.m] | J [$m^4$] | $C_w$ [$m^6$] |
|---|---|---|---|---|---|---|---|
| 1.89E-04 | 1.33E-05 | 9.44E-04 | 1.07E-03 | 334 969 | 379 424 | 2.00E-07 | 5.08E-07 |

Abaqus has a built-in function for reporting the Load Proportionality Factor (LPF) versus the arc length. The XY-data was manipulated by multiplying the LPF with the reference force to arrive at the non-linear response curve for the particular model, as depicted in Figure 3.7. In the figure, a linear response is noted until a sharp reduction in member strength takes place. Figures 3.7 and 3.8 illustrate what takes place at the different stages of loading, with the latter figure displaying the von Mises stresses that occur in different parts during increased loading.

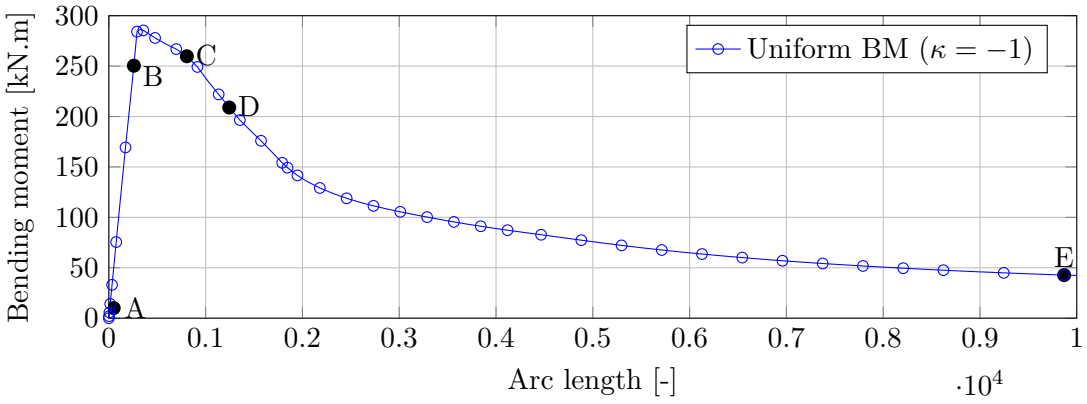


Figure 3.7: Load-arc length response curve using Riks analysis

At point A, little to no stress is observed within the beam as the bending moment is initialised. The bending moment then increases linearly until point B where almost all of the bending moment was carried by the flanges until the end of the elastic range. From here, increasing amounts of out-of-plane deformation was noticed as well as partial yielding on the inside of the bowed flange, which is in compression at mid height. Point C was found on the downward path of the load curve with yielding also being observed on the other free edge of the compression flange until the entire compression flange reached the point of yield (point D). Lastly, point E is provided only to show the crumpled shape of the beam under the applied loading. This stage is not of any use in design as it is characterised by large strain behaviour that leads to strain-hardening, which is not included in the current material model.

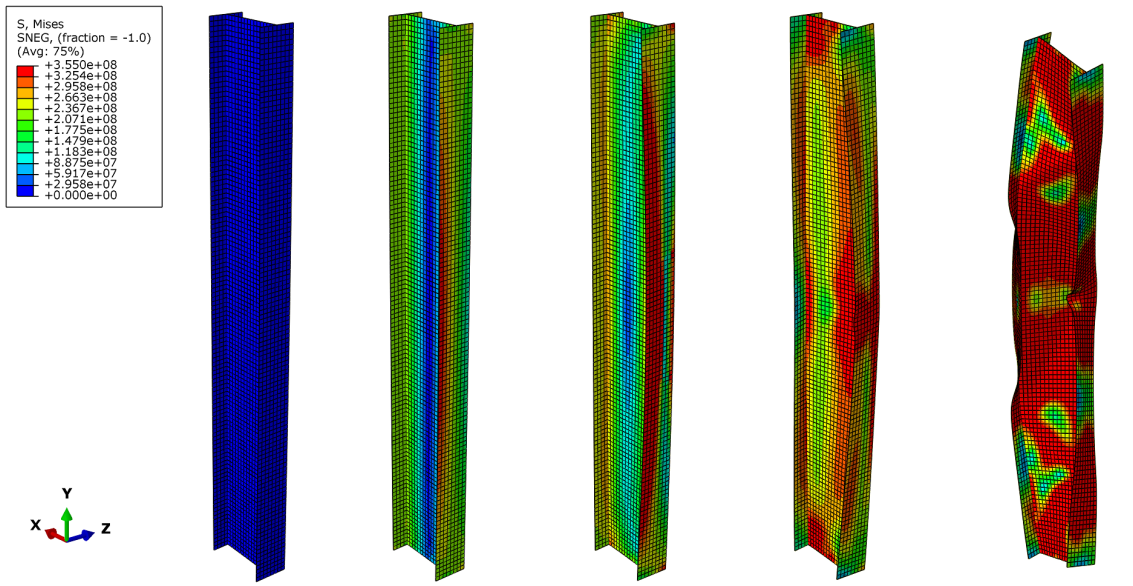


(a) Point A (b) Point B (c) Point C (d) Point D (e) Point E

Figure 3.8: Riks analysis load stages

The ultimate uniform bending moment found for the section was 281 kN.m. This compares well with SANS 10162-1 (2011) where the predicted ultimate load carrying capacity is 293 kN.m (+4%).

## 3.4 Validation of the numerical techniques against prismatic structural members

Sections 3.2 to 3.3, considered the methods employed in Abaqus for the study of the structural behaviour and ultimate load capacity of thin-walled elements. This section deals with the performance of the proposed numerical techniques for the three different loading models as depicted in Figure 3.9.

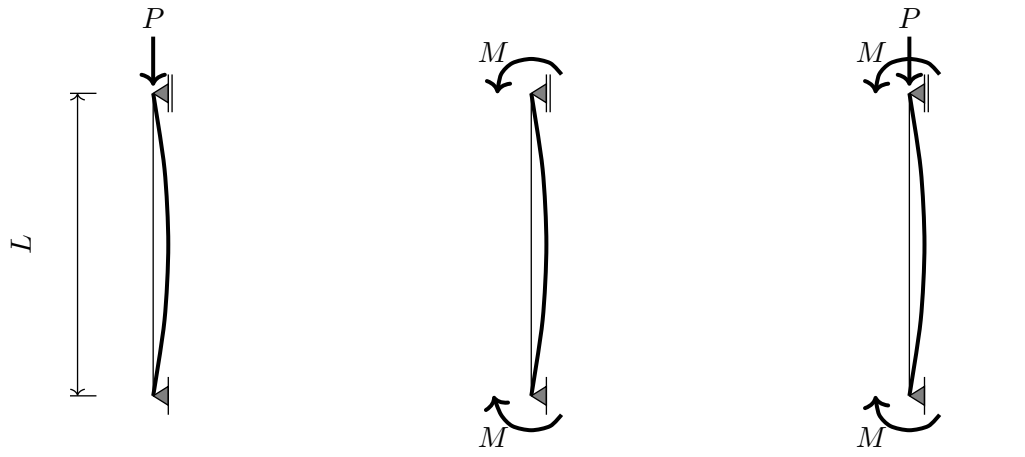


(a) Column (b) Beam (c) Beam-column

Figure 3.9: Applied loading considered for validation

Firstly, in-plane column behaviour was affected through the application of an axial compression load through the centreline of the member and the boundary conditions described in Section 3.2.4. Secondly, the lateral-torsional buckling capacity was determined for beams subjected to uniform bending moment through the application of equal and opposite end moments. Finally, the response of a structural member regarding in-plane and out-of-plane action was investigated under combined axial load and uniform bending moment.

The prismatic section defined earlier in Table 3.2 was used in all cases. The analyses were conducted according to various discrete lengths and eccentricities to account for geometric and material imperfections (see Section 3.2.3), in order to determine the effectiveness of the numerical procedure. In total, more than 125 full non-linear analyses with different configurations were conducted against which the performance of the numerical models were validated.

### 3.4.1 Column resistances

The cross-sections were first classified for axial compression, based on the design specifications included in this study (see Table 3.3). In all cases, the flange plates were found to be sufficiently compact so that local instabilities may be neglected, while the web plate was considered slender by all the specifications. The effective area was determined according to each of the design specifications' method for dealing with local plate instabilities. This, along with the different resistance factors employed by each of the design specifications, led to different predicted factored axial compressive resistances. The results obtained from the numerical procedure were then superimposed on the factored in-plane flexural buckling curves of the design specifications and presented in Figure 3.10.

Table 3.3: Axial load cross-sectional classification for 400x200 (8W, 10F)

| | Flanges | Web | $A_g$ [mm$^2$] | $A_{eff}$ [mm$^2$] | $C_{r,max}$ [kN] |
|---|---|---|---|---|---|
| SANS/CSA | Class $< 4$ | Class 4 | | 6286 | 2008 |
| AISC | Non-slender | Slender | 7040 | 6421 | 2052 |
| EC3 | Class 3 | Class 4 | | 6117 | 2172 |

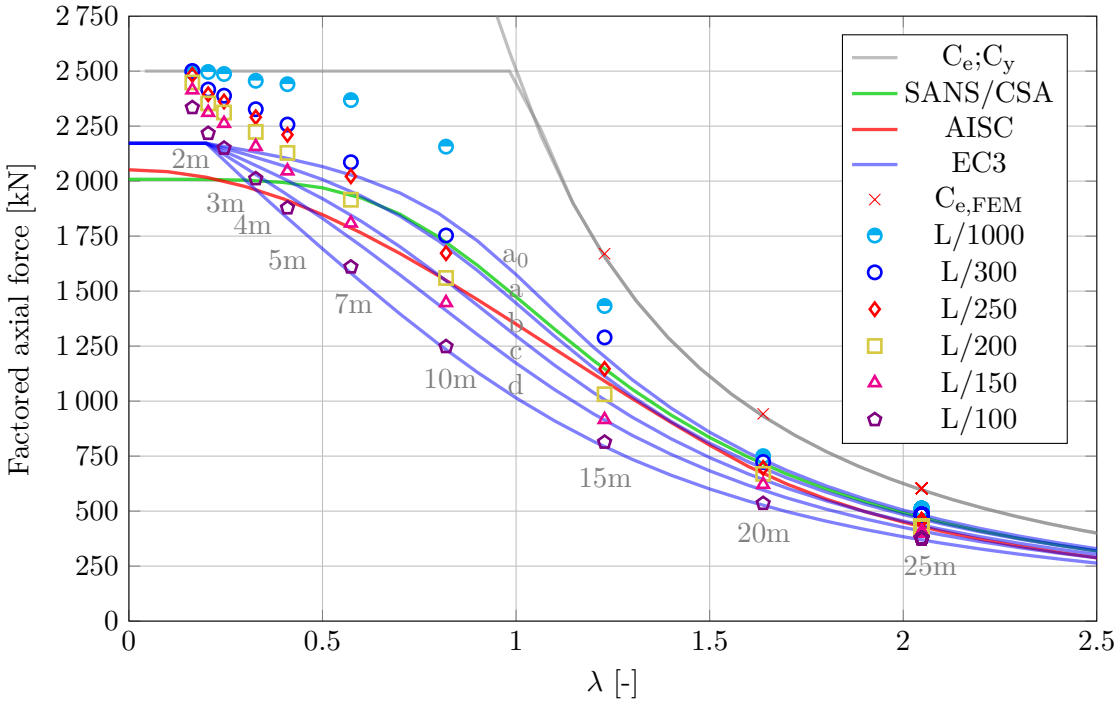


Figure 3.10: Flexural buckling curves for 400x200 (8W, 10F)

The results obtained through FEA correlate well with the EC3 buckling curves. Additional capacity was noted in the plastic region, as the column was able to redistribute stress until the entire cross-section reached yield stress (equal to $C_y = 2500$ kN). The effect of increased eccentricity can be observed from the plot for $L/1000$ that acts as a baseline when only geometric

imperfections are considered, without accounting for material imperfections. The welded column found here is, however, categorised as being of curve type b in Table 3.1, which corresponds to the $L/200$ curve. The SANS/CSA and AISC curves follow this curve reasonably well with some conservatism noted in the plastic range. A slight overestimation occurs in the SANS/CSA curve over the inelastic region with the largest deviation approximately equal to +9%.

### 3.4.2 Beam resistances

The focus of the numerical validation is turned next towards beams under a uniform bending moment. The classification of the cross-section for flexural members according to the different design specifications are provided in Table 3.4.

Table 3.4: Bending moment cross-sectional classification for 400x200 (8W, 10F)

| | Flanges | Web | Section | $M_{r,max}$ [kN.m] |
|---|---|---|---|---|
| SANS/CSA | Class 3 | Class 1 | Class 3 | $0.9 \cdot M_y = 301$ |
| AISC | Non-compact | Compact | NC(F),C(W) | $0.9 \cdot M_p = 341$ |
| EC3 | Class 3 | Class 1 | Class 3 | $M_y/1.0 = 335$ |

The difference with which each of the design specifications considers the moment of resistance becomes apparent from the above table. This is brought on mainly by the classifications used in the specifications, with AISC considering the current cross-section capable of attaining a part of the plastic moment. Conversely, SANS 10162-1, CSA S16 and EC3 determines the maximum moment of resistance based on the yield moment. Apart from the use of a resistance factor equal to unity by the latter, all of these design specifications follow a similar methodology. In Figure 3.11, the finite element analysis results are again superimposed on the lateral-torsional buckling curves produced by the design specifications, for ease of reference.

The results from the finite element analyses form gradual curves, as is to be expected. The plot for beams modelled with a geometric imperfection of $L/1000$ again overestimates the ultimate load carrying capacity of the member, while a narrow band of results is noted when introducing the equivalent geometric imperfections that account for material imperfections. These results converge with the band formed by the design guides. The EC3 criterion for welded beam members requires design based on curve c and is represented by the $L/150$ plot in Figure 3.11. It can be seen that the numerical analysis marginally exceeds the results predicted by EC3, suggesting that EC3 is on the safe side. The $L/150$ results correlate well with the SANS/CSA buckling curve with the largest variance of approximately +10% found in the inelastic range. The difference in the AISC maximum resistance becomes noticeable in the above figure as the moment of resistance of the particular cross-section is based on the plastic moment, whereas the other design specifications used the elastic moment. This results in an increased moment of resistance for the particular beam throughout the slenderness range.

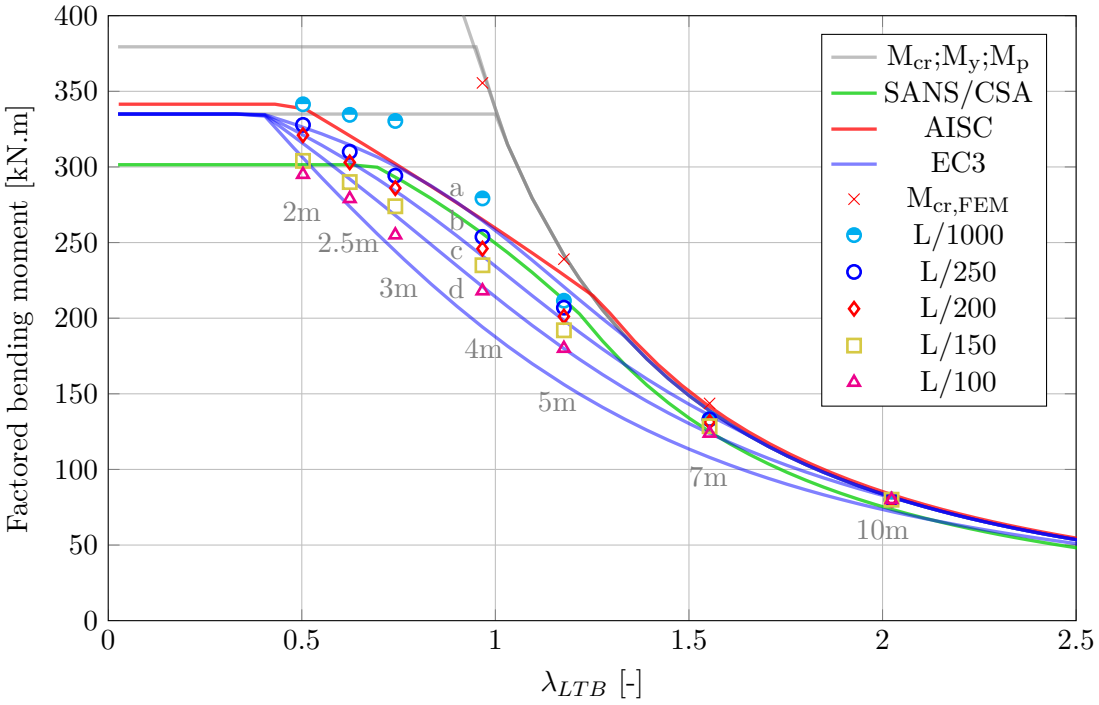


Figure 3.11: Lateral-torsional buckling curves for 400x200 (8W, 10F)

### 3.4.3 Beam-column resistances

The final case to consider was that in which axial and bending force acted simultaneously on a structural member. To this end, a member with a specific length was selected (5 m) with the previously stated cross-sectional properties. The beam-column capacity was obtained for two cases, namely overall member strength and lateral-torsional buckling strength, by adapting the boundary conditions during the finite element analyses to either permit or restrict out-of-plane action, as discussed earlier in this chapter. The member was modelled using a maximum eccentricity of $L/150$, and the maximum resistance results obtained by finite element analysis are listed in Table 3.5. The interaction formula from SANS/CSA was used as an illustration of the predicted member capacities against the numerically obtained results. This was based on the maximum factored resistance to axial loads and bending moments as specified in SANS 10162-1 and CSA S16. These resistances and the differences when comparing them to the numerically obtained values are also indicated in Table 3.5.

Table 3.5: Maximum resistances for 5 m 400x200 (8W, 10F) member

| | Overall member strength | | Lateral-torsional buckling | |
|---|---|---|---|---|
| | $C_{r,max}$ [kN] | $M_{r,max}$ [kN.m] | $C_{r,max}$ [kN] | $M_{r,max}$ [kN.m] |
| FEM | 2045.9 | 298.3 | 908.0 | 192.0 |
| SANS/CSA | 1984.5 | 301.5 | 812.5 | 212.0 |
| Difference | -3% | +1% | -11% | +10% |

Good correlation was obtained between the design specification and finite element analysis for the pure axial or pure bending values in the overall member strength model. During the numerical analysis, significant moment redistribution was noted in the beam-column when subjected to small axial-high moment loads. This additional capacity is not accounted for in the SANS/CSA interaction curve, in which a linear relationship connects the resistances at zero moment and zero axial force for class 3 beam-columns, thus negating any beneficial influences on strength past the point of first yield. The fact that the member here is classified as being of class 3, only on account of the flanges marginally exceeding the upper boundary for class 2 flanges according to SANS/CSA, caused the additional strength identified by the finite element analysis.

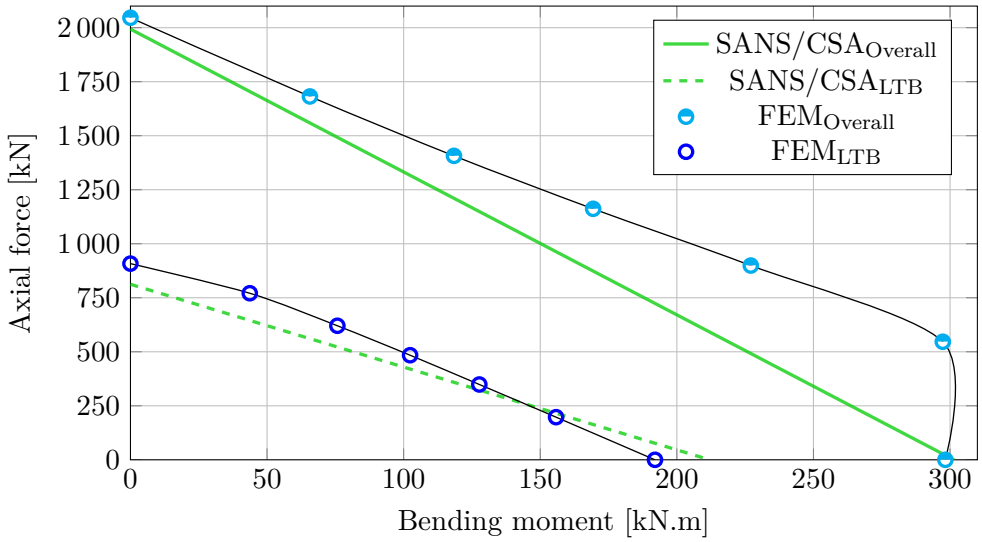


Figure 3.12: Beam-column interaction for 5 m 400x200 (8W, 10F) member

Of the two cases considered, it is clear that lateral-torsional buckling would govern for the specific member if no lateral support was provided. No significant moment redistribution was noted during the analysis of this mode. Unsafe results were obtained for low axial-high moment loading configurations, but these can be attributed to the differences already observed between the maximum predicted moments of resistance in Section 3.4.2.

## 3.5 Conclusions

The numerical techniques presented in this chapter considered various aspects about modelling thin-walled structural members. These techniques describe the effects of non-linear geometric and material behaviour brought on by imperfections and sufficient methods to address these issues during modelling. The use of equivalent geometric imperfections according to EC3 was seen to produce comparable results to those of the different international design specifications considered in this study. This reduced the complex modelling issues that arise when introducing residual stress as a separate load step in Abaqus. Furthermore, the residual stress profiles in

web-tapered beams are still relatively unknown with few sources found to confirm these stress distributions during the literature study.

Eigenvalue buckling analysis was used to derive mode shapes associated with structural failure and used to introduce geometric imperfections into the Riks model for non-linear analysis. The method proved effective in predicting the ultimate load capacity of columns, beams and beam-columns. This is mainly attributed to the finite element model's ability to simulate the effects of local and out-of-plane actions.

Due to a lack of published results on web-tapered member resistances, it is accepted that the numerical techniques, as presented in this chapter, will suffice for modelling web-tapered members.

# Chapter 4

# Web-tapered member design approach

## 4.1 Introduction

The background to prominent design specifications was considered, along with guidelines found in the literature for the design of web-tapered members in Chapter 2. The underlying principles for the design of structural steel members were seen to be closely related between steel specifications. It was found that the guidelines in DG25 for web-tapered members could be implemented with design specifications other than AISC. The methods proposed by Marques, da Silva, Rebelo, et al. (2014) are specific to EC3 as they were derived using the Ayrton–Perry model and are heavily dependent on detailed finite element analyses, which makes them difficult to implement on a routine basis. The same author proved that accurate to conservative estimated member resistances could be found by using the normal prismatic buckling curves, similar to the method employed by DG25.

It was decided that DG25 would be the most fitting approach for use with SANS 10162-1 (and CSA S16) for the design of web-tapered members. Based on the review of available literature it is believed that DG25 will tend towards a conservative approach and will not require any advanced finite element analysis. This makes it more suited to implementing with the structural optimisation procedure developed in Chapter 5.

## 4.2 Web-tapered columns

### 4.2.1 Proposed design approach

A complex strategy is implemented in DG25 for the design of web-tapered columns. In determining the critical cross-section within a column, the internal stresses and resistances have to be calculated at various locations. In AISC 360 the area reduction is calculated as a function

of the stress and plate dimensions at any cross-section. The critical section in a web-tapered member is then determined as the cross-section with the highest resulting internal stresses after accounting for any area reductions, as shown in Figure 4.1.

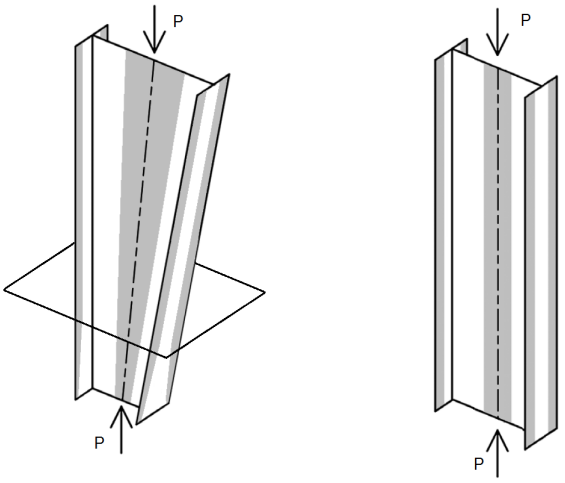


Figure 4.1: Mapping of web-tapered column, adapted from White and Kim (2006)

Various assumptions that limit the scope of this study were made in Section 1.4, the most notable being that flanges subject to local instability are excluded. This makes the identification of the critical section considerably less onerous, as only the web is allowed to display signs of local instability. The benefit of this assumption is further discussed later in Section 4.3. A simplified approach is proposed for capacity checks of web-tapered columns in the form of the flow diagram in Figure 4.2. The steps are based on the procedure in DG25 and discussed below with reference to the provisions of SANS 10162-1.

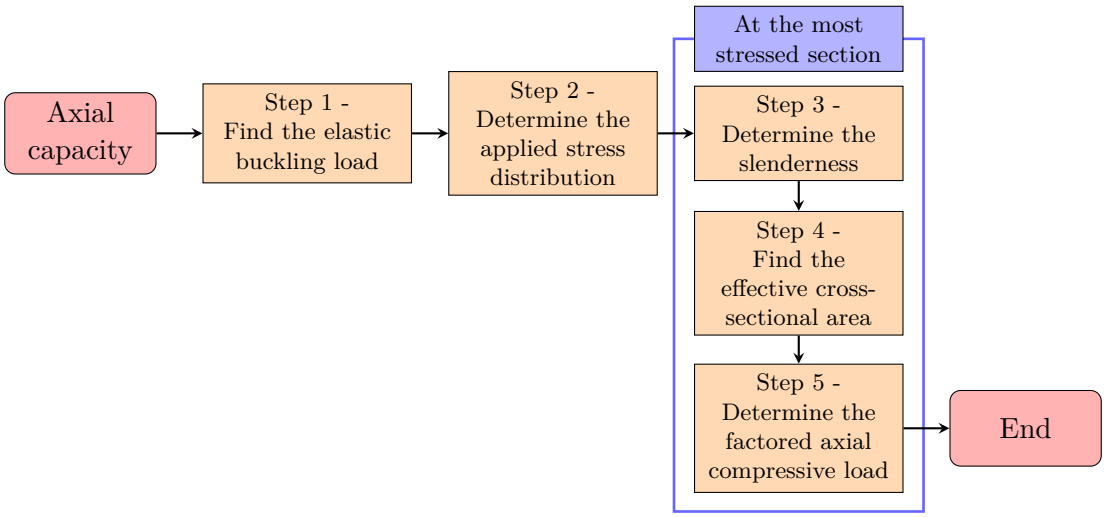


Figure 4.2: Design approach for web-tapered columns

**Step 1: Elastic buckling load**

Various methods were presented in Sections 2.3.1.2.1 and 2.5.3 for determining the elastic flexural buckling load of a web-tapered column. The effort associated with each method may differ significantly, ranging from empirical approximations to numerical and energy-based computational methods. The use and implementation of these methods are considered next, along with the appropriate strategies for each mode of failure.

a) Strong-axis flexural buckling:

To investigate the use of the elastic flexural buckling methods, an ideally pin-ended web-tapered column was considered from literature (Chang, 2006; Kaehler et al., 2011). The configuration and design parameters are presented in Appendix A.1. The elastic flexural buckling load was determined using the empirical approximation, an eigenvalue buckling analysis using beam elements and the method of successive approximations. The comparison was implemented in Matlab and used a discretised beam consisting of 10 prismatic elements. Newmark's method of successive approximations was allowed to converge to a point where no significant change was observed using finite difference expressions (see Appendix A.1). The results for the different methods are presented in Table 4.1. The method of successive approximations, as reported by Kaehler et al. (2011), is used as a reference value.

Table 4.1: Comparison of strong-axis elastic flexural buckling methods

| Study | Method | $C_e$ [kN] | Diff. [%] |
|---|---|---|---|
| Kaehler et al. (2011) | Empirical approx. | 17 663 | -0.20 |
| | Successive approx. | 17 698 | - |
| Chang (2006) | Eigenvalue buckling | 17 250 | -2.53 |
| Aucamp (2016 - Current) | Empirical approx. | 17 663 | -0.20 |
| | Successive approx. | 17 698 | 0.00 |
| | Eigenvalue buckling | 17 671 | -0.15 |

The elastic flexural buckling loads show a close correlation, the minor exception being the result from Chang (2006). The most significant outcome of the comparison was the close correlation of the empirical approximation with the numerically determined values, considering that the empirical formula requires considerably less effort to perform.

An extended investigation was performed to determine the accuracy of the empirical formula for different structural members against numerically determined elastic flexural buckling loads. The results are presented in Appendix A.2, where a similar correlation was observed for various combinations of plate sizes, web-tapering ratios and column lengths. The values resulting from the elastic buckling load methods were indistinguishable from

each other for all practical implications, with differences between the methods never exceeding more than 3.5%. It was concluded that the empirical approximation provides an accurate means for typical member lengths and tapering ratios, while requiring minimal effort.

b) Weak-axis flexural buckling:
The elastic flexural buckling load for the weak-axis may either be calculated by numerical methods or approximated by Euler's formula (Equation 2.1), using the section properties at mid-height. This is regarded as a sufficient approximation as the moment of inertia variation is insignificant in the weak-axis plane, for typical tapering ratios (Kaehler et al., 2011). The weak-axis flexural resistance can thus easily be obtained and not investigated further in this study.

**Step 2: Applied stress distribution**

The critical cross-section is found by using the force distribution in the column to determine the point of the highest internal axial stress. This method is identical to finding the cross-section with the highest utilisation ratio as discussed by Marques, Taras, et al. (2012).

**Step 3: Non-dimensional slenderness parameter**

The equivalent prismatic member is determined from the elastic flexural buckling load ($C_e$) and the critical cross-section's area ($A_{crit}$) in the previous two steps. The non-dimensional slenderness parameter ($\lambda$) is thus a unique value determined for a specific unbraced length and axis orientation.

$$\lambda = \sqrt{\frac{f_y}{f_e}} = \sqrt{\frac{A_{crit} \cdot f_y}{C_e}} \tag{4.1}$$

**Step 4: Effective cross-sectional area**

The effective width method is used to account for local elastic instabilities in plate members. The method employed by the 2011 edition of SANS 10162-1 determines a stable plate width based on the applied stress over the cross-section, from which the effective area $A_{eff}$ is computed. This results in a parabolic variation of the neglected portion of the web as seen in Figure 4.3. When columns are subjected to high axial stress, this neglected portion increases to correspond to the class 3 limit, which may conservatively be used as it requires less effort to determine.

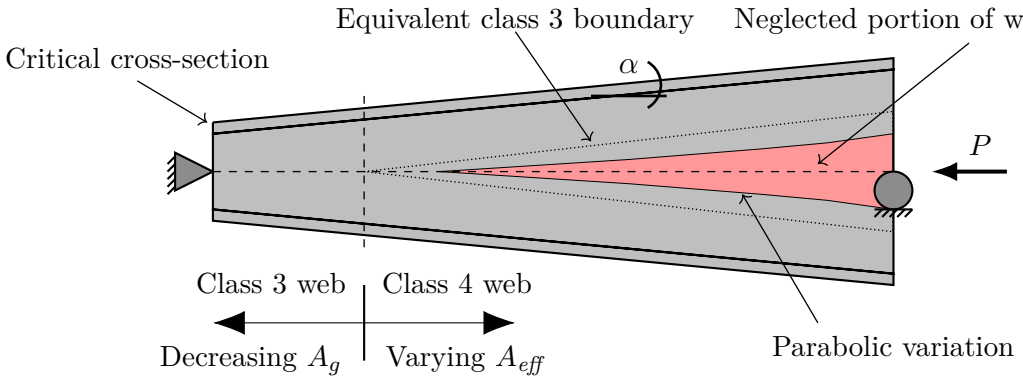


Figure 4.3: Area reduction in web-tapered column with intermediate transition from class 3 to class 4 web

**Step 5: Axial compressive resistance**

Columns are assumed to be fabricated from welded plate members with flame cut edges in this study (see Section 1.4), thus making use of the $n = 2.24$ curve in SANS 10162-1. The axial compressive resistance ($C_r$) is calculated using Equation 2.4, based on the slenderness ratio of members calculated on the basis of their gross sectional properties (Step 3) and the reduced area at the critical section (Step 4).

### 4.2.2 Verification of web-tapered column resistance

A parametric study was undertaken to validate the proposed approach and to compare it against results obtained through full non-linear analysis using the techniques explored in Chapter 3. The effects of various tapering angles ($\alpha$) (defined in Figure 4.3) were investigated over lengths ranging from 2 m to 15 m. The section was defined by flange plates that are 200 mm by 10 mm in dimension and a web plate thickness of 8 mm. As the column length increased, the variable $h$ was adjusted according to the taper angle being considered. A summary of the main variables considered in the investigation appears in Table 4.2.

Table 4.2: Main variables of web-tapered members investigated

| Case | Length [m] | 0 | 2 | 4 | 6 | 8 | 10 | 15 |
|---|---|---|---|---|---|---|---|---|
| | $\alpha$ [Deg] | h [m] | | | | | | |
| 1 | 2.5° | 0.250* | 0.425 | 0.599 | 0.774 | 0.949 | 1.123 | 1.560 |
| 2 | | 0.400 | 0.575 | 0.749 | 0.924 | 1.099 | 1.273 | 1.710 |
| 3 | 5.0° | 0.250* | 0.600 | 0.950 | 1.300 | 1.650 | 2.000 | 2.875 |
| 4 | | 0.400 | 0.750 | 1.100 | 1.450 | 1.800 | 2.150 | 3.025 |

The values in Table 4.2 above that are marked with an asterisk indicate situations where the web plate was still considered less than class 4. Furthermore, a maximum out-of-straightness eccentricity of $L/200$ was used to model equivalent geometric imperfections in Abaqus (see Table 3.1). Figure 4.4 depicts the stress distribution in a 2 m long column from case 2 above at the point of ultimate load with areas in red equal to the material's yield stress and blue approximately half of that.

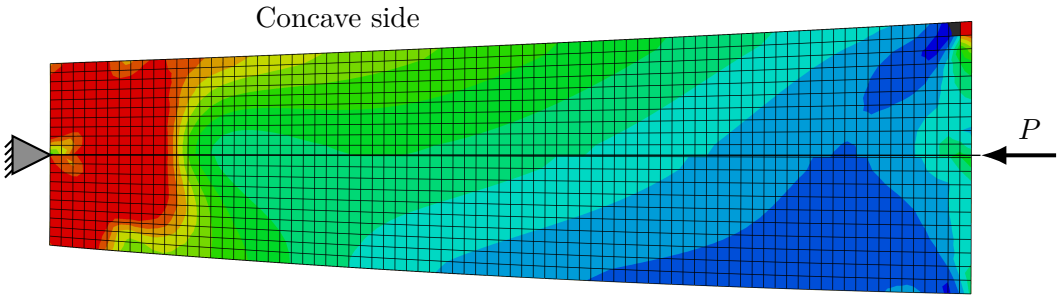


Figure 4.4: Web-tapered column stress at ultimate load

The critical cross-section in this case is clearly at the smallest end of the column, which is in line with the proposed design methodology. An anti-symmetric stress distribution can be seen to form around the longitudinal axis, as is to be expected when geometric imperfections are introduced. The flange on the concave side of the column is seen to transmit a larger portion of the load to the support at the other end. The ultimate axial load capacity found in this particular case was $C_r = 2565$ kN, which slightly exceeds the smallest section's yield capacity ($C_y = 2500$ kN).

The modes of failure for the columns in case 1 and 4 are depicted in the Figure 4.5. These represent the opposite limits of the range of structural failure observed, with cases 2 and 3 exhibiting behaviour somewhere between these modes. Columns from each case studied were noted to fail similarly throughout the length range, with more slender columns displaying marginally more flexural rotation and buckling at a location further up the column height. Conversely, the critical location for more stocky columns was progressively closer to the smaller end. For all practical purposes, failures were governed by the same mechanism, i.e. cross-sectional yielding, which is often seen with stockier columns.

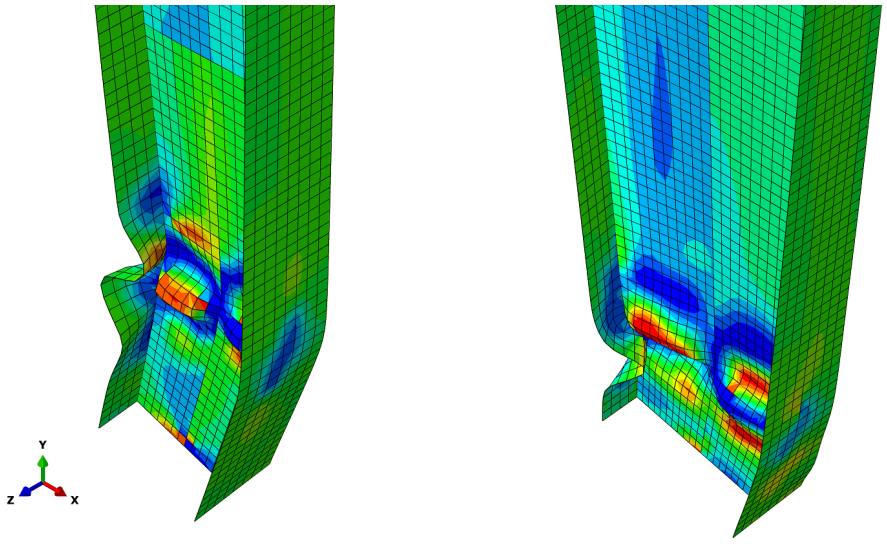


(a) Case 1 (b) Case 4

Figure 4.5: Typical web-tapered column squash deformation at smaller end experienced during investigation

Although columns were tested up to a height of 15 m, it was found that their equivalent slenderness always fell within the plastic and inelastic range for in-plane flexural buckling. This was due to the increased in-plane elastic critical buckling load produced by web-tapered columns leading to a lower value of $\lambda$ (see Equation 4.1).

An overview of the findings is presented in Figures 4.6 (a) to (d) along with an extract of the calculations in Appendix A.3. It can be seen that the proposed approach follows the elastic and flexural resistance curves predicted by SANS/CSA based on the smallest cross-section. The crucial difference lies in the determination of the equivalent slenderness parameter, which causes the predicted results of the proposed method to shift to a lower slenderness position along the SANS/CSA curve, thus enabling web-columns to be handled as stockier prismatic members and increasing the predicted capacity accordingly.

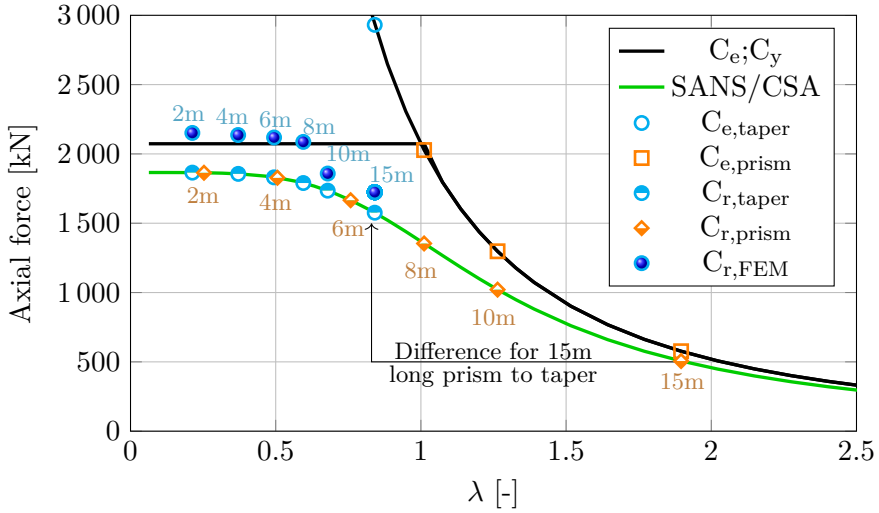


(a) Case 1: $\alpha$=2.5°, $h_{small}$=0.250 m

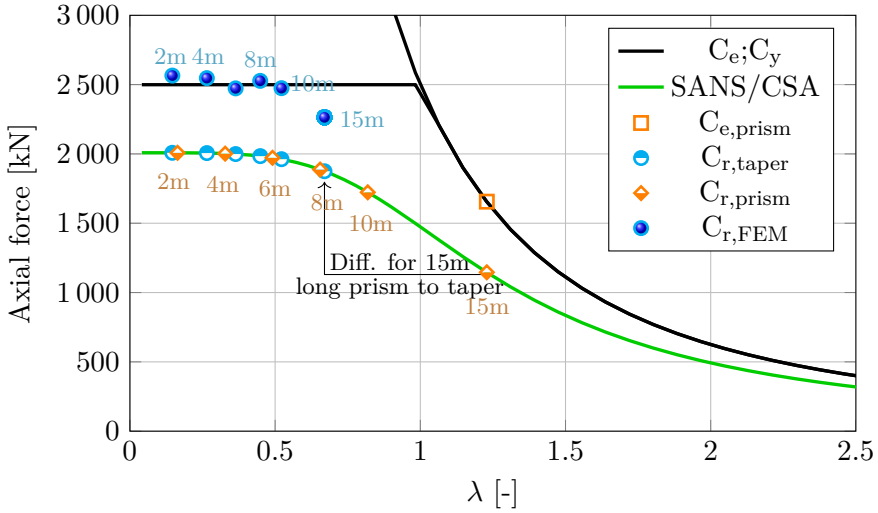


(b) Case 2: $\alpha$=2.5°, $h_{small}$=0.400 m

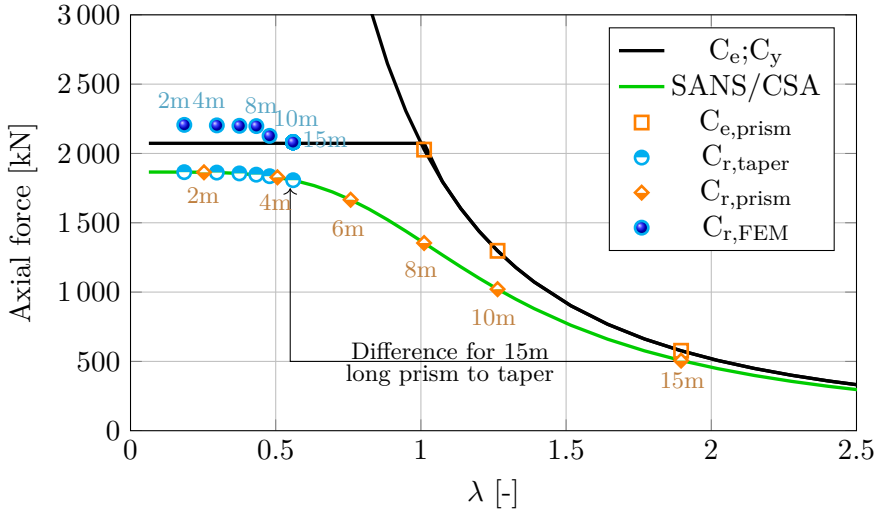


(c) Case 3: $\alpha$=5.0°, $h_{small}$=0.250 m

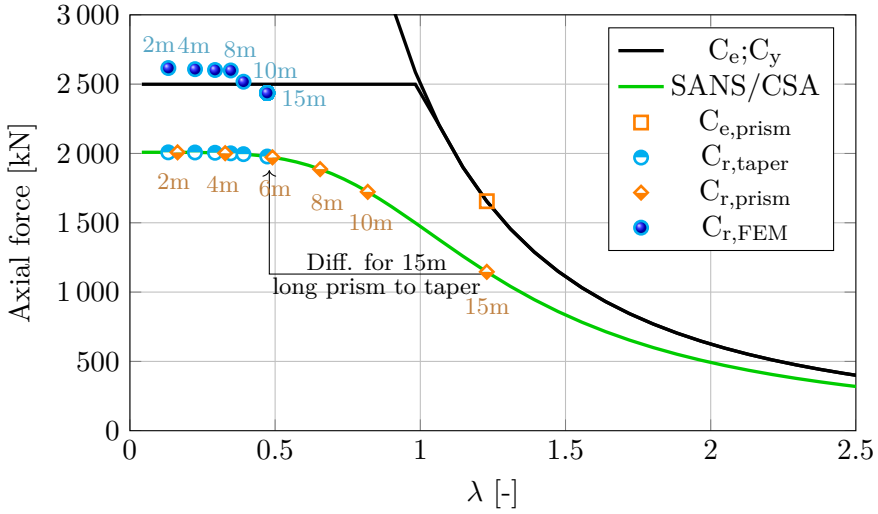


(d) Case 4: $\alpha$=5.0°, $h_{small}$=0.400 m

Figure 4.6: Results for web-tapered columns from the proposed design approach and finite element analysis

This method was validated in a process that required approximately 50 finite element analyses to be conducted for obtaining the mode shapes for imperfection modelling and eventual non-linear analysis. In all cases the proposed method was found to be safe when compared to the numerical procedures. In cases 1 and 2, a degree of inelastic behaviour was predicted by the proposed method, which correlated well with the decrease in axial compression resistance found in this region when using the numerical models. Cases 3 and 4 were generally found to be within the plastic region with the predicted results from the numerical procedure generally conforming to the axial yield capacity in these regions. The investigation did not deal with longer columns, as modelling of larger members becomes increasingly demanding of computing resources, while it was also decided that columns in excess of the current length limit are not feasible, as their web-plates become impractically large for manufacturing.

## 4.3 Web-tapered beams

### 4.3.1 Proposed design approach

In various parts of this paper thus far, the mode of failure of prismatic beams without continuous lateral support that restricts torsional twisting of the section was considered. This may lead to lateral-torsional buckling, which is considered for web-tapered beams in the following section.

The design procedure in DG25 allows for the use of slender flanges in flexure, resulting in an additional limit state to be considered, i.e. compression flange local buckling. By limiting the scope of study to exclude class 4 flanges (see Section 1.4), a simplified approach for capacity checks of web-tapered beams is proposed based on the flow diagram in Figure 4.7. This is due to the fact that SANS 10162-1 does not cover the design of beams with potential local instability in both a flange and the web. In such a case the designer has to consult the cold-formed steel specifications, which fall outside the scope of this study.

The simplified approach will be presented in terms of the SANS 10162-1 design specifications in Step 1 to Step 7. As the moment of resistance in SANS 10162-1 is calculated based on the critical elastic lateral-torsional buckling moment instead of stable lengths (as in AISC), no adaptation of the current SANS formulae is required and these may be readily applied to the proposed procedure below.

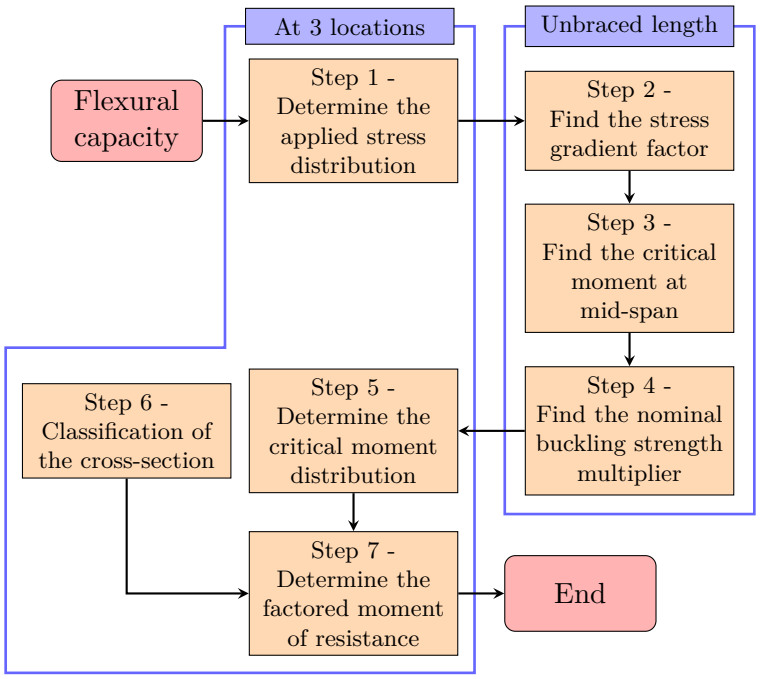


Figure 4.7: Design approach for web-tapered beams

**Step 1: Applied stress distribution**

The distribution of flexural stress in the compression flange must be determined through inspection at various locations. DG25 recommends inspection to be done at three locations, i.e. at both ends of the unbraced length and the middle.

**Step 2: Stress gradient factor**

Following the study by Kim (2010), the AASHTO method for determining the stress gradient factor ($C_b$) is recommended when used with Step 3 (see Section 2.3.2.2.1). It should be noted that a beam subject to double curvature has a unique stress distribution in each flange if both flanges are subject to compression stress at some point, requiring them to be considered separately. Thus, each flange will be defined by a unique value for $C_b$.

**Step 3: Preliminary critical elastic lateral-torsional buckling stress at mid-span**

The method investigated by Kim (2010), determines a preliminary critical elastic lateral-torsional buckling stress ($f_{cr,mid}$) for web-tapered beams using the mid-span properties. This may be done directly from Equation 2.11. The value of $f_{cr,mid}$ represents a basic value to be scaled later in Step 5.

**Step 4: Nominal buckling strength multiplier**

The use of the nominal buckling strength multiplier ($\gamma_{eLTB}$) was discussed in Section 2.3.2.2.1. The $\gamma_{eLTB}$ multiplier represents the ratio of $f_{cr,mid}$ to the maximum compression flange stress found through the inspection process in Step 1 and is used in scaling the stress found in the compression flange at several locations to a critical stress that signifies lateral-torsional buckling.

**Step 5: Final critical elastic lateral-torsional buckling moment distribution**

The previous two steps provide a convenient means to determine $f_{cr}$ at any position along the beam based on $f_{cr,mid}$ and the applied stress distribution in the compression flange. Although it may not be apparent, the method is synonymous with the computational methods used in prismatic beams for dealing with moment gradients. This is discussed further in Section 4.3.2.1.

**Step 6: Cross-section classification**

As an intermediate step, the cross-section at each inspection point must be classified for flexure according to table 4 in SANS 10162-1.

**Step 7: Moment of resistance**

Once the distribution of the critical stress in the compression flange is known for a given stress gradient, the moment of resistance at each inspection point can be calculated. The appropriate design formula is selected based on the cross-section classification at each of the specified locations. When dealing with class 4 webs, the moment of resistance should be reduced in accordance with section 14.3.4 of SANS 10162-1.

### 4.3.2 Verification of predicted web-tapered beam resistance

An important difference in the design of web-tapered beams is the consideration of stress in the compression flange rather than bending moments. The design approach for web-tapered beams that was presented in Section 4.3.1 is illustrated next for different beam configurations.

#### 4.3.2.1 Verification of the stress-based approach against prismatic beams

The stress-based approach for dealing with a web-tapered member remains applicable to a prismatic beam, i.e. when $\alpha = 0^o$. This is illustrated next for the 6 m prismatic beam in Figure 4.8 that consists of the cross-section from Table 3.2 and the end moment ratios ($\kappa$) of -1, 0 and 1.

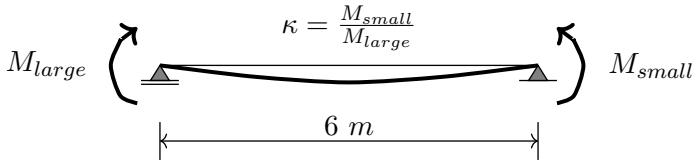


Figure 4.8: Definition of end moment ratio

#### 4.3.2.1.1 Prismatic beam under uniform bending moment

First, the fundamental and most adverse loading condition is considered when uniform bending moment is applied to the beam. The design of the prismatic beam is considered by following the steps of the proposed web-tapered beam design approach (see Figure 4.7).

1. An arbitrary bending moment is considered to be applied to the ends of the beam, of equal and opposite direction and thus causing a uniform internal bending moment of 100 kN.m. This equates to a constant compression flange stress of 106 MPa.

2. In Step 2 the stress gradient is determined using the AASHTO formula (Equation 2.22). On account of the uniform stress gradient in the compression flange determined in the previous step, no increase in the critical bending capacity is made ($C_b = 1$).

3. In Step 3 the critical moment based on the mid-span section properties is 178 kN.m, which is equivalent to a flange stress of 188.5 MPa for $f_{cr,mid}$.

4. The nominal buckling strength multiplier is determined in Step 4 using Equation 2.23 and is equal to $\gamma_{eLTB} = 1.779$.

5. In Step 5 the stress distribution in the compression flange is scaled by $\gamma_{eLTB}$ to find the stress distribution in the compression flange at the point of elastic lateral-torsional buckling. As the flange stress distribution is uniform for the particular case, the resulting $f_{cr}$ distribution becomes equal to $f_{cr,mid}$ throughout the length of the beam.

6. Next, in Step 6 the section classification is performed according to the SANS 10162-1 provisions. In the case considered, the flange is regarded as class 3 and the web as class 1, resulting in an overall section classification of class 3. Thus, the SANS 10162-1 equations for beams based on the yield moment are used.

7. Finally, the resistance moment distribution is calculated in Step 7. In this case a constant moment of resistance of $M_r = 160$ kN.m is found. When divided by the elastic section modulus of the prismatic beam, this results in a constant compression flange stress of $f_r = 169.7$ MPa.

A familiar design sequence can be seen when comparing the stress-based approach to load and resistance factor design. The method described above arrives at the same moment of resistance when compared to SANS 10162-1. The most notable difference is the recommended use of the AASHTO stress gradient factor in DG25 that is based on the research by Kim (2010). The results of the uniform case is shown for each step in Table 4.3.

Table 4.3: Beam utilisation under uniform bending moment: $\alpha = 0^o$, L = 6 m, 400x200 (8W, 10F)

| $\kappa$ [-] | Position [m] | Step 1 $f_{c\text{-flange}}$ [MPa] | Step 2 $C_b$ [-] | Step 3 $f_{cr,mid}$ [MPa] | Step 4 $\gamma_{eLTB}$ [-] | Step 5 $f_{cr}$ [MPa] | Step 6+7 $f_r$ [MPa] | Utilisation [%] |
|---|---|---|---|---|---|---|---|---|
| | 0 | 106.0 | | | | 188.5 | 169.7 | 62% |
| | 1 | 106.0 | | | | 188.5 | 169.7 | 62% |
| | 2 | 106.0 | | | | 188.5 | 169.7 | 62% |
| -1 | 3 | 106.0 | 1.00 | 188.5 | 1.779 | 188.5 | 169.7 | 62% |
| | 4 | 106.0 | | | | 188.5 | 169.7 | 62% |
| | 5 | 106.0 | | | | 188.5 | 169.7 | 62% |
| | 6 | 106.0 | | | | 188.5 | 169.7 | 62% |

The calculations above show that the beam is only loaded to 62% of its design resistance, and that each inspection point is equally utilised due to the even spread of compression flange stresses. A Riks non-linear analysis was conducted to study the distribution of stress using a maximum equivalent imperfection of $L/150$. Figure 4.9 provides a graphical illustration of the regular stress distribution seen throughout the length of the beam at the point of bifurcation, with some stress build-up noticeable at the concave edge of the top flange. The stress values as measured at the compression flange to web connection are reported below at various stages of loading and compared with the design values from Table 4.3.

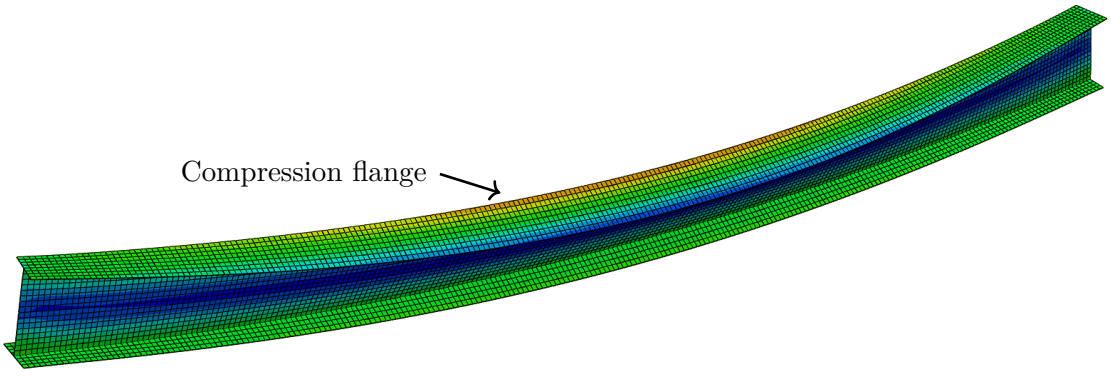


Figure 4.9: Deformation and Von Mises stresses for uniform bending moment at the point of bifurcation

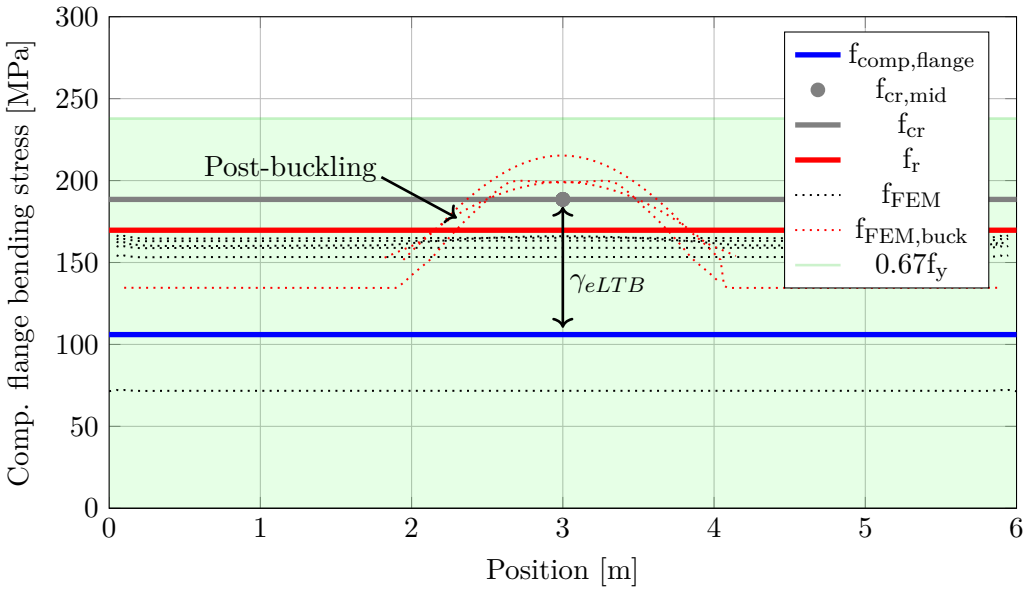


Figure 4.10: Compression flange stress distribution for uniform bending moment ($\kappa = -1$)

From Figure 4.10 it is observed how the steps from the stress-based approach interact with one another. As $f_{cr} < 0.67f_y$, the beam's moment of resistance is calculated based on $\phi f_{cr}$ when the SANS 10162-1 moment of resistance formulae (see Equation 2.19) are converted in terms of stress through division by the elastic section modulus. A very close correlation can be seen between the maximum attainable stress reported from the Riks analysis during the increments leading up to the predicted design resistance. Thereafter, rapid loss of stability is noted at mid-span as the stress build-up on the inner edge of the compression flange encroaches on the plate junction area with increasing lateral-torsional deformation. This is indicated as the post-buckling results that exceed $f_r$.

#### 4.3.2.1.2 Prismatic beam under non-uniform bending moment

The uniform moment case considered before illustrates a trivial design situation as any given cross-section is considered to be critical. The comparison is expanded in this section to include beams that are subjected to non-uniform stress gradients, where a unique critical location can be found.

**Triangular bending moment distribution ($\kappa = 0$)**

The first case studied was that of a triangular bending moment distribution, resulting from $\kappa = 0$. Here, a critical location arises from the non-uniform application of load at the end of the beam where the load is being applied. At this point the beam is stressed to 41% of the permitted stress for the given stress gradient and the stresses decrease to zero at the other end of

Table 4.4: Beam utilisation under triangular bending moment: $\alpha = 0^o$, L = 6 m, 400x200 (8W, 10F)

| $\kappa$ [-] | Position [m] | Step 1 $f_{c\text{-flange}}$ [MPa] | Step 2 $C_b$ [-] | Step 3 $f_{cr,mid}$ [MPa] | Step 4 $\gamma_{eLTB}$ [-] | Step 5 $f_{cr}$ [MPa] | Step 6+7 $f_r$ [MPa] | Utilisation [%] |
|---|---|---|---|---|---|---|---|---|
| | 0 | 106.0 | | | | 329.9 | 256.7 | 41% |
| | 1 | 88.3 | | | | 274.9 | 234.6 | 38% |
| | 2 | 70.7 | | | | 219.9 | 197.9 | 36% |
| 0 | 3 | 53.0 | 1.75 | 329.9 | 3.113 | 164.9 | 148.5 | 36% |
| | 4 | 35.3 | | | | 110.0 | 99.0 | 36% |
| | 5 | 17.7 | | | | 55.0 | 49.5 | 36% |
| | 6 | 0.0 | | | | 0.0 | 0.0 | 0% |

the beam. A characteristic of the procedure can be seen from the utilisation column in Table 4.4 where a constant usage percentage is found between the positions 2 m to 5 m. This results from $f_{cr} < 0.67 f_y$ in this region and $f_r$ being determined as a fraction of the $f_{cr}$. However, the critical elastic stress exceeds this limit at positions 0 m and 1 m, requiring the stress variant of Equation 2.18 to be used.

The region that is highly stressed on the one side of the beam is depicted in the figure below, which gives rise to an unsymmetrical deflected shape coupled with lateral-torsional deformation near the left hand side (the loaded end). The stress distribution in the compression flange at a moment close to structural failure is illustrated in Figure 4.12.

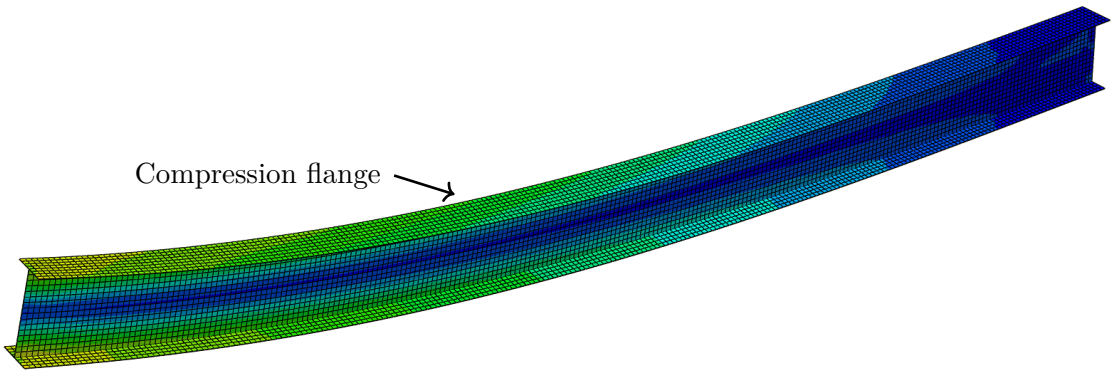


Figure 4.11: Deformation and Von Mises stresses for triangular bending moment at the point of bifurcation

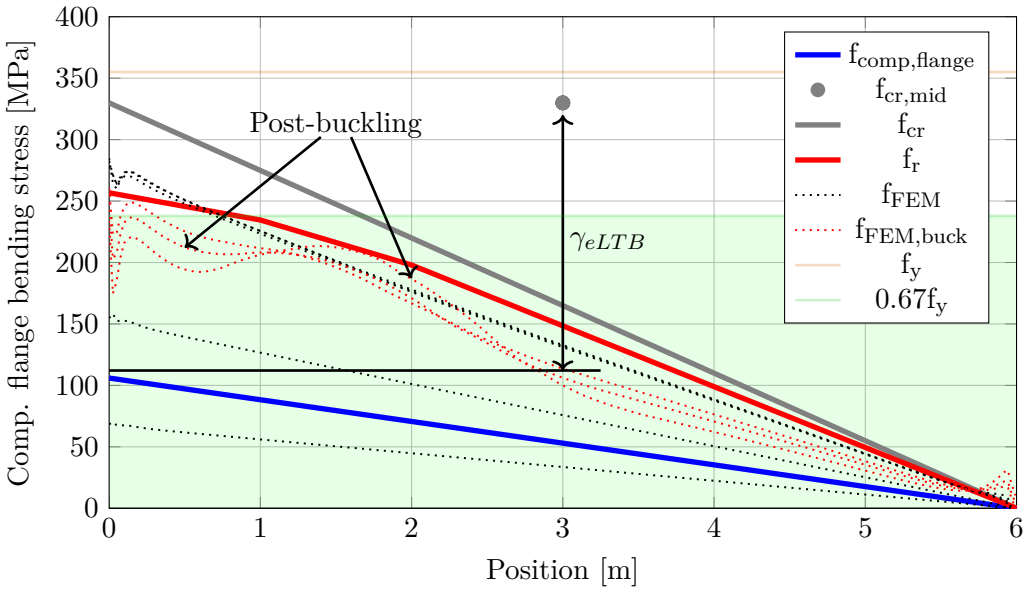


Figure 4.12: Compression flange stress distribution for triangular bending moment ($\kappa = 0$)

The benefit of the simplified approach for obtaining the distribution of elastic critical stress becomes apparent in the figure above. The scalar value of $\gamma_{eLTB}$ is found as the ratio of the elastic critical stress at mid-span to the maximum applied stress in the compression flange. In this instance the resisting stress permitted ($f_r$) between the positions 1 m and 6 m is $\phi f_{cr}$ as $f_{cr} < 0.67 f_y$. Thereafter, the gradient of $f_r$ changes due to the SANS beam formula for plastic-inelastic behaviour. The maximum allowed stress in the compression flange at the critical cross-section is equal to $f_r = 256.7$ MPa, which is equivalent to a moment of resistance $M_r = 242$ kN.m, as is also found when this configuration is designed using SANS 10162-1. The stress measurements from the numerical analysis show the incremental change in the stress gradient as it asymptotically approaches the predicted stress limit until it becomes almost parallel. The SANS 10162-1 marginally overestimated the allowable stress distribution when compared with the results obtained by Abaqus at the point of lateral-torsional instability. At this point the left hand side exceeds the predicted stress and lateral-torsional buckling manifests, similar to the previous example, but at a position of approximately 1.3 m from the loaded beam end.

### Double curvature moment distribution ($\kappa = +1$)

As a final review of the method, the situation is considered where double curvature is induced through the application of end moments that are equal in both size and direction. This results in a double curvature deformation that is designated as $\kappa = +1$ and leads to an increase in the stress gradient factor equal to the limit allowed by AASHTO of 2.3. Table 4.5 provides an overview of the calculation results.

Table 4.5: Beam utilisation under double curvature bending moment: $\alpha = 0^o$, L = 6 m, 400x200 (8W, 10F)

| $\kappa$ [-] | Position [m] | Step 1 $f_{top\text{-}flange}$ [MPa] | Step 2 $C_b$ [-] | Step 3 $f_{cr,mid}$ [MPa] | Step 4 $\gamma_{eLTB}$ [-] | Step 5 $f_{cr}$ [MPa] | Step 6+7 $f_r$ [MPa] | Utilisation [%] |
|---|---|---|---|---|---|---|---|---|
| | 0 | 106.0 | | | | 433.6 | 283.2 | 37% |
| | 1 | 70.7 | | | | 289.1 | 241.1 | 29% |
| | 2 | 35.3 | | | | 144.5 | 130.1 | 27% |
| +1 | 3 | 0.0 | 2.30 | 433.6 | 4.091 | 0.0 | 0.0 | - |
| | 4 | -35.3 | | | | -144.5 | -130.1 | 27% |
| | 5 | -70.7 | | | | -289.1 | -241.1 | 29% |
| | 6 | -106.0 | | | | -433.6 | -283.2 | 37% |

A symmetric utilisation curve applies with two critical positions noted at the ends of the beam (37% utilisation) and a point of zero stress at the centre of the beam. The critical stress at the central inspection positions, i.e. 2 m, 3 m and 4 m, are determined to fall within the $0.67f_y$ = 237.9 MPa limit, with the resistance stress in the remaining positions calculated based on the plastic/inelastic behaviour. The distribution of stress is again shown visually, as determined using finite element analysis in Figure 4.13 and summarised along with the design results in Figure 4.14.

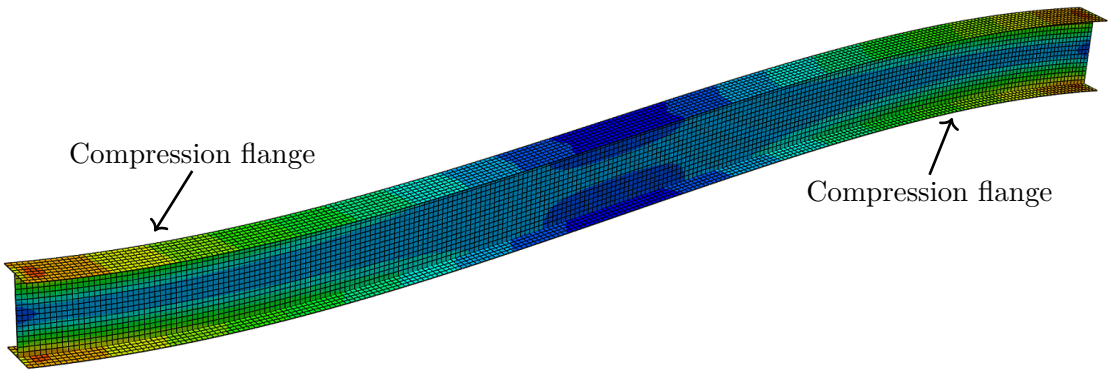


Figure 4.13: Deformation and Von Mises stresses for double curvature bending moment at the point of bifurcation

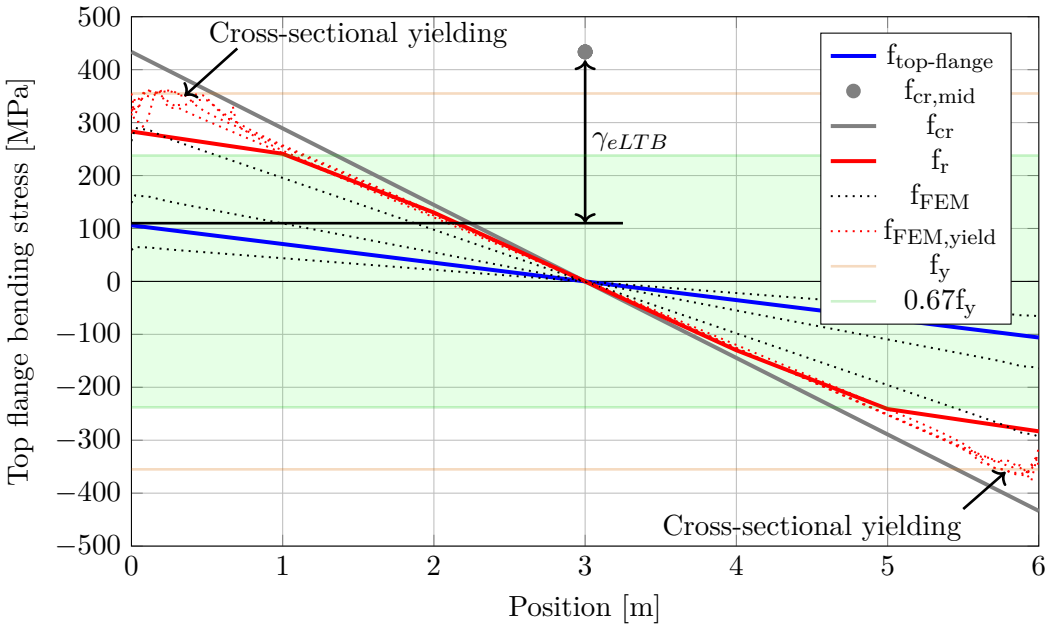


Figure 4.14: Compression flange stress distribution for double curvature bending moment ($\kappa = +1$)

The symmetrical utilisation is observed above and reported in terms of the top flange stress. The maximum stress allowed to form at either end of the beam is equal to $f_r = 283.2$ MPa, corresponding to $M_r = 267$ kN.m (equal to SANS 10162-1). The readings from the numerical analysis progressively increase by rotating around the central inspection point where the stress is zero. A linear stress reading is noted that eventually reaches the maximum permissible limit predicted for top flange stress, whereafter capacity soon deteriorates near the beam ends. This is due to the redistribution of stress into the web, as the failure mechanism is characterised by cross-sectional yielding with limited out-of-plane deformation observed at the first point of structural failure.

To conclude, the stress-based approach was considered for prismatic beam members and highlights several aspects in conventional member design that may not always be apparent. This is due to designs being based on the critical cross-section where the highest internal stress prevails. To this end, the stress is dependent on the internal bending moment diagram ($\kappa$) and the cross-sectional properties, which are regarded as uniform in prismatic beams. Thus, the critical cross-section is easily identifiable for prismatic beams.

#### 4.3.2.2 Stress-based approach for web-tapered beam design

Beams with linearly varying web depths are studied in this section. This brings another design variable into consideration, namely tapering angle ($\alpha$). The critical cross-section can no longer be intuitively located as both the internal forces and the section modulus are non-uniform. The

stress-based approach holds the advantage of being able to reduce the number of variables that have to be actively considered when dealing with web-tapered members, by focussing only on the stress in the compression flange. Essentially, the procedure that was outlined in the previous section for dealing with stress gradients is again employed to take into account the variation in cross-sectional properties.

Beams with angles of taper $\alpha = 2.5^{o}$ and $5.0^{o}$ were studied to investigate the stress-based approach adapted from DG25. The beams are 6 m in length with the cross-section at the smaller end defined by the properties in Table 3.2. The different load configurations examined are presented in Figure 4.15 below with an arbitrary bending moment of 100 kN.m at one or both ends. End moment ratios, $\kappa$ of -1, 0 and +1 were considered, with the moment in $\kappa = 0$ applied either to the smaller or larger end. The latter case was designated as $\kappa = 0^{*}$.

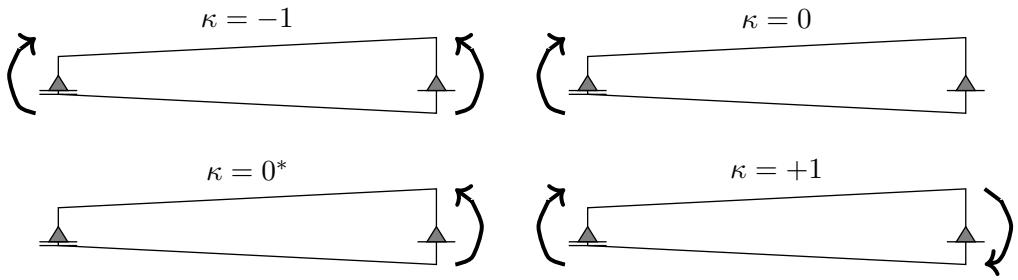


Figure 4.15: Applied bending moment to web-tapered beams

**Design of web-tapered beams with $\alpha = 2.5^{o}$**

The procedure required the applied stress to be scaled according to $\gamma_{eLTB}$ to determine the critical flange stress, on which the allowable compression stress ($f_r$) is based. The calculations for the design of these web-tapered beams are presented in Appendix B. In these calculations the locations where the web plate becomes classified as class 4 are indicated by an asterisk and the moment of resistance decreased according to section 14.3.4 in SANS 10162-1.

The predicted bending resistances were compared with results obtained from various finite element models. To simulate the flaws associated with geometric and material imperfections, an equivalent geometric imperfection of $L/100$ was used in modelling the beams. This accounted for the slender section classification typically found at the larger end of the beams and corresponds to the most conservative imperfection bow from Table 3.1. The Von Mises stress distribution at the point of failure for each of the loading configurations is indicated in Figure 4.16 below.

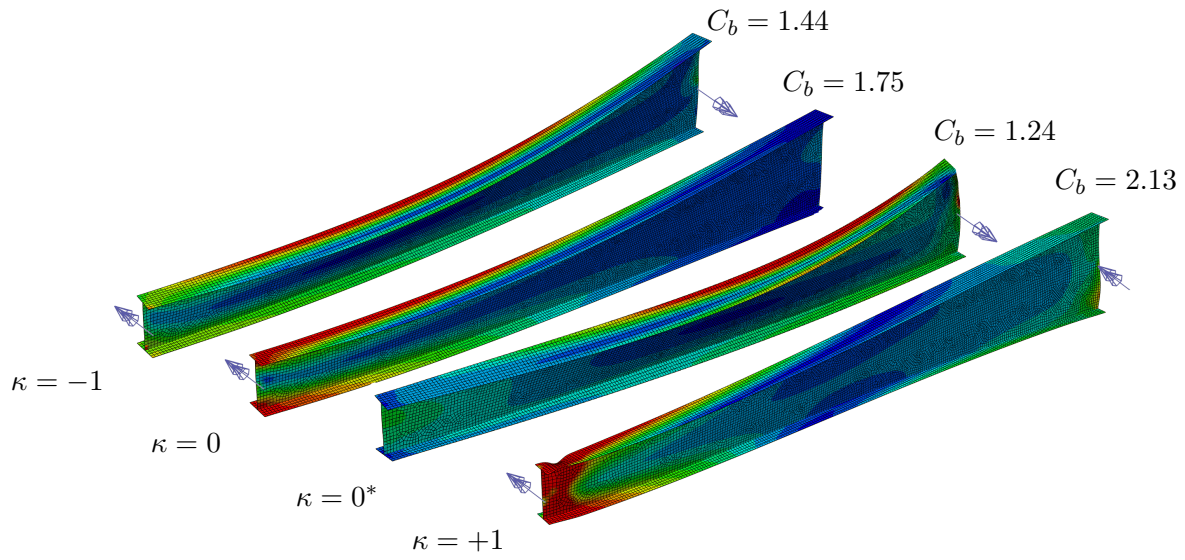


Figure 4.16: Deformation and Von Mises stresses for 2.5° web-tapered beams

In the first three instances (namely $\kappa = -1$, 0 and $0^*$) the beams displayed lateral-torsional buckling as modes of failure. Here, the maximum out-of-plane deflection was found at positions at the centre of the beam or near the beam end that was loaded in bending. However, the beam for $\kappa = +1$ displayed cross-sectional yielding at the smaller end, resulting from the increased critical buckling load resulting from a steep stress gradient ($C_b = 2.13$). A graphical overview of the top flange stress distributions is presented in Figure 4.17.

Good correlation can be observed between the stress curves patterns produced by the allowable flange stress and the Riks analysis results for the top flange. Furthermore, the results are accurate to conservative, as the numerical results in all cases were able to reach the predicted capacity or remained stable past this point. Figure 4.17 (a) to (c) shows how the stress distribution rapidly changes near the centre of the beam after the ultimate load has been reached as lateral-torsional buckling takes place. Quite different stress curves are seen to form between the two cases with a single end moment. Although the magnitude of the applied moment is the same (and linear) a concave or convex upward stress curve results on account of the change in section modulus for $\kappa = 0$ and $\kappa = 0^*$, respectively. This resulted in different stress gradient values to be determined when using the AASHTO method. As mentioned before, lateral-torsional buckling was not noted for $\kappa = +1$, where instead the smaller beam end failed via cross-sectional yielding. This mode of failure can be seen in the stress diagram in Figure 4.17 (d) where the smaller beam end reaches the material's yield point. It is interesting to note that the load configuration $\kappa = 0$ also nearly reached this point but failed in lateral-torsional buckling first with a pertinent post-buckling increase forming between the inspection locations 1 m and 2 m.

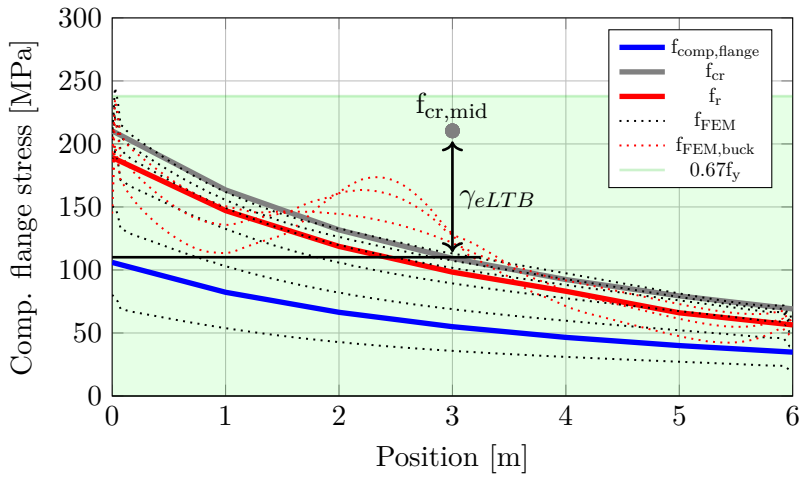


(a) $\kappa = -1$

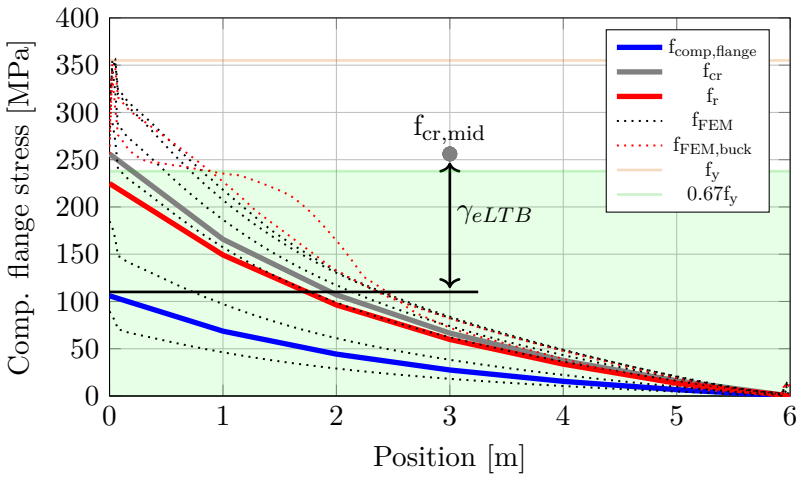


(b) $\kappa = 0$

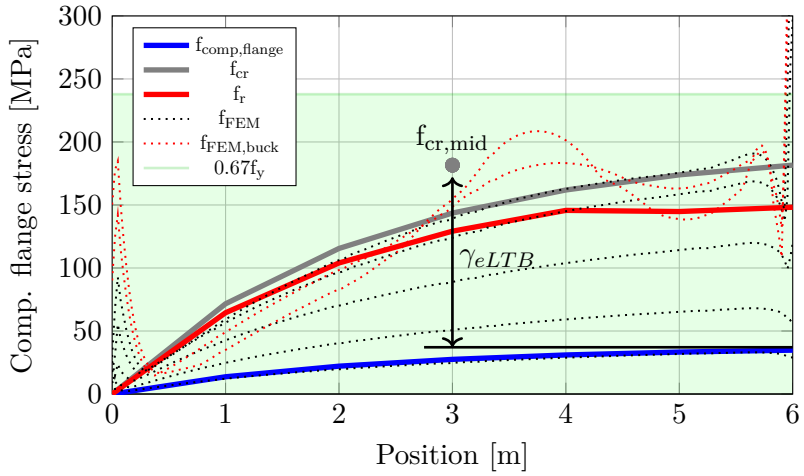


(c) $\kappa = 0^*$

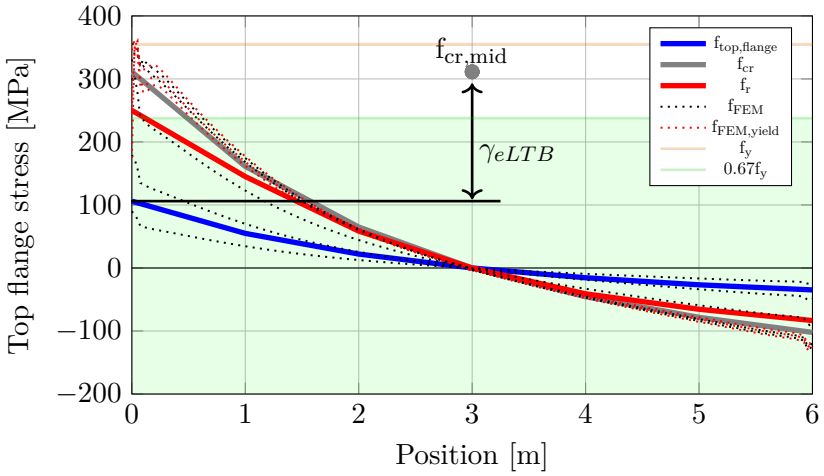


(d) $\kappa = +1$

Figure 4.17: Results for web-tapered beams with $\alpha = 2.5^o$ from the proposed design approach and finite element analysis

**Design of web-tapered beams with $\alpha = 5.0^o$**

In this set of beams under the same loading actions the angle of taper was increased to $\alpha = 5.0^o$. The results of the proposed approach are available in Appendix B. The change in section modulus leads to different stress curves in the compression flange and new values for $C_b$, as seen in Figure 4.18, when compared with the beams discussed before.

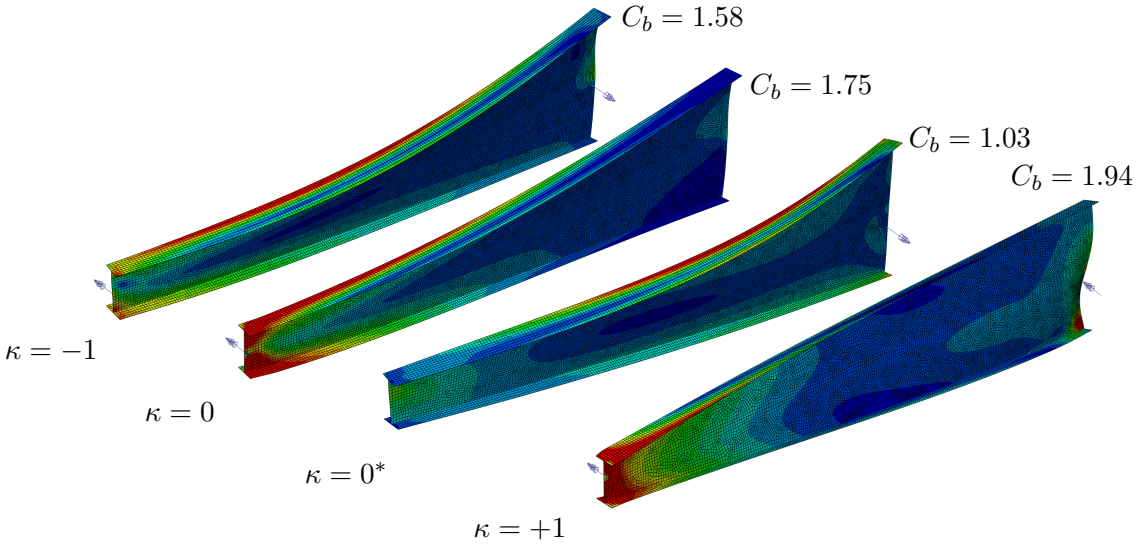


Figure 4.18: Von Mises stress distribution for 5.0° web-tapered beams

By analysing the beams using full non-linear finite element analysis, it was found that lateral-torsional buckling only governed as the mode of failure for $\kappa = -1$ and $0^*$, while cross-sectional yielding occurred at the small end in the case of $\kappa = +1$ (see Figure 4.18). A combination of these two mechanisms develop for $\kappa = 0$ at the ultimate load and can be attributed to the increased average in-plane stiffness that decreases rotation in the deeper parts of the beam. The results for the increased angle of taper are presented in Figure 4.19.

In Figure 4.19 a similar set of stress curve patterns can be observed as before. Again, safe results were obtained in all cases as the stable stress curves exceed the predicted limits. The conservatism is, however, increased with the larger tapering ratios, attributed to the $\gamma_{eLTB}$ scaling procedure from DG25 to obtain the critical stress distribution, which is known to be an oversimplification. To compensate for this, DG25 permits the critical stress curve to be determined by more sophisticated methods that can accurately predict out-of-plane buckling.

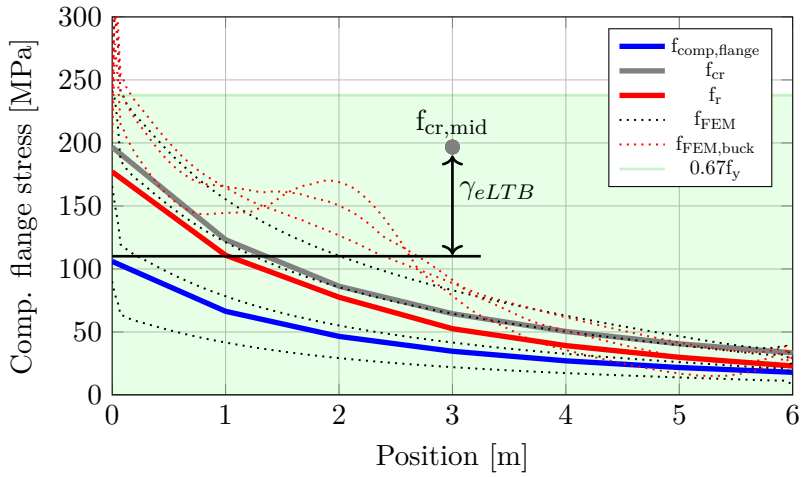


(a) $\kappa = -1$

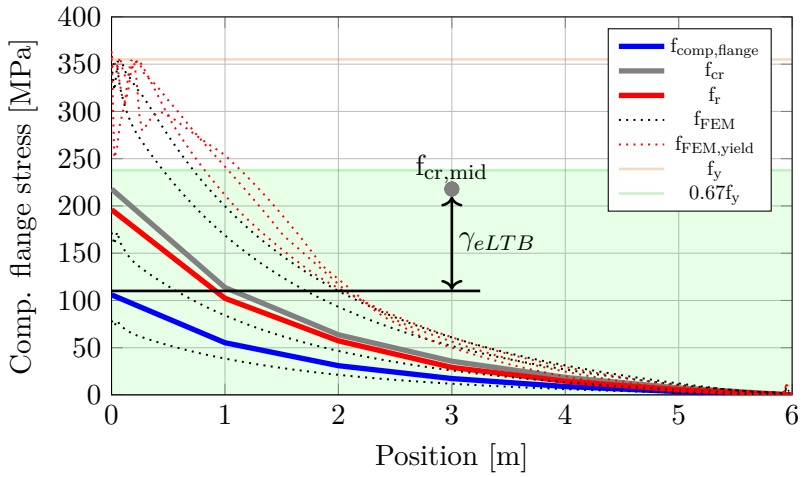


(b) $\kappa = 0$

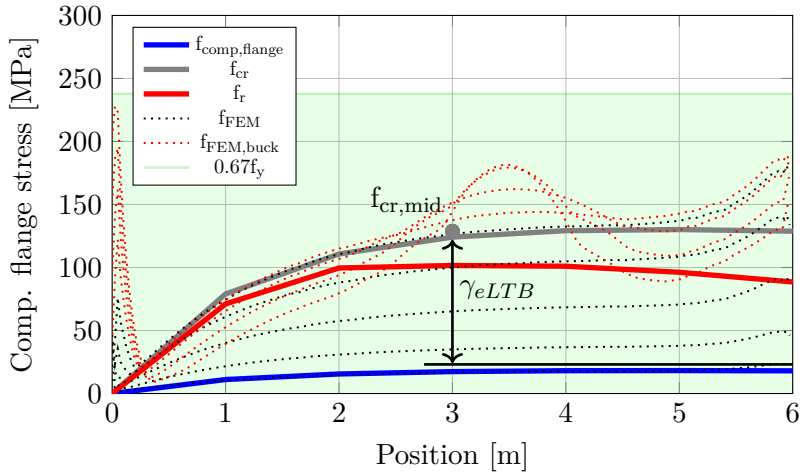


(c) $\kappa = 0^*$

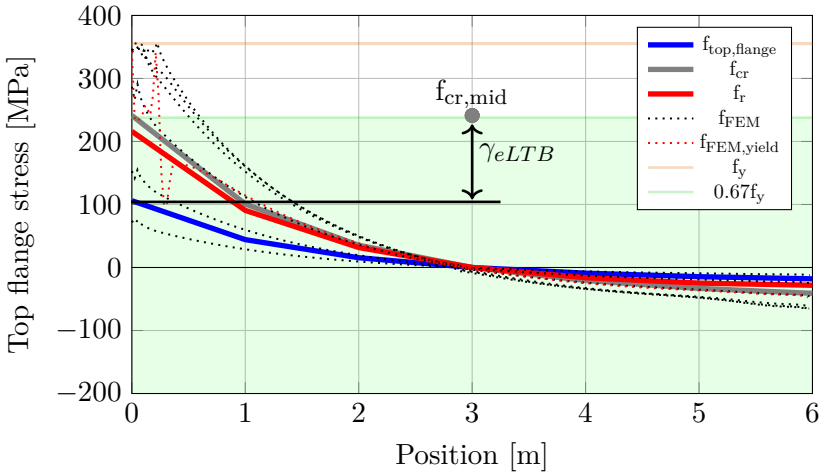


(d) $\kappa = +1$

Figure 4.19: Results for web-tapered beams with $\alpha = 5.0^o$ from the proposed design approach and finite element analysis

#### 4.3.2.2.1 Review of the DG25 scaling procedure for lateral-torsional buckling

The preceding discussion proves that the scale factor method by DG25 for determining the critical elastic stress distribution succeeds in replicating the stress curves produced during finite element analysis for small angles of taper. Reasonably accurate and consistently safe allowable stress distributions were predicted with the proposed approach for modest angles of taper, without resorting to advanced procedures to determine the elastic lateral-torsional buckling loads of web-tapered members.

However, it was found that the predicted resistance tends to become overly conservative of the critical stress for larger angles of taper. This might be attributed to the inability of the DG25 method to account adequately for the inclination of the flanges. This can typically only be addressed using shell elements or the specialised finite beam elements developed by the likes of Boissonnade and Maquoi (2005), Andrade, Camotim, and Dinis (2007), and Jeong (2014) as discussed earlier in Section 2.5.4. In the research by Kim (2010), on which DG25 is based, high levels of conservatism was specifically noted for the singly symmetric I-beams when subjected to reverse curvature.

# Chapter 5

# Development of an automated design and optimisation procedure for portal frames

## 5.1 Introduction

The next objective of this study, as defined in Section 1.3, is to determine the weight savings benefit of optimally designed portal frames consisting of web-tapered members, as opposed to conventional prismatic plate-girders.

The genetic algorithm concept was selected to perform this task as it is well suited to dealing with the discrete search spaces typically found in the field of structural optimisation. The current chapter describes the implementation of the genetic algorithm by regularly referring to the underlying theory presented in Section 2.6.2. Here, the Matlab numerical computing environment is used to implement the algorithm by first verifying the optimisation procedure against a mathematical test function before extending it to problems of an engineering nature.

The optimal portal frame will be determined using an automated structural analysis procedure based on Timoshenko beam elements and the proposed design approach for web-tapered members from the previous chapter. This approach is based on DG25 and verified in Chapter 4 for use in both prismatic and web-tapered member design according to SANS 10162-1. This design approach was selected as none of the design specifications considered could design web-tapered member or required detailed finite element analysis to be performed for each member. Also, the procedures for attaining the critical buckling loads can be predicted on a routine basis with this approach, making it ideal for the structural optimisation technique employed here.

## 5.2 Verification of the optimisation procedure

The genetic algorithm consists of several components that mimic species behaviour in nature. In principle, the role of the algorithm is to produce a population of solutions that is allowed to reproduce and improve based on desirable traits that are of interest to the user. Formal definitions vary throughout literature and lead to various implementations of this process. Figure 5.1 illustrates the genetic algorithm used in this study, where the reproduction process is controlled through a combination of selection, elitism and crossover with mutation as clarified in Section 2.6.2.

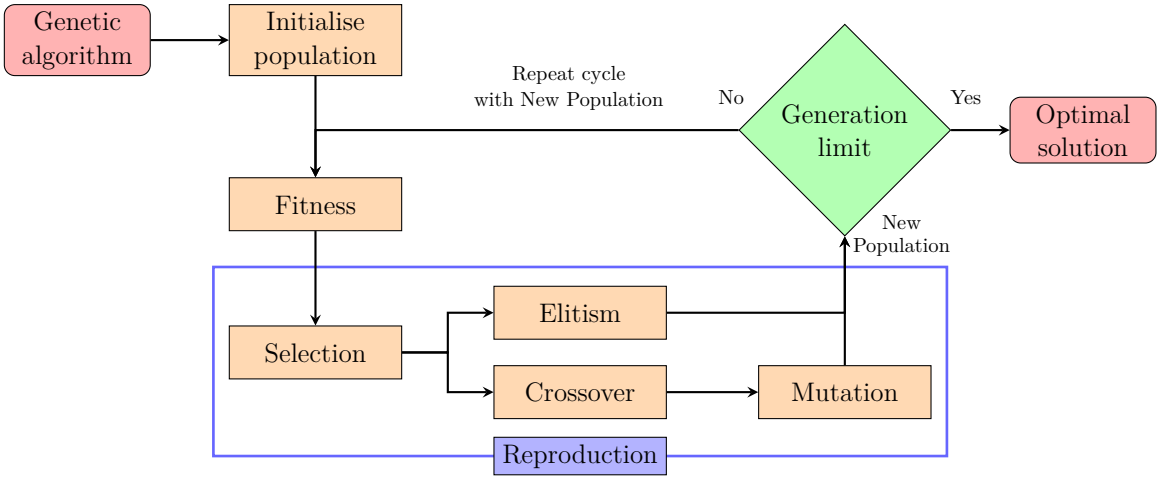


Figure 5.1: Flow diagram of genetic algorithm

The optimisation procedure was evaluated for a purely mathematical problem, before using the GA for structural optimisation in Section 5.3. Several test functions are available as a means to evaluate optimisation algorithms, with known mathematical optimisation targets. Popular test functions often encountered in research, describing continuous mathematical solutions, are available from Molga and Smutnicki (2005). The performance of the genetic algorithm was tested for the so-called "six-hump camel back function" with two variables ($x$ and $y$), as presented in Equation 5.1 and Figure 5.2.

$$S(x,y) = \left(4 - 2.1x^2 + {}^1\!/_3 x^4\right) x^2 + (x \cdot y) + (-4 + 4y^2)y^2 \tag{5.1}$$

In Figure 5.2, six regions of local minima are visible of which two locations are both regarded as the global minima with equal values. In the domain defined by $-2 \leq x \leq 2$ and $-1 \leq y \leq 1$, the known global minima are:

$$S(x,y) = -1.0316 \text{ at } (-0.0898, 0.7126) \text{ and } (0.0898, -0.7126) \tag{5.2}$$

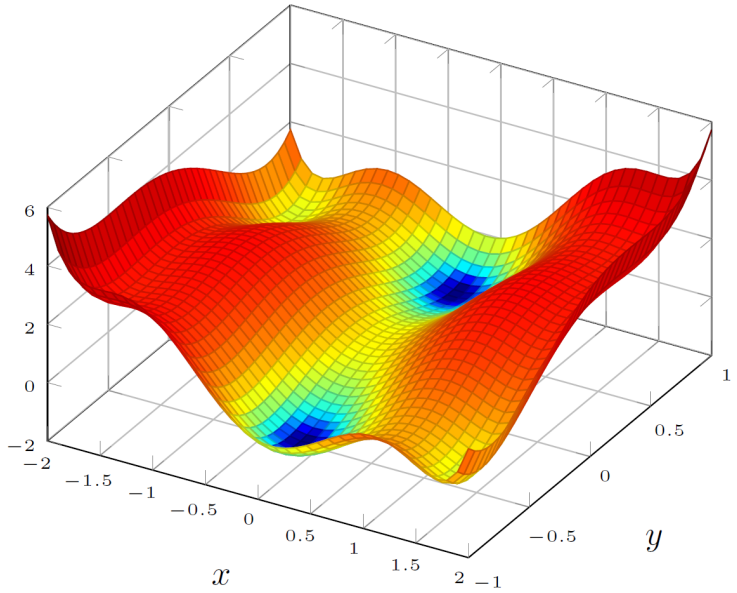


Figure 5.2: Six-hump camel back mathematical test function

The position of the global minimum for $S(x, y)$ is determined by inspecting a limited number of the coordinates within the domain. The GA generates an initial population of chromosomes, which represent a set of possible solutions from randomly selected coordinates (genes), $x$ and $y$. The fitness is readily determined by inserting the coordinates into Equation 5.1 for a solution. As a correct solution is obtainable for any position within the domain, the mathematical formula is continuous and no penalty function is required. All the solutions are sorted by rank in ascending order for the value of $S(x, y)$. Thus, the top ranked solution corresponds to the lowest value as the search is for the global minimum. Here, the reproduction process in Figure 5.1 is simulated using a split between directly transferring the fittest solutions to the next generation (elitism) and the pairing of the fittest solutions using the two-point crossover procedure with a uniform mutation. The mutation operator is employed to introduce new properties into the system. This aids in introducing new genes into the population when mostly poor properties exists that would only replicate into offspring with similar traits. The newly obtained population recirculates back to the fitness function and the process is repeated until the maximum generation limit has been reached. The total number of generations was kept constant at 100 to evaluate the effect of population size and operator parameters on the results and computing time, as summarised in Table 5.1.

Table 5.1: Genetic algorithm parameters and results for the six-hump camel back function

| Case | Population size | Crossover proportion ($p_c$) | Mutation proportion ($p_m$) | Location x | Location y | S(x,y) | Run time |
|---|---|---|---|---|---|---|---|
| A | 500 | 0.8 | 0.2 | -0.0909 | 0.7125 | -1.0316 | 11 sec |
| B | 500 | 0.5 | 0.8 | 0.0906 | -0.7103 | -1.0316 | 11 sec |
| C | 1000 | 0.8 | 0.2 | -0.0884 | 0.7115 | -1.0316 | 32 sec |
| D | 1000 | 0.5 | 0.8 | 0.0888 | -0.7100 | -1.0316 | 33 sec |
| E | 2000 | 0.8 | 0.2 | -0.0890 | 0.7130 | -1.0316 | 109 sec |
| F | 2000 | 0.5 | 0.8 | -0.0918 | 0.7137 | -1.0316 | 112 sec |

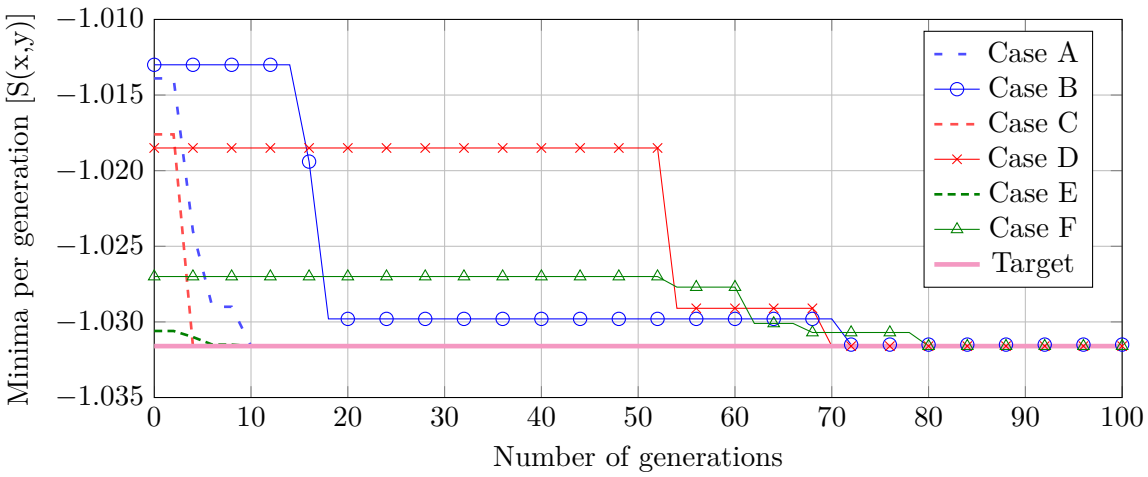


Figure 5.3: Genetic algorithm historical results for the six-hump camel back function

In all the cases the target value of $S(x, y) = -1.0316$ was reached in the vicinity of one of the two global minima. It is evident from Figure 5.3 that each run took a different and unpredictable path, but eventually converged to the target value. The unpredictable paths are due to the random method used to populate the initial set of solutions. The cases with the smallest population (cases A and B) typically started with the poorest sets of initial solutions, while the largest populations (cases E and F) had a higher probability of containing better solutions from the outset to replicate into improved solutions. However, by considering the balance between exploiting better properties in the system (crossover) and exploring new properties (mutation) the time required to complete each run can be drastically reduced. Thus, a small population could prove to be equally effective in finding the optimal solution.

## 5.3 Structural optimisation procedure

The mathematical function presented above consists of a continuous surface, defined by two variables $(x, y)$ and a solution $(S)$, which can be represented graphically in three dimensions. As problems in structural optimisation tend to consist of a vast number of discrete variables, the search space becomes discontinuous and disjointed. The genetic algorithm is well suited to these types of problems as it navigates the search space without prior knowledge of the landscape in search of the optimal valid solution. The implementation of each of the components required for structural optimisation is outlined in the sections that follow.

### 5.3.1 Implementation of the genetic algorithm to structural problems

The GA that was used to verify the optimisation procedure in the previous section was altered to include the structural engineering components in the form depicted by Figure 5.4.

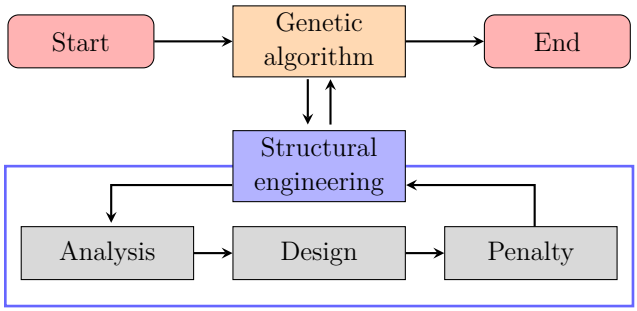


Figure 5.4: Flow diagram of genetic algorithm with structural optimisation functions

The GA initialises a population of chromosomes, where each gene is selected at random from a list of discrete values that describe the plate element size. This initial population and subsequent generations thereof are evaluated in the structural engineering component of the algorithm. During each generation, several structural analyses are performed to determine the forces to be withstood for each solution, followed by member capacity checks in the design function. If it is found that the capacity of any single solution is inadequate, a penalty is registered against that solution in proportion to the degree of insufficiency and reported back to the genetic algorithm. This value is then used to alter the fitness of inferior solutions by making them less desirable for reproduction into the next generation. As the objective here is to find the lightest possible structure, the penalty is applied by increasing the weight of the inadequate frames.

A dynamic penalty was employed with the constants $c = 0.05$ and $\alpha = 1.5$ as defined in Section 2.6.2.7. This scheme did not penalise borderline solutions harshly during the early stages of the algorithm, but increased the penalty severity during later generations. A rank-based selection procedure is then implemented to sort all the solutions per generation according to the

number of constraint violations followed by their modified weight. The top 20% of solutions of each generation was allowed to progress into the next generation without any alteration through the process of elitism. Furthermore, the first 80% of solutions was paired using a two-point crossover and replaced by the newly formed offspring in the new generation. This corresponds to a value for $p_c = 0.8$. These offspring also underwent a uniform mutation with 20% of all new genes in a generation being altered at random ($p_m = 0.2$). The newly formed population was then reintroduced into the GA until the prescribed number of generations had been completed. The final solution to the structural optimisation should then fulfil all the design requirements and succeed in reaching a near optimal solution.

### 5.3.2 Analysis function

In this function, a structural analysis is implemented using the direct stiffness method coupled with an automated stepped-representation procedure. In this regard, several prismatic beams of varying size are used to simulate the distribution of mass and stiffness throughout a portal frame. This process tends to create finite beam elements that are short in relation to their overall depth and cause the formation of ill-conditioned stiffness matrices that overestimate the in-plane stiffness of beams. This effect is avoided through the use of Timoshenko beam elements with the theory that was established earlier in Section 2.5.2.

By performing a structural analysis, the unknown degrees of freedom were determined by the known deformations and external forces using primal-dual solvers. A linear elastic analysis was selected as the contribution of second-order effects on portal frames is relatively small. To account for different load combinations, each solution iterates through a unique set of external forces representing each load combination, resulting in multiple deformation and force vectors for the Ultimate Limit State (ULS) and Serviceability Limit State (SLS). A limited number of load combinations were selected for this study to bring about the most severe cases under gravitational load or upward thrust. The following combinations of Dead Load (DL), Live Load (LL) and Wind Loads (WL) were considered that included action combination factors.

$$\begin{aligned} \text{ULS1} &= (1.2)\text{DL} + (1.6)\text{LL} \quad \text{(Unfavourable)} \\ \text{ULS2} &= (0.9)\text{DL} + (1.3)\text{WL} \quad \text{(Favourable)} \end{aligned} \tag{5.3}$$

$$\begin{aligned} \text{SLS1} &= (1.1)\text{DL} + (1.0)\text{LL} \quad \text{(Unfavourable)} \\ \text{SLS2} &= (1.0)\text{DL} + (0.6)\text{WL} \quad \text{(Favourable)} \end{aligned} \tag{5.4}$$

Equations 5.3 and 5.4 lead to multiple load cases that have to be evaluated in the design function against the member capacities. The unfavourable and favourable ULS load combinations bring about bending moment diagrams that describe sagging or uplift of the structure as shown in Figure 5.5.

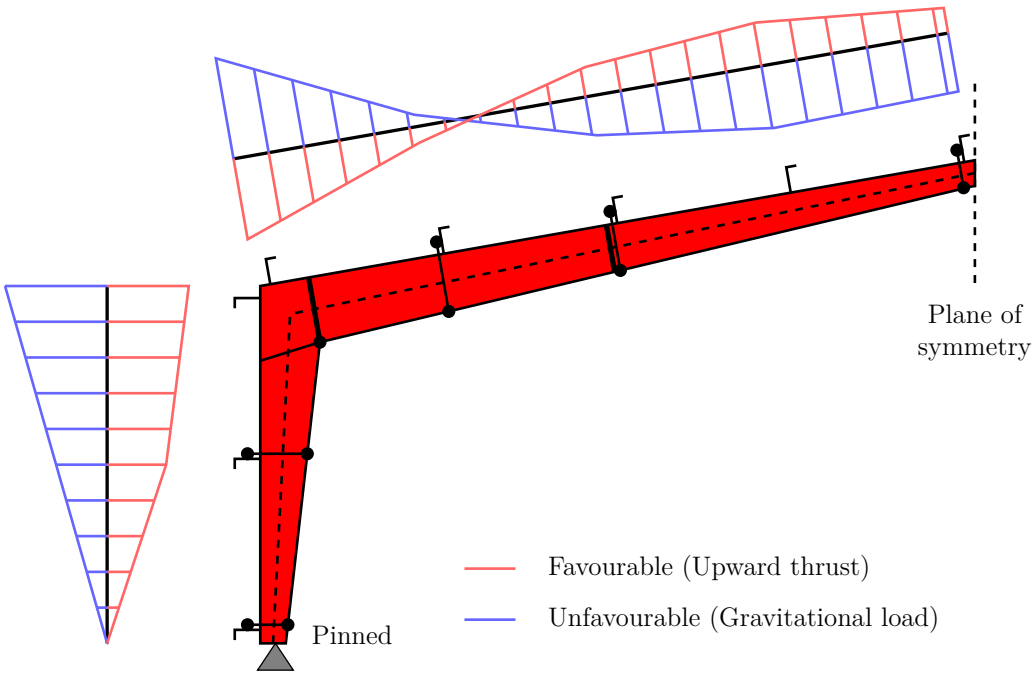


Figure 5.5: Bending moment diagrams for unfavourable and favourable load combinations

MBS buildings are typically constructed with vertical cladding systems to the walls by slanting the columns inward when dealing with web-tapered frames, as seen in the illustration above. This results in a shift of the nodal connection position in the finite element analysis where member centrelines intersect. This point of intersection constantly changes due to the different plate dimensions received from the genetic algorithm. The structural analysis considered this attribute for each frame and recalculated the new nodal positions that describe the frame geometry of each solution considered.

Notional loads were applied with all load combinations in accordance with SANS 10162-1 equal to 0.5% of the total factored gravitational load at the eaves in the direction of the dominant lateral forces.

### 5.3.3 Design function

The implementation of the design function is considered next as part of the structural optimisation procedure. The resistance utilisation ratios that are determined here will later be used to evaluate each solution received from the genetic algorithm.

#### 5.3.3.1 Combined axial compression and bending resistance

The resistance of portal frames under the combined influence of axial compression and bending is considered for the required checks of overall member strength and lateral-torsional buckling strength. The interaction equation in SANS 10162-1 is condensed to Equations 5.5 and 5.6 below as the factor accounting for $P-\delta$ and moment gradient effects ($U_1$) will be assumed to be equal to unity. This assumption is made as portal frames are classified as unbraced structures where this assumption is permitted in SANS 10162-1 and due to the relatively small axial loads witnessed in standard portal frames.

$$\frac{C_u}{C_r} + \frac{0.85M_{u,x}}{M_{r,x}} \leq 1.0, \qquad \text{if class 1 or 2} \tag{5.5}$$

$$\frac{C_u}{C_r} + \frac{M_{u,x}}{M_{r,x}} \leq 1.0, \qquad \text{if class 3 or 4} \tag{5.6}$$

In Chapter 4, a simplified design approach was proposed for the design of web-tapered members based on the methodologies from DG25. The most significant benefit of the simplified procedure is that it provides a means to perform member resistance calculations on a routine basis and predict the critical buckling loads of web-tapered members. The buckling loads would otherwise require sophisticated numerical modelling techniques that are inefficient and difficult to implement in the automated design and optimisation procedure. This approach to web-tapered member design was verified extensively against full non-linear analyses and found to be accurate to conservative throughout Chapter 4. The resistances used in each of the strength checks are summarised as follows:

Overall member strength:

1. $C_r$ is calculated using the web-tapered column design approach of Section 4.2.1 for in-plane axial resistance.
2. $M_{r,x}$ is determined according to section 13.5 of SANS 10162-1 using the bending resistance of the smallest cross-section over the length of a member.

Lateral-torsional buckling strength:

1. $C_r$ was determined in this study by only considering the weak-axis flexural resistance using the cross-sectional properties midway between lateral-torsional restraints of a beam.
2. $M_{r,x}$ is found using the web-tapered beam design approach in Section 4.3.1 that considers lateral-torsional buckling.

#### 5.3.3.2 Combined axial tension and bending resistance

The two interaction formulae from SANS 10162-1 in Equations 5.7 and 5.8 will be considered to evaluate the combined effect of axial tension and bending. This could typically occur when portal frames are subjected to upwards thrust induced by wind loads.

$$\frac{T_u}{T_r} + \frac{M_u}{M_r} \leq 1.0 \tag{5.7}$$

$$\frac{M_u}{M_r} - \frac{T_u \cdot Z}{M_r \cdot A} \leq 1.0 \tag{5.8}$$

In the equations above $T_u$ and $M_u$ represent the applied tensile force and bending moment in the member respectively, while $T_r$ and $M_r$ are used for the tensile and bending moment resistances. The section modulus ($Z$) and $M_r$ are defined based on the elastic or plastic properties, depending on the cross-section classification. In the latter equation, $M_r$ will be determined using the design approach for web-tapered beams. The interaction equations are then inspected at the ends and middle of each unbraced beam segment.

#### 5.3.3.3 Shear resistance

The contribution of inclined flanges in web-tapered members to the shear forces in the web will be assumed to be negligible. This assumption allows the shear resistance to be determined using conventional formulae, based on the recommendation by Galambos (1988). The shear capacity ($V_r$) will be evaluated on a cross-sectional basis using the following equation, where $V_u$ is the factored shear force.

$$\frac{V_u}{V_r} \leq 1.0 \tag{5.9}$$

with,

$$V_r = \phi \cdot h_w \cdot t_w \cdot f_s$$

The ultimate shear stress ($f_s$) in Equation 5.9 is determined in accordance with section 13.4.1 of SANS 10162-1. It will be assumed for the calculation of $f_s$ that transverse stiffeners are spaced far apart in relation to the web height of the members. This results in a constant shear buckling coefficient, with $k_v = 5.34$, and no tension-field stress after buckling ($f_t = 0$).

### 5.3.4 Penalty function

The role of the penalty function is considered next as the final component of the structural engineering procedure that was depicted earlier in Figure 5.4.

The genetic algorithm is naturally applicable to dealing with unconstrained optimisation problems, where all solutions in the search space are feasible, as illustrated by the mathematical test function in Section 5.2. However, the portal frames have to comply with specific design criteria that constrain the number of feasible solutions in the search space. The portal frame solutions that are found to be invalid are dealt with by increasing their total structural weight, which amounts to decreasing their fitness. This increase in weight makes them less likely to be recirculated into subsequent generations.

The penalty function is incorporated into the optimisation procedure to fulfil this task by differentiating between solutions that are structurally sound and those that transgress the limits imposed in terms of member capacity or deflection. In this regard, the penalty function receives information from the structural analysis and design functions in Sections 5.3.2 and 5.3.3. Each violation recorded is stored for that solution. When all the checks are completed, the dynamic penalty is implemented by penalising invalid solutions according to the number of violations.

The individual member capacities are checked against the internal forces that arise under ULS loading conditions based Section 5.3.3. The displacements under the serviceability limit state are evaluated using the allowable deflection criteria for industrial buildings in annexure D of SANS 10162-1 of height/200 and span/180 for horizontal and vertical deformation, respectively.

# Chapter 6

# Optimal portal frame results and comparisons

## 6.1 Introduction

In the previous chapter, an automated design procedure was proposed, based on the design approach presented in Chapter 4. This approach is a simplification of Design Guide 25 and suitable for the design of both prismatic and web-tapered members. The automated procedure is capable of optimising designs to find the lightest possible portal frame through the use of a genetic algorithm.

The potential of web-tapered portal frames to reduce material consumption is reviewed in this chapter by considering the results from the genetic algorithm for several portal frame geometries. The conditions will be established for the study of optimal portal frames, whereafter the optimal results from the genetic algorithm are presented for two types of frame elements, i.e. conventional plate-girders and web-tapered members. Preliminary conclusions about the material usage are made for these frame elements that is followed by a review of the optimal frame capacities.

The optimised portal frame designs derived from the genetic algorithm will also be compared with designs produced by a commercial software package for MBS buildings.

## 6.2 Conditions accepted for portal frame optimisation

Until this point, only the implementation of the structural optimisation procedure was discussed. The conditions that describe the portal frames that will be optimised regarding the chromosome structure, load cases and positions of lateral restraint are detailed next. These factors are important and have a marked influence on the constraints that are imposed by the automated design and optimisation procedure.

### 6.2.1 Assembly of the genetic algorithm chromosome

The structural optimisation procedure receives information from the genetic algorithm in the form of chromosomes. Each chromosome consist of the information necessary to describe different structural configurations that will be analysed. The portal frame in Figure 6.1 was considered for this study and consists of equal-flange I-shaped members. Assuming the frame to be symmetrical, a chromosome length of 10 (variables 1 to 10) is used to define a web-tapered frame. Conversely, a shortened chromosome with a length of 8 variables is used for portal frames constructed from prismatic plate-girders as variables $1 = 2$ and $6 = 7$. The dimensions of plate thickness or plate width as stipulated in Table 6.1 defines each variable (or "gene") in the chromosome.

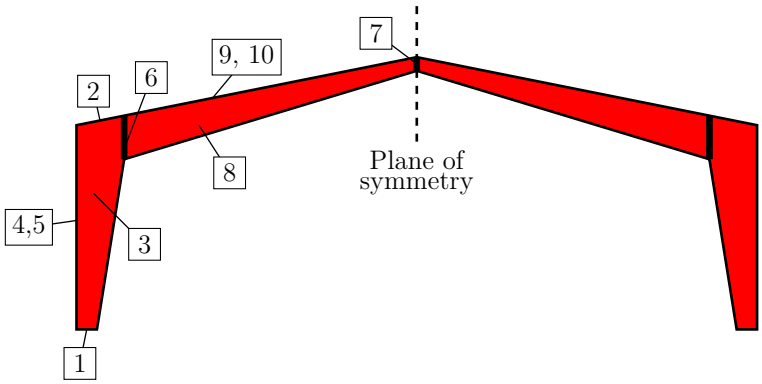


Figure 6.1: Chromosome variable identification

The plate widths are assumed to be cut in increments of 10 mm from hot-rolled plates with standard thicknesses. The limit for the minimum thickness was set at 6 mm to avoid plate distortion during the welding process. The maximum and minimum plate widths were selected between 250 mm and 1500 mm as this represents the range of plate sizes that typical automated submerged arc welding machines can accommodate.

The total number of solutions in the search space is calculated as the product of the number of discrete values per variable and equates to 20.9 trillion solutions. To put this into perspective, if each solution could be calculated and evaluated in 0.1 seconds, it would require 663 centuries to evaluate all the possible combinations. The GA only requires a fraction of this time to find (near) optimal solutions.

Table 6.1: Design variables considered for web-tapered portal frames

| Variable | Dimension | Discrete values [mm] | Number of discrete values |
|---|---|---|---|
| 1 | Web width | 250 : +10 : 1500 | 126 |
| 2 | Web width | 250 : +10 : 1500 | 126 |
| 3 | Web thickness | 6, 8, 10, 12 | 4 |
| 4 | Flange width | 130 : +10 : 300 | 18 |
| 5 | Flange thickness | 6, 8, 10, 12 | 4 |
| 6 | Web width | 250 : +10 : 1500 | 126 |
| 7 | Web width | 250 : +10 : 1500 | 126 |
| 8 | Web thickness | 6, 8, 10, 12 | 4 |
| 9 | Flange width | 130 : +10 : 300 | 18 |
| 10 | Flange thickness | 6, 8, 10, 12 | 4 |

### 6.2.2 Loading conditions investigated

The portal frames are subjected to a fixed set of external loads. The forces were selected to provide typical load magnitudes found in portal frames, while being simple to replicate when verified against commercial software. Table 6.2 lists these uniformly distributed loads with an illustration provided in Figure 6.2.

Table 6.2: Applied loading to portal frames

| DL [kN/m$^2$] | LL [kN/m$^2$] | $WL_1$ [kN/m$^2$] | $WL_2$ [kN/m$^2$] | $WL_3$ [kN/m$^2$] | $WL_4$ [kN/m$^2$] |
|---|---|---|---|---|---|
| 0.25* | 0.25 | 0.40 | 1.00 | 0.65 | 0.40 |

*Excluding the own weight of the primary frame

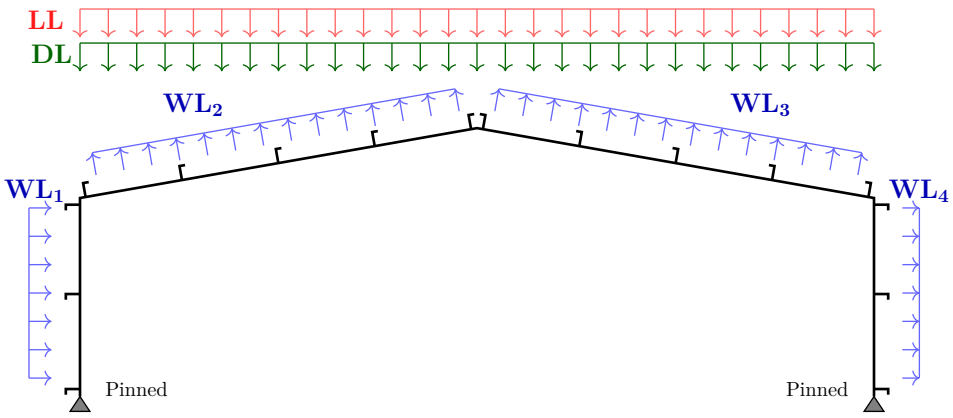


Figure 6.2: Applied loading to portal frames

The loads caused by the cladding systems, secondary frame members, and services are included in DL, while the own weight of the primary framing is excluded on account of it being dependent on the specific solution that is considered. To this end, the weight and its distribution are calculated dynamically for each portal frame configuration that is analysed. The provisions in SANS 10160-2 for inaccessible roofs under general operating conditions were used to determine LL. A simplified wind load case was selected that excluded regions of localised high wind pressure. These uniform loads are of a magnitude commonly found when designing portal frame structures according to SANS 10160-3. Furthermore, only a single wind direction was considered to limit the number of load case iterations required from the structural analysis program and induce uplift thrust. The wind load selected assumed the wind to act only from one direction and directly into an open doorway, thus creating a positive internal pressure and a net upward thrust on the frame. This simplification was made as routine wind load calculations for different portal frames were excluded from the scope of the study.

### 6.2.3 Portal frame case studies

In total, four portal frame geometries are investigated using the automated design and optimisation procedure from the previous chapter. The frame geometries studied are summarised in Table 6.3.

Table 6.3: Summary of portal frame case studies

| Case study | Eaves height [m] | Span [m] | Rafter slope | Frame spacing [m] |
|---|---|---|---|---|
| 1 | 4.5 | 20 | 1:10 | 5 |
| 2 | | 30 | | |
| 3 | | 40 | | |
| 4 | | 50 | | |

The frames are first optimised using only prismatic plate-girders to establish the frame weight thresholds when using conventional design techniques. After that, the process is repeated with web-tapered members. The results of the portal frames optimised by these two methods will then be compared to determine the material savings benefit when using web-tapered members.

The presence and positions of lateral supports to the primary framing have a marked impact on the stability of a structure. The structural capacity of a portal frame can be maximised by providing lateral support that is continuous or at regular intervals, but this becomes impractical and costly. Lateral support can be provided by purlins, side girts and knee-bracing, but is typically specified only when and where it is required. Usually, the product specifications will dictate the attachment point for the cladding systems on the external flanges, while any excessive compression stress in the interior flange will require the addition of a knee-brace.

It was decided to use the lateral support positions as determined by a commercial MBS software program. The commercial design drawings are available in Appendix C for each of the frames studied and show all the positions where lateral support is provided. By using these points of support, the designs produced by the automated procedure can be compared to those by commercial software.

## 6.3 Results for optimal portal frame size and weight using the genetic algorithm

The optimisation algorithm was run for each case study using either prismatic or tapering members as methods for construction. The algorithm ran a total of 40 times for the different cases (five times per construction method for each of the four frames) with an average run-time of 35 minutes. At the commencement of each cycle, a unique solution was generated that differed from the other runs, but reached similar optimal weights for either of the two construction methods. Figures 6.3 (a) to (d) present the historical results, which show that the algorithm succeeded in identifying near optimal solutions during the prescribed number of generations (100).

If the process started off with a feasible but heavy frame it progressively decreased in weight through the generations. However, if it started with a frame that was not feasible, as in the case of span lengths between 30 m and 50 m, the algorithm increased the overall weight of the portal frame until a solution was obtained that complied with the design constraints. After that, a gradual decrease took place until the optimal solution emerged.

When viewing the historical results, it is clear that the algorithm is initially very active, with improved solutions found at frequent intervals. However, in the later part of a run the optimal solution sometimes stagnates over several generations, followed by a series of improved results. This behaviour is attributed to the mutation operator that introduces new genes into the population. The introduction of this added diversity caused new combinations to form, through the crossover operator, which explains the short succession of subsequent improvements.

Certain groupings emerged from the data in Figure 6.3 that either described prismatic or web-tapered portal frames. The results indicate a decrease in the overall weight of the portal frames when using web-tapered members in comparison with conventional prismatic members. The optimal frames are considered next to evaluate the material savings potential for each type of portal frame.

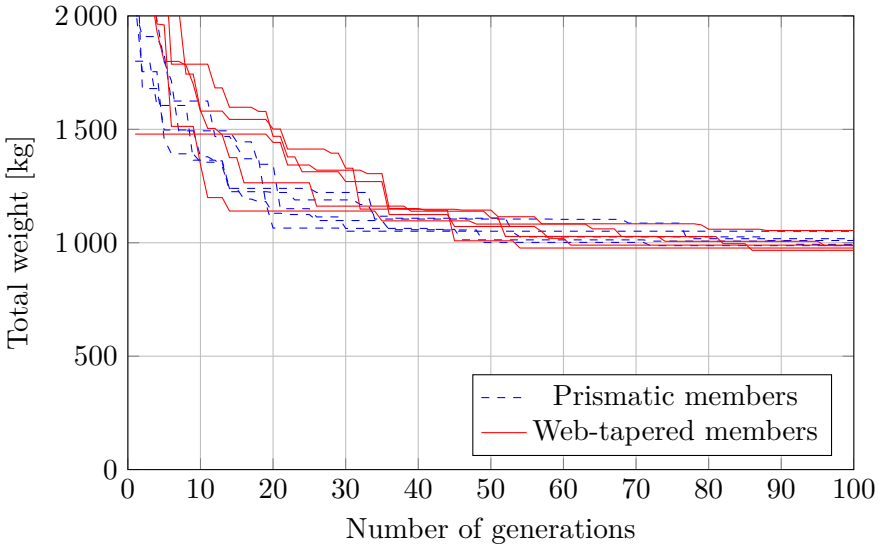


(a) Case study 1: 20 m x 4.5 m

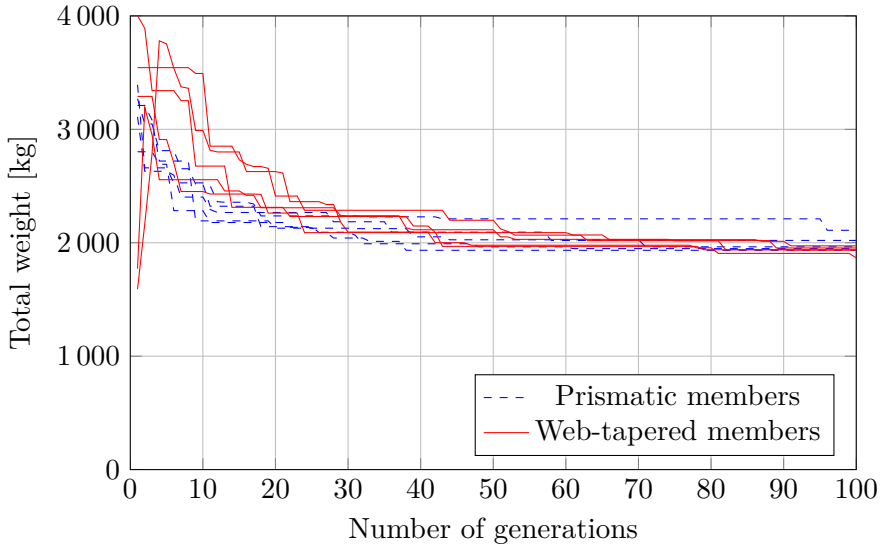


(b) Case study 2: 30 m x 4.5 m

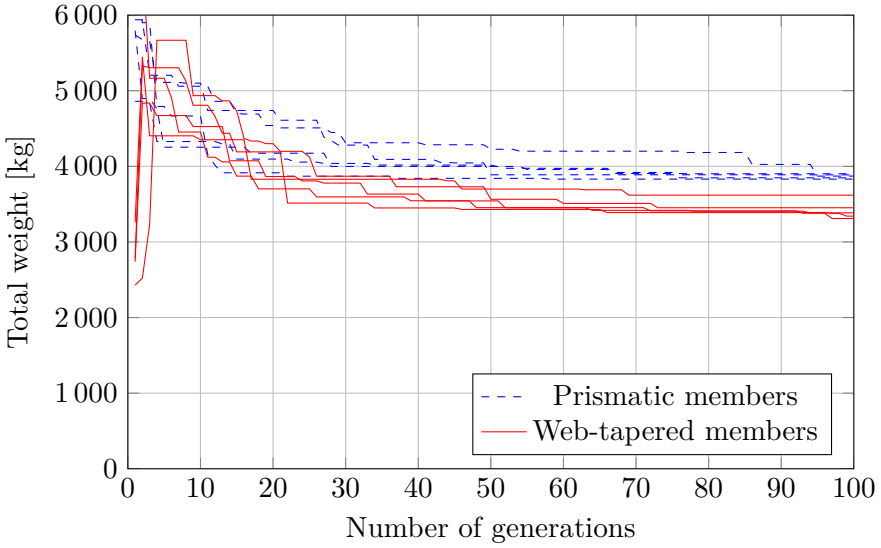


(c) Case study 3: 40 m x 4.5 m

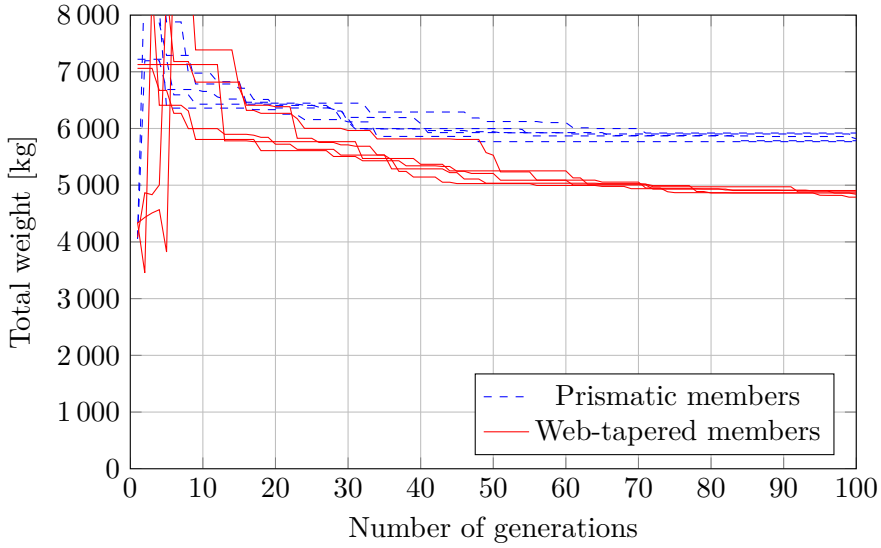


(d) Case study 4: 50 m x 4.5 m

Figure 6.3: Results for the optimisation of portal frames

### 6.3.1 Preliminary findings concerning reduced material requirements by web-tapered portal frames

Table 6.4 presents the optimal solutions for the portal frames in terms of plate dimensions and total weight. Progressively larger members that correlate to the increase in clear span length were required for both construction methods. The algorithm identified optimal combinations without any bias regarding the expected solution. This disregard is especially noted for the column in the 40 m x 4.5 m web-tapered frame. In this case, the algorithm opted for a shallow web depth (250 mm) at the bottom in combination with a relatively deep beam (730 mm) at the top and a thicker web plate, in contrast with the web plates used for the web-tapered span lengths of 30 m and 50 m.

Table 6.4: Summary of the optimal results found for each portal frame

| Case study | 20 m x 4.5 m | 30 m x 4.5 m | 40 m x 4.5 m | 50 m x 4.5 m |
|---|---|---|---|---|
| Prismatic portal frames | | | | |
| Column: | | | | |
| $h_w$ [mm] | 310 | 360 | 490 | 710 |
| $t_w$ [mm] | 6 | 6 | 6 | 10 |
| b [mm] | 150 | 180 | 190 | 210 |
| $t_f$ [mm] | 8 | 10 | 12 | 12 |
| Rafter: | | | | |
| $h_w$ [mm] | 300 | 470 | 800 | 910 |
| $t_w$ [mm] | 6 | 6 | 6 | 6 |
| b [mm] | 130 | 150 | 200 | 240 |
| $t_f$ [mm] | 8 | 10 | 12 | 12 |
| Weight [kg] | 988 | 1933 | 3831 | 5768 |
| Weight per area [kg/m$^2$] | 9.88 | 12.89 | 19.16 | 23.07 |
| Web-tapered portal frames | | | | |
| Column: | | | | |
| $h_{w,bot}$ [mm] | 260 | 290 | 250 | 280 |
| $h_{w,top}$ [mm] | 310 | 390 | 730 | 1190 |
| $t_w$ [mm] | 6 | 6 | 8 | 6 |
| b [mm] | 150 | 180 | 200 | 200 |
| $t_f$ [mm] | 8 | 10 | 10 | 12 |
| Rafter: | | | | |
| $h_{w,bot}$ [mm] | 300 | 570 | 720 | 1310 |
| $h_{w,top}$ [mm] | 290 | 370 | 250 | 250 |
| $t_w$ [mm] | 6 | 6 | 6 | 6 |
| b [mm] | 130 | 140 | 210 | 200 |
| $t_f$ [mm] | 8 | 10 | 12 | 12 |
| Weight [kg] | 969 | 1868 | 3310 | 4790 |
| Weight per area [kg/m$^2$] | 9.69 | 12.45 | 16.55 | 19.16 |
| Weight difference [%] | -1.9 | -3.4 | -13.6 | -17.0 |

An interesting tendency was noted where the optimum column size was found to be smaller than the rafter size near the eaves connection, regardless of the method of construction. By studying the results during the generations leading up to the final solutions, it was noted how different combinations could exist with nearly the same frame weights but an entirely different arrangement of plate elements. Here, small column sections with larger rafter sections could easily make way for the opposite relation between the two without significant variation in the material required. The different geometries that are feasible with nearly the same weight savings potential indicated that the search space could be described as "flat" with no clearly defined optimal solution found during the investigation.

The frame weights displayed a divergence between the two construction methods at longer spans lengths. This growing difference in material saving is indicative of the findings by Firoz et al. (2012), who agreed that web-tapered construction is most economical in longer span applications. The difference was found to be insignificant at spans smaller than 30 m, but becomes pronounced during the investigation of longer spans, as seen in Table 6.4 and Figure 6.3. At the maximum span, this difference in material requirements was found to be 17% lower when using web-tapered members instead of conventional prismatic plate-girders. This reduction is largely attributed to the efficient use of material near the points of restraint and the removal of excess self-weight from the rafters near the centre ridge. Based on these results, significant benefits were noted preliminarily by using web-tapered portal frames in long span applications to reduce steel consumption.

## 6.4 Examination of the structural optimisation procedure

The optimised portal frames are considered next by inspecting the displacements and load capacity of the individual members found in the structure. The genetic algorithm automatically generates a design and optimisation report after each run. The report contains information regarding the solutions from the start of the algorithm and a summary of the final optimal structure. The summary includes information on the displacements, internal forces and the design constraints during each load combination. An extract of the 50 m x 4.5 m web-tapered portal frame report is available in Appendix D.

### 6.4.1 Comparison of the structural analysis according to displacements

The maximum displacements as determined by the genetic algorithm under the serviceability limits states, are summarised below in Table 6.5. The table includes displacement results when modelling the optimal portal frames in Prokon's second-order frame analysis. This was done to justify the use of the linear elastic structural analysis used by the algorithm.

Table 6.5: Comparison of maximum displacements under serviceability loads

| Case study | Analysis | Prismatic portal frames | | | | Web-tapered portal frames | | | |
|---|---|---|---|---|---|---|---|---|---|
| | | SLS1 | | SLS2 | | SLS1 | | SLS2 | |
| | | X [mm] | Y [mm] | X [mm] | Y [mm] | X [mm] | Y [mm] | X [mm] | Y [mm] |
| 20 m x 4.5 m | GA | 12.5 | -101.8 | 5.3 | 30.8 | 13.7 | -107.1 | 5.7 | 32.5 |
| | Prokon | 8.7 | -101.9 | 13.6 | 31.4 | 9.4 | -108.4 | 14.1 | 33.0 |
| 30 m x 4.5 m | GA | 16.4 | -154.7 | 6.2 | 38.7 | 17.7 | 158.3 | 7 | 41.6 |
| | Prokon | 12.8 | -153.6 | 4.5 | 37.5 | 13.9 | -161.2 | 4.1 | 40.4 |
| 40 m x 4.5 m | GA | 12.3 | -127.6 | 3.6 | 19.1 | 18.5 | -191.1 | 11.4 | 43.5 |
| | Prokon | 9.6 | -126.7 | 2 | 17.3 | 17.6 | -194.2 | 8.5 | 37.0 |
| 50 m x 4.5 m | GA | 11.6 | -147.4 | 5.0 | 18.4 | 12.1 | -137.1 | 9.2 | 33.8 |
| | Prokon | 11.0 | -149.2 | 3.7 | 14.1 | 11.3 | -134.7 | 6.9 | 32.9 |

The results display a strong correlation between the two approaches, despite the fact that the genetic algorithm only made use of a linear elastic analysis. The differences between these two methods was demonstrated to be rather insignificant and warranted the use of the linear elastic method when analysing portal frames. The insignificance of second-order effects are attributed to the low axial loads that arise from typical South African loading conditions, in combination with the small lateral deflections due to the large span-to-height ratios of portal frames.

### 6.4.2 Design capacity and deflection checks

A summary of the maximum utilisation ratios along with the modes of failure per limit state is provided in Tables 6.6 and 6.7. Deformation under SLS1 was identified as the critical mode of failure for all of the shorter span portal frames (spans 20 m and 30 m). The vertical deflection limit of span/180 was reached at the centre ridge for these load combinations, while the horizontal deflection had no influence on any of the designs as utilisation in this sense remained below 30%.

In the short span frames, the ULS1 load combination became close to being the critical load state as high utilisation was noted for lateral-torsional buckling in the region near the eaves connections. The lateral-torsional buckling was found either in the column or the rafter segment adjacent to the fixed beam connection and is attributed to the inner flange that is in compression under gravitational loading, but only supported at discrete points where knee-braces had been placed. From this, it can be concluded that the lateral support of the flanges specified in Section 6.2.3 succeeded in stabilising the frame sufficiently without lateral-torsional buckling being induced.

Table 6.6: Critical utilisation ratio per limit state for prismatic portal frames

| Case study | Limit state | Max util. | Mode of failure |
|---|---|---|---|
| 20 m x 4.5 m | ULS1 | 0.950 | Lateral-torsional buckling in column at eaves |
| | ULS2 | 0.730 | In-plane overall strength in column below eaves |
| | SLS1 | 0.958 | Vertical deflection below centre ridge |
| | SLS2 | 0.302 | Vertical deflection near centre of windward rafter |
| 30 m x 4.5 m | ULS1 | 0.901 | Lateral-torsional buckling in column below eaves |
| | ULS2 | 0.686 | Lateral-torsional buckling at centre of rafter |
| | SLS1 | 0.952 | Vertical deflection near centre ridge |
| | SLS2 | 0.238 | Vertical deflection near centre of windward rafter |
| 40 m x 4.5 m | ULS1 | 0.931 | Lateral-torsional buckling in rafter near eaves |
| | ULS2 | 0.572 | In-plane overall strength in column below eaves |
| | SLS1 | 0.587 | Vertical deflection at centre ridge |
| | SLS2 | 0.088 | Vertical deflection near centre of windward rafter |
| 50 m x 4.5 m | ULS1 | 0.845 | Lateral-torsional buckling in rafter near eaves |
| | ULS2 | 0.466 | In-plane overall strength in rafter near eaves |
| | SLS1 | 0.543 | Vertical deflection at centre ridge |
| | SLS2 | 0.068 | Vertical deflection near centre of windward rafter |

Table 6.7: Critical utilisation ratio per limit state for web-tapered portal frames

| Case study | Limit state | Max util. | Mode of failure |
|---|---|---|---|
| 20 m x 4.5 m | ULS1 | 0.967 | Lateral-torsional buckling in column below eaves |
| | ULS2 | 0.730 | In-plane overall strength in column below eaves |
| | SLS1 | 0.997 | Vertical deflection at centre ridge |
| | SLS2 | 0.302 | Vertical deflection near centre of windward rafter |
| 30 m x 4.5 m | ULS1 | 0.941 | Lateral-torsional buckling in rafter below eaves |
| | ULS2 | 0.654 | In-plane overall strength in column below eaves |
| | SLS1 | 0.972 | Vertical deflection at centre ridge |
| | SLS2 | 0.255 | Vertical deflection near centre of windward rafter |
| 40 m x 4.5 m | ULS1 | 0.999 | Lateral-torsional buckling in rafter near eaves |
| | ULS2 | 0.597 | In-plane overall strength in column below eaves |
| | SLS1 | 0.874 | Vertical deflection at centre ridge |
| | SLS2 | 0.199 | Vertical deflection near centre of windward rafter |
| 50 m x 4.5 m | ULS1 | 0.999 | Lateral-torsional buckling in rafter near eaves |
| | ULS2 | 0.522 | In-plane overall strength in column below eaves |
| | SLS1 | 0.501 | Vertical deflection at centre ridge |
| | SLS2 | 0.123 | Vertical deflection near centre of windward rafter |

Conversely, for all the longer span portal frames, lateral-torsional buckling of the rafter between the eaves connection and the first knee-brace for the ULS1 condition was the controlling issue. In this regard, the web-tapered frames reached an utilisation ratio of 0.999 for the lateral-torsional buckling design checks in both the 40 m and 50 m span lengths. This high degree of utilisation is believed to be indicative of web-tapered frames' ability to suit the prevailing loading conditions when optimised with the genetic algorithm. The prismatic portal frames, on the other hand, struggled to reach maximum utilisation levels above 95% despite several hours of optimisation calculations. This shortfall of the member resistances in prismatic frames (especially in long span applications) is believed to be caused by the greater difficulty the genetic algorithm experienced in refining combinations. The search space for the problem was deemed to become over-constrained as the prismatic frame components could not adapt to the same degree as the non-prismatic members.

It is interesting to note that although the effects of combined axial tension and bending, and shear were considered during the study, it proved to play an insignificant role in the capacity of portal frames.

Based on these observations, it was deemed that structural optimisation algorithm can succeed in identifying (near) optimal solutions. These solutions complied with the set parameters for member capacity and deflection checks under a variety of load combinations using either prismatic or web-tapered elements. This provides meaningful results as the material efficiency of web-tapered frames can be compared directly with an equally optimal prismatic frame.

## 6.5 Review of the optimisation results when compared with commercial MBS design software

The optimised portal frames found in this study are compared next to designs generated using commercial MBS software, with the purpose of providing some insights into the current MBS industry.

The frame geometries and fundamental conditions that were accepted for optimisation in Section 6.2 were applied in the MBS software to produce the design drawings shown in Appendix C. A close resemblance is observed in the total weight and layout between these design drawings and the frames found in Table 6.4, especially for shorter spans. However, the commercial designs show multiple properties not catered for by the genetic algorithm as the span length increases, as will be discussed in due course. A comparison of the different designs is provided next in a chart that describes the total frame weight for each case study and design method.

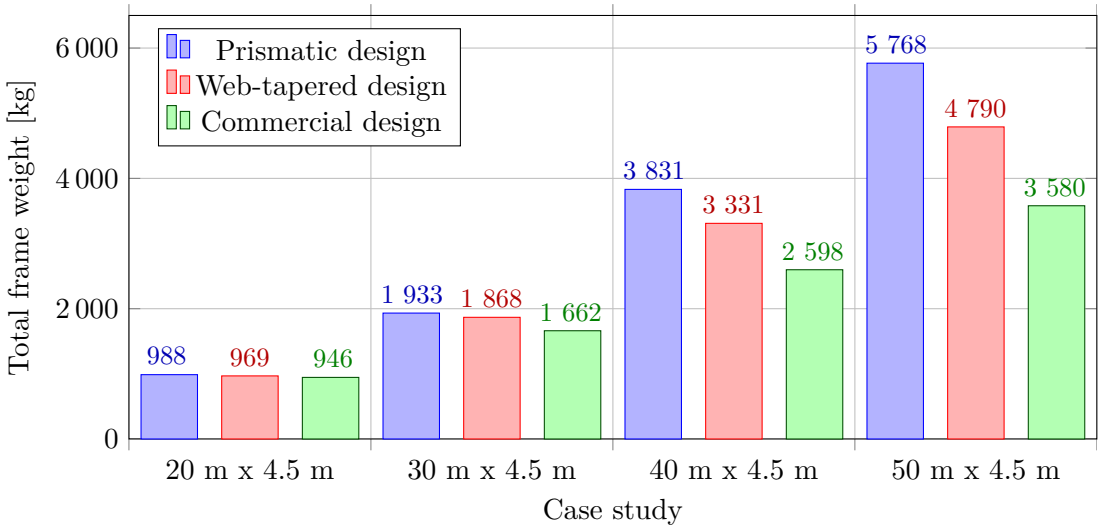


Figure 6.4: Portal frame weights achieved using the genetic algorithm when compared to commercial design software

The difference in the total frame weights is immediately apparent when viewing Figure 6.4. Again, a close correlation is observed between the prismatic and tapered designs in short span applications, while large differences are found as the spans increase. The differences in material usage are summarised in Table 6.8 below.

Table 6.8: Summary of the material usages per case study and design program

| Case study | Genetic algorithm | | | Commercial software | |
|---|---|---|---|---|---|
| | Prismatic [kg] | Web-tapered [kg] | Diff. [%] | Web-tapered [kg] | Diff. [%] |
| 20 m x 4.5 m | 988 | 969 | -1.9% | 946 | -4.3% |
| 30 m x 4.5 m | 1933 | 1868 | -3.4% | 1662 | -14.0% |
| 40 m x 4.5 m | 3831 | 3331 | -13.1% | 2598 | -32.2% |
| 50 m x 4.5 m | 5768 | 4790 | -17.0% | 3580 | -37.9% |

The designs produced by the commercial design software far surpass the reduction of material achieved by the genetic algorithm for longer span structures. The findings in Table 6.8 resonates with those reported by Saka (1997), Müller et al. (1999), Meera (2013), Zende et al. (2013), Roa and Vishwanath (2014), and Mckinstray et al. (2015). These researchers in the field of web-tapered portal frames have found savings to lie between 10% and 40%. Several reasons exist for the significant savings found when using the commercial software as opposed to the automated design procedure developed in this study.

The enhanced capabilities of the commercial design software include the following considerations:

a) The use of singly symmetric sections is permitted.

b) Slender flanges were permitted.

c) The software is capable of changing the angles of the web plates at intermediate intervals in the rafter, while only a single linear taper of the web was considered in this study.

d) Intermediate changes in plate thickness and width are permitted at locations where cross-sections are stiffened by end plates.

e) Plate thicknesses of as little as 5 mm thick are used in some instances.

In addition to the variances above, it is believed that the MBS software utilises advanced finite beam elements similar to those developed by researchers such as Boissonnade and Maquoi (2005), Andrade, Camotim, and Dinis (2007), and Jeong (2014). In Section 4.3.2.2 it was proven that a significant portion of a beam capacity might be underestimated when using the $\gamma_{eLTB}$-scaling method from DG25. The accurate determination of the beam's lateral-torsional resistance is thought to play a major role in the results provided by the MBS design software, but the internal design and analysis methods are not commonly shared with third parties for review.

# Chapter 7

# Conclusions and recommendations

## 7.1 Research overview

Web-tapered portal frames are advocated by MBS manufacturers as a cost-effective alternative to conventional construction techniques. The use of web-tapered members that are produced from welded plates also avoids the current unstable supply of hot-rolled structural sections recently witnessed in South Africa. These attributes led to an interest in the use of web-tapered portal frames by South African stakeholders related to the portal frames industry. However, some concerns were identified regarding the design and behaviour of these structures, as current design specifications either do not consider structures with tapered members, or only provide limited aid to design engineers.

The unfamiliar nature of web-tapered portal frames required a comprehensive literature review to be undertaken in Chapter 2. As the study did not include physical experimentation, a full non-linear finite element analysis procedure was described in Chapter 3 to investigate member capacities and behaviour. The principles in DG25 were found to be universal for steel specifications (Ziemian, 2010), which led to a new approach being developed in this study based on SANS 10162-1 that was subsequently validated in Chapter 4. This approach was implemented in an automated design optimisation procedure using a genetic algorithm in Chapter 5. Multiple case studies were specified in this dissertation to find optimal portal frames under different load configurations and plate dimensions. The optimal results were presented and discussed in Chapter 6 and then compared with designs produced by commercial MBS design software.

In this chapter, a summary of the research findings along with conclusions are presented in Section 7.2 in conjunction with the objectives defined in Chapter 1. This is followed by several recommendations in Section 7.3 for the design of web-tapered members. During the study, certain matters were identified that require additional investigation in the future. These are discussed in Section 7.4.

## 7.2 Findings and conclusions

The findings and conclusions concerning each of the research objectives from Section 1.3 are listed and discussed below:

1. *Determine what principles and procedures are currently employed internationally for the design of web-tapered members.*

    a) SANS 10162-1 and CSA S16 make no provisions for the design of web-tapered members. The EC3 specification for steel structures contains provisions for non-uniform members, by combining finite element analysis with the design process. However, despite the added complexities of incorporating finite element analysis, it was found to provide inconsistent and sometimes very conservative member capacities. Marques, da Silva, Greiner, et al. (2013) questioned the current EC3 provisions for non-uniform members and proposed that completing a full non-linear analysis would require basically the same amount of effort but would be more accurate. In addition, newer versions of AISC 360 no longer include any guidelines on the design of web-tapered members. Thus, it can be concluded that none of the conventional steel design specifications that were investigated contain adequate provisions for the design of web-tapered members.

    b) The most comprehensive guidelines for designing web-tapered portal frame structures were found in DG25, which is based on AISC 360. It utilises the concept of an equivalent prismatic member, whereby the web-tapered member capacity is determined using the conventional resistance formulae for prismatic members. This is done, firstly, by using the cross-sectional properties at various positions along the length of the member to identify the critical cross-section that represents the most detrimental combination of axial and bending forces. Secondly, the slenderness is determined using the elastic buckling load and the nominal cross-sectional resistance of the web-tapered member. DG25 suggests an empirical approach or numerical analysis that can accurately account for out-of-plane actions to derive the elastic buckling load, as no closed-form solution is available for web-tapered members.

2. *Select or develop an adequate methodology for designing web-tapered portal frames in South Africa.*

    a) DG25 was selected as the basis for designing web-tapered portal frames in this study as it represents the most complete guideline currently available for the design of web-tapered members. However, it is written specifically for designers accustomed to AISC 360 and in most instances resorts to written examples to describe the implementation thereof. This leaves many of the underlying principles overlooked, thus

causing DG25 to be difficult to interpret and overly complex to follow.

b) It was found that the equivalent prismatic member concept made the principles contained in DG25 universally compatible with other design specifications (Ziemian, 2010), although the implementation thereof was unknown and untested.

c) Consequently, a design approach was proposed in this study in terms of SANS 10162-1 (and CSA S16), but can readily be adapted for use with EC3 as well. The approach is presented using clearly defined steps to aid in the design of web-tapered members.

d) The adapted approach only considered flanges to a maximum of class 3 slenderness, in combination with slender web-plates (class 4) to comply with the specifications of SANS 10162-1. This simplified the process of identifying the critical cross-section under axial loading, as no area reductions of the flange plates were required.

3. *Review how the methodology from objective 2 performs by comparing the findings to full non-linear finite element analysis in Abaqus.*

a) Several methods are proposed by DG25 to determine the in-plane elastic buckling load of web-tapered columns. The numerical procedures, which include Newmark's method of successive approximations and eigenvalue buckling analysis, were compared against the simple empirical formula in DG25 that is based on Euler's formula. It was found that the empirical formula accurately predicted the in-plane elastic buckling load for a variety of cross-sections with typical angles of taper witnessed in MBS portal frames. This formula significantly reduces the complexity of designing web-tapered columns and is a suitable substitution when performing hand calculations.

b) It was observed that the critical cross-section of web-tapered columns subjected to pure axial loads is found in the vicinity of the smallest end, as this corresponds to the cross-section with the highest internal stress. However, an increased elastic buckling load is achieved when using web-tapered columns in comparison to prismatic columns with the same critical cross-section. This increase of the elastic buckling load can be seen as being equivalent to using a less slender column, whereby an increase in axial resistances is determined when using the SANS 10162-1 formula.

c) The method was reviewed using full non-linear analysis that incorporated imperfections. The predicted resistance of the web-tapered columns was found to be safe, with most cases failing plastically as the yield load of the smaller cross-section was reached.

d) An adequate means to predict the elastic flexural buckling load of web-tapered members about the weak-axis is to use the mid-height section properties in combination with Euler's formula. This is attributed to the negligible variation of the weak-axis

moment of inertia over the height of the column. The axial resistance about the weak-axis can then be determined using the normal prismatic formula.

e) DG25 provides a simplified method to predict the elastic lateral-torsional buckling moment in web-tapered beams without resorting to advanced finite element analysis. This approach utilises a nominal buckling strength multiplier to scale the applied stress in the compression flange to approximate the distribution and shape of the critical lateral-torsional buckling stress. The effective slenderness can then be determined at various locations along the length of the beam as a function of the elastic lateral-torsional buckling load and the cross-sectional moment of resistance. By knowing this ratio, the appropriate SANS 10162-1 formula can be used to predict the laterally unsupported resistance moment of the member.

f) The method in DG25 that approximates the elastic lateral-torsional buckling load was investigated extensively and found to be safe for a variety of configurations. This study determined that the DG25 method's prediction of the lateral-torsional buckling was accurate when modest angles of taper ($\alpha$) and stress gradients ($C_b$) applied. However, it can become very conservative for large angles of taper or steep stress gradients. The consequence thereof is an underestimation of the actual moment resistance of web-tapered beams and a loss of benefit from using web-tapered members.

4. *Create a structural optimisation algorithm capable of finding the lightest possible frame, when subjected to various load combinations and design constraints.*

a) A structural optimisation program that produces lightweight prismatic or web-tapered portal frame designs was developed in Matlab, the source code to which, is made available in Appendix E.

b) The program makes use of a genetic algorithm to perform optimisation tasks. The algorithm was verified using the six-hump camel back test function, which represents an unconstrained continuous mathematical surface with multiple positions of local optima. The verification proved the effectiveness of the genetic algorithm to negotiate complex search spaces in search of the global optimum.

c) The algorithm was subsequently expanded for structural engineering by including functions for structural analysis and member design. Structural configurations that did not comply with the design constraints were then systematically removed from the pool of possible solutions, using a dynamic penalty function, until the optimal feasible solution was found. The genetic algorithm proved to be effective in identifying the optimal frame within a large discontinuous search space and managed to converge at approximately 35 minutes over the course of several repeated runs.

d) A linear elastic structural analysis was coded into the program, which did not account for secondary moments that arose from $P - \Delta$ effects. This assumption was proven to be justified for portal frames under typical South African loading conditions, by comparing the displacement results from the linear elastic analysis with a second-order analysis in Prokon. No significant difference was observed between the methods of analysis as a result of the low axial loads and small lateral deflections of typical portal frames found locally.

e) The algorithm utilises the proposed design approach for web-tapered members and can consider the effects of multiple load combinations when applied to the portal frame. Only two types of loading were considered, namely gravitational loads and upward thrust, which were deemed to be representative of the most detrimental conditions to be expected in South Africa. It was found that the run time of the program dramatically increased for each additional load combination.

5. *Confirm the reported material savings potential of web-tapered portal frames designed with the method in objective 2 against conventional portal frames with prismatic plate-girders designed according to SANS 10162-1.*

a) The optimisation algorithm was used to establish a threshold to which conventional portal frames can be optimised when using prismatic plate-girders. The optimal portal frame weights per plan area were calculated to lie between 9.88 kg/m$^2$ to 23.07 kg/m$^2$ for clear spans ranging from 20 m to 50 m, under the conditions and brace configurations specified for this study.

b) Similarly, the optimal web-tapered portal frames were calculated to have a weight per plan area of 9.69 kg/m$^2$ to 19.16 kg/m$^2$ for the clear spans between 20 m and 50 m.

c) The maximum material saving was achieved in the longest span considered during the study, namely 50 m. The reduction in steel, in this case, amounted to 17% when using web-tapered portal frames.

d) The advantage of web-tapered members in portal frames was noted to become less apparent as clear span distances decreased. The shortest clear span considered during the study was 20 m, for which only a 2% reduction in steel was obtained. This effect corresponds to reports by previous researchers who found web-tapered construction to be most effective for long span applications.

e) Portal frames are conventionally constructed with large columns in combination with smaller rafter sections. The structural optimisation data showed that the ideal portal frame could either have large columns - small rafter configurations or the opposite,

with both being feasible and of almost equal total frame weight. This is believed to show that the search space in structural optimisation problems is described as relatively "flat" with no clear optimal solutions.

f) Vertical deflection near the centre ridge of the portal frames due to gravitational loads was in all cases the dominant serviceability limit state and governed the design for short spans. However, for longer spans (40 m to 50 m), the frame capacities were controlled by the ultimate limit state when subjected to gravitational loads. In these cases, the critical mode of failure was caused by lateral-torsional buckling of the rafter between the eaves connection and the first knee-brace.

g) It is believed that the full vertical deflection limit at the centre ridge can be reached for the span lengths from 40 m to 50 m if additional knee-braces are fitted to the rafter in the vicinity of the eaves connection. In doing so, a lighter portal frame could be achieved.

6. *Evaluate the optimal portal frames produced in the study against portal frames generated by the automated design software by Metal Building Software Incorporated.*

a) A commercial design package by Metal Building Software Incorporated was used to design the portal frames considered in the case studies and subjected to the same conditions. The MBS software further reduced the material requirement for web-tapered members by incorporating several additional aspects into the design of portal frames, which include intermediate changes in plate sizes and tapering angles, the consideration of very thin and slender flange plates and the use of singly symmetric sections. In addition to these issues, it is believed that advanced finite beam elements for tapered members are utilised by commercial MBS software that can accurately predict elastic lateral-torsional buckling. It was shown in this study that very conservative and inefficient approximations can result in some cases when using the DG25 method to predict the elastic lateral-torsional buckling load. The accurate determination of the elastic lateral-torsional buckling load is believed to contribute to a significant increase in the economical use of material when using commercial MBS software.

b) A comparison of the results revealed a good correlation in clear spans less than 30 m. However, the designs generated by the commercial MBS software surpassed those produced by the structural optimisation procedure developed for this study in terms of weight savings when large clear spans were considered. By using the MBS software, a maximum material reduction was achieved for the 50 m clear span of approximately 38% relative to the optimal prismatic portal frame from objective 5.

c) The findings regarding the material reduction potential of web-tapered members confirm the economical use of steel resources that is advocated by MBS manufacturers.

## 7.3 Recommendations for web-tapered member design

Based on the findings of this study, the following recommendations are made for the design of web-tapered members:

a) Newmark's method of successive approximations or an eigenvalue buckling analysis can be used to obtain the in-plane flexural buckling load of web-tapered members. However, these methods require some effort to implement and are not ideal for routine analysis. In this regard, the empirical approximation in Equation 2.6 is recommended, as it was found to provide almost indistinguishable results from the numerical techniques.

b) The $\gamma_{eLTB}$-scaling method in DG25 is safe to perform routine designs for web-tapered beams, but can become overly conservative in certain cases. A more accurate means should be considered when designing web-tapered beams with the goal of an optimised frame. In this regard, a finite element analysis using shell elements could be considered for the thin-walled sections but can prove difficult to implement and resource-intensive during iterative design. Another promising means is with the use of finite beam elements that can account for tapered members and accurately predict out-of-plane deformation. It should be noted that an eigenvalue buckling analysis with conventional finite beam elements is not suitable for predicting the elastic lateral-torsional buckling load of web-tapered beams even when using a fine discretisation process.

## 7.4 Future studies

The following proposals are made for further research:

a) A shortage of previous experimental work on web-tapered members was noted during the literature study and will continue to hinder the validation of finite element analysis models in the future. Currently, many of the uncertainties are addressed, based on knowledge obtained from prismatic member studies and may not always be representative of web-tapered members. In this regard, data on the geometric imperfections and residual stress distribution in web-tapered members could prove beneficial.

b) During the presentation of literature and theories, it was found that the behaviour of single-sided welds is not well researched. Members with these welds require less handling but can easily be prone to bow about their weak-axes when unsymmetrical residual stresses are formed by the welding process.

c) The portal frame industry can benefit from a study of the ideal connection that is cost effective, practical to manufacture and easy to assemble. Furthermore, a study of the behaviour of the web-panel at the eaves connection can prove useful in understanding the

complex distribution of stresses in that vicinity. Design issues relating to stiffening these web-panels can be derived based on this understanding.

d) This research project was focused mainly on establishing the design principles of web-tapered portal frames and reporting on whether this method is safe and worth pursuing. The results proved a clear benefit regarding material savings and it was assumed that the reduction of material would correlate to an overall reduction of the building costs. However, the added financial cost that arises from manufacturing web-tapered members should also be considered in the future to evaluate the feasibility of web-tapered portal frames.

e) Portal frames are constructed with discrete positions of lateral support, as each connection has an inherent cost to be considered. The optimisation procedure in this study can be expanded to include the layout of purlins and knee-braces as part of the primary design variable to determine the most cost-effective portal frame. Furthermore, the supports of a portal frame are typically designed as pinned. A lighter and more economical portal frame is feasible when using fixed supports, but the increased cost associated with larger foundations will need consideration.

f) The reliability of web-tapered portal frame structures remains an unexplored field that is to be addressed in the future.

## 7.5 Concluding statement

The research study examined the use of web-tapered members in portal frame applications. This method is rarely seen in South Africa, but many local portal frame manufacturers have expressed an interest in this technique due to the apparent financial advantage it provides. This method of construction also makes use of hot-rolled plates, as opposed to rolled sections for which the local supply has recently become sporadic. The study addressed many of the current concerns from industry as this technique is largely unknown locally and serves to provide a framework for future investigations. The study set out to address several objectives, which were all successfully met.

# References


AASHTO (2007). *LRFD Bridge Design Specifications* (cit. on pp. 23, 24).

AISC (2010). *Specification for Steel Buildings (Including additional commentary on the specification, 22 June 2010)*. American Institute of Steel Construction, Chicago (cit. on pp. 11, 17, 24, 25, 32, 33).

AISI-CSA (2007). *North American Specification for the design of cold-formed steel structural members*. CSA S136-07 (cit. on p. 19).

Andrade, A. and D. Camotim (2005a). "Elastic Lateral-Torsional Buckling Behavior of Doubly Symmetric Tapered Beam-Columns". In: *Annual Technical Session*. Strucutral Stability Research Council. University of Missouri, Rolla, MO, pp. 445–468 (cit. on pp. 46, 47).

Andrade, A. and D. Camotim (2005b). "Lateral-torsional buckling of singly symmetric tapered beams: theory and applications". In: *Journal of engineering mechanics* 131.6, pp. 586–597 (cit. on p. 47).

Andrade, A., P. Providência, and D. Camotim (2010). "Elastic lateral-torsional buckling of restrained web-tapered I-beams". In: *Computers & structures* 88.21, pp. 1179–1196 (cit. on p. 47).

Andrade, A., D. Camotim, and P. B. Dinis (2007). "Lateral-torsional buckling of singly symmetric web-tapered thin-walled I-beams: 1D model vs. shell FEA". In: *Computers & Structures* 85.17, pp. 1343–1359 (cit. on pp. 47, 99, 122).

Atkinson, R., K. Bradfield, and R. Southwell (1937). "Relaxation Methods Applied to a spar of varying Section, Deflected by Transverse Loading Combined with End Thrust or Tension". In: *Reports and Memoranda No.1822* (cit. on p. 44).

AWS (1998). "Structural Welding Code - Steel". In: *American Welding Society D1.1-98* (cit. on p. 39).

Badari, B. and F. Papp (2015). "On Design Method of Lateral-torsional Buckling of Beams: State of the Art and a New Proposal for a General Type Design Method". In: *Periodica Polytechnica. Civil Engineering* 59.2, p. 179 (cit. on pp. 12, 21).

Baker, K. and D. Kennedy (1984). "Resistance factors for laterally unsupported steel beams and biaxially loaded steel beam columns". In: *Canadian Journal of Civil Engineering* 11.4, pp. 1008–1019 (cit. on p. 20).

Baptista, A. and J. Muzeau (1998). "Design of tapered compression members according to Eurocode 3". In: *Journal of Constructional Steel Research* 1.46, pp. 146–148 (cit. on pp. 14, 15, 57).

Beer, H. and G. Schultz (1970). "Theoretical basis for the European column curves". In: *Construction Métallique* 3, p. 58 (cit. on pp. 10, 62).

Bhatti, M. (2006). *Advanced topics in finite element analysis of structures: with Mathematica and MATLAB computations*. John Wiley & Sons, Inc. (cit. on p. 48).

Bjorhovde, R. (1972). *Deterministic and probabilistic approaches to the strength of steel columns*. Lehigh University. (cit. on pp. 10, 62).

Bjorhovde, R. (1978). "The safety of steel columns". In: *Journal of the Structural Division* 104.3, pp. 463–477 (cit. on p. 10).

Bjorhovde, R. and L. Tall (1971). "Maximum column strength and the multiple column curve concept". In: *Fritz Engineering Laboratory Report* 337 (cit. on p. 10).

Bleich, F. (1932). "Stahlhochbauten ihre theorie, berechnung und bauliche gestaltung". In: *Berlin, Verlag von Julius Springer* (cit. on p. 37).

Blodgett, O. (1966). "Design of welded structures". In: *Cleveland: James F. Lincoln Arc Welding Foundation, 1966* 1 (cit. on p. 37).

Boissonnade, N. and R. Maquoi (2005). "A Geometrically and Materially Non-linear 3-D Beam Finite Element for the Analysis of Tapered Steel Members". In: *International Journal of Steel Structures* 5.5, pp. 413–419 (cit. on pp. 46, 47, 99, 122).

Bradfield, K. and R. Southwell (1937). "Relaxation Methods Applied to Engineering Problems. I. The Deflexion of Beams under Transverse Loading". In: *Proceedings of the Royal Society of London. Series A, Mathematical and Physical Sciences*, pp. 155–181 (cit. on p. 44).

Cazacu, R. and L. Grama (2014). "Comparative study for the size optimization of a tapered pipe cantilever beam using genetic algorithms". In: *Proceedings of the Annual Session of Scientific Papers \IMT Oradea* 13.23, p. 1 (cit. on p. 55).

CEN (1995). *Eurocode 3: Design of Steel Structures. Part 1-2: General rules. Structural fire design*. Comité Europeo de Normalización (cit. on p. 61).

CEN (2005). *Eurocode 3: Design of Steel Structures. Part 1-1: General Rules and Rules for Buildings*. Comité Europeo de Normalización (cit. on p. 35).

Chang, C. (2006). *GT-Sabre User Manual* (cit. on pp. 47, 78).

Chen, Y., Z. Shen, Q. Zheng, and C. Chen (2001). "Experimental study on the performance of single weld joints in H-shaped steel members". In: *International Journal of Steel Structures*, pp. 201–211 (cit. on p. 39).

Coley, D. (1999). *An introduction to genetic algorithms for scientists and engineers*. World scientific (cit. on p. 55).

Cook, R., D. Malkus, M. Plesha, and R. Witt (2001). *Concepts and applications of finite element analysis*. 4th. John Wiley & Sons (cit. on pp. 41–43, 45–48).

Cowper, G. (1966). "The shear coefficient in Timoshenko′s beam theory". In: *Journal of applied mechanics* 33.2, pp. 335–340 (cit. on p. 42).

Craig, R. (1999). *Mechanics of Materials*. 2nd. John Wiley & Sons (cit. on pp. 9, 40).

CSA (2013). *Design of steel structures*. Canadian Standards Association, Mississauga, Ontario, Canada (cit. on p. 34).

Dassault Systems (2013). "Abaqus Analysis User′s Guide 6.13". In: *Simulia Corporation* (cit. on pp. 61, 65, 67).

Davison, B., G. Owens, D. Brown, M. Burdekin, et al. (2011). *Steel designers' manual*. John Wiley & Sons (cit. on p. 3).

Dibley, J. (1969). "Lateral torsional buckling of I-shaped sections in grade 55 steel". In: *Proceedings of the Institution of Civil Engineers* 43.4, pp. 599–627 (cit. on p. 20).

Dong, S., C. Alpdogan, and E. Taciroglu (2010). "Much ado about shear correction factors in Timoshenko beam theory". In: *International Journal of Solids and Structures* 47.13, pp. 1651–1665 (cit. on p. 42).

Driver, R. (2014). *Design of steel structures overview*. University Lecture (cit. on pp. 33, 34, 41).

ECCS (1976). "ECCS Manual on the Stability of Steel Structures". In: European Convention for Constructional Steelwork, Brussels, Belgium (cit. on p. 11).

Engesser, F. (1909). "Über die knickfestigkeit von stäben veränderlichen trägheitsmomentes". In: *Zeitschrift des österreichischen Ingenieur- und architektenvereins* 61, pp. 544–548 (cit. on p. 44).

Firoz, S., S. Kumar, and S. Rao (2012). "Design Concept of Pre-Engineered Building". In: *International Journal of Research in Applications* 2.2, pp. 267–272 (cit. on pp. 3, 8, 117).

Galambos, T. (1988). *Guide to stability design criteria for metal structures* (cit. on pp. 38, 108).

Galambos, T. (1998). *Guide to stability design criteria for metal structures*. John Wiley & Sons (cit. on p. 11).

Galambos, T. and A. Surovek (2008). *Structural stability of steel: concepts and applications for structural engineers*. John Wiley & Sons (cit. on pp. 10, 16, 18).

Ghali, A., A. Neville, and T. Brown (2009). *Structural analysis: A unified classical and matrix approach*. 6th. Taylor & Francis (cit. on p. 44).

Goldberg, D. et al. (1989). *Genetic algorithms in search optimization and machine learning*. Vol. 412. Addison-wesley Reading Menlo Park (cit. on p. 49).

Goldberg, D. and M. Samtani (1986). "Engineering optimization via genetic algorithm". In: *Electronic Computation (1986)*. ASCE, pp. 471–482 (cit. on p. 56).

Guney, E. and D. White (2007). *Ensuring Sufficient Accuracy of Second-Order Frame Analysis Software*. Tech. rep. Georgia Institute of Technology, Atlanta, GA: Structural Engineering Mechanics & Materials Report No. 55, School of Civil & Environmental Engineering (cit. on p. 8).

Haftka, R. and Z. Gürdal (1992). *Elements of structural optimization*. Kluwer Academic Publishers (cit. on pp. 49, 50).

Hayalioglu, M. and M. Saka (1992). "Optimum design of geometrically nonlinear elastic-plastic steel frames with tapered members". In: *Computers & structures* 44.4, pp. 915–924 (cit. on p. 2).

Hendy, C. and R. Johnson (2006). "Chapter 5 Structural analysis". In: *Designers' Guide to EN 1994-2 Eurocode 4: Design of Steel and Composite Structures: Part 2: General Rules and Rules for Bridges*. Thomas Telford Publishing, pp. 29–66 (cit. on p. 63).

Jacquet, J. (1970). "Column test and analysis of their results". In: *Construction Métallique* 3, pp. 13–36 (cit. on p. 10).

Jeong, W. (2014). "Structural analysis and optimized design of general nonprismatic I-section members". In: (cit. on pp. 47, 99, 122).

Kaehler, R., D. White, and Y. Kim (2011). "Frame design using web-tapered members". In: *Design Guide 25* (cit. on pp. 1, 8, 13, 22–24, 28, 33, 35, 37, 38, 40, 44, 46, 57, 78, 79).

Kim, Y. (2010). "Behavior and design of metal building frames using general prismatic and web-tapered steel I-section members". In: (cit. on pp. 9, 19, 23–25, 36, 58, 85, 88, 99).

Kim, Y. and D. White (2006a). *Benchmark Problems for Second-Order Analysis of Frames with Tapered-Web Members*. Tech. rep. Georgia Institute of Technology, Atlanta, GA: Structural Engineering Mechanics & Materials Report No. 56, School of Civil & Environmental Engineering (cit. on p. 8).

Kim, Y. and D. White (2006b). *Full Nonlinear Finite Element Analysis Simulation of the LB-3 Test from Prawel et al. (1974)*. Tech. rep. Georgia Institute of Technology, Atlanta, GA: Structural Engineering Mechanics & Materials Report No. 56, School of Civil & Environmental Engineering (cit. on pp. 8, 23).

Kim, Y. and D. White (2007a). "Practical Buckling Solutions for Tapered Beam Members". In: *Annual Technical Session, Structural Stability Research Council*. Ed. by M. University of Missouri Rolla (cit. on pp. 8, 23).

Kim, Y. and D. White (2007b). *Assessment of Nominal Resistance Calculations for Web-Tapered I-shaped Members: Comparison to Experimental Tests and to Finite Element Simulations of Experimental Tests*. Tech. rep. Georgia Institute of Technology, Atlanta, GA: Structural Engineering Mechanics & Materials Report No. 31, School of Civil & Environmental Engineering (cit. on pp. 8, 23).

Kirby, P. and D. Nethercot (1979). *Design for structural stability*. Halsted Press (cit. on pp. 17, 20).

Kulak, G. and G. Grondin (2002). *Limit states design in structural steel*. 7th. Canadian Institute of Steel Construction, Willowdate, Ontario (cit. on pp. 31, 32).

Lagaros, N., M. Papadrakakis, and G. Kokossalakis (2002). "Structural optimization using evolutionary algorithms". In: *Computers & structures* 80.7, pp. 571–589 (cit. on p. 56).

Lee, G., M. Morell, and R. Ketter (1972). *Design of Tapered Members*. Tech. rep. DTIC Document (cit. on pp. 9, 57).

Lee, G. and M. Morrell (1975). "Application of AISC design provisions for tapered members". In: *Engineering Journal* 12.1, pp. 1–13 (cit. on pp. 9, 36).

Li, G. and J. Li (2002). "A tapered Timoshenko–Euler beam element for analysis of steel portal frames". In: *Journal of Constructional Steel Research* 58.12, pp. 1531–1544 (cit. on p. 41).

Loov, R. (1996). "A simple equation for axially loaded steel column design curves". In: *Canadian Journal of Civil Engineering* 23.1, pp. 272–276 (cit. on p. 11).

Marques, L. (2012). "Tapered steel members: Flexural and lateral-torsional buckling". PhD thesis. Universidade de Coimbra, Portugal (cit. on pp. 1, 26, 28, 36, 37, 57).

Marques, L., L. da Silva, R. Greiner, C. Rebelo, and A. Taras (2013). "Development of a consistent design procedure for lateral–torsional buckling of tapered beams". In: *Journal of Constructional Steel Research* 89, pp. 213–235 (cit. on pp. 25–29, 47, 58, 124).

Marques, L., L. da Silva, C. Rebelo, and A. Santiago (2014). "Extension of EC3-1-1 interaction formulae for the stability verification of tapered beam-columns". In: *Journal of Constructional Steel Research* 100, pp. 122–135 (cit. on pp. 36, 37, 57, 76).

Marques, L., A. Taras, L. da Silva, R. Greiner, and C. Rebelo (2012). "Development of a consistent buckling design procedure for tapered columns". In: *Journal of Constructional Steel Research* 72, pp. 61–74 (cit. on pp. 13–15, 35, 79).

MBMA (2012). *Metal Buildings Systems Manual* (cit. on pp. 39, 40).

MBMA (2016). *About MBMA & Industry trends*. Metal Building Manufacturers Association. URL: `http://www.mbma.com/` (cit. on p. 3).

Mckinstray, R., J. Lim, T. Tanyimboh, D. Phan, and W. Sha (2015). "Optimal design of long-span steel portal frames using fabricated beams". In: 104, pp. 104–114 (cit. on pp. 2, 50, 121).

Meera, C. (2013). "Pre-engineered building design of an industrial warehouse". In: *International Journal of Engineering Sciences & Emerging Technologies* 2, pp. 75–82 (cit. on pp. 2, 121).

Mitchell, M. (1998). *An introduction to genetic algorithms*. MIT press (cit. on pp. 50–54).

Molga, M. and C. Smutnicki (2005). "Test functions for optimization needs". In: *Test functions for optimization needs* (cit. on p. 101).

Müller, A., F. Werner, and P. Osterrieder (1999). "Optimal Design of Steel Frames with Non-Uniform Members". In: *Advances in Steel Structures ICASS '99*. Vol. 2. Institute of Steel Structures, Bauhaus-University Weimar, Germany, pp. 1073–1080 (cit. on pp. 2, 121).

Murthy, P. (2013). "Interactive behavior of restrained elements in metal building systems". In: (cit. on pp. 38, 39).

Nanakorn, P. and K. Meesomklin (2001). "An adaptive penalty function in genetic algorithms for structural design optimization". In: *Computers & Structures* 79.29, pp. 2527–2539 (cit. on p. 55).

Nelson, P. and T. Murray (1979). *Development of Simplified Design Methodology for Tapered Beams*. Tech. rep. School of Civil Engineering and Environmental Science, University of Oklahoma, Norman, Oklahoma: Star Manufacturing Co. (cit. on p. 7).

Newman, A. (2004). *Metal building systems: design and specifications*. McGraw-Hill Professional (cit. on pp. 2, 3, 7, 8).

Newmark, N. (1943). "Numerical procedure for computing deflections, moments, and buckling loads". In: *Transactions of the American Society of Civil Engineers* 108.1, pp. 1161–1188 (cit. on pp. 43, 44).

Niles, A. and J. Newell (1938). *Airplane structures*. Vol. 1 & 2. J. Wiley & sons, inc. (cit. on p. 44).

Ostwald, W. (1910). "Klassiker der exakten Wissenschaften". In: *Nr* 175 (cit. on p. 7).

Outinen, J. et al. (2007). *Mechanical properties of structural steels at high temperatures and after cooling down*. Helsinki University of Technology (cit. on p. 61).

Ozgur, C., Y. Kim, and D. White (2007). *Consideration of End Restraint Effects in Web-Tapered Members*. Tech. rep. Georgia Institute of Technology, Atlanta, GA: Structural Engineering Mechanics & Materials Report No. 32, School of Civil & Environmental Engineering (cit. on p. 8).

Prawel, S., M. Morrell, and G. Lee (1974). "Bending and buckling strength of tapered structural members". In: *Welding Journal* 53.2, pp. 75–84 (cit. on pp. 23, 38, 39).

Rajeev, S. and C. Krishnamoorthy (1992). "Discrete optimization of structures using genetic algorithms". In: *Journal of structural engineering* 118.5, pp. 1233–1250 (cit. on p. 50).

Rao, S. (2009). *Engineering optimization: Theory and practice*. John Wiley & Sons (cit. on pp. 49, 50, 54, 55).

Roa, K. and K. Vishwanath (2014). "Design optimisation of an Industrial Structure from Steel Frame to Pre-Engineered Building". In: *International Journal of Research in Advent Technology* 2.9, pp. 6–10 (cit. on pp. 2, 51, 121).

Rudman, C. (2009). "Investigation into the structural behavior of portal frames". MA thesis. University of Stellenbosch (cit. on p. 1).

Saitou, K., K. Izui, S. Nishiwaki, and P. Papalambros (2005). "A survey of structural optimization in mechanical product development". In: *Journal of Computing and Information Science in Engineering* 5.3, pp. 214–226 (cit. on p. 48).

Saka, M. (1997). "Optimum design of steel frames with tapered members." In: *Computer & structures* 63(4), pp. 797–811 (cit. on p. 121).

Salter, J., D. Anderson, and I. May (1980). "Tests on tapered steel columns". In: *Struct. Eng. A* 58.6, pp. 189–193 (cit. on p. 23).

Salvadori, M. (1955). "Lateral buckling of I-beams". In: *Transactions of the American Society of Civil Engineers* 120.1, pp. 1165–1177 (cit. on pp. 20, 23).

SANS 10162-1 (2011). "South African standard code of practice for the structural use of steel: Part 1: Limit states design of hot-rolled steelwork". In: *SABS* (cit. on pp. 16, 70).

SANS 2001-CS1 (2005). "South African standard code of practice for construction works: Part CS1: Structural steelwork". In: *SABS* (cit. on p. 62).

Serna, M., A. López, I. Puente, and D. Yong (2006). "Equivalent uniform moment factors for lateral–torsional buckling of steel members". In: *Journal of Constructional Steel Research* 62.6, pp. 566–580 (cit. on p. 61).

Sfintesco, D. (1970). "Experimental basis of the European column curves". In: *Construction Métallique* 7.3 (cit. on p. 10).

Shiomi, H., S. Nishikawa, and M. Kurata (1983). "Tests on tapered steel beam-columns". In: *Transactions of JSCE* 15, pp. 99–101 (cit. on p. 23).

Timoshenko, S. and J. Gere (1961). "Theory of elastic stability. 1961". In: *McGrawHill-Kogakusha Ltd, Tokyo* (cit. on pp. 9, 16, 17, 19, 21, 43, 44, 46, 57).

Timoshenko, S. and J. Goodier (1970). *Theory of Elasticity* (cit. on p. 38).

Trahair, N. (1993). *Flexural-torsional buckling of structures*. Vol. 6. CRC Press (cit. on p. 64).

Trahair, N., M. Bradford, D. Nethercot, and L. Gardner (2008). *The behaviour and design of steel structures to EC3*. 4th. Taylor & Francis (cit. on pp. 12, 14, 15, 29–31, 34, 35, 57).

Tsavdaridis, K., J. Kingman, and V. Toropov (2015). "Application of structural topology optimisation to perforated steel beams". In: *Computers & Structures* 158, pp. 108–123 (cit. on p. 49).

Vianello, L. (1898). "Graphische Untersuchung der Knickfestigkeit gerader Stäbe". In: *Zeitschrift für Deutsche Ing* 42, pp. 1436–1443 (cit. on p. 44).

Walls, R. and C. Viljoen (2016). "A comparison of technical and practical aspects of Eurocode 3-1-1 and SANS 10162-1 hot-rolled steelwork design codes". In: *Journal of the South African Institution of Civil Engineering* 58.1, pp. 16–25 (cit. on pp. 12, 21).

White, D. (2006). *Structural Behavior of Steel*. Tech. rep. Georgia Institute of Technology, Atlanta, GA: Structural Engineering Mechanics & Materials Report No. 2006-43, School of Civil & Environmental Engineering (cit. on pp. 8, 23).

White, D., M. Barker, and A. Azizinamini (2008). "Shear strength and moment-shear interaction in transversely stiffened steel I-girders". In: *Journal of structural engineering* 134.9, pp. 1437–1449 (cit. on p. 38).

White, D. and C. Chang (2007). "Improved Flexural Stability Design of I-Section Members in AISC (2005) - A Case Study Comparison to AISC (1989) ASD". In: *Engineering journal* 44.4, p. 291 (cit. on p. 9).

White, D. and M. Clarke (1997). "Design of beam-columns in steel frames. I: Philosophies and procedures". In: *Journal of Structural Engineering* 123.12, pp. 1556–1564 (cit. on p. 32).

White, D. and Y. Kim (2006). "A Prototype Application of the AISC (2005) Stability Analysis and Design Provisions to Metal Building Structural Systems". In: *Report to Metal Building Manufacturers Association, School of Civil and Environmental Engineering, Georgia Institute of Technology, Atlanta, GA, September* (cit. on pp. 8, 23, 77).

Wong, E. and R. Driver (2010). "Critical evaluation of equivalent moment factor procedures for laterally unsupported beams". In: *Engineering journal* 47.1, p. 1 (cit. on pp. 16, 20, 23).

Younes, R., G. Abu-Farsakh, and Y. Hunaiti (2009). "Effect of Welding on Lateral-Torsional Buckling Resistance of I-Shaped Built-up Steel". In: *Jordan Journal of Civil Engineering* 3.4 (cit. on p. 39).

Yura, J. and T. Helwig (1996). "Bracing for stability". In: *Structural stability research council* (cit. on pp. 23, 58).

Zende, A., A. Kulkarni, and A. Hutagi (2013). "Comparative Study of Analysis and Design of Pre-Engineered-Buildings and Conventional Frames". In: *Journal of Mechanical and Civil Engineering*, pp. 32–43 (cit. on pp. 2, 3, 121).

Ziemian, R. (2010). *Guide to stability design criteria for metal structures*. John Wiley & Sons (cit. on pp. 3, 9–13, 15, 16, 22, 32, 33, 37, 41, 43, 57, 123, 125).

Zoad, D. (2012). "Evaluation of Pre-Engineered Structure Design by IS-800 as against Pre-Engineering Structure Design by AISC". In: *International Journal of Research & Technology* 1.5, pp. 1–9 (cit. on p. 3).

# Appendices

# Appendix A

# Design of web-tapered columns

## A.1 Newman's method of successive approximations

| E [MPa] | $f_y$ [MPa] | $P_{ref}$ [kN] | $\phi$ [-] | b [mm] | $t_f$ [mm] | $t_w$ [mm] |
|---|---|---|---|---|---|---|
| 199 948 | 379.21 | 1 | 0.9 | 152.4 | 6.35 | 3.175 |

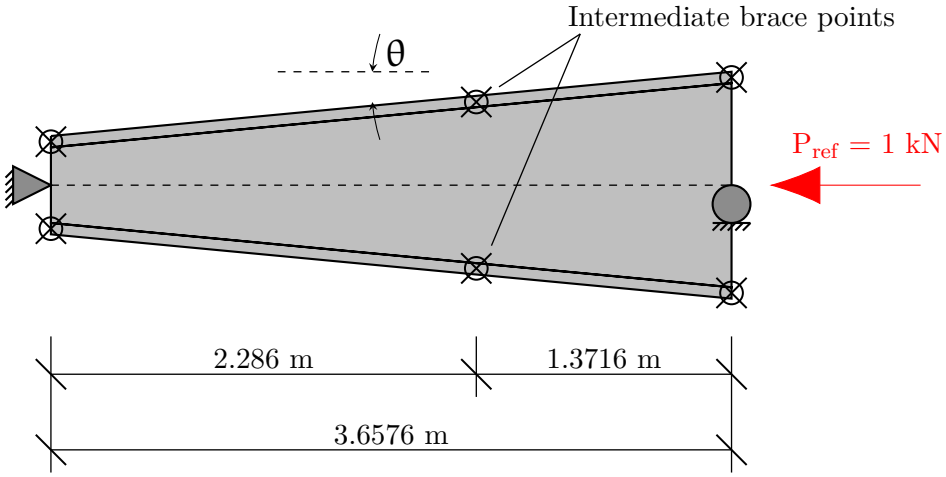


Table A.1: Newark's method of successive approximations: 1st iteration

| | 0 Left | 1L | 1R | 2L | 2R | 3L | 3R | 4L | 4R | 5L | 5R | 6L | 6R | 7L | 7R | 8L | 8R | 9L | 9R | 10 Right |
|---|---|---|---|---|---|---|---|---|---|---|---|---|---|---|---|---|---|---|---|---|
| Station | 0 | 1 | | 2 | | 3 | | 4 | | 5 | | 6 | | 7 | | 8 | | 9 | | 10 |
| Assumed curve (rad) | 0 | 0.314 | | 0.628 | | 0.942 | | 1.257 | | 1.571 | | 1.885 | | 2.199 | | 2.513 | | 2.827 | | 3.142 |
| Assumed δ (norm) | 0 | 30.9 | | 58.8 | | 80.9 | | 95.1 | | 100.0 | | 95.1 | | 80.9 | | 58.8 | | 30.9 | | 0 |
| $h_w$ (m) | 0.305 | 0.335 | | 0.366 | | 0.396 | | 0.427 | | 0.457 | | 0.488 | | 0.518 | | 0.549 | | 0.579 | | 0.610 |
| $I_i$ ($m^4$) | 5.43E-05 | 6.65E-05 | | 8.00E-05 | | 9.49E-05 | | 1.11E-04 | | 1.29E-04 | | 1.49E-04 | | 1.70E-04 | | 1.93E-04 | | 2.17E-04 | | 2.44E-04 |
| $I_i/I_{max}$ (-) | 0.223 | 0.273 | | 0.328 | | 0.390 | | 0.457 | | 0.531 | | 0.611 | | 0.698 | | 0.792 | | 0.892 | | 1.000 |
| $P_{ref}$ (kN) | 1 | 1 | | 1 | | 1 | | 1 | | 1 | | 1 | | 1 | | 1 | | 1 | | 1 |
| $P_{ref}$*$y_1$/EI (1000/m) | 0 | 2.326E-06 | | 3.677E-06 | | 4.264E-06 | | 4.273E-06 | | 3.869E-06 | | 3.197E-06 | | 2.381E-06 | | 1.525E-06 | | 7.114E-07 | | 0 |
| Con M'/EI (1000/m) | 0 | 8.209E-07 | | 1.322E-06 | | 1.542E-06 | | 1.550E-06 | | 1.407E-06 | | 1.165E-06 | | 8.696E-07 | | 5.591E-07 | | 2.633E-07 | | 0 |
| (M'/EI)*x (-) | 0 | 3.00E-07 | | 9.67E-07 | | 1.69E-06 | | 2.27E-06 | | 2.57E-06 | | 2.56E-06 | | 2.23E-06 | | 1.64E-06 | | 8.67E-07 | | 0 |
| Avg θ (rad) | 5.37E-06 | | 4.55E-06 | | 3.23E-06 | | 1.69E-06 | | 1.39E-07 | | -1.27E-06 | | -2.43E-06 | | -3.30E-06 | | -3.86E-06 | | -4.12E-06 | |
| $y_2$ (m) | 0 | 1.97E-06 | | 3.63E-06 | | 4.81E-06 | | 5.43E-06 | | 5.48E-06 | | 5.02E-06 | | 4.13E-06 | | 2.92E-06 | | 1.51E-06 | | 0 |
| $y_1/y_2$ (kN) | 0 | 15 721 | | 16 188 | | 16 809 | | 17 512 | | 18 242 | | 18 952 | | 19 595 | | 20 124 | | 20 484 | | 0 |
| $y_2$ (norm) | 0 | 35.9 | | 66.2 | | 87.8 | | 99.1 | | 100.0 | | 91.5 | | 75.3 | | 53.3 | | 27.5 | | 0 |

Table A.2: Newark's method of successive approximations: 2nd iteration

| | 0 Left | 1L | 1R | 2L | 2R | 3L | 3R | 4L | 4R | 5L | 5R | 6L | 6R | 7L | 7R | 8L | 8R | 9L | 9R | 10 Right |
|---|---|---|---|---|---|---|---|---|---|---|---|---|---|---|---|---|---|---|---|---|
| Station | 0 | 1 | | 2 | | 3 | | 4 | | 5 | | 6 | | 7 | | 8 | | 9 | | 10 |
| $y_2$ (norm) | 0 | 35.9 | | 66.2 | | 87.8 | | 99.1 | | 100.0 | | 91.5 | | 75.3 | | 53.3 | | 27.5 | | 0 |
| $h_w$ (m) | 0.305 | 0.335 | | 0.366 | | 0.396 | | 0.427 | | 0.457 | | 0.488 | | 0.518 | | 0.549 | | 0.579 | | 0.610 |
| $I_i$ ($m^4$) | 5.43E-05 | 6.65E-05 | | 8.00E-05 | | 9.49E-05 | | 1.11E-04 | | 1.29E-04 | | 1.49E-04 | | 1.70E-04 | | 1.93E-04 | | 2.17E-04 | | 2.44E-04 |
| $I_i/I_{max}$ (-) | 0.223 | 0.273 | | 0.328 | | 0.390 | | 0.457 | | 0.531 | | 0.611 | | 0.698 | | 0.792 | | 0.892 | | 1.000 |
| $P_{ref}$ (kN) | 1 | 1 | | 1 | | 1 | | 1 | | 1 | | 1 | | 1 | | 1 | | 1 | | 1 |
| $P_{ref}$*$y_2$/EI (1000/m) | 0 | 2.70E-06 | | 4.14E-06 | | 4.63E-06 | | 4.45E-06 | | 3.87E-06 | | 3.08E-06 | | 2.22E-06 | | 1.38E-06 | | 6.33E-07 | | 0 |
| Con M'/EI (1000/m) | 0 | 9.49E-07 | | 1.49E-06 | | 1.67E-06 | | 1.62E-06 | | 1.41E-06 | | 1.12E-06 | | 8.12E-07 | | 5.08E-07 | | 2.35E-07 | | 0 |
| (M'/EI)*x (-) | 0 (-) | 3.47E-07 | | 1.09E-06 | | 1.84E-06 | | 2.36E-06 | | 2.58E-06 | | 2.47E-06 | | 2.08E-06 | | 1.49E-06 | | 7.74E-07 | | 0 |
| Avg θ (rad) | 5.71E-06 | | 4.76E-06 | | 3.27E-06 | | 1.60E-06 | | -1.78E-08 | | -1.43E-06 | | -2.55E-06 | | -3.36E-06 | | -3.87E-06 | | -4.10E-06 | |
| $y_3$ (m) | 0 | 2.09E-06 | | 3.83E-06 | | 5.02E-06 | | 5.61E-06 | | 5.60E-06 | | 5.08E-06 | | 4.15E-06 | | 2.92E-06 | | 1.50E-06 | | 0 |
| $y_2/y_3$ (kN) | 0 | 17 183 | | 17 310 | | 17 480 | | 17 669 | | 17 855 | | 18 025 | | 18 165 | | 18 268 | | 18 329 | | 0 |
| $y_3$ (norm) | 0 | 37.2 | | 68.2 | | 89.6 | | 100.0 | | 99.9 | | 90.6 | | 73.9 | | 52.0 | | 26.8 | | 0 |

Table A.3: Newark's method of successive approximations: 10th iteration

| | 0 Left | 1L | 1R | 2L | 2R | 3L | 3R | 4L | 4R | 5L | 5R | 6L | 6R | 7L | 7R | 8L | 8R | 9L | 9R | 10 Right |
|---|---|---|---|---|---|---|---|---|---|---|---|---|---|---|---|---|---|---|---|---|
| Station | 0 | 1 | | 2 | | 3 | | 4 | | 5 | | 6 | | 7 | | 8 | | 9 | | 10 |
| $y_9$ (norm) | 0 | 37.6 | | 68.7 | | 89.9 | | 100.0 | | 99.5 | | 90.0 | | 73.3 | | 51.5 | | 26.5 | | 0 |
| $h_w$ (m) | 0.305 | 0.335 | | 0.366 | | 0.396 | | 0.427 | | 0.457 | | 0.488 | | 0.518 | | 0.549 | | 0.579 | | 0.610 |
| $I_i$ ($m^4$) | 5.43E-05 | 6.65E-05 | | 8.00E-05 | | 9.49E-05 | | 1.11E-04 | | 1.29E-04 | | 1.49E-04 | | 1.70E-04 | | 1.93E-04 | | 2.17E-04 | | 2.44E-04 |
| $I_i/I_{max}$ (-) | 0.223 | 0.273 | | 0.328 | | 0.390 | | 0.457 | | 0.531 | | 0.611 | | 0.698 | | 0.792 | | 0.892 | | 1.000 |
| $P_{ref}$ (kN) | 1 | 1 | | 1 | | 1 | | 1 | | 1 | | 1 | | 1 | | 1 | | 1 | | 1 |
| $P_{ref}$*$y_9$/EI (1000/m) | 0 | 2.83E-06 | | 4.30E-06 | | 4.74E-06 | | 4.49E-06 | | 3.85E-06 | | 3.02E-06 | | 2.16E-06 | | 1.34E-06 | | 6.09E-07 | | 0 |
| Con M'/EI (1000/m) | 0 | 9.93E-07 | | 1.54E-06 | | 1.71E-06 | | 1.63E-06 | | 1.40E-06 | | 1.10E-06 | | 7.90E-07 | | 4.91E-07 | | 2.26E-07 | | 0 |
| (M'/EI)*x (-) | 0 | 3.63E-07 | | 1.13E-06 | | 1.88E-06 | | 2.39E-06 | | 2.57E-06 | | 2.42E-06 | | 2.02E-06 | | 1.44E-06 | | 7.45E-07 | | 0 |
| Avg θ (rad) | 5.81E-06 | | 4.81E-06 | | 3.27E-06 | | 1.56E-06 | | -7.23E-08 | | -1.48E-06 | | -2.58E-06 | | -3.37E-06 | | -3.86E-06 | | -4.09E-06 | |
| $y_{10}$ (m) | 0 | 2.12E-06 | | 3.88E-06 | | 5.08E-06 | | 5.65E-06 | | 5.62E-06 | | 5.08E-06 | | 4.14E-06 | | 2.91E-06 | | 1.50E-06 | | 0 |
| $y_9/y_{10}$ (kN) | 0 | 17 698 | | 17 698 | | 17 698 | | 17 698 | | 17 698 | | 17 698 | | 17 698 | | 17 698 | | 17 698 | | 0 |
| δ 10th iter (norm) | 0 | 37.6 | | 68.7 | | 89.9 | | 100.0 | | 99.5 | | 90.0 | | 73.3 | | 51.5 | | 26.5 | | 0 |

## A.2 Elastic in-plane flexural buckling load: Empirical vs Numerical comparison

Table A.4: Comparison of elastic in-plane flexural buckling: E = 199 948 MPa, b = 152.4 mm, $t_f$ = 6.35 mm, $t_w$ = 3.175 mm, $\alpha = 2.386^o$

| L [mm] | $h_{w,small}$ [mm] | $h_{w,large}$ [mm] | $x_{crit}$ [mm] | $h_{w,crit}$ [mm] | Numerical [kN] | | | | Empirical [kN] | |
|---|---|---|---|---|---|---|---|---|---|---|
| | | | | | Successive approximations | | Eigenvalue Buckling Analysis | | $P_{ex}$ | Max deviation |
| | | | | | 10 elements | 100 elements | 10 elements | 100 elements | | |
| 500 | 304.8 | 346.5 | 245.1 | 325.2 | 491 869 | 491 889 | 491 873 | 491 888 | 491 818 | -0.01% |
| 600 | 304.8 | 354.8 | 293.0 | 329.2 | 350 525 | 350 539 | 350 521 | 350 538 | 350 470 | -0.02% |
| 700 | 304.8 | 363.1 | 340.6 | 333.2 | 264 155 | 264 165 | 264 147 | 264 165 | 264 098 | -0.03% |
| 800 | 304.8 | 371.5 | 387.9 | 337.1 | 207 357 | 207 365 | 207 345 | 207 364 | 207 299 | -0.03% |
| 900 | 304.8 | 379.8 | 434.9 | 341.0 | 167 909 | 167 915 | 167 895 | 167 914 | 167 850 | -0.04% |
| 1000 | 304.8 | 388.1 | 481.6 | 344.9 | 139 329 | 139 334 | 139 313 | 139 333 | 139 271 | -0.05% |
| 1100 | 304.8 | 396.5 | 528.0 | 348.8 | 117 915 | 117 919 | 117 898 | 117 918 | 117 857 | -0.05% |
| 1200 | 304.8 | 404.8 | 574.1 | 352.6 | 101 424 | 101 427 | 101 405 | 101 427 | 101 367 | -0.06% |
| 1300 | 304.8 | 413.1 | 619.9 | 356.5 | 88 431 | 88 434 | 88 412 | 88 433 | 88 375 | -0.07% |
| 1400 | 304.8 | 421.5 | 665.5 | 360.3 | 77 996 | 77 998 | 77 976 | 77 998 | 77 941 | -0.07% |
| 1500 | 304.8 | 429.8 | 710.8 | 364.0 | 69 476 | 69 477 | 69 455 | 69 477 | 69 422 | -0.08% |
| 2000 | 304.8 | 471.5 | 934.0 | 382.6 | 43 484 | 43 485 | 43 462 | 43 485 | 43 435 | -0.11% |
| 2500 | 304.8 | 513.1 | 1151.7 | 400.8 | 30 748 | 30 748 | 30 724 | 30 748 | 30 704 | -0.15% |
| 3000 | 304.8 | 554.8 | 1364.8 | 418.5 | 23 448 | 23 448 | 23 423 | 23 448 | 23 408 | -0.17% |
| 3500 | 304.8 | 596.5 | 1573.6 | 435.9 | 18 817 | 18 816 | 18 791 | 18 816 | 18 780 | -0.19% |
| 4000 | 304.8 | 638.1 | 1778.7 | 453.0 | 15 662 | 15 661 | 15 634 | 15 661 | 15 629 | -0.21% |
| 4500 | 304.8 | 679.8 | 1980.3 | 469.8 | 13 396 | 13 395 | 13 368 | 13 395 | 13 367 | -0.22% |
| 5000 | 304.8 | 721.5 | 2178.8 | 486.4 | 11 703 | 11 701 | 11 673 | 11 701 | 11 676 | -0.23% |

Table A.5: Comparison of elastic in-plane flexural buckling: E = 199 948 MPa, b = 152.4 mm, $t_f$ = 6.35 mm, $t_w$ = 3.175 mm, $\alpha = 5.0^o$

| L [mm] | $h_{w,small}$ [mm] | $h_{w,large}$ [mm] | $x_{crit}$ [mm] | $h_{w,crit}$ [mm] | Numerical [kN] | | | | Empirical [kN] | |
|---|---|---|---|---|---|---|---|---|---|---|
| | | | | | Successive approximations | | Eigenvalue Buckling Analysis | | $P_{ex}$ | Max deviation |
| | | | | | 10 elements | 100 elements | 10 elements | 100 elements | | |
| 500 | 304.8 | 392.3 | 240.4 | 346.9 | 563 977 | 563 996 | 563 905 | 563 995 | 563 723 | -0.05% |
| 600 | 304.8 | 409.8 | 286.5 | 354.9 | 411 332 | 411 344 | 411 249 | 411 343 | 411 084 | -0.06% |
| 700 | 304.8 | 427.3 | 332.0 | 362.9 | 316 888 | 316 897 | 316 800 | 316 896 | 316 649 | -0.08% |
| 800 | 304.8 | 444.8 | 377.1 | 370.8 | 254 034 | 254 040 | 253 940 | 254 039 | 253 803 | -0.09% |
| 900 | 304.8 | 462.3 | 421.6 | 378.6 | 209 874 | 209 878 | 209 777 | 209 877 | 209 653 | -0.11% |
| 1000 | 304.8 | 479.8 | 465.7 | 386.3 | 177 524 | 177 527 | 177 424 | 177 525 | 177 312 | -0.12% |
| 1100 | 304.8 | 497.3 | 509.3 | 393.9 | 153 025 | 153 026 | 152 922 | 153 025 | 152 821 | -0.13% |
| 1200 | 304.8 | 514.8 | 552.5 | 401.5 | 133 962 | 133 962 | 133 856 | 133 961 | 133 766 | -0.15% |
| 1300 | 304.8 | 532.3 | 595.4 | 409.0 | 118 792 | 118 792 | 118 684 | 118 791 | 118 605 | -0.16% |
| 1400 | 304.8 | 549.8 | 637.8 | 416.4 | 106 490 | 106 489 | 106 380 | 106 488 | 106 311 | -0.17% |
| 1500 | 304.8 | 567.3 | 679.9 | 423.8 | 96 352 | 96 350 | 96 240 | 96 349 | 96 180 | -0.18% |
| 2000 | 304.8 | 654.8 | 885.6 | 459.8 | 64 691 | 64 686 | 64 569 | 64 685 | 64 552 | -0.22% |
| 2500 | 304.8 | 742.2 | 1084.3 | 494.5 | 48 545 | 48 538 | 48 413 | 48 537 | 48 434 | -0.23% |
| 3000 | 304.8 | 829.7 | 1277.1 | 528.3 | 38 966 | 38 957 | 38 824 | 38 956 | 38 877 | -0.23% |
| 3500 | 304.8 | 917.2 | 1464.9 | 561.1 | 32 703 | 32 691 | 32 549 | 32 690 | 32 633 | 0.26% |
| 4000 | 304.8 | 1004.7 | 1648.3 | 593.2 | 28 320 | 28 306 | 28 155 | 28 304 | 28 267 | 0.40% |
| 4500 | 304.8 | 1092.2 | 1827.9 | 624.6 | 25 098 | 25 080 | 24 921 | 25 079 | 25 059 | 0.55% |
| 5000 | 304.8 | 1179.7 | 2004.0 | 655.4 | 22 637 | 22 616 | 22 447 | 22 614 | 22 610 | 0.72% |

Table A.6: Comparison of elastic in-plane flexural buckling: E = 199 948 MPa, b = 152.4 mm, $t_f$ = 6.35 mm, $t_w$ = 3.175 mm, $\alpha = 10.0^o$

| L [mm] | $h_{w,small}$ [mm] | $h_{w,large}$ [mm] | $x_{crit}$ [mm] | $h_{w,crit}$ [mm] | Numerical [kN] | | | | Empirical [kN] | |
|---|---|---|---|---|---|---|---|---|---|---|
| | | | | | Successive approximations | | Eigenvalue Buckling Analysis | | $P_{ex}$ | Max deviation |
| | | | | | 10 elements | 100 elements | 10 elements | 100 elements | | |
| 500 | 304.8 | 481.1 | 232.7 | 386.9 | 712 437 | 712 446 | 712 029 | 712 442 | 711 577 | -0.12% |
| 600 | 304.8 | 516.4 | 276.1 | 402.2 | 537 853 | 537 854 | 537 424 | 537 850 | 537 063 | -0.15% |
| 700 | 304.8 | 551.7 | 318.7 | 417.2 | 427 730 | 427 724 | 427 282 | 427 720 | 427 004 | -0.17% |
| 800 | 304.8 | 586.9 | 360.6 | 432.0 | 353 107 | 353 096 | 352 642 | 353 092 | 352 441 | -0.19% |
| 900 | 304.8 | 622.2 | 401.9 | 446.5 | 299 786 | 299 771 | 299 305 | 299 767 | 299 175 | -0.20% |
| 1000 | 304.8 | 657.5 | 442.5 | 460.8 | 260 102 | 260 082 | 259 604 | 260 078 | 259 541 | -0.22% |
| 1100 | 304.8 | 692.7 | 482.6 | 475.0 | 229 595 | 229 572 | 229 081 | 229 567 | 229 081 | -0.22% |
| 1200 | 304.8 | 728.0 | 522.1 | 488.9 | 205 521 | 205 495 | 204 991 | 205 490 | 205 051 | -0.23% |
| 1300 | 304.8 | 763.3 | 561.2 | 502.7 | 186 107 | 186 077 | 185 560 | 186 072 | 185 678 | -0.23% |
| 1400 | 304.8 | 798.5 | 599.8 | 516.3 | 170 164 | 170 130 | 169 600 | 170 125 | 169 772 | -0.23% |
| 1500 | 304.8 | 833.8 | 638.0 | 529.8 | 156 866 | 156 828 | 156 284 | 156 823 | 156 509 | -0.23% |
| 2000 | 304.8 | 1010.1 | 823.4 | 595.2 | 114 113 | 114 053 | 113 439 | 114 047 | 113 900 | 0.40% |
| 2500 | 304.8 | 1186.4 | 1001.0 | 657.8 | 91 276 | 91 190 | 90 502 | 91 184 | 91 172 | 0.73% |
| 3000 | 304.8 | 1362.8 | 1172.3 | 718.2 | 77 215 | 77 099 | 76 332 | 77 092 | 77 193 | 1.12% |
| 3500 | 304.8 | 1539.1 | 1338.3 | 776.8 | 67 740 | 67 588 | 66 738 | 67 580 | 67 780 | 1.54% |
| 4000 | 304.8 | 1715.4 | 1499.9 | 833.7 | 60 944 | 60 751 | 59 816 | 60 742 | 61 031 | 1.99% |
| 4500 | 304.8 | 1891.7 | 1657.5 | 889.3 | 55 844 | 55 604 | 54 582 | 55 595 | 55 966 | 2.47% |
| 5000 | 304.8 | 2068.1 | 1811.7 | 943.7 | 51 883 | 51 592 | 50 481 | 51 581 | 52 029 | 2.98% |

Table A.7: Comparison of elastic in-plane flexural buckling: E = 199 948 MPa, b = 160 mm, $t_f$ = 10 mm, $t_w$ = 6 mm, $\alpha = 2.386^o$

| L [mm] | $h_{w,small}$ [mm] | $h_{w,large}$ [mm] | $x_{crit}$ [mm] | $h_{w,crit}$ [mm] | Numerical [kN] | | | | Empirical [kN] | |
|---|---|---|---|---|---|---|---|---|---|---|
| | | | | | Successive approximations | | Eigenvalue Buckling Analysis | | $P_{ex}$ | Max deviation |
| | | | | | 10 elements | 100 elements | 10 elements | 100 elements | | |
| 500 | 304.8 | 346.5 | 245.0 | 325.2 | 890 951 | 890 986 | 890 957 | 890 986 | 890 830 | -0.02% |
| 600 | 304.8 | 354.8 | 292.9 | 329.2 | 635 249 | 635 273 | 635 241 | 635 273 | 635 120 | -0.02% |
| 700 | 304.8 | 363.1 | 340.4 | 333.2 | 478 965 | 478 983 | 478 948 | 478 982 | 478 832 | -0.03% |
| 800 | 304.8 | 371.5 | 387.7 | 337.1 | 376 167 | 376 181 | 376 144 | 376 180 | 376 033 | -0.04% |
| 900 | 304.8 | 379.8 | 434.6 | 341.0 | 304 756 | 304 767 | 304 729 | 304 766 | 304 622 | -0.05% |
| 1000 | 304.8 | 388.1 | 481.2 | 344.9 | 253 009 | 253 017 | 252 979 | 253 017 | 252 875 | -0.06% |
| 1100 | 304.8 | 396.5 | 527.5 | 348.8 | 214 228 | 214 235 | 214 196 | 214 235 | 214 096 | -0.07% |
| 1200 | 304.8 | 404.8 | 573.5 | 352.6 | 184 357 | 184 363 | 184 323 | 184 362 | 184 226 | -0.07% |
| 1300 | 304.8 | 413.1 | 619.3 | 356.4 | 160 818 | 160 823 | 160 783 | 160 823 | 160 689 | -0.08% |
| 1400 | 304.8 | 421.5 | 664.8 | 360.2 | 141 910 | 141 914 | 141 873 | 141 913 | 141 782 | -0.09% |
| 1500 | 304.8 | 429.8 | 710.0 | 364.0 | 126 468 | 126 472 | 126 430 | 126 471 | 126 342 | -0.10% |
| 2000 | 304.8 | 471.5 | 932.4 | 382.5 | 79 341 | 79 343 | 79 299 | 79 342 | 79 224 | -0.15% |
| 2500 | 304.8 | 513.1 | 1149.4 | 400.6 | 56 230 | 56 230 | 56 184 | 56 229 | 56 121 | -0.19% |
| 3000 | 304.8 | 554.8 | 1361.4 | 418.3 | 42 973 | 42 972 | 42 925 | 42 972 | 42 873 | -0.23% |
| 3500 | 304.8 | 596.5 | 1569.1 | 435.6 | 34 557 | 34 556 | 34 507 | 34 555 | 34 464 | -0.27% |
| 4000 | 304.8 | 638.1 | 1772.9 | 452.5 | 28 820 | 28 819 | 28 768 | 28 818 | 28 735 | -0.30% |
| 4500 | 304.8 | 679.8 | 1973.2 | 469.2 | 24 699 | 24 697 | 24 645 | 24 696 | 24 620 | -0.32% |
| 5000 | 304.8 | 721.5 | 2170.2 | 485.7 | 21 617 | 21 614 | 21 560 | 21 614 | 21 544 | -0.34% |

Table A.8: Comparison of elastic in-plane flexural buckling: E = 199 948 MPa, b = 160 mm, $t_f$ = 10 mm, $t_w$ = 6 mm, $\alpha = 5.0^o$

| L [mm] | $h_{w,small}$ [mm] | $h_{w,large}$ [mm] | $x_{crit}$ [mm] | $h_{w,crit}$ [mm] | Numerical [kN] | | | | Empirical [kN] | |
|---|---|---|---|---|---|---|---|---|---|---|
| | | | | | Successive approximations | | Eigenvalue Buckling Analysis | | $P_{ex}$ | Max deviation |
| | | | | | 10 elements | 100 elements | 10 elements | 100 elements | | |
| 500 | 304.8 | 392.3 | 240.2 | 346.8 | 1 024 384 | 1 024 418 | 1 024 246 | 1 024 416 | 1 023 798 | -0.06% |
| 600 | 304.8 | 409.8 | 286.2 | 354.9 | 747 893 | 747 915 | 747 737 | 747 913 | 747 319 | -0.08% |
| 700 | 304.8 | 427.3 | 331.6 | 362.8 | 576 757 | 576 772 | 576 589 | 576 770 | 576 199 | -0.10% |
| 800 | 304.8 | 444.8 | 376.5 | 370.7 | 462 818 | 462 829 | 462 642 | 462 827 | 462 276 | -0.12% |
| 900 | 304.8 | 462.3 | 421.0 | 378.5 | 382 740 | 382 747 | 382 556 | 382 745 | 382 215 | -0.14% |
| 1000 | 304.8 | 479.8 | 464.9 | 386.1 | 324 057 | 324 061 | 323 868 | 324 059 | 323 549 | -0.16% |
| 1100 | 304.8 | 497.3 | 508.4 | 393.8 | 279 601 | 279 603 | 279 406 | 279 601 | 279 109 | -0.18% |
| 1200 | 304.8 | 514.8 | 551.4 | 401.3 | 244 999 | 244 999 | 244 798 | 244 997 | 244 522 | -0.19% |
| 1300 | 304.8 | 532.3 | 594.0 | 408.7 | 217 455 | 217 454 | 217 250 | 217 452 | 216 994 | -0.21% |
| 1400 | 304.8 | 549.8 | 636.3 | 416.1 | 195 113 | 195 110 | 194 903 | 195 108 | 194 667 | -0.23% |
| 1500 | 304.8 | 567.3 | 678.2 | 423.5 | 176 694 | 176 690 | 176 480 | 176 688 | 176 263 | -0.24% |
| 2000 | 304.8 | 654.8 | 882.6 | 459.2 | 119 136 | 119 127 | 118 901 | 119 125 | 118 770 | -0.31% |
| 2500 | 304.8 | 742.2 | 1079.8 | 493.7 | 89 751 | 89 738 | 89 495 | 89 735 | 89 441 | -0.35% |
| 3000 | 304.8 | 829.7 | 1270.9 | 527.2 | 72 302 | 72 284 | 72 024 | 72 281 | 72 040 | -0.36% |
| 3500 | 304.8 | 917.2 | 1456.8 | 559.7 | 60 884 | 60 860 | 60 582 | 60 858 | 60 664 | -0.36% |
| 4000 | 304.8 | 1004.7 | 1638.2 | 591.4 | 52 890 | 52 860 | 52 564 | 52 858 | 52 707 | -0.35% |
| 4500 | 304.8 | 1092.2 | 1815.5 | 622.5 | 47 009 | 46 973 | 46 657 | 46 970 | 46 860 | 0.43% |
| 5000 | 304.8 | 1179.7 | 1989.3 | 652.9 | 42 515 | 42 473 | 42 136 | 42 469 | 42 396 | 0.61% |

Table A.9: Comparison of elastic in-plane flexural buckling: E = 199 948 MPa, b = 160 mm, $t_f$ = 10 mm, $t_w$ = 6 mm, $\alpha = 10.0^o$

| L [mm] | $h_{w,small}$ [mm] | $h_{w,large}$ [mm] | $x_{crit}$ [mm] | $h_{w,crit}$ [mm] | Numerical [kN] | | | | Empirical [kN] | |
|---|---|---|---|---|---|---|---|---|---|---|
| | | | | | Successive approximations | | Eigenvalue Buckling Analysis | | $P_{ex}$ | Max deviation |
| | | | | | 10 elements | 100 elements | 10 elements | 100 elements | | |
| 500 | 304.8 | 481.1 | 232.3 | 386.7 | 1 300 597 | 1 300 613 | 1 299 825 | 1 300 605 | 1 298 537 | -0.16% |
| 600 | 304.8 | 516.4 | 275.6 | 402.0 | 983 748 | 983 748 | 982 933 | 983 740 | 981 820 | -0.20% |
| 700 | 304.8 | 551.7 | 318.0 | 416.9 | 783 766 | 783 754 | 782 913 | 783 746 | 781 961 | -0.23% |
| 800 | 304.8 | 586.9 | 359.6 | 431.6 | 648 176 | 648 155 | 647 288 | 648 146 | 646 487 | -0.26% |
| 900 | 304.8 | 622.2 | 400.6 | 446.1 | 551 245 | 551 214 | 550 322 | 551 206 | 549 663 | -0.29% |
| 1000 | 304.8 | 657.5 | 441.0 | 460.3 | 479 067 | 479 029 | 478 110 | 479 020 | 477 587 | -0.31% |
| 1100 | 304.8 | 692.7 | 480.8 | 474.3 | 423 559 | 423 513 | 422 567 | 423 504 | 422 174 | -0.33% |
| 1200 | 304.8 | 728.0 | 520.0 | 488.2 | 379 738 | 379 685 | 378 711 | 379 675 | 378 442 | -0.34% |
| 1300 | 304.8 | 763.3 | 558.8 | 501.9 | 344 386 | 344 326 | 343 324 | 344 316 | 343 174 | -0.35% |
| 1400 | 304.8 | 798.5 | 597.1 | 515.4 | 315 344 | 315 276 | 314 245 | 315 266 | 314 211 | -0.36% |
| 1500 | 304.8 | 833.8 | 634.9 | 528.7 | 291 112 | 291 037 | 289 977 | 291 026 | 290 056 | -0.36% |
| 2000 | 304.8 | 1010.1 | 818.3 | 593.4 | 213 151 | 213 031 | 211 820 | 213 019 | 212 419 | -0.34% |
| 2500 | 304.8 | 1186.4 | 993.6 | 655.2 | 171 464 | 171 290 | 169 916 | 171 277 | 170 992 | 0.63% |
| 3000 | 304.8 | 1362.8 | 1162.5 | 714.8 | 145 781 | 145 541 | 143 995 | 145 526 | 145 521 | 1.05% |
| 3500 | 304.8 | 1539.1 | 1325.9 | 772.4 | 128 467 | 128 149 | 126 423 | 128 133 | 128 381 | 1.53% |
| 4000 | 304.8 | 1715.4 | 1484.8 | 828.4 | 116 050 | 115 641 | 113 726 | 115 623 | 116 106 | 2.05% |
| 4500 | 304.8 | 1891.7 | 1639.6 | 883.0 | 106 734 | 106 222 | 104 114 | 106 202 | 106 907 | 2.61% |
| 5000 | 304.8 | 2068.1 | 1791.0 | 936.4 | 99 503 | 98 877 | 96 570 | 98 855 | 99 770 | 3.21% |

## A.3 Web-tapered column resistances using the proposed approach

Table A.10: Web-tapered column resistance: Case 1 $\alpha = 2.5^o$, with a unit load

| Length [m] | Position | h [mm] | $A_g$ [mm$^2$] | Step 1 $C_e$ [kN] | $f_e$ [MPa] | Step 2 $C_{applied}$ [kN] | $f_{applied}$ [MPa] | Step 3 $\lambda$ [-] | Step 4 $A_{eff}$ [mm$^2$] | Step 5 $C_r$ [kN] |
|---|---|---|---|---|---|---|---|---|---|---|
| | Small end | 250 | 5840 | 45730 | 7830 | 1000 | 171 | 0.213 | 5840 | 1865 |
| 2 | Middle | 294 | 6189 | | 7389 | | 162 | | | |
| | Large end | 337 | 6539 | | 6994 | | 153 | | | |
| | Small end | 250 | 5840 | 15091 | 2584 | 1000 | 171 | 0.371 | 5840 | 1856 |
| 4 | Middle | 337 | 6539 | | 2308 | | 153 | | | |
| | Large end | 425 | 7237 | | 2085 | | 138 | | | |
| | Small end | 250 | 5840 | 8484 | 1453 | 1000 | 171 | 0.494 | 5840 | 1831 |
| 6 | Middle | 381 | 6888 | | 1232 | | 145 | | | |
| | Large end | 512 | 7936 | | 1069 | | 126 | | | |
| | Small end | 250 | 5840 | 5856 | 1003 | 1000 | 171 | 0.595 | 5840 | 1790 |
| 8 | Middle | 425 | 7237 | | 809 | | 138 | | | |
| | Large end | 599 | 8634 | | 678 | | 116 | | | |
| | Small end | 250 | 5840 | 4495 | 770 | 1000 | 171 | 0.679 | 5840 | 1735 |
| 10 | Middle | 468 | 7586 | | 592 | | 132 | | | |
| | Large end | 687 | 9333 | | 482 | | 107 | | | |
| | Small end | 250 | 5840 | 2931 | 502 | 1000 | 171 | 0.841 | 5840 | 1576 |
| 15 | Middle | 577 | 8460 | | 346 | | 118 | | | |
| | Large end | 905 | 11079 | | 265 | | 90 | | | |

# Appendix B

# Design of web-tapered beams

## B.1 Web-tapered beam resistances using the proposed approach

Table B.1: Web-tapered beam utilisation: L = 6 m, 400x200 (8W, 10F), $\alpha = 2.5^o$

| $\kappa$ [-] | Position [m] | Step 1 $f_{top\ flange}$ [MPa] | Step 2 $C_b$ [-] | Step 3 $f_{cr,mid}$ [MPa] | Step 4 $\gamma_{eLTB}$ [-] | Step 5 $f_{cr}$ [MPa] | Step 6+7 $f_r$ [MPa] | Utilisation [%] |
|---|---|---|---|---|---|---|---|---|
| | 0 | 106.0 | | | | 210.4 | 189.3 | 56% |
| | 1 | 82.3 | | | | 163.5 | 147.1 | 56% |
| | 2 | 66.4 | | | | 131.8 | 118.7 | 56% |
| -1 | 3 | 55.0 | 1.44 | 210.4 | 1.985 | 109.2 | 98.3 | 56% |
| | 4 | 46.5 | | | | 92.4 | 83.1 | 56% |
| | 5 | 40.0 | | | | 79.4 | 66.0* | 61% |
| | 6 | 34.8 | | | | 69.1 | 56.4* | 62% |
| | 0 | 106.0 | | | | 256.1 | 224.8 | 47% |
| | 1 | 68.6 | | | | 165.8 | 149.2 | 46% |
| | 2 | 44.3 | | | | 107.0 | 96.3 | 46% |
| 0 | 3 | 27.5 | 1.75 | 256.1 | 2.416 | 66.5 | 59.8 | 46% |
| | 4 | 15.5 | | | | 37.5 | 33.7 | 46% |
| | 5 | 6.7 | | | | 16.1 | 13.5* | 49% |
| | 6 | 0.0 | | | | 0.0 | 0.0* | - |
| | 0 | 0.0 | | | | 0.0 | 0.0 | - |
| | 1 | 13.7 | | | | 71.6 | 64.5 | 21% |
| | 2 | 22.1 | | | | 115.5 | 104.0 | 21% |
| $0_*$ | 3 | 27.5 | 1.24 | 181.6 | 5.219 | 143.6 | 129.2 | 21% |
| | 4 | 31.0 | | | | 161.9 | 145.7 | 21% |
| | 5 | 33.3 | | | | 173.9 | 144.8 | 23% |
| | 6 | 34.8 | | | | 181.6 | 148.2 | 23% |
| | 0 | 106.0 | | | | 311.3 | 250.1 | 42% |
| | 1 | 54.9 | | | | 161.2 | 145.1 | 38% |
| | 2 | 22.1 | | | | 65.0 | 58.5 | 38% |
| +1 | 3 | 0.0 | 2.13 | 311.3 | 2.937 | 0.0 | 0.0 | - |
| | 4 | -15.5 | | | | -45.6 | -41.0 | 38% |
| | 5 | -26.7 | | | | -78.3 | -65.5* | 41% |
| | 6 | -34.8 | | | | -102.2 | -83.4* | 42% |

Table B.2: Web-tapered beam utilisation: L = 6 m, 400x200 (8W, 10F), $\alpha = 5.0^o$

| $\kappa$ [-] | Position [m] | Step 1 $f_{top\ flange}$ [MPa] | Step 2 $C_b$ [-] | Step 3 $f_{cr,mid}$ [MPa] | Step 4 $\gamma_{eLTB}$ [-] | Step 5 $f_{cr}$ [MPa] | Step 6+7 $f_r$ [MPa] | Utilisation [%] |
|---|---|---|---|---|---|---|---|---|
| | 0 | 106.0 | | | | 196.7 | 177.1 | 60% |
| | 1 | 66.4 | | | | 123.2 | 110.9 | 60% |
| | 2 | 46.5 | | | | 86.3 | 77.6 | 60% |
| -1 | 3 | 34.7 | 1.58 | 196.7 | 1.856 | 64.5 | 52.6* | 66% |
| | 4 | 27.1 | | | | 50.4 | 39.2* | 69% |
| | 5 | 21.8 | | | | 40.6 | 29.9* | 73% |
| | 6 | 18.0 | | | | 33.5 | 23.0* | 78% |
| | 0 | 106.0 | | | | 217.9 | 196.1 | 54% |
| | 1 | 55.3 | | | | 113.7 | 102.3 | 54% |
| | 2 | 31.0 | | | | 63.7 | 57.3 | 54% |
| 0 | 3 | 17.4 | 1.75 | 217.9 | 2.056 | 35.7 | 29.2* | 59% |
| | 4 | 9.0 | | | | 18.6 | 14.6* | 62% |
| | 5 | 3.6 | | | | 7.5 | 5.6* | 65% |
| | 6 | 0.0 | | | | 0.0 | 0.0* | - |
| | 0 | 0.0 | | | | 0.0 | 0.0 | - |
| | 1 | 11.1 | | | | 79.0 | 71.1 | 16% |
| | 2 | 15.5 | | | | 110.7 | 99.6 | 16% |
| $0_*$ | 3 | 17.4 | 1.03 | 128.8 | 7.072 | 124.1 | 101.6 | 17% |
| | 4 | 18.1 | | | | 129.2 | 101.0 | 18% |
| | 5 | 18.2 | | | | 130.1 | 96.2 | 19% |
| | 6 | 18.0 | | | | 128.8 | 88.5 | 20% |
| | 0 | 106.0 | | | | 241.2 | 216.0 | 49% |
| | 1 | 44.2 | | | | 100.7 | 90.6 | 49% |
| | 2 | 15.5 | | | | 35.3 | 31.7 | 49% |
| +1 | 3 | 0.0 | 1.94 | 241.2 | 2.276 | 0.0 | 0.0* | - |
| | 4 | -9.0 | | | | -20.6 | -16.2* | 56% |
| | 5 | -14.6 | | | | -33.2 | -24.8* | 59% |
| | 6 | -18.0 | | | | -41.0 | -28.2* | 64% |

# Appendix C

# Web-tapered portal frame designs by commercial software

| SPLICE BOLT TABLE | | | | | | |
|---|---|---|---|---|---|---|
| Mark | Qty Top | Bot | Int | Type | Dia | Length |
| SP-1 | 4 | 4 | 0 | Gr8.8 | 20 | 70 |
| SP-2 | 4 | 4 | 0 | Gr8.8 | 16 | 40 |

FLANGE BRACES: Both Sides(U.N.)
FBxxA(1): xx=length(mm)
A - L40x4

| MEMBER TABLE | | | | | | | |
|---|---|---|---|---|---|---|---|
| Mark | Weight | Length | Web Depth Start/End | Web Plate Thick | Web Plate Length | Outside Flange W x Thk x Length | Inside Flange W x Thk x Length |
| RF2-1 | 155 | 4314 | 250/ 400 | 6 | 3876 | 150 x 6 x 4296 | 150 x 6 x 3878 |
| | | | 400/ 354 | 8 | 457 | 150 x 6 x 558 | |
| RF2-2 | 318 | 9466 | 350/ 350 | 6 | 9438 | 150 x 8 x 1235 | 150 x 6 x 6000 |
| | | | | | | 150 x 6 x 6000 | 150 x 6 x 3402 |
| | | | | | | 150 x 6 x 2202 | |

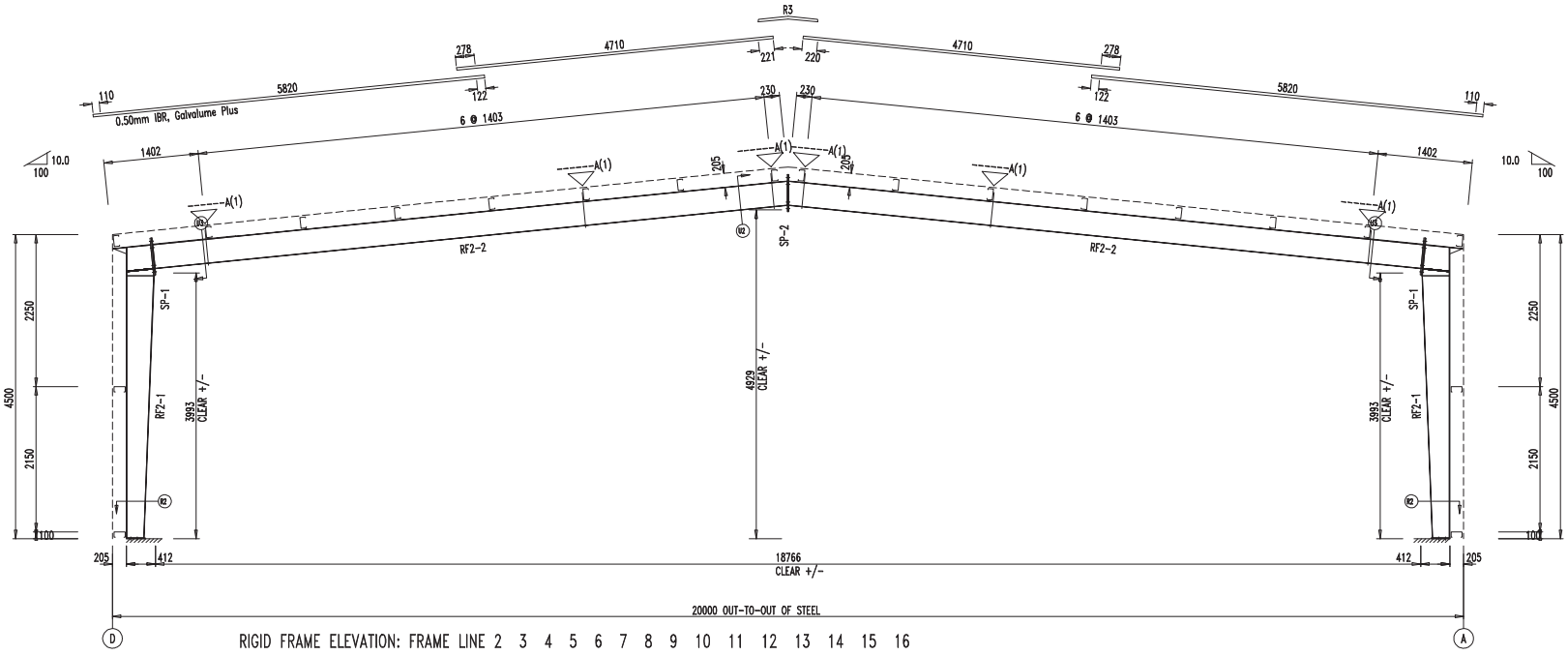


RIGID FRAME ELEVATION: FRAME LINE 2 3 4 5 6 7 8 9 10 11 12 13 14 15 16

| NO. | DATE | DETAILS | DES | DRW | CHK |
|---|---|---|---|---|---|
| 0 | 9/17/16 | . | DES | DET | . |

REVISIONS

CUSTOMER
Customer
Customer Address Two

CUSTOMER JOB No :

PROJECT
Project
Project Address One
Project Address Two

LOCATION

CLOTAN BUILDING SYSTEMS
*Ora et Labora*
130 Hertz Blvd., NW7, Vanderbijlpark, South Africa
Ph: +27 (0)16 986 8000 +27 (0)16 986 8050 (fax)

DRG.TITLE
RIGID FRAME ELEVATION

Case study 1:
20 m x 4.5 m

| APPRD. | DATE | SCALE |
|---|---|---|
| . | 9/17/16 | N.T.S. |

| JOB NO. | BUILDING NO. | DRAWING NO. | REV. |
|---|---|---|---|
| US_Test_20x80 | . | of | 0 |

| SPLICE BOLT TABLE | | | | | | |
|---|---|---|---|---|---|---|
| Mark | Qty Top | Bot | Int | Type | Dia | Length |
| SP-1 | 4 | 4 | 0 | Gr8.8 | 24 | 75 |
| SP-2 | 4 | 4 | 0 | Gr8.8 | 16 | 40 |

FLANGE BRACES: Both Sides(U.N.)
FBxxB(1): xx=length(mm)
B - L50x5
A - L40x4

| MEMBER TABLE | | | | | | | |
|---|---|---|---|---|---|---|---|
| Mark | Weight | Length | Web Depth Start/End | Web Plate Thick | Web Plate Length | Outside Flange W x Thk x Length | Inside Flange W x Thk x Length |
| RF2-1 | 254 | 4340 | 250/ 500 | 5 | 3703 | 180 x 10 x 4318 | 180 x 12 x 3711 |
| | | | 500/ 434 | 10 | 659 | 180 x 10 x 641 | |
| RF2-2 | 401 | 8378 | 550/ 398 | 5 | 2496 | 180 x 10 x 6000 | 180 x 10 x 2351 |
| | | | 398/ 300 | 5 | 5850 | 180 x 10 x 2346 | 180 x 10 x 6000 |
| | | | | | | | 180 x 10 x 0 |
| RF2-3 | 176 | 6025 | 300/ 300 | 5 | 6000 | 150 x 6 x 6000 | 150 x 6 x 5969 |

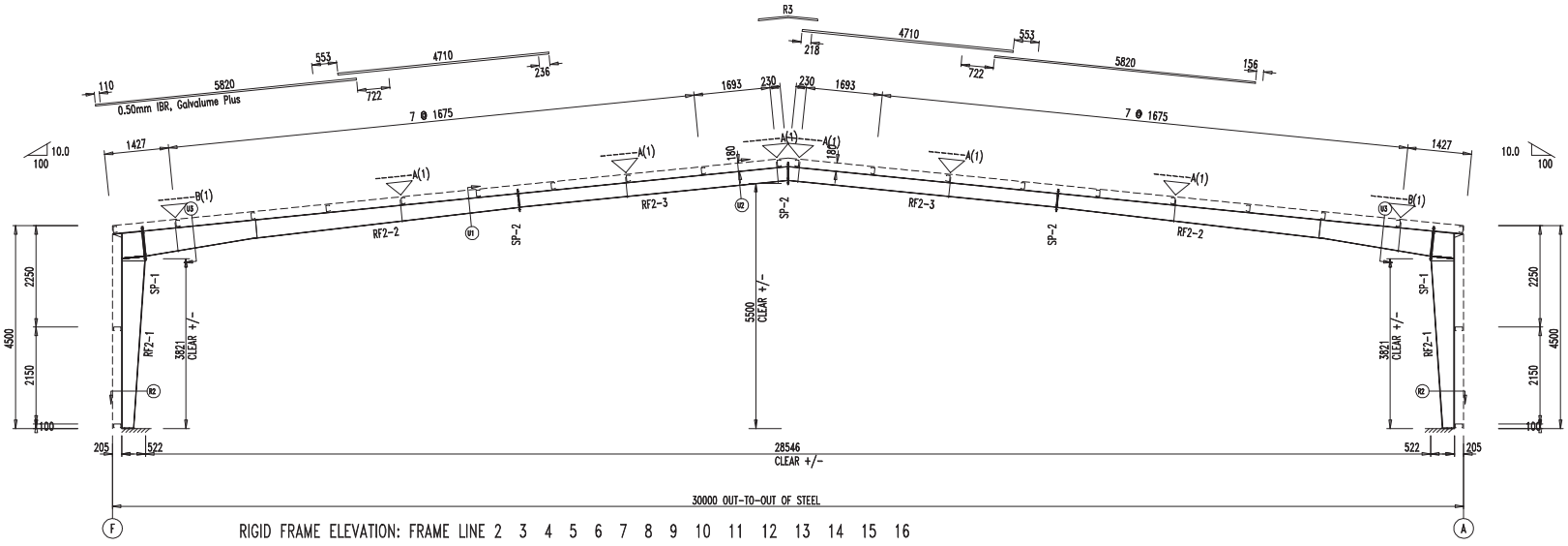


RIGID FRAME ELEVATION: FRAME LINE 2 3 4 5 6 7 8 9 10 11 12 13 14 15 16

| NO. | DATE | DETAILS | DES | DRW | CHK |
|---|---|---|---|---|---|
| 0 | 9/18/16 | . | DES | DET | . |

REVISIONS

CUSTOMER
Customer
Customer Address Two

CUSTOMER JOB No :

PROJECT
Project
Project Address One
Project Address Two

LOCATION

CLOTAN BUILDING SYSTEMS
Ora et Labora
130 Hertz Blvd., NW7, Vanderbijlpark, South Africa
Ph: +27 (0)16 986 8000 +27 (0)16 986 8050 (fax)

DRG.TITLE
RIGID FRAME ELEVATION

Case study 2:
30 m x 4.5 m

| APPRD. | DATE | SCALE |
|---|---|---|
| . | 9/18/16 | N.T.S. |

| JOB NO. | BUILDING NO. | DRAWING NO. | REV. |
|---|---|---|---|
| US_Test_30x80 | . | of | 0 |

| SPLICE BOLT TABLE | | | | | | |
|---|---|---|---|---|---|---|
| Mark | Qty Top | Bot | Int | Type | Dia | Length |
| SP-1 | 4 | 4 | 2 | Gr8.8 | 24 | 75 |
| SP-2 | 4 | 4 | 0 | Gr8.8 | 16 | 40 |

FLANGE BRACES: Both Sides(U.N.)
FBxxB(1): xx=length(mm)
B - L50x5
A - L40x4

| MEMBER TABLE | | | | | | | |
|---|---|---|---|---|---|---|---|
| Mark | Weight | Length | Web Depth Start/End | Web Plate Thick | Web Plate Length | Outside Flange W x Thk x Length | Inside Flange W x Thk x Length |
| RF2-1 | 349 | 4340 | 450/ 850 | 6 | 3488 | 200 x 10 x 4318 | 200 x 10 x 3510 |
| | | | 850/ 759 | 8 | 907 | 200 x 10 x 968 | |
| RF2-2 | 454 | 7052 | 850/ 842 | 5 | 1232 | 180 x 12 x 1082 | 180 x 12 x 1082 |
| | | | 842/ 551 | 5 | 5789 | 180 x 10 x 5939 | 180 x 10 x 5946 |
| RF2-3 | 219 | 6024 | 550/ 350 | 5 | 6000 | 150 x 6 x 6000 | 150 x 6 x 6000 |
| | | | | | | | 150 x 6 x 3 |
| RF2-4 | 277 | 6025 | 350/ 350 | 5 | 6000 | 180 x 10 x 6000 | 180 x 10 x 5964 |

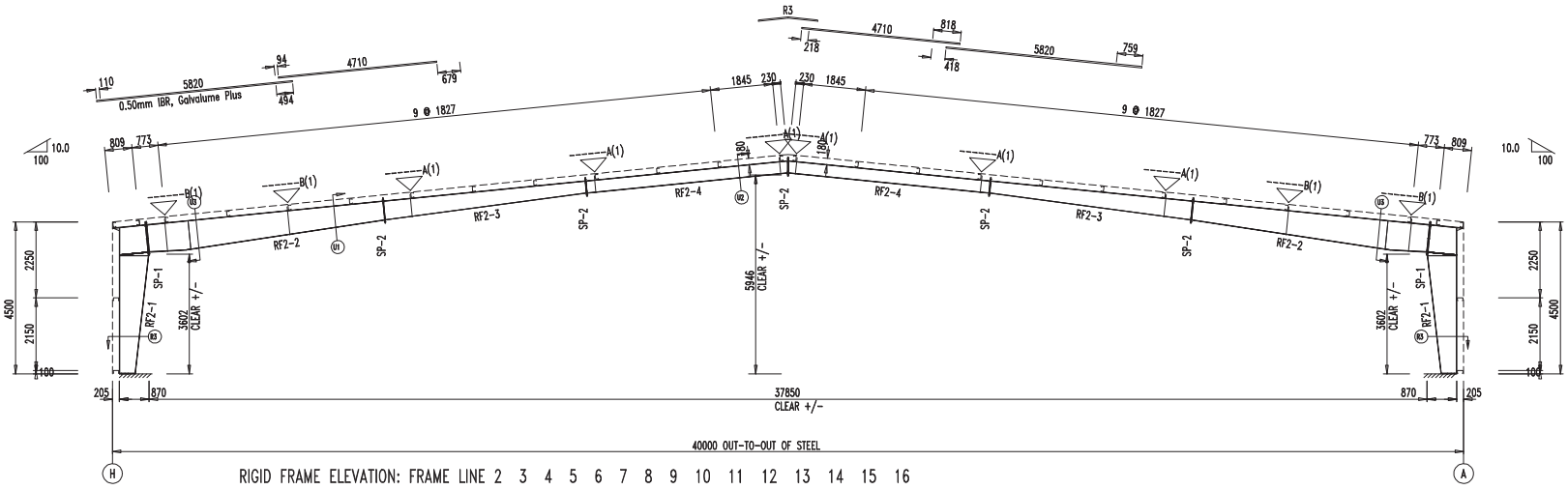


RIGID FRAME ELEVATION: FRAME LINE 2 3 4 5 6 7 8 9 10 11 12 13 14 15 16

| NO. | DATE | DETAILS | DES | DRW | CHK |
|---|---|---|---|---|---|
| 0 | 9/18/16 | . | DES | DET | . |

REVISIONS

CUSTOMER
Customer
Customer Address Two

CUSTOMER JOB No :

PROJECT
Project
Project Address One
Project Address Two

LOCATION

CLOTAN BUILDING SYSTEMS
*Ora et Labora*
130 Hertz Blvd., NW7, Vanderbijlpark, South Africa
Ph: +27 (0)16 986 8000 +27 (0)16 986 8050 (fax)

DRG.TITLE
RIGID FRAME ELEVATION

Case study 3:
40 m x 4.5 m

| APPRD. | DATE | SCALE |
|---|---|---|
| . | 9/18/16 | N.T.S. |

| JOB NO. | BUILDING NO. | DRAWING NO. | REV. |
|---|---|---|---|
| US_Test_40x80 | . | of | 0 |

| SPLICE BOLT TABLE | | | | | | |
|---|---|---|---|---|---|---|
| Mark | Qty Top | Bot | Int | Type | Dia | Length |
| SP-1 | 4 | 4 | 2 | Gr8.8 | 24 | 75 |
| SP-2 | 4 | 4 | 2 | Gr8.8 | 20 | 70 |
| SP-3 | 4 | 4 | 0 | Gr8.8 | 16 | 40 |

FLANGE BRACES: Both Sides(U.N.)
FBxxA(1): xx=length(mm)
A – L40x4
B – L50x5

| MEMBER TABLE | | | | | | | |
|---|---|---|---|---|---|---|---|
| Mark | Weight | Length | Web Depth Start/End | Web Plate Thick | Web Plate Length | Outside Flange W x Thk x Length | Inside Flange W x Thk x Length |
| RF2-1 | 484 | 4340 | 650/1250 | 8 | 4431 | 180 x 10 x 4318<br>180 x 10 x 1335 | 180 x 10 x 3230 |
| RF2-2 | 487 | 5786 | 1150/1038<br>1038/ 801 | 6<br>5 | 2900<br>2850 | 180 x 10 x 5750 | 180 x 10 x 2752<br>180 x 10 x 3009 |
| RF2-3 | 533 | 12028 | 799/ 596<br>596/ 450 | 5<br>5 | 6150<br>5850 | 150 x 8 x 6000<br>150 x 6 x 6000 | 150 x 8 x 6000<br>150 x 8 x 3<br>150 x 6 x 6000<br>150 x 6 x 2 |
| RF2-4 | 286 | 5946 | 450/ 350 | 5 | 5921 | 180 x 10 x 5921 | 180 x 10 x 5885 |

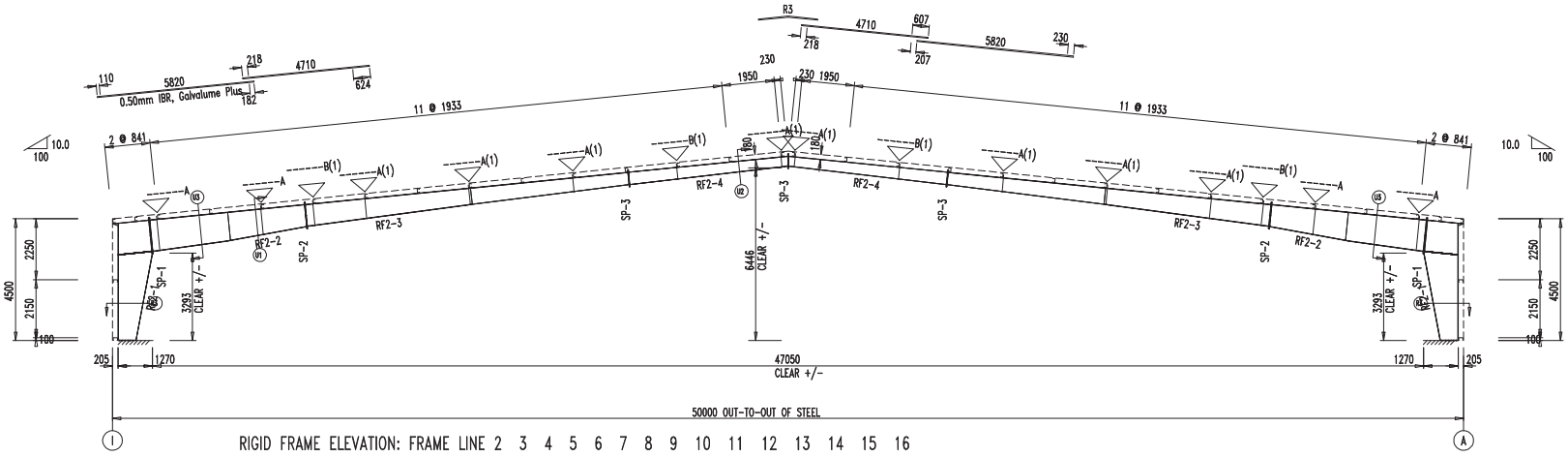


RIGID FRAME ELEVATION: FRAME LINE 2 3 4 5 6 7 8 9 10 11 12 13 14 15 16

| NO. | DATE | DETAILS | DES | DRW | CHK |
|---|---|---|---|---|---|
| | | | | | |
| | | | | | |
| | | | | | |
| 0 | 9/18/16 | . | DES | DET | . |

REVISIONS

CUSTOMER
Customer
Customer Address Two

CUSTOMER JOB No :

PROJECT
Project
Project Address One
Project Address Two

LOCATION

CLOTAN BUILDING SYSTEMS
*Ora et Labora*
130 Hertz Blvd., NW7, Vanderbijlpark, South Africa
Ph: +27 (0)16 986 8000 +27 (0)16 986 8050 (fax)

DRG.TITLE
RIGID FRAME ELEVATION

Case study 4:
50 m x 4.5 m

| APPRD. | DATE | SCALE |
|---|---|---|
| . | 9/18/16 | N.T.S. |
| JOB NO. | BUILDING NO. | DRAWING NO. / REV. |
| US_Test_50x80 | . | of / 0 |

# Appendix D

# Structural optimisation report sheet

50mx4.5WebTaperReport.txt

GA operators:

| 'Variables' | 'Population Size' | 'Generations' |
|---|---|---|
| [10] | [50] | [100] |
| 'Stop Criteria' | '% Completed' | 'Forced Stop' |
| [0.9800] | [100] | 'No' |
| 'Replace Rate' | 'Select. Rate' | '-' |
| [0.2000] | [0.8000] | '-' |
| 'Replace Pop' | 'Select Pop' | '-' |
| [10] | [40] | '-' |
| 'Total Genes' | 'Mutat. Rate' | 'Mutations/Gen' |
| [500] | [0.2000] | [100] |

| 'Optimum (kg)' | 'Violations' |
|---|---|
| [4789.7] | [0] |

Combination =

```
     4    95     1     8     4   107     1     1     8
4
```

Column

| 'hw bot' | 'hw top' | 'tw' | 'b' | 'tf' |
|---|---|---|---|---|
| [0.2800] | [1.1900] | [0.0060] | [0.2000] | [0.0120] |

Rafter

| 'hw bot' | 'hw top' | 'tw' | 'b' | 'tf' |
|---|---|---|---|---|
| [1.3100] | [0.2500] | [0.0060] | [0.2000] | [0.0120] |

Deflections:

| '-----' | 'X (mm)' | 'Y (mm)' |
|---|---|---|
| 'Limit' | [33.3750] | [ 274.0000] |
| '-----' | '------' | '------' |
| 'Load Comb' | 'X (mm)' | 'Y (mm)' |
| 'SLS1' | [12.0759] | [-137.1394] |
| 'SLS2' | [-9.1658] | [ 33.7721] |

Servicebility limit state:

| 'Displacement' | 'Unity' | 'Node' |
|---|---|---|
| 'Horizontal' | [0.3618] | [ 63] |
| 'Vertical' | [0.5005] | [ 41] |

Ultimate limit state:

| 'Shear' | 'Unity' | 'Node' |
|---|---|---|
| 'Shear (Purlin)' | [0.5324] | [ 93] |

| 'Comb Axi+Bending' | 'Unity' | 'Node' |
|---|---|---|
| 'Global (Purlin)' | [0.5221] | [ 91] |
| 'Torsion (Brace)' | [0.9987] | [ 57] |
| 'Torsion (Purlin)' | [0.5153] | [ 91] |

| 'Comb Ten+Bending' | 'Unity' | 'Node' |
|---|---|---|
| 'Method 1(Purlin)' | [0.3363] | [ 44] |
| 'Method 2(Purlin)' | [0.1856] | [ 42] |

History

| 'Gen' | 'Opt sol' | 'Viol' |
|---|---|---|
| ans = | | |
| 1 | 7021.3 | 0 |
| 2 | 7021.3 | 0 |
| .... | | |
| .... | | |
| .... | | |
| 99 | 4789.7 | 0 |
| 100 | 4789.7 | 0 |

Displacement at FEM nodes [DOF1=Ux,2=Uy,3=Rz, ...]

| '[m / Rad]' | '[m / Rad]' | '[m / Rad]' | '[m / Rad]' |
|---|---|---|---|
| 'SLS1' | 'SLS2' | 'ULS1' | 'ULS2' |
| ans = | | | |
| 0 | 0 | 0 | 0 |
| 0 | 0 | 0 | 0 |
| 0.0059 | 0.0005 | 0.0076 | -0.0032 |
| -0.0013 | -0.0001 | -0.0016 | 0.0007 |
| 0.0001 | 0.0000 | 0.0002 | -0.0001 |
| 0.0058 | 0.0005 | 0.0074 | -0.0031 |
| -0.0025 | -0.0002 | -0.0032 | 0.0013 |
| 0.0002 | 0.0000 | 0.0003 | -0.0001 |
| 0.0055 | 0.0005 | 0.0071 | -0.0028 |
| .... | | | |
| .... | | | |
| .... | | | |
| .... | | | |

# Appendix E

# Matlab source code to the structural optimisation algorithm

## GAscript.m

```
%% MAIN SCRIPT:
% Excutable script to optimizing the structural problem.
% Herman Aucamp.
% 15045471.
%% Clear all parameters:
% Clear memory.
% Close all figures.
% Clear command window.
% Use a compact format in command window
% ------------------------------------------------------------------------
clear all
close all
clc
format compact
%% GA Variables:
% Number of optimization variables.
% List of angles including m,A,rx,ry.
% Variable minimum limit.
% Variable maximum limit.
% Number of generations.
% Population size.
% Mutation rate ratio of all genes in population.
% Selection ratio.
% Replace ratio.
% Selection population size.
% Replaced populations size.
% Number of matings between Chromosomes.
% Number of mutations in populations total genes.
% Stopping criteria ratio in population becomes the same
% ------------------------------------------------------------------------
[NumVar,Var,List] = LISTfunc();
NumGen            = 100;
PopSize           = 50;
MutRate           = 0.2;
SelectR           = 0.8;
ReplaceR          = 1-SelectR;
SelectSize        = ceil(PopSize*SelectR);
ReplaceSize       = PopSize-SelectSize;
NumMutate         = ceil(PopSize*NumVar*MutRate);
StopCrit          = 0.98;
%% Create initial population:
% Assign generation counter.
% Create an array of each generation.
% Use function to select a random initial population.
% Allocate memory.
% Evaluate fitness of initial population.
% ------------------------------------------------------------------------
iGen        = 1;
Gen         = 1:NumGen;
flag        = 0;
Population      = INITfunc(PopSize);
Opt_data    = zeros(NumGen,1);
Viol_data   = zeros(NumGen,1);
Pop_data    = zeros(NumGen,NumVar);
fitness     = zeros(PopSize,1);
viol        = zeros(PopSize,1);
for i=1:PopSize
    [fitness(i),viol(i)] = FITNESSfunc(Population(i,:),iGen);
end
%% Initialise a graphical output:
% Print full screen.
% Display with major gridlines.
% Retain current plot after each generation.
% Allocate memory.
% ------------------------------------------------------------------------
figure('units','normalized','outerposition',[0 0 1 1]);
grid on; hold on;
%% Loop Selection/ Replacement/ Crossover/ Mutation, assemble a New Pop:
while iGen<=NumGen
% Clear command window
% Show percentage complete continuously.
% ------------------------------------------------------------------------
clc
if iGen > 1
    Combination=Pop_data(iGen-1,:);
    Percentage_complete=floor(((iGen)/NumGen)*100);
    display('------------------------------------------------------------')
    display('GA operators:');
    display({'Variables' 'Population Size' 'Generations'; ...
        NumVar PopSize NumGen; ...
        'Stop Criteria' '% Completed' 'Forced Stop'; ...
        StopCrit Percentage_complete flag; ...
        'Replace Rate' 'Select. Rate' '-'; ...
        ReplaceR SelectR '-'; ...
        'Replace Pop' 'Select Pop' '-'; ...
        ReplaceSize SelectSize '-'; ...
        'Total Genes' 'Mutat. Rate' 'Mutations/Gen'; ...
        NumVar*PopSize MutRate NumMutate})
    display('------------------------------------------------------------')
    display({'Optimum' 'Violations';Opt_data(iGen-1) Viol_data(iGen-1)})
    display('------------------------------------------------------------')
    display(Combination)
    display('------------------------------------------------------------')
    display('Column')
    display({'hw bot' 'hw top' 'tw' 'b' 'tf';...
        List{1}(Combination(1)) List{2}(Combination(2))...
        List{3}(Combination(3)) List{4}(Combination(4))...
        List{5}(Combination(5))})
    display('Rafter')
    display({'hw bot' 'hw top' 'tw' 'b' 'tf';...
        List{6}(Combination(6)) List{7}(Combination(7))...
        List{8}(Combination(8)) List{9}(Combination(9))...
        List{10}(Combination(10))})
    display('------------------------------------------------------------')
    [~, ~,~, ~, ~, ~, ~, D, ~, ~, ~, LimH, LimV, ~, ~, ~] =...
        FEMfunc(Combination);
    display('Deflections:');
    if max(D(1:3:end,1))<=abs(min(D(1:3:end,1)))
        MaxDispl_X1mm = min(D(1:3:end,1))*1000;
    else
        MaxDispl_X1mm = max(D(1:3:end,1))*1000;
    end
    if max(D(2:3:end,1))<=abs(min(D(2:3:end,1)))
        MaxDispl_Y1mm = min(D(2:3:end,1))*1000;
    else
        MaxDispl_Y1mm = max(D(2:3:end,1))*1000;
    end
    if max(D(1:3:end,2))<=abs(min(D(1:3:end,2)))
        MaxDispl_X2mm = min(D(1:3:end,2))*1000;
    else
        MaxDispl_X2mm = max(D(1:3:end,2))*1000;
    end
    if max(D(2:3:end,2))<=abs(min(D(2:3:end,2)))
        MaxDispl_Y2mm = min(D(2:3:end,2))*1000;
    else
        MaxDispl_Y2mm = max(D(2:3:end,2))*1000;
    end
```

```
    display({'-----'  'X (mm)' 'Y (mm)';...
        'Limit' LimH*1000 LimV*1000;...
        '-----' '------' '------';...
        'Load Comb' 'X (mm)' 'Y (mm)';...
        'SLS1'      MaxDispl_X1mm MaxDispl_Y1mm;...
        'SLS2'      MaxDispl_X2mm MaxDispl_Y2mm})
    display('------------------------------------------------------------')
    display(Percentage_complete)
end
%% Selection of individuals into mating pool:
% "Sort according to chromosome fitness & remove to weakest (heaviest)...
% ...solution(s) from the population".
% Allocate memory.
% Give a [PopSize x NumVar] matrix and add the fitness...
% ...(total weight of the solution) as a final column.
% Sort population according to the last row which...
% ...contains the fitness of the "chromosome".
% The fitness column (to be removed) after the sorting is completed.
% Actually remove the fitness column.
% Assign the fittest candidates to a temporary population with the size...
% of the "selected" population.
% -------------------------------------------------------------------------
SelectPop  = zeros(SelectSize,NumVar);
TempPop = [Population,fitness,viol];
TempPop = sortrows(TempPop,[NumVar+2,NumVar+1]);
cols2remove = [NumVar+1,NumVar+2];
TempPop(:,cols2remove)=[];
for i=1:SelectSize
    SelectPop(i,:) = TempPop(i,:);
end
%% Replacement by Elitism into next generation:
% "Skim the fittest (lighest) solution from the temporary population...
% to be carried forward without modification into the next generation".
% Assign this population as the "Replaced" population.
% -------------------------------------------------------------------------
ReplacePop = zeros(ReplaceSize,NumVar);
for i=1:ReplaceSize
    ReplacePop(i,:) = SelectPop(i,:);
end
%% Crossover:
% Choose 2 random parent chromosome index numbers after the...
% ...selection routine.
% Eliminate the case where the same parent breads with itself.
% Two-point crossover technique of crossing the genes.
% The RHS chromosome "addresses" to be switched between parents.
% Switch the chromosomes: i.e. Parent 1 LHS and Parent 2 RHS.
% -------------------------------------------------------------------------
for i=1:SelectSize
    ParentIndex1 = randi([1,SelectSize]);
    ParentIndex2 = randi([1,SelectSize]);
    while ParentIndex2 == ParentIndex1
        ParentIndex2 = randi([1,SelectSize]);
    end
    CrossIndex1 = randi([1,NumVar-2]);
    CrossIndex2 = randi([CrossIndex1,NumVar-1]);
    j=(CrossIndex1+1):CrossIndex2;
    for j=(CrossIndex1+1):CrossIndex2
        SelectPop(ParentIndex1,j) = SelectPop(ParentIndex2,j);
        SelectPop(ParentIndex2,j) = SelectPop(ParentIndex1,j);
    end
end
%% Mutation:
% Choose a random chromosome index number after the selection routine...
% ...and after the population has undercone crossover; change...
% ...1 gene for every number of mutations.
% Thus 1 chromosome may have zero, 1 or more gene mutations.
% Uniform mutation technique (UMT), one random gene is considered.
% UMT: Gene is randomly replaced by any value between the boundaries to...
% ...allow for diversity.
% -------------------------------------------------------------------------
for i=1:NumMutate
    ParentIndex1 = randi([1,SelectSize]);
    GeneIndex = randi([1,NumVar]);
    SelectPop(ParentIndex1,GeneIndex) = ...
        randi([1,length(List{GeneIndex})]);
end
%% Create new Population:
% Replace fittest solutions from previous generation into new population.
% Allocate memory.
% -------------------------------------------------------------------------
Population = zeros(PopSize,NumVar);
for i=1:ReplaceSize
    Population(i,:) = ReplacePop(i,:);
end
for i=ReplaceSize+1:PopSize
    Population(i,:) = SelectPop(i-ReplaceSize,:);
end
fitness = zeros(PopSize,1);
for i=1:PopSize
    % %Force prismatic member (also change ativate comment at INITfunc)
%     Population(i,1)=subs(Population(i,2));
%     Population(i,7)=subs(Population(i,6));
    [fitness(i),viol(i)]=FITNESSfunc(Population(i,:),iGen);
end
%% Stopping criterion:
% Create a [PopSize x NumVar] temp matrix and add the fitness...
% ...(total weight of the solution) and violations as final columns.
% Sort population according to the row which contains...
% ...the fitness of the "chromosome".
% Check if the x % of the most fit chromosomes are the same; if so the...
% ...break the while loop and give summary.
% -------------------------------------------------------------------------
stopValue = ceil(StopCrit*PopSize);
iPop = 0;
for i=2:PopSize
    TempPop = [Population,fitness,viol];
    TempPop = sortrows(TempPop,[NumVar+2,NumVar+1]);
    if TempPop(1,NumVar+1) == TempPop(i,NumVar+1)
        iPop = iPop + 1;
        if iPop == stopValue
            flag = 1;
        end
    end
end
if flag == 1
    break
end
%% Continuous graphical output:
% Report generation's optimum weight and number of violations...
% ...if there are no violations.
% Else report generation's maximum optimum weight and...
% number of violations if there are no violations.
% Plot the updated optimum_data vs the number of generations.
% Adjust vertical axis to 3 times the current optimal weight.
% -------------------------------------------------------------------------
for i=1:PopSize
    if TempPop(i,NumVar+2) == 0
        Opt_data(iGen) = TempPop(i,NumVar+1);
        Viol_data(iGen) = TempPop(i,NumVar+2);
```

```
        Pop_data(iGen,:) = TempPop(i,1:NumVar);
    else
        Opt_data(iGen) = min(TempPop(:,NumVar+1));
        Viol_data(iGen) = mean(TempPop(i,NumVar+2));
        Pop_data(iGen,:) = TempPop(i,1:NumVar);
    end
    break
end
FXfunc(NumGen,iGen,Gen,Opt_data,Pop_data(iGen,:));
drawnow;
iGen = iGen +1;
end
%% Summary of results:
% Find the fittest solution throughtout all the generations...
% without any violations then break before looking at unfitter solutions.
% Calculate the displ + forces for the fittest chromosome for reporting.
% ------------------------------------------------------------------------
TempPop = [Pop_data,Opt_data,Viol_data];
TempPop = sortrows(TempPop,[NumVar+2,NumVar+1]);
for i=1:NumGen
    if TempPop(i,NumVar+2) == 0
        Combination = TempPop(i,1:NumVar);
        Optimum = TempPop(i,NumVar+1);
        NumViol = TempPop(i,NumVar+2);
        break
    else
        Combination = zeros(1,NumVar);
        Optimum = min(TempPop(:,NumVar+1));
        NumViol = min(TempPop(i,NumVar+2));
    end
end
if flag == 0
    flag = 'No';
else
    flag = 'Yes';
end
clc
[~, ~, ~, ~, ~, ~, P,...
    D, axial, shear, moment,...
    LimH, LimV, ~, horzUnity, vertUnity] =...
    FEMfunc(Combination);
[~,CRX_ratio,CRYP_ratio,CRYB_ratio,MRB_ratio,MRP_ratio,...
    VRP_ratio,COMBPG,COMBBT,COMBPT,...
    COMBTP1,COMBTP2] = DESIGNfunc(Combination,axial,shear,moment);
display('------------------------------------------------------------')
display('GA operators:');
display({'Variables' 'Population Size' 'Generations'; ...
    NumVar PopSize NumGen; ...
    'Stop Criteria' '% Completed' 'Forced Stop'; ...
    StopCrit Percentage_complete flag; ...
    'Replace Rate' 'Select. Rate' '-'; ...
    ReplaceR SelectR '-'; ...
    'Replace Pop' 'Select Pop' '-'; ...
    ReplaceSize SelectSize '-'; ...
    'Total Genes' 'Mutat. Rate' 'Mutations/Gen'; ...
    NumVar*PopSize MutRate NumMutate})
display('------------------------------------------------------------')
display({'Optimum' 'Violations';Optimum NumViol})
display('------------------------------------------------------------')
display(Combination)
display('------------------------------------------------------------')
display('Column')
display({'hw bot' 'hw top' 'tw' 'b' 'tf';...
    List{1}(Combination(1)) List{2}(Combination(2))...
    List{3}(Combination(3)) List{4}(Combination(4))...
    List{5}(Combination(5))})
display('Rafter')
display({'hw bot' 'hw top' 'tw' 'b' 'tf';...
    List{6}(Combination(6)) List{7}(Combination(7))...
    List{8}(Combination(8)) List{9}(Combination(9))...
    List{10}(Combination(10))})
display('------------------------------------------------------------')
display('Deflections:');
    if max(D(1:3:end,1))<=abs(min(D(1:3:end,1)))
        MaxDispl_X1mm = min(D(1:3:end,1))*1000;
    else
        MaxDispl_X1mm = max(D(1:3:end,1))*1000;
    end
    if max(D(2:3:end,1))<=abs(min(D(2:3:end,1)))
        MaxDispl_Y1mm = min(D(2:3:end,1))*1000;
    else
        MaxDispl_Y1mm = max(D(2:3:end,1))*1000;
    end
    if max(D(1:3:end,2))<=abs(min(D(1:3:end,2)))
        MaxDispl_X2mm = min(D(1:3:end,2))*1000;
    else
        MaxDispl_X2mm = max(D(1:3:end,2))*1000;
    end
    if max(D(2:3:end,2))<=abs(min(D(2:3:end,2)))
        MaxDispl_Y2mm = min(D(2:3:end,2))*1000;
    else
        MaxDispl_Y2mm = max(D(2:3:end,2))*1000;
    end
display({'-----'  'X (mm)' 'Y (mm)';...
    'Limit' LimH*1000 LimV*1000;...
    '-----' '------' '------';...
    'Load Comb' 'X (mm)' 'Y (mm)';...
    'SLS1'      MaxDispl_X1mm MaxDispl_Y1mm;...
    'SLS2'      MaxDispl_X2mm MaxDispl_Y2mm})
display('------------------------------------------------------------')
display('Servicebility limit state:');
horzUnityt = max(horzUnity(:,1),horzUnity(:,2));
vertUnityt = max(vertUnity(:,1),vertUnity(:,2));
[horzM, horzMi] = max(horzUnityt);
[vertM, vertMi] = max(vertUnityt);
display({'Displacement'  'Unity' 'Node'; ...
    'Horizontal' horzM, horzMi; ...
    'Vertical'   vertM, vertMi})
display('------------------------------------------------------------')
display('Ultimate limit state:');
CRXt_ratio    = subs(max(CRX_ratio(:,1),CRX_ratio(:,2)));
CRYPt_ratio   = subs(max(CRYP_ratio(:,1),CRYP_ratio(:,2)));
CRYBt_ratio   = subs(max(CRYB_ratio(:,1),CRYB_ratio(:,2)));
MRBt_ratio    = subs(max(MRB_ratio(:,1),MRB_ratio(:,2)));
MRPt_ratio    = subs(max(MRP_ratio(:,1),MRP_ratio(:,2)));
VRPt_ratio    = subs(max(VRP_ratio(:,1),VRP_ratio(:,2)));
COMBPGt       = subs(max(COMBPG(:,1),COMBPG(:,2)));
COMBBTt       = subs(max(COMBBT(:,1),COMBBT(:,2)));
COMBPTt       = subs(max(COMBPT(:,1),COMBPT(:,2)));
COMBTP1t      = subs(max(COMBTP1(:,1),COMBTP1(:,2)));
COMBTP2t      = subs(max(COMBTP2(:,1),COMBTP2(:,2)));
[CRX,CRXi]    = max(CRXt_ratio);
[CRYP,CRYPi]  = max(CRYPt_ratio);
[CRYB,CRYBi]  = max(CRYBt_ratio);
[MRB,MRBi]    = max(MRBt_ratio);
[MRP,MRPi]    = max(MRPt_ratio);
[VRP,VRPi]    = max(VRPt_ratio);
[PG, PGi]     = max(COMBPGt);
[BT, BTi]     = max(COMBBTt);
[PT, PTi]     = max(COMBPTt);
```

```
[P1, P1i]    = max(COMBTP1t);
[P2, P2i]    = max(COMBTP2t);
display({'Axial'              'Unity'     'Node';
    'Axial   (Strong)'  CRX,        CRXi;
    'Axial    (Brace)'  CRYB,       CRYBi;
    'Axial   (Purlin)'  CRYP,       CRYPi})
display('----------------------')
display({'Moment'             'Unity'     'Node';
    'Moment   (Brace)'  MRB,        MRBi;
    'Moment  (Purlin)'  MRP,        MRPi})
display('----------------------')
display({'Shear'              'Unity'     'Node';
    'Shear   (Purlin)'  VRP,        VRPi})
display('----------------------')
display({'Comb Axi+Bending'   'Unity'     'Node';
    'Global  (Purlin)'  PG,         PGi;
    'Torsion  (Brace)'  BT,         BTi;
    'Torsion (Purlin)'  PT,         PTi})
display('----------------------')
display({'Comb Ten+Bending'   'Unity'     'Node';
    'Method 1(Purlin)'  P1,         P1i;
    'Method 2(Purlin)'  P2,         P2i})
display('------------------------------------------------------------')
display('History')
display({'Gen' 'Opt sol' 'Viol'})
[Gen' Opt_data Viol_data]
display('------------------------------------------------------------')
display('Displacement')
display({'X (Unity)' '-' 'Y (Unity)' '-';...
    'SLS1' 'SLS2' 'SLS1' 'SLS2'})
[horzUnity,vertUnity]
display('----------------------')
display('Axial')
display({'Strong-axis' '-';...
    'ULS1'     'ULS2'})
CRX_ratio
display('----------------------')
display({'Weak (Braces)' '-';...
    'ULS1' 'ULS2'})
CRYB_ratio
display('----------------------')
display({'Weak (Purlin)' '-';...
    'ULS1' 'ULS2'})
CRYP_ratio
display('------------------------------------------------------------')
display('Bending')
display({'Braces' '-';...
    'ULS1' 'ULS2'})
MRB_ratio
display('----------------------')
display({'Purlin' '-';...
    'ULS1' 'ULS2'})
MRP_ratio
display('------------------------------------------------------------')
display('Shear')
display({'Purlin' '-';...
    'ULS1' 'ULS2'})
VRP_ratio
display('------------------------------------------------------------')
display('Combination: Axial+Bend (Brace)')
display({'COMBBT'     '-';...
    'ULS1'      'ULS2'})
[COMBBT]
display('----------------------')
display('Combination: Axial+Bend (Purlin)')
display({'COMBPG'     '-'     'COMBPT'     '-';...
    'ULS1'      'ULS2'  'ULS1'      'ULS2'})
[ COMBPG  COMBPT]
display('------------------------------------------------------------')
display('Combination: Tension+Bend (Purlin)')
display({'COMBTP1'    '-'     'COMBTP2'    '-';...
    'ULS1'     'ULS2'  'ULS1'      'ULS2'})
[COMBTP1  COMBTP1]
display('------------------------------------------------------------')
```

## LISTfunc.m

```
%% FUNCTION-TYPE:
% Specify the attributes of the cross sections used in the GA.
% Herman Aucamp.
% 15045471.
% ------------------------------------------------------------------------
function[NumVar,Var,List] = LISTfunc()
% ------------------------------------------------------------------------
% Define the sectional options
% Plate thickness up to 16mm have the same yield stress.
% ------------------------------------------------------------------------
% Var 1  - Bottom Web height Column
% Var 2  - Top Web height Column
% Var 3  - Web thickness Column
% Var 4  - Flange width Column
% Var 5  - Flange thickness Column
% Var 6  - Bottom Web height Rafter
% Var 7  - Top Web height Rafter
% Var 8  - Web thickness Rafter
% Var 9  - Flange width Rafter
% Var 10 - Flange thickness Rafter
% ------------------------------------------------------------------------
%% Define variables
```

```
Var{1}  = 1;
List{1} = [250 260 270 280 290,...
           300 310 320 330 340 350 360 370 380 390,...
           400 410 420 430 440 450 460 470 480 490,...
           500 510 520 530 540 550 560 570 580 590,...
           600 610 620 630 640 650 660 670 680 690,...
           700 710 720 730 740 750 760 770 780 790,...
           800 810 820 830 840 850 860 870 880 890,...
           900 910 920 930 940 950 960 970 980 990,...
           1000 1010 1020 1030 1040 1050 1060 1070 1080 1090,...
           1100 1110 1120 1130 1140 1150 1160 1170 1180 1190,...
           1200 1210 1220 1230 1240 1250 1260 1270 1280 1290,...
           1300 1310 1320 1330 1340 1350 1360 1370 1380 1390,...
           1400 1410 1420 1430 1440 1450 1460 1470 1480 1490 1500]'/1000;
Var{2}  = 2;
List{2} = [250 260 270 280 290,...
           300 310 320 330 340 350 360 370 380 390,...
           400 410 420 430 440 450 460 470 480 490,...
           500 510 520 530 540 550 560 570 580 590,...
           600 610 620 630 640 650 660 670 680 690,...
           700 710 720 730 740 750 760 770 780 790,...
           800 810 820 830 840 850 860 870 880 890,...
           900 910 920 930 940 950 960 970 980 990,...
           1000 1010 1020 1030 1040 1050 1060 1070 1080 1090,...
           1100 1110 1120 1130 1140 1150 1160 1170 1180 1190,...
           1200 1210 1220 1230 1240 1250 1260 1270 1280 1290,...
```

```
            1300 1310 1320 1330 1340 1350 1360 1370 1380 1390,...
            1400 1410 1420 1430 1440 1450 1460 1470 1480 1490 1500]'/1000;
Var{3}  = 3;
List{3} = [6 8 10 12]'/1000;
Var{4}  = 4;
List{4} = [130 140 150 160 170 180 190,...
            200 210 220 230 240 250 260 270 280 290 300]'/1000;
Var{5}  = 5;
List{5} = [6 8 10 12]'/1000;
Var{6}  = 6;
List{6} = [250 260 270 280 290,...
            300 310 320 330 340 350 360 370 380 390,...
            400 410 420 430 440 450 460 470 480 490,...
            500 510 520 530 540 550 560 570 580 590,...
            600 610 620 630 640 650 660 670 680 690,...
            700 710 720 730 740 750 760 770 780 790,...
            800 810 820 830 840 850 860 870 880 890,...
            900 910 920 930 940 950 960 970 980 990,...
            1000 1010 1020 1030 1040 1050 1060 1070 1080 1090,...
            1100 1110 1120 1130 1140 1150 1160 1170 1180 1190,...
            1200 1210 1220 1230 1240 1250 1260 1270 1280 1290,...
            1300 1310 1320 1330 1340 1350 1360 1370 1380 1390,...
            1400 1410 1420 1430 1440 1450 1460 1470 1480 1490 1500]'/1000;
Var{7}  = 7;
List{7} = [250 260 270 280 290,...
            300 310 320 330 340 350 360 370 380 390,...
            400 410 420 430 440 450 460 470 480 490,...
            500 510 520 530 540 550 560 570 580 590,...
            600 610 620 630 640 650 660 670 680 690,...
            700 710 720 730 740 750 760 770 780 790,...
            800 810 820 830 840 850 860 870 880 890,...
            900 910 920 930 940 950 960 970 980 990,...
            1000 1010 1020 1030 1040 1050 1060 1070 1080 1090,...
            1100 1110 1120 1130 1140 1150 1160 1170 1180 1190,...
            1200 1210 1220 1230 1240 1250 1260 1270 1280 1290,...
            1300 1310 1320 1330 1340 1350 1360 1370 1380 1390,...
            1400 1410 1420 1430 1440 1450 1460 1470 1480 1490 1500]'/1000;
Var{8}  = 8;
List{8} = [6 8 10 12]'/1000;
Var{9}  = 9;
List{9} = [130 140 150 160 170 180 190,...
            200 210 220 230 240 250 260 270 280 290 300]'/1000;
Var{10} = 10;
List{10}= [6 8 10 12]'/1000;
NumVar=size(Var,2);
end
```

## INITfunc.m

```
%% FUNCTION-TYPE:
% Create the initial population of candidate solutions.
% Herman Aucamp.
% 15045471.
% ------------------------------------------------------------------------
function[Population] = INITfunc(PopSize)
% ------------------------------------------------------------------------
% Call variables from list.
% Allocate memory to initial Population.
% Iterate through the population and assign random variables from list.
% ------------------------------------------------------------------------
%% Initilise population
[NumVar,Var,List]=LISTfunc();
Population=zeros(PopSize,NumVar);
for i=1:PopSize
for j=1:NumVar
if ismember(j,Var{j})==1
Population(i,j)=randi([1,length(List{j})]);
end
end
% % Force prismatic members  (also change GAscript at create new Pop)
% Population(i,2)=subs(Population(i,1));
% Population(i,7)=subs(Population(i,6));
end
end
```

## FITNESSfunc.m

```
%% FUNCTION-TYPE:
% Calculate the fitness of each individual candidate solution.
% Herman Aucamp.
% 15045471.
% ------------------------------------------------------------------------
function[fitness,viol] = FITNESSfunc(Chromosome,counter)
% ------------------------------------------------------------------------
% Call information from List-, Nodes- and Global functions.
% Define material parameters in SI-units.
% Allocate memory to temporary lengthlist and volumelist (m, m3).
% Determine the length, volumes and weight of each chromosome.
% Penalised all solutions with class 4 flanges.
% Complete FEM analysis.
% Complete Design checks.
% Penalise any violations and determine the fitness  (kg)
% ------------------------------------------------------------------------
[NumVar,~,List] = LISTfunc();
[NumEl,~,~,xCoord,yCoord] = NODEfunc();
[~,~,rho,~,~,~,fy,~,~,~,~,~,~,~,~,~,~,~,~,~] = GLOBALfunc();
LengthList = zeros(2,1);
for i=1:NumEl/2
    x1 = xCoord(i,1);
    x2 = xCoord(i+1,1);
    y1 = yCoord(i,1);
    y2 = yCoord(i+1,1);
    LengthList(i) = sqrt((x2-x1)^2+(y2-y1)^2);
end
VolList=zeros(2,1);
j=1;
for i=1:5:NumVar
    VolList(j)=...
    ((List{i}(Chromosome(1,i),1)+List{i+1}(Chromosome(1,i+1),1))/2)*...
    List{i+2}(Chromosome(1,i+2),1)*LengthList(j)...
    +...
    List{i+3}(Chromosome(1,i+3),1)*List{i+4}(Chromosome(1,i+4),1)*2*...
    LengthList(j)...
    +...
    List{i}(Chromosome(1,i),1)*3.5*List{i+3}(Chromosome(1,i+3),1)*...
    List{i+4}(Chromosome(1,i+4),1)...
    +...
    List{i+1}(Chromosome(1,i+1),1)*3.5*List{i+3}(Chromosome(1,i+3),1)*...
    List{i+4}(Chromosome(1,i+4),1);
    VolList(j) = VolList(j);
    j=j+1;
end
```

```
WeightList = 2*rho*VolList;
%% Ignore Class 4 flanges
CLSViol = 0;
for i=1:5:NumVar
    b  = List{i+3}(Chromosome(1,i+3),1);
    tf = List{i+4}(Chromosome(1,i+4),1);
    ratio = b/(2*tf);
    Lim = 200/sqrt(fy*10^(-6));
    if ratio>Lim
        CLSViol = CLSViol + 10*(ratio-Lim)^2;
    end
end
viol = CLSViol;
%% Limit shape to Column bottom < top; Rafter bottom > top
SHPViol = 0;
if List{1}(Chromosome(1,1),1) > List{2}(Chromosome(1,2),1)
    SHPViol = (List{1}(Chromosome(1,1),1)...
              - List{1}(Chromosome(1,2),1))/10;
end
if List{7}(Chromosome(1,7),1) > List{6}(Chromosome(1,6),1)
    SHPViol = SHPViol + (List{7}(Chromosome(1,7),1)...
                        - List{6}(Chromosome(1,6),1))/10;
end
viol = viol + SHPViol;
%% Serviceability Limit State
[~, ~, ~, ~, ~, ~, ~, ~, axial, shear, moment, ~, ~, FEMViol, ~, ~] =...
        FEMfunc(Chromosome);
viol = viol + FEMViol;
%% Ultimate Limit State
if viol < 50
    [DESViol,~,~,~,~,~,~,~,~,~,~,~] =...
        DESIGNfunc(Chromosome,axial,shear,moment);
else
    DESViol = viol*2;
end
viol = viol + DESViol;
%% Penalty
penaltyWeight = 0;
alpha = 1.5;
c = 0.05;
penaltyWeight = penaltyWeight+viol*(c*counter)^alpha;
viol = viol';
fitness = sum(WeightList)+penaltyWeight;
end
```

## FEMfunc.m

```
%% FUNCTION-TYPE:
% Finite Element Method for descrizing 2D Frames.
% Herman Aucamp.
% 15045471.
% ------------------------------------------------------------------------
function [sNod, sEl,   hw,     u, v, DEG, P,...
          D,    axial, shear, moment,...
          LimH, LimV,  viol,  horzUnity, vertUnity] =...
          FEMfunc(Chromosome)
% ------------------------------------------------------------------------
%% Input geometry data
% Call for material and physical properties.
% Mirror image chromosome for symmetry (flips left to right).
% Define degrees of freedom for the planar analysis.
% Allocate memory.
% Web height at geometry definitions (hw).
% Flange thickness at geometry definitions (tf).
% Web thickness at geometry definitions (tw).
% Width of flange at geometry definitions (b).
% ------------------------------------------------------------------------
[~,Var,List]=LISTfunc();
[NumEl,~,Nod,~,~] = NODEfunc();
[~,E,rho,mu,G,g,~,~,s,~,~,~,~,~,~,~,~,tClad,LoadComb] = GLOBALfunc();
Nod(1,1) = Nod(1,1) + (tClad + List{1}(Chromosome(1))/2);
Nod(1,2) = Nod(1,2);
Nod(2,1) = Nod(2,1) + (tClad + List{2}(Chromosome(2))/2);
Nod(2,2) = Nod(2,2) - (tClad + List{3}(Chromosome(3))/2);
Nod(3,1) = Nod(3,1);
Nod(3,2) = Nod(3,2) - (tClad + List{7}(Chromosome(7))/2);
Nod(4,1) = Nod(4,1) - (tClad + List{2}(Chromosome(2))/2);
Nod(4,2) = Nod(4,2) - (tClad + List{3}(Chromosome(3))/2);
Nod(5,1) = Nod(5,1) - (tClad + List{1}(Chromosome(1))/2);
Nod(5,2) = Nod(5,2);
xCoord = Nod(:,1);
yCoord = Nod(:,2);
Chromosome = [Chromosome,fliplr(Chromosome)];
Dof = 3;
j=1;
hw=zeros(NumEl/2,2);
tw=zeros(NumEl/2,1);
b=zeros(NumEl/2,1);
tf=zeros(NumEl/2,1);
for i=1:5:length(Chromosome)/2
    if ismember(i,Var{i})==1
    hw(j,1)  = List{i}(Chromosome(i));
    hw(j,2)  = List{i+1}(Chromosome(i+1));
    end
    j=j+1;
end
hw=[hw;fliplr(flipdim(hw,1))];
j=1;
for i=3:5:length(Chromosome)/2
    if ismember(i,Var{i})==1
    tw(j,1)  = List{i}(Chromosome(i));
    end
    j=j+1;
end
tw=[tw;flipdim(tw,1)];
j=1;
for i=4:5:length(Chromosome)/2
    if ismember(i,Var{i})==1
    b(j,1)  = List{i}(Chromosome(i));
    end
    j=j+1;
end
b=[b;flipdim(b,1)];
j=1;
for i=5:5:length(Chromosome)/2
    if ismember(i,Var{i})==1
    tf(j,1)  = List{i}(Chromosome(i));
    end
    j=j+1;
end
tf=[tf;flipdim(tf,1)];
%% Height at discretization point
% Allocate memory.
% Discretize values over member length linearly.
% Reasemble columns to [nx1] array.
% ------------------------------------------------------------------------
```

```
hwTemp  = zeros(size(hw,1),s);
tfTemp = zeros(size(hw,1),s);
twTemp = zeros(size(hw,1),s);
bTemp  = zeros(size(hw,1),s);
for i = 1:size(hw,1)
    hwTemp(i,:) = linspace(hw(i,1),hw(i,2),s)';
    tfTemp(i,:)= linspace(tf(i),tf(i),1)';
    twTemp(i,:)= linspace(tw(i),tw(i),1)';
    bTemp(i,:) = linspace(b(i),b(i),1)';
end
hw = hwTemp'; tf = tfTemp'; tw = twTemp'; b = bTemp';
hw = subs(hw(:)); tf = subs(tf(:)); tw = subs(tw(:)); b = subs(b(:));
%% Prismatic equivalent sections
% Allocate memory.
% For each sub-member.
% Average height per sub-member.
% Remove the double web height entries at member ends.
% Average heights per sub-member.
% ------------------------------------------------------------------------
hwTemp   = zeros(1,size(hw,1)-1);
tfTemp  = zeros(1,size(hw,1)-1);
twTemp  = zeros(1,size(hw,1)-1);
bTemp   = zeros(1,size(hw,1)-1);
for i = 1:size(hw,1)-1
    hwTemp(i) = (hw(i)+hw(i+1))/2;
    tfTemp(i) = (tf(i)+tf(i+1))/2;
    twTemp(i) = (tw(i)+tw(i+1))/2;
    bTemp(i) = (b(i)+b(i+1))/2;
end
hwTemp(s:s:size(hwTemp,2)-1) = [];
tfTemp(s:s:size(tfTemp,2)-1) = [];
twTemp(s:s:size(twTemp,2)-1) = [];
bTemp(s:s:size(bTemp,2)-1) = [];
hw = hwTemp';tf = tfTemp'; tw = twTemp'; b = bTemp';
%% Area of equivalent prismatic members
% Allocate memory.
% For each sub-member.
% Area calculation.
% ------------------------------------------------------------------------
A = zeros(1,size(hw,1));
for i = 1:size(hw,1)
    A(i) = (tw(i)*hw(i))+2*(b(i)*tf(i));
end
A = A';
%% Inertia of equivalent prismatic members
% Allocate memory.
% For each sub-member.
% Second moment of area calculation.
% ------------------------------------------------------------------------
I = zeros(1,size(hw,1));
for i = 1:size(hw,1)
    I(i)  = (((tw(i)*(hw(i)).^3)/12)+...
            ((b(i)*((((hw(i))+2*tf(i)).^3)-...
            (hw(i)).^3))/12));
end
I = I';
%% Subnode positions due to discretization
% Allocate memory.
% For each sub-member determine the physical position in the frame.
% ------------------------------------------------------------------------
sNodx = zeros(1,s);
sNody = zeros(1,s);
for i = 1:size(Nod,1)-1
    sNodx(i,:)= linspace(Nod(i,1),Nod(i+1,1),s);
    sNody(i,:)= linspace(Nod(i,2),Nod(i+1,2),s);
end
sNodx = sNodx'; sNodx(s:s:size(sNodx,1)*size(sNodx,2)-1) = [];
if size(Nod,1) >= 3
    sNodx = sNodx';
end
sNody = sNody'; sNody(s:s:size(sNody,1)*size(sNody,2)-1) = [];
if size(Nod,1) >= 3
    sNody = sNody';
end
sNod  = [sNodx, sNody];
%% Connecting sub-element to sub-node positions
% Allocate memory.
% Describe how submember join each other physically.
% ------------------------------------------------------------------------
sEl = zeros(size(sNod,1)-1,size(sNod,2));
for i = 1:size(sNod,1)-1
    sEl(i,:)= [i i+1];
end
%% Pre-processing
% Determine the number of subnodes.
% Te total number of degress of freedom.
% [1 0 0 1 0 0...]': a list of hor disp dofs
% [0 1 0 0 1 0...]': a list of ver disp dofs
% [0 0 1 0 0 1...]': a list of rot disp dofs
% ------------------------------------------------------------------------
nSNod       = size(sEl,1)+1;
nDof        = Dof*nSNod;
u           = INDEXfunc(1:3:nDof,nDof);
v           = INDEXfunc(2:3:nDof,nDof);
% r           = Index_func(3:3:nDof,nDof);
%% Allocate memory
% Allocate memory.
% Use sparsity prop of stiffness matrix to save on memory.
% ------------------------------------------------------------------------
K = spalloc(nDof,nDof,9);
D = zeros(nDof,length(LoadComb(:,1)));
P = zeros(nDof,length(LoadComb(:,1)));
axial    = zeros(size(sEl,1),length(LoadComb(:,1)));
shear    = zeros(size(sEl,1),length(LoadComb(:,1)));
moment   = zeros(size(sEl,1)+1,length(LoadComb(:,1)));
%% Input boundary conditions (support and forces) data
% Predefined (p) and free (f) d.o.fs
% Only translation d.o.fs at supports are set to zero.
% Detemine the slope of each subnode and weight.
% ------------------------------------------------------------------------
p       = INDEXfunc([Dof-2 Dof-1 nDof-2 nDof-1],nDof);
f       = ~p;
D(p)    = [ 0 0 0 0 ];
for iel=1:size(sEl,1)
    vec = sNod(sEl(iel,2),:) - sNod(sEl(iel,1),:);
    L(iel)    = norm(vec);
    a(iel)    = atan2(vec(2),vec(1));
    adeg(iel) = rad2deg(a(iel));
    W(iel)    = g*rho*A(iel)*L(iel);
end
%% Systen assenbly and solution
% Generate the element stiffness matrix, using Timoshenko beams.
% See Cowper (1966) on Timoshenko beams.
% Consider each element in turn, get the rotation matrix per element.
% ------------------------------------------------------------------------
ROT     = cell(size(sEl,1),1);
KL      = cell(size(sEl,1),1);
```

```
TOPO    = cell(size(sEl,1),1);
DEG     = cell(size(sEl,1),1);
for iel     = 1:size(sEl,1)
rot = [ cos(a(iel))     -sin(a(iel))  0       0       0       0
        sin(a(iel))      cos(a(iel))  0       0       0       0
        0           0       1       0       0       0
        0           0       0       cos(a(iel)) -sin(a(iel))  0
        0           0       0       sin(a(iel))  cos(a(iel))  0
        0           0       0       0       0       1];
kelA    = E*A(iel)/L(iel)*...
          [   1   0   0  -1   0   0
              0   0   0   0   0   0
              0   0   0   0   0   0
             -1   0   0   1   0   0
              0   0   0   0   0   0
              0   0   0   0   0   0];
eta     = b(iel)/(hw(iel)+2*tf(iel));
beta    = (2*b(iel)*tf(iel))/((hw(iel)+2*tf(iel))*tw(iel));
alpha   = 12+(72*beta)+(150*beta^2)+(90*beta^3)+...
          mu*(12+(66*beta)+(135*beta^2)+(90*beta^3))+...
          30*(eta^2)*beta*(1+beta)+...
          5*mu*(eta^2)*beta*(8+9*beta);
k       = (10*(1+mu)*((1+3*beta)^2))/alpha;
phi     = (12*E*I(iel)*k)/(A(iel)*G*(L(iel)^2));
psi     = (12*E*I(iel))/((1+phi)*L(iel)^2);
kelB    = ...
          [0 0           0                       0  0           0
           0 psi/L(iel)  psi/2                   0 -psi/L(iel)  psi/2
           0 psi/2 psi*(4+phi)*L(iel)/12 0 -psi/2 psi*(2-phi)*L(iel)/12
           0 0           0                       0  0           0
           0 -psi/L(iel) -psi/2                   0  psi/L(iel) -psi/2
           0 psi/2 psi*(2-phi)*L(iel)/12 0 -psi/2 psi*(4+phi)*L(iel)/12];
%% Assemble system stiffness matrix
% Get the address and add the element matrix into the right position.
% -------------------------------------------------------------------------
topo        = [ 3*(sEl(iel,1)-1)+(1:3)...
                3*(sEl(iel,2)-1)+(1:3)];
K(topo,topo)= K(topo,topo) + rot*(kelA+kelB)*rot';
ROT{iel}    = rot;
KL{iel}     = kelA+kelB;
TOPO{iel}   = topo;
DEG{iel}    = adeg(iel);
end
%% Primal-dual solver
% Find the applied loading from the loading function per load comb.
% Solve for the free d.o.fs on the right hand side (forces).
% -------------------------------------------------------------------------
[DL,LL,WL,NL] = LOADINGfunc(sNod,sEl,nDof,a,W,L);
for z=1:length(LoadComb(:,1))
P(:,z) = LoadComb(z,1)*DL + LoadComb(z,2)*LL + LoadComb(z,3)*WL+...
         (LoadComb(z,1)*abs(sum(DL)) + LoadComb(z,2)*abs(sum(LL)))*NL;
    D(f,z) = (K(f,f)) \ (P(f,z)-K(f,p)*D(p,z));
    P(p,z) = K(p,f)*D(f,z) + K(p,p)*D(p,z);
%% Back-calculate for internal forces
% Solve for the free d.o.fs on the left hand side (displacements).
```

## NODEfunc.m

```
%% FUNCTION-TYPE:
% Specify node coordinates, elements, known forces and displacements.
% Herman Aucamp.
% 15045471.
% -------------------------------------------------------------------------
function[NumEl,NumNod,Nod,xCoord,yCoord] = NODEfunc()
% -------------------------------------------------------------------------
```

```
% Rotate members into local coordinate system.
% Global forces = global stiffness * displacements (fg).
% Local forces = rotated global forces (fl).
% Create vector of internal forces (axial, shear and moment).
% If member has shortened (= compressed)
% If member has elongated (= tension)
% Logical procedure due to a moment entries = NoOfMembers+1
% -------------------------------------------------------------------------
    fg = cell(size(sEl,1),1);
    fl = cell(1,size(sEl,1));
    for iel = 1:size(sEl,1)
        fg{iel} = (ROT{iel}*KL{iel}*ROT{iel}')*D(TOPO{iel}',z);
        fl{iel} = (ROT{iel}'*fg{iel});
    end
    horz(:,z) = sNod(:,1)+D(u,z);
    vert(:,z) = sNod(:,2)+D(v,z);
    for i = 1:size(sEl,1)
        old = [sNod(sEl(i,:),1),sNod(sEl(i,:),2)];
        new = [horz(sEl(i,:),z),vert(sEl(i,:),z)];
        vec1 = old(2,:)-old(1,:);
        L1   = norm(vec1);
        vec2 = new(2,:)-new(1,:);
        L2   = norm(vec2);
        if L1-L2>0
            axial(i,z) = fl{i}(1);
        else
            axial(i,z) = -abs(fl{i}(1));
        end
        shear(i,z) = (fl{i}(2));
        if i < size(sEl,1)
            moment(i,z) = fl{i}(3);
        else
            moment(i,z) = fl{i}(3);
            moment(i+1,z) = fl{i}(6);
        end
    end
%% Count SLS displacement violations
% Define the limits for displacement Ter Haar+Retief+Dunaiski (1998).
% Count the violations per SLS load combination.
% -------------------------------------------------------------------------
LimH    = (max(yCoord)-min(yCoord))/200;
LimV    = (max(xCoord)-min(xCoord))/180;
viol(1) = sum(abs(D(u,1))>=LimH) + sum(abs(D(v,1))>=LimV);
viol(2) = sum(abs(D(u,2))>=LimH) + sum(abs(D(v,2))>=LimV);
horzUnity(:,z) = abs(D(u,z))/LimH;
vertUnity(:,z) = abs(D(v,z))/LimV;
if viol(1) > 0 && viol(2) > 0
    viol = subs((viol(1)*viol(2))*ceil(nDof/10));
else
    viol = subs((sum(viol))*ceil(nDof/10));
end
end
% Loads_kN = [P(u,:)/1000 P(v,:)/1000]
% Displ_mm = [D(u,2)*1000 D(v,2)*1000]
```

```
% Provide the coordinates of portal frame (2D and 4 members)
% Purlin positions should be changed in PURLINfunc to realistic values...
% for each frame-span configuration.
% Unhide the frame to be inspected.
% -------------------------------------------------------------------------
%% Nodes
Nod = [ 0 0 ; 0 4.5 ; 10 5.50 ; 20 4.5 ; 20 0];
% Nod = [ 0 0 ; 0 4.5 ; 15 6.00 ; 30 4.5 ; 30 0];
```

```
% Nod = [ 0 0 ; 0 4.5 ; 20 6.50 ; 40 4.5 ; 40 0];
% Nod = [ 0 0 ; 0 4.5 ; 25 7.00 ; 50 4.5 ; 50 0];
NumEl = size(Nod,1)-1;
```

## GLOBALfunc.m

```
%% FUNCTION-TYPE:
% General parameters used throughout the GA.
% Herman Aucamp.
% 15045471.
% ------------------------------------------------------------------------
function[phi,E,rho,mu,G,g,fy,fu,...
    s,n,sz,conv,maxsPurl,omega1,sFrame,wClad,Qi,tClad,LoadComb] =...
    GLOBALfunc()
% ------------------------------------------------------------------------
% All units in SI-units.
% Material properties of S355JR steel according to SAISC HB, 6th ed, 2008.
% Resistance factor for steel SANS10162-1.
% Modulus of Elasticity (Pa).
% Density of S355JR (rho - kg/m3).
% Poison ratio (mu).
% Shear modulus (G - Pa).
% Gravitational acceleration (g m/s2).
% S355JR Yield stress (fy - Pa).
% S355JR Ultimate stress (fu - Pa).
% Member discretisation points (s).
% SANS10162-1 buckling curve (n = 1.34 or 2.24).
% Successive approximations: Number of discretizations.
% Successive approximations: Converenge criteria.
% Maximum purlin spacing (maxsPurl - m).
% Small P-delta effect (omega1 - distr loads btwn supports).
% Frame spacing in meters (sFrame - m).
% Lip channel 150x65x20x2.5 (wPurl - 5.912334 kg/m).
```

## INDEXfunc.m

```
%% FUNCTION-TYPE:
% General parameters used throughout the GA.
% Herman Aucamp.
% 15045471.
% ------------------------------------------------------------------------
function[i] = INDEXfunc(d,length)
% ------------------------------------------------------------------------
% The following routine generates so-called logical index arrays,
% that acts as "fillers" that allow access to selected elements of
```

## LOADINGfunc.m

```
%% FUNCTION-TYPE:
% Defining the loading vectors for the FEM function.
% Herman Aucamp.
% 15045471.
% ------------------------------------------------------------------------
function [DL,LL,WL,NL] = LOADINGfunc(sNod,sEl,nDof,a,W,L)
% ------------------------------------------------------------------------
% [1 0 0 1 0 0...]': a list of hor disp dofs.
% [0 1 0 0 1 0...]': a list of ver disp dofs.
% DL - Dead loads (forces).
% LL - Live loads (forces).
% WL - Wind loads(forces).
% NL - Notional loads (forces).
```

```
NumNod = size(Nod,1);
xCoord = Nod(:,1);
yCoord = Nod(:,2);
end
```

```
% 0.50 mm ISQ550 IBR sheets (wClad - 5.269 kg/m2).
% Inaccessible roof 250 Pa (SANS 10160-2).
% Load combinations [SLS1 SLS2 ULS1 ULS2].
% ------------------------------------------------------------------------
%% General parameter shared by functinos
phi      = 0.9;
E        = 200e9;
rho      = 7850;
mu       = 0.3;
G        = 77e9;
g        = 9.81;
fy       = 355e6;
fu       = 470e6;
s        = 21;
n        = 2.24;
sz       = 100;
conv     = 10^(-2);
maxsPurl= 2.5;
omega1   = 1.0;
sFrame   = 5;
wClad    = 25.4842*g;
Qi       = 250;
tClad = 0.2;
LoadComb(1,:) = [1.1, 1.0, 0.0];
LoadComb(2,:) = [1.0, 0.0, 0.6];
LoadComb(3,:) = [1.2, 1.6, 0.0];
LoadComb(4,:) = [0.9, 0.0, 1.3];
end
```

```
% an array. One example would be to use this in order to access
% only horizontal displacements in a displacement vector.
% ------------------------------------------------------------------------
%% INDEX returns logical array
i    = zeros(length,1);
     i(d(d>0 & d<=length))=1;
i    = logical(i);
end
```

```
% ------------------------------------------------------------------------
[NumEl,~,~,~,~] = NODEfunc();
[~,~,~,~,~,~,~,~,s,~,~,~,~,~,~,sFrame,wClad,Qi,~,~] = GLOBALfunc();
[xPurl,yPurl,M,~,~,~,LiPurl,~] = PURLINfunc();
u = INDEXfunc(1:3:nDof,nDof);
v = INDEXfunc(2:3:nDof,nDof);
DL = zeros(nDof,1);
NL = zeros(nDof,1);
LL = zeros(nDof,1);
WL = zeros(nDof,1);
%% Dead loads:
% Step 1: Assign own weight of frame (internal).
% Step 2: Assign cladding, purlin and girts own weight (external).
% Find the subnode index nearest to the purlin position.
```

```
% Complete interation per members (i.e. LHS Column or RHS Rafter).
% ------------------------------------------------------------------------
for i=1:size(sEl,1)
    if i==1
        DL(i*3-1) = DL(i*3-1)-W(i);
    else
        DL(i*3-1) = DL(i*3-1)-W(i-1);
    end
end
for i=s:3*s-3
        DL(i*3-1) = DL(i*3-1)-(L(i)*wClad*sFrame);
end
%% Live loads:
% Find the subnode index nearest to the purlin position.
% Complete interation per members (i.e. LHS Column or RHS Rafter).
% ------------------------------------------------------------------------
for i=s:3*s+1
        LL(i*3-1) = LL(i*3-1)-(L(i)*Qi*sFrame);
end
%% Wind loads:
% Define peak wind pressure at eave (qpe) and ridge (qpr) (Pa or N/m2)
% Define wind pressure coeficients per area (-).
% Find the subnode index nearest to the purlin position.
% ------------------------------------------------------------------------
%% Pressure and pressure coefficients
qpe  = 1000;
qpr  = 1000;
cr_A  = 0.40;
cr_B  = 1.00;
cr_C  = 0.65;
cr_D  = 0.40;
for i=1:4*s-3
    if i>=1 && i<s
        WL(i*3-2) = WL(i*3-2)+cos(a(i))*(L(i)*cr_A*qpe*sFrame);
        WL(i*3-1) = WL(i*3-1)+sin(a(i))*(L(i)*cr_A*qpe*sFrame);
    elseif i>=s && i<2*s
        WL(i*3-2) = WL(i*3-2)-sin(a(i))*(L(i)*cr_B*qpe*sFrame);
        WL(i*3-1) = WL(i*3-1)+cos(a(i))*(L(i)*cr_B*qpe*sFrame);
    elseif i>=2*s && i<3*s+1
        WL(i*3-2) = WL(i*3-2)-sin(a(i))*(L(i)*cr_C*qpe*sFrame);
        WL(i*3-1) = WL(i*3-1)+cos(a(i))*(L(i)*cr_C*qpe*sFrame);
    else
        WL(i*3-2) = WL(i*3-2)-sin(a(i-1))*(L(i-1)*cr_D*qpe*sFrame);
        WL(i*3-1) = WL(i*3-1)+cos(a(i-1))*(L(i-1)*cr_D*qpe*sFrame);
    end
end
%% Notional loads:
% Applied at eave height, hortizontally.
% ------------------------------------------------------------------------
NL(s*3-2) = NL(s*3-2)+0.005;
end
```

## DESIGNfunc.m

```
%% FUNCTION-TYPE:
% Design code check (ULS)
% Herman Aucamp.
% 15045471.
% ------------------------------------------------------------------------
function [viol,CRX_ratio,CRYP_ratio,CRYB_ratio,MRB_ratio,MRP_ratio,...
    VRP_ratio,COMBPG,COMBBT,COMBPT,...
    COMBTP1,COMBTP2] = DESIGNfunc(Chromosome,axial,shear,moment)
% ------------------------------------------------------------------------
%% Chromosome and portal frame properties
% All geometric and material parameters in SI-units.
% Determine member axial-, shear- and flexural capacity.
% Check interaction formula.
% Mirror image of portal frame.
% mi denotes purlin numbers.
% ni denotes brace numbers.
% Find beam cross section prop. at all FEM, Purlin and Brace Positions.
% ------------------------------------------------------------------------
[phi,E,~,~,G,~,fy,~,s,~,~,~,~,~,~,~,~,~,~,LoadComb] = GLOBALfunc();
[NumVar,~,List]=LISTfunc();
[NumEl,~,~,xCoord,yCoord] = NODEfunc();
[~,~,M,~,~,N,LiPurl,LiBrace] = PURLINfunc();
Chromosome = [Chromosome,fliplr(Chromosome)];
hw=zeros(NumEl/2,2);
tw=zeros(NumEl/2,1);
b =zeros(NumEl/2,1);
tf=zeros(NumEl/2,1);
L =zeros(NumEl,1);
j=1;
for i=1:5:NumVar
    hw(j,1)  = List{i}(Chromosome(i));
    hw(j,2)  = List{i+1}(Chromosome(i+1));
    tw(j,1)  = List{i+2}(Chromosome(i+2));
    b(j,1)   = List{i+3}(Chromosome(i+3));
    tf(j,1)  = List{i+4}(Chromosome(i+4));
    j=j+1;
end
hw = [hw;fliplr(flipdim(hw,1))]';
tw = [tw;flipdim(tw,1)]';
b  = [b;flipdim(b,1)]';
tf = [tf;flipdim(tf,1)]';
for i=1:NumEl
    L(i) = sqrt((xCoord(i+1)-xCoord(i))^2+(yCoord(i+1)-yCoord(i))^2);
    for si=1:s
        if si==1
            Lxi{i}(si) = 0;
        else
            Lxi{i}(si) = Lxi{i}(si-1)  +  (L(i)/(s-1));
        end
    end
    for mi=1:M(i)-1
        LyiP{i}{mi}(1) = LiPurl{i}(mi);
        LyiP{i}{mi}(2) = (LiPurl{i}(mi)+LiPurl{i}(mi+1))/2;
        LyiP{i}{mi}(3) = LiPurl{i}(mi+1);
    end
    for ni=1:N(i)-1
        LyiB{i}{ni}(1) = LiBrace{i}(ni);
        LyiB{i}{ni}(2) = (LiBrace{i}(ni)+LiBrace{i}(ni+1))/2;
        LyiB{i}{ni}(3) = LiBrace{i}(ni+1);
    end
    [hwEl{i}, AgEl{i}, AwEl{i}, AfEl{i},...
        IxEl{i}, ZexEl{i}, MexEl{i},...
        ZplxEl{i}, MplxEl{i}, rxEl{i},...
        IyEl{i}, ZeyEl{i}, ZplyEl{i}, ryEl{i},...
        JEl{i}, CwEl{i}, IpEl{i}, rtEl{i},...
        IeffEl{i}, ZeffEl{i}] =...
        BEAMPROPfunc(L(i), Lxi{i},...
        hw(:,i), tw(i), b(i), tf(i),s);
    for mi=1:M(i)-1
        [hwP{i}{mi}, AgP{i}{mi}, AwP{i}{mi}, AfP{i}{mi},...
            IxP{i}{mi}, ZexP{i}{mi}, MexP{i}{mi},...
            ZplxP{i}{mi}, MplxP{i}{mi}, rxP{i}{mi},...
            IyP{i}{mi}, ZeyP{i}{mi}, ZplyP{i}{mi}, ryP{i}{mi},...
```

```
            JP{i}{mi}, CwP{i}{mi}, IpP{i}{mi}, rtP{i}{mi},...
            IeffP{i}{mi}, ZeffP{i}{mi}] =...
            BEAMPROPfunc(L(i), LyiP{i}{mi},...
            hw(:,i), tw(i), b(i), tf(i),3);
    end
    for ni=1:N(i)-1
        [hwB{i}{ni}, AgB{i}{ni}, AwB{i}{ni}, AfB{i}{ni},...
            IxB{i}{ni}, ZexB{i}{ni}, MexB{i}{ni},...
            ZplxB{i}{ni}, MplxB{i}{ni}, rxB{i}{ni},...
            IyB{i}{ni}, ~, ~, ryB{i}{ni},...
            JB{i}{ni}, CwB{i}{ni}, ~, rtB{i}{ni},...
            IeffB{i}{ni}, ZeffB{i}{ni}] =...
            BEAMPROPfunc(L(i), LyiB{i}{ni},...
            hw(:,i), tw(i), b(i), tf(i),3);
    end
end
%% Start loop for ULS load combination
% -------------------------------------------------------------------------
% Initialise Axial (Cu), Shear (Vu) and Moment (Mu) vectors per member.
% Populate cell array per member using data received from FEM analysis.
% Set axial value at end equal to value in member.
% Set shear value at end equal to value in member.
% -------------------------------------------------------------------------
Cu{NumEl} = zeros(s,1);
Vu{NumEl} = zeros(s,1);
Mu{NumEl} = zeros(s,1);
viol = 0;
for z=3:length(LoadComb(:,1))
for i=1:NumEl
Cu{i} = axial((i-1)*(s-1)+1:(i)*(s-1),z);
Vu{i} = shear((i-1)*(s-1)+1:(i)*(s-1),z);
Mu{i} = moment((s*(i-1))-(i-2):(s*(i))-(i-1),z);
Cu{i}(s) = Cu{i}(s-1);
Vu{i}(s) = Vu{i}(s-1);
end
%% AXIAL COMPRESSION
% -------------------------------------------------------------------------
% Check axial capacity of each member strong axis.
% Check axial capacity of each member weak axis between purlins.
% Check axial capacity of each member weak axis between brace points.
% Step 1: Elastic flexural buckling load (Ce)
% Step 2: Applied compressive stress (f)
% Step 3: Slenderness ratio (gamma_e)
% Step 4: Nominal axial compressive resistance stress
% Step 5: Area reduction
% Step 6: Maximum applied compressive stress
% Step 7: True axial compressive resistance (Cr)
% -------------------------------------------------------------------------
for i=1:NumEl
    [Felas] = SUCAPPROXfunc(hwEl{i}(1), hwEl{i}(s),...
        L(i), b(i), tw(i), tf(i), max(Cu{i}));
    Cex{i} = Felas*max(Cu{i});
    [~,fr] = NOMRESISTfunc(Cex{i},min(AgEl{i}));
    [~,~,f_tap] = ELASBUCKfunc(max(Cu{i}),AgEl{i},fr,s);
    [~,~,Q,~,~,imax] = EWMfunc(max(Cu{i}),...
        hwEl{i},tw(i),b(i),tf(i),AgEl{i},f_tap,s);
    [~,Crx{i}] = FLEXRESISTfunc(Q(imax),...
        AgEl{i}(imax),Cex{i});
Crx_ratio{i} = max(Cu{i})/Crx{i};
    if Crx_ratio{i} < 0
        Crx_ratio{i} = 0;
        end
    for mi=1:M(i)-1
        CeyP{i}(mi) = (pi()^2)*E*IyP{i}{mi}(2)/...
            ((LyiP{i}{mi}(3)-LyiP{i}{mi}(1))^2);
        [~,fr] = NOMRESISTfunc(CeyP{i}(mi),min(AgP{i}{mi}));
        [~,~,f_tap] = ELASBUCKfunc(max(Cu{i}),AgP{i}{mi},fr,3);
        [~,~,Q,~,~,imax] = EWMfunc(max(Cu{i}),...
            hwP{i}{mi},tw(i),b(i),tf(i),AgP{i}{mi},f_tap,3);
        [~,CryP{i}(mi)] = FLEXRESISTfunc(Q(imax),...
            AgP{i}{mi}(imax),CeyP{i}(mi));
        CryP_ratio{i}(mi) = max(Cu{i})/CryP{i}(mi);
        if CryP_ratio{i}(mi) < 0
            CryP_ratio{i}(mi) = 0;
        end
    end
    for ni=1:N(i)-1
        CeyB{i}(ni) = (pi()^2)*E*IyB{i}{ni}(2)/...
            ((LyiB{i}{ni}(3)-LyiB{i}{ni}(1))^2);
        [~,fr] = NOMRESISTfunc(CeyB{i}(ni),min(AgB{i}{ni}));
        [~,~,f_tap] = ELASBUCKfunc(max(Cu{i}),AgB{i}{ni},fr,3);
        [~,~,Q,~,~,imax] = EWMfunc(max(Cu{i}),...
            hwB{i}{ni},tw(i),b(i),tf(i),AgB{i}{ni},f_tap,3);
        [~,CryB{i}(ni)] = FLEXRESISTfunc(Q(imax),...
            AgB{i}{ni}(imax),CeyB{i}(ni));
        CryB_ratio{i}(ni) = max(Cu{i})/CryB{i}(ni);
        if CryB_ratio{i}(ni) < 0
            CryB_ratio{i}(ni) = 0;
        end
    end
end
CRX_ratio(:,z-2) = cell2mat(Crx_ratio)';
CRYP_ratio(:,z-2) = cell2mat(CryP_ratio)';
CRYB_ratio(:,z-2) = cell2mat(CryB_ratio)';
%% FLEXURAL STRENGTH
% Inside flanges
% -------------------------------------------------------------------------
% Sequence to find Cu and Mu at bottom, middle, top of each subElement
% (i)  Consider each element.
% (ni) Consider each unbraced length between brace points.
% (k)  Bottom/Middle/Top of each unbraced length.
% (c=0.005) If close enough use original FEM moments.
% Interpolate to find moment and axial force.
% Interpolate - Lower the index value if nearer to top.
% -------------------------------------------------------------------------
for i=1:NumEl
    for ni=1:N(i)-1
        for k=1:3
            [c, index] = min(abs(Lxi{i}-LyiB{i}{ni}(k)));
            if c<=0.005
                MuB{i}{ni}(k) = Mu{i}(index);
                CuB{i}{ni}(k) = Cu{i}(index);
            elseif Lxi{i}(index)<LyiB{i}{ni}(k)
                X = (LyiB{i}{ni}(k));
                A = (Lxi{i}(index));
                B = (Lxi{i}(index+1));
                CMom = (Mu{i}(index));
                DMom = (Mu{i}(index+1));
                MuB{i}{ni}(k) = (X-A)*((DMom-CMom)/(B-A))+(CMom);
                CAxi = (Cu{i}(index));
                DAxi = (Cu{i}(index+1));
                CuB{i}{ni}(k) = (X-A)*((DAxi-CAxi)/(B-A))+(CAxi);
            else
                index = index-1;
                X = (LyiB{i}{ni}(k));
                A = (Lxi{i}(index));
                B = (Lxi{i}(index+1));
                CMom = (Mu{i}(index));
                DMom = (Mu{i}(index+1));
```

```
                MuB{i}{ni}(k) = (X-A)*((DMom-CMom)/(B-A))+(CMom);
                CAxi = (Cu{i}(index));
                DAxi = (Cu{i}(index+1));
                CuB{i}{ni}(k) = (X-A)*((DAxi-CAxi)/(B-A))+(CAxi);
            end
        end
    end
end
% -------------------------------------------------------------------------
% Step 1: Cross section classification.
% Step 2: Calculate the stress inside flange...
%         per unbraced length at 3-points. (+ for compr/ - for tension).
% Step 3: Calculate the stress gradient factor of each unbraced length.
% -------------------------------------------------------------------------
% Calculate the unbraced length of each subelement...
% if unbraced length is in tension throughtout the unbraced length...
% is set to infinitely short.
% -------------------------------------------------------------------------
% Step 4: Calc the critical stress at midspan for unbraced length (Yura).
% Step 5: Scale the elastic LTB load for the 3-points.
% Step 6: Calculate the moment of resistance at 3-points.
% Step 7: Check moment capacity at 3-points.
% -------------------------------------------------------------------------
% Allow a nominal moment for equation to hold if moment = zero.
% -------------------------------------------------------------------------
flg_class2 = 170/sqrt(fy*10^(-6));
flg_class4 = 200/sqrt(fy*10^(-6));
for i=1:NumEl
    for ni=1:N(i)-1
        for k=1:3
            flg_ratio{i} = b(i)/(2*tf(i));
            web_ratio{i}{ni}(k) = hwB{i}{ni}(k)/tw(i);
            web_class2{i}{ni}(k) = ...
                (1700/sqrt(fy*10^(-6)))*...
                (1-0.61*((CuB{i}{ni}(k)/(phi*AgB{i}{ni}(k)*fy))));
            web_class4{i}{ni}(k) = ...
                ((1900/sqrt(fy*10^(-6)))*...
                (1-0.65*(CuB{i}{ni}(k)/(phi*AgB{i}{ni}(k)*fy))));
            fB{i}{ni}(k) = (MuB{i}{ni}(k))/(ZexB{i}{ni}(k));
        end
        f2 = max(fB{i}{ni});
        if f2<=0
            f2=0;
        end
        fmid = fB{i}{ni}(2);
        f0   = min(fB{i}{ni});
        [omega2B{i}{ni}] = STRESSGRADfunc(f2,fmid,f0);
        if fB{i}{ni}<0
            sBrace{i}{ni} = 0.001;
        else
            sBrace{i}{ni} = max(LyiB{i}{ni})-min(LyiB{i}{ni});
        end
        McrB_mid{i}{ni} = ((omega2B{i}{ni}*pi())/(sBrace{i}{ni}*(1)))*...
            sqrt(E*IyB{i}{ni}(2)*G*JB{i}{ni}(2) +...
            (((pi()*E)/(sBrace{i}{ni}*(1)))^2)*...
            IyB{i}{ni}(2)*CwB{i}{ni}(2));
        if max(fB{i}{ni}) == 0
            gammaLTB_B{i}{ni} = 100000;
        else
            gammaLTB_B{i}{ni} = ...
                (McrB_mid{i}{ni}/ZexB{i}{ni}(2))/(max(fB{i}{ni}));
        end
        for k=1:3
            if MuB{i}{ni}(k)==0
                MuB_ = 1;
            else
                MuB_ = MuB{i}{ni}(k);
            end
            McrB{i}{ni}(k) = ...
                abs((fB{i}{ni}(k)*gammaLTB_B{i}{ni}*ZexB{i}{ni}(k)));
            if flg_ratio{i} <= flg_class2 && ...
                    web_ratio{i}{ni}(k) <= web_class2{i}{ni}(k)
                if McrB{i}{ni}(k)>0.67*MplxB{i}{ni}(k)
                    MrB{i}{ni}(k) = min(1.15*phi*MplxB{i}{ni}(k)*...
                        (1-(0.28*MplxB{i}{ni}(k))/McrB{i}{ni}(k)),...
                        phi*MplxB{i}{ni}(k));
                else
                    MrB{i}{ni}(k) = phi*McrB{i}{ni}(k);
                end
                if MrB{i}{ni}(k) < 1
                    MrB{i}{ni}(k) = 1;
                end
                MrB_ratio{i}{ni}(k) = abs(MuB{i}{ni}(k))/MrB{i}{ni}(k);
            elseif flg_ratio{i} <= flg_class4
                if McrB{i}{ni}(k)>0.67*MexB{i}{ni}(k)
                    Mr_B{i}{ni}(k) = min([1.15*phi*MexB{i}{ni}(k)*...
                        (1-(0.28*MexB{i}{ni}(k))/McrB{i}{ni}(k)),...
                        phi*MexB{i}{ni}(k),phi*ZeffB{i}{ni}(k)*fy]);
                else
                    Mr_B{i}{ni}(k) = phi*McrB{i}{ni}(k);
                end
                if web_ratio{i}{ni}(k) > web_class4{i}{ni}(k)
                    MrB{i}{ni}(k) = Mr_B{i}{ni}(k)*(1-0.0005*...
                        (AwB{i}{ni}(k)/AfB{i}{ni}(k))*...
                        ((hwB{i}{ni}(k)/tw(i))-...
                        (1900/sqrt(abs(MuB_)/(phi*ZexB{i}{ni}(k))))));
                else
                    MrB{i}{ni}(k) = Mr_B{i}{ni}(k);
                end
                if MrB{i}{ni}(k) < 1
                    MrB{i}{ni}(k) = 1;
                end
                MrB_ratio{i}{ni}(k) = abs(MuB{i}{ni}(k))/MrB{i}{ni}(k);
            else
                MrB{i}{ni}(k) = 1;
                MrB_ratio{i}{ni}(k) = abs(MuB{i}{ni}(k))/MrB{i}{ni}(k);
            end
            if MrB_ratio{i}{ni}(k) < 0
                MrB_ratio{i}{ni}(k) = 0;
            end
        end
    end
end
MRB = cell2mat([MrB{:,:}])';
MRB_ratio(:,z-2) = cell2mat([MrB_ratio{:,:}])';
%% Outside flanges
% -------------------------------------------------------------------------
% Sequence to find Cu and Mu at bottom, middle, top of each subElement
% (i)  Consider each member.
% (mi) Consider each unbraced length between purlins.
% (k)  Bottom/Middle/Top of unbraced length.
% (c = 5 mm) If close enough use original FEM moments.
% Interpolate to find moment, shear (Shear checks later) + axial force.
% Interpolate - Lower the index value if nearer to top.
% -------------------------------------------------------------------------
for i=1:NumEl
    for mi=1:M(i)-1
        for k=1:3
            [c, index] = min(abs(Lxi{i}-LyiP{i}{mi}(k)));
            if c<=0.005
                MuP{i}{mi}(k) = Mu{i}(index);
                VuP{i}{mi}(k) = Vu{i}(index);
                CuP{i}{mi}(k) = Cu{i}(index);
            elseif Lxi{i}(index)<LyiP{i}{mi}(k)
```

```
                X = (LyiP{i}{mi}(k));
                A = (Lxi{i}(index));
                B = (Lxi{i}(index+1));
                CMom = (Mu{i}(index));
                DMom = (Mu{i}(index+1));
                MuP{i}{mi}(k) = (X-A)*((DMom-CMom)/(B-A))+(CMom);
                CAxi = (Cu{i}(index));
                DAxi = (Cu{i}(index+1));
                CuP{i}{mi}(k) = (X-A)*((DAxi-CAxi)/(B-A))+(CAxi);
                CShr = (Vu{i}(index));
                DShr = (Vu{i}(index+1));
                VuP{i}{mi}(k) = (X-A)*((DShr-CShr)/(B-A))+(CShr);
            else
                index = index-1;
                X = (LyiP{i}{mi}(k));
                A = (Lxi{i}(index));
                B = (Lxi{i}(index+1));
                CMom = (Mu{i}(index));
                DMom = (Mu{i}(index+1));
                MuP{i}{mi}(k) = (X-A)*((DMom-CMom)/(B-A))+(CMom);
                CAxi = (Cu{i}(index));
                DAxi = (Cu{i}(index+1));
                CuP{i}{mi}(k) = (X-A)*((DAxi-CAxi)/(B-A))+(CAxi);
                CShr = (Vu{i}(index));
                DShr = (Vu{i}(index+1));
                VuP{i}{mi}(k) = (X-A)*((DShr-CShr)/(B-A))+(CShr);
            end
        end
    end
end
% ------------------------------------------------------------------------
% Step 1: Cross section classification.
% Step 2: Calculate the stress inside flange...
%         per unbraced length at 3-points. (+ for compr/ - for tension).
% Step 3: Calculate the stress gradient factor of each unbraced length.
% ------------------------------------------------------------------------
% Calculate the unbraced length of each subelement...
% if unbraced length is in tension throughtout the unbraced length...
% is set to infinitely short.
% ------------------------------------------------------------------------
% Step 4: Calc the critical stress at midspan for unbraced length (Yura).
% Step 5: Scale the elastic LTB load for the 3-points.
% Step 6: Calculate the moment of resistance at 3-points.
% Step 7: Check moment capacity at 3-points.
% ------------------------------------------------------------------------
% Allow a nominal moment for equation to hold if moment = zero.
% ------------------------------------------------------------------------
for i=1:NumEl
    for mi=1:M(i)-1
        for k=1:3
% Step 1
            web_ratio{i}{mi}(k)  = hwP{i}{mi}(k)/tw(i);
            web_class2{i}{mi}(k) = ....
                (1700/sqrt(fy*10^(-6)))*...
                (1-0.61*((CuP{i}{mi}(k)/(phi*AgP{i}{mi}(k)*fy))));
            web_class4{i}{mi}(k) = ...
                ((1900/sqrt(fy*10^(-6)))*...
                (1-0.65*(CuP{i}{mi}(k)/(phi*AgP{i}{mi}(k)*fy))));
% Step 2
            fP{i}{mi}(k) = (-MuP{i}{mi}(k))/(ZexP{i}{mi}(k));
        end
% Step 3
        f2 = max(fP{i}{mi});
        if f2<=0
            f2=0;
        end
        fmid = fP{i}{mi}(2);
        f0   = min(fP{i}{mi});
        [omega2P{i}{mi}] = STRESSGRADfunc(f2,fmid,f0);
% Unbraced length
        if fP{i}{mi}<=0
            sPurl{i}{mi} = 0.001;
        else
            sPurl{i}{mi} = max(LyiP{i}{mi})-min(LyiP{i}{mi});
        end
% Step 4
        McrP_mid{i}{mi} = ((omega2P{i}{mi}*pi())/(sPurl{i}{mi}*(1)))*...
            sqrt(E*IyP{i}{mi}(2)*G*JP{i}{mi}(2) +...
            (((pi()*E)/(sPurl{i}{mi}*(1)))^2)*...
            IyP{i}{mi}(2)*CwP{i}{mi}(2));
        if max(fP{i}{mi}) <= 0
            gammaLTB_P{i}{mi} = 100000;
        else
            gammaLTB_P{i}{mi} = ...
            (McrP_mid{i}{mi}/ZexP{i}{mi}(2))/(max(fP{i}{mi}));
        end
        for k=1:3
            if MuP{i}{mi}(k)==0
                MuP_ = 1;
            else
                MuP_ = MuP{i}{mi}(k);
            end
% Step 5
            McrP{i}{mi}(k) = abs((fP{i}{mi}(k)*...
            gammaLTB_P{i}{mi}*ZexP{i}{mi}(k)));
% Step 6 + 7
            if flg_ratio{i} <= flg_class2 && ...
            web_ratio{i}{mi}(k) <= web_class2{i}{mi}(k)
                if McrP{i}{mi}(k)>0.67*MplxP{i}{mi}(k)
                    MrP{i}{mi}(k) = min(1.15*phi*MplxP{i}{mi}(k)*...
            (1-(0.28*MplxP{i}{mi}(k))/McrP{i}{mi}(k)),...
            phi*MplxP{i}{mi}(k));
                else
                    MrP{i}{mi}(k) = phi*McrP{i}{mi}(k);
                end
                if MrP{i}{mi}(k) < 1
                    MrP{i}{mi}(k) = 1;
                end
                MrP_ratio{i}{mi}(k) = abs(MuP{i}{mi}(k))/MrP{i}{mi}(k);
            elseif flg_ratio{i} <= flg_class4
                if McrP{i}{mi}(k)>0.67*MexP{i}{mi}(k)
                    Mr_P{i}{mi}(k) = min([1.15*phi*MexP{i}{mi}(k)*...
            (1-(0.28*MexP{i}{mi}(k))/McrP{i}{mi}(k)),...
            phi*MexP{i}{mi}(k),phi*ZeffP{i}{mi}(k)*fy]);
                else
                    Mr_P{i}{mi}(k) = phi*McrP{i}{mi}(k);
                end
                if web_ratio{i}{mi}(k) > web_class4{i}{mi}(k)
                    MrP{i}{mi}(k) = Mr_P{i}{mi}(k)*(1-0.0005*...
            (AwP{i}{mi}(k)/AfP{i}{mi}(k))*((hwP{i}{mi}(k)/tw(i))-...
            (1900/sqrt(abs(MuP_)/(phi*ZexP{i}{mi}(k))))));
                else
                    MrP{i}{mi}(k) = Mr_P{i}{mi}(k);
                end
                if MrP{i}{mi}(k) < 1
                    MrP{i}{mi}(k) = 1;
                end
                MrP_ratio{i}{mi}(k) = abs(MuP{i}{mi}(k))/MrP{i}{mi}(k);
            else
                MrP{i}{mi}(k) = 1;
                MrP_ratio{i}{mi}(k) = abs(MuP{i}{mi}(k))/MrP{i}{mi}(k);
            end
            if MrP_ratio{i}{mi}(k) < 0
```

```
                MrP_ratio{i}{mi}(k) = 0;
            end
        end
    end
end
MRP = cell2mat([MrP{:,:}])';
MRP_ratio(:,z-2) = cell2mat([MrP_ratio{:,:}])';
%% SHEAR
% ------------------------------------------------------------------------
% Check unbraced lengths between purling positions (outer flange).
% Step 1: Accept that no web-stiffners are provided (conservative)
% Step 2: Calc the cross sectional Cu based on zero slenderness...
%         and at 3-points.
% Step 3: Calc the cross sectional Mu based on lat. supported section.
% ------------------------------------------------------------------------
for i=1:NumEl
    for mi=1:M(i)-1
        for k=1:3
            kv{i}{mi}(k) = 5.34 + 4/((L(i)/hwP{i}{mi}(k))^2);
            if web_ratio{i}{mi}(k) <= 440*sqrt((kv{i}{mi}(k))/(fy/1000000))
                fs{i}{mi}(k) = 0.66*fy;
            elseif web_ratio{i}{mi}(k) > ...
                    440*sqrt((kv{i}{mi}(k))/(fy/1000000))...
                && web_ratio{i}{mi}(k) <= ...
                500*sqrt((kv{i}{mi}(k))/(fy/1000000))
                fs{i}{mi}(k) = ...
                    1000000*290*(sqrt((fy/1000000)*kv{i}{mi}(k)))/...
                                (web_ratio{i}{mi}(k));
            elseif web_ratio{i}{mi}(k) > ...
                    500*sqrt((kv{i}{mi}(k))/(fy/1000000))...
                && web_ratio{i}{mi}(k) <= ...
                620*sqrt((kv{i}{mi}(k))/(fy/1000000))
                fcri = 290*(sqrt((fy/1000000)*kv{i}{mi}(k)))/...
                                (web_ratio{i}{mi}(k));
                ka = 1/sqrt(1+(L(i)/hwP{i}{mi}(k))^2);
                ft = ka*(0.5*(fy/1000000)-0.866*fcri);
                fs{i}{mi}(k) = (fcri+ft)*1000000;
            else
                fcre = (180000*kv{i}{mi}(k))/(web_ratio{i}{mi}(k)^2);
                ka = 1/sqrt(1+(L(i)/hwP{i}{mi}(k))^2);
                ft = ka*(0.5*(fy/1000000)-0.866*fcre);
                fs{i}{mi}(k) = (fcre+ft)*1000000;
            end
            VrP{i}{mi}(k) = phi*hwP{i}{mi}(k)*tw(i)*fs{i}{mi}(k);
            VrP_ratio{i}{mi}(k) = abs(VuP{i}{mi}(k))/VrP{i}{mi}(k);
            if VrP_ratio{i}{mi}(k) < 0
                VrP_ratio{i}{mi}(k) = 0;
            end
        end
    end
end
VRP = cell2mat([VrP{:,:}])';
VRP_ratio(:,z-2) = cell2mat([VrP_ratio{:,:}])';
%% A) Overall member strength'))
% ------------------------------------------------------------------------
% Check unbraced lengths between purlin position (outer flange).
% As overall member strength checks use cross section characteristics...
% only purlin is invetigated here.
% Step 1: Use U1=1 (moment grad + 2nd order) for unbraced frames.
% Step 2: Calc the cross sectional Cu based on zero slenderness...
%         and at 3-points.
% Step 3: Calc the cross sectional Mu based on the section class.
% ------------------------------------------------------------------------
% Penalise sections with class 4 flanges is to force a design violation.
% ------------------------------------------------------------------------
% Step 4: Combine into appropriate interaction formula.
% ------------------------------------------------------------------------
for i=1:NumEl
    for mi=1:M(i)-1
        for k=1:3
            U1P{i}{mi}(k) = 1;
            if flg_ratio{i}<=flg_class2 && ...
            web_ratio{i}{mi}(k)<=web_class2{i}{mi}(k)
                MrPG{i}{mi}(k) = phi*MplxP{i}{mi}(k);
            elseif flg_ratio{i}<=flg_class4 && ...
            web_ratio{i}{mi}(k)<=web_class4{i}{mi}(k)
                MrPG{i}{mi}(k) = phi*MexP{i}{mi}(k);
            elseif flg_ratio{i}<=flg_class4 && ...
            web_ratio{i}{mi}(k)>web_class4{i}{mi}(k)
                if MuP{i}{mi}(k)==0
                    MuP_ = 1;
                else
                    MuP_ = MuP{i}{mi}(k);
                end
                MrPG{i}{mi}(k) = (phi*MexP{i}{mi}(k))*...
            (1-0.0005*(AwP{i}{mi}(k)/AfP{i}{mi}(k))*...
            ((hwP{i}{mi}(k)/tw(i))-(1900/sqrt(abs(MuP_)/...
            (phi*ZexP{i}{mi}(k))))));
            elseif flg_ratio{i}>flg_class4
                MrPG{i}{mi}(k) = 1;
            end
            if flg_ratio{i}<=flg_class2 && ...
            web_ratio{i}{mi}(k)<=web_class2{i}{mi}(k)
                CombPG{i}{mi}(k) = (CuP{i}{mi}(k)/Crx{i})+...
            ((0.85*U1P{i}{mi}(k)*-MuP{i}{mi}(k))/(MrPG{i}{mi}(k)));
            else
                CombPG{i}{mi}(k) = (CuP{i}{mi}(k)/Crx{i})+...
            ((U1P{i}{mi}(k)*-MuP{i}{mi}(k))/(MrPG{i}{mi}(k)));
            end
            if CombPG{i}{mi}(k) < 0
                CombPG{i}{mi}(k) = 0;
            end
        end
    end
end
COMBPG(:,z-2) = cell2mat([CombPG{:,:}])';
%% B) Lateral-torsional buckling strength
% ------------------------------------------------------------------------
% Check unbraced lengths between brace points (inner flange).
% Different critical lengths.
% Step 1: Use U1=1 (moment grad + 2nd order) for unbraced frames.
% Step 2: Calc the cross sectional Cu based on K=1 and...
%         uniaxial strong axis bending and at 3-points.
% Step 3: Calc the cross sectional Mu based on lat. supported section.
% ------------------------------------------------------------------------
% Penalise sections with class 4 flanges is to force a design violation.
% ------------------------------------------------------------------------
% Step 4: Combine into appropriate interaction formula.
% ------------------------------------------------------------------------
for i=1:NumEl
    for ni=1:N(i)-1
        for k=1:3
            U1B{i}{ni}(k) = 1;
            if flg_ratio{i}<=flg_class2 && ...
            web_ratio{i}{ni}(k)<=web_class2{i}{ni}(k)
                CombBT{i}{ni}(k) = (CuB{i}{ni}(k)/CryB{i}(ni))+...
            ((0.85*U1B{i}{ni}(k)*MuB{i}{ni}(k))/(MrB{i}{ni}(k)));
            else
                CombBT{i}{ni}(k) = (CuB{i}{ni}(k)/CryB{i}(ni))+...
            ((U1B{i}{ni}(k)*MuB{i}{ni}(k))/(MrB{i}{ni}(k)));
            end
            if CombBT{i}{ni}(k) < 0
```

```
                CombBT{i}{ni}(k) = 0;
            end
        end
    end
end
COMBBT(:,z-2) = cell2mat([CombBT{:,:}])';
% ------------------------------------------------------------------------
% Check unbraced lengths between purlin position (outer flange).
% Different critical lengths.
% Step 1: Use U1=1 (moment grad + 2nd order) for unbraced frames.
% Step 2: Calc the cross sectional Cu based on zero slenderness...
%         and at 3-points.
% Step 3: Calc the cross sectional Mu based on the section class.
% ------------------------------------------------------------------------
% Penalise sections with class 4 flanges is to force a design violation.
% ------------------------------------------------------------------------
% Step 4: Combine into appropriate interaction formula.
% ------------------------------------------------------------------------
for i=1:NumEl
    for mi=1:M(i)-1
        for k=1:3
            U1P{i}{mi}(k) = 1;
            if flg_ratio{i}<=flg_class2 && ...
            web_ratio{i}{mi}(k)<=web_class2{i}{mi}(k)
                CombPT{i}{mi}(k) = (CuP{i}{mi}(k)/CryP{i}(mi))+...
            ((0.85*U1P{i}{mi}(k)*-MuP{i}{mi}(k))/(MrP{i}{mi}(k)));
            else
                CombPT{i}{mi}(k) = (CuP{i}{mi}(k)/CryP{i}(mi))+...
            ((U1P{i}{mi}(k)*-MuP{i}{mi}(k))/(MrP{i}{mi}(k)));
            end
            if CombPT{i}{mi}(k) < 0
                CombPT{i}{mi}(k) = 0;
            end
        end
    end
end
COMBPT(:,z-2) = cell2mat([CombPT{:,:}])';
%% COMBINED TENSION AND FLEXURE
% ------------------------------------------------------------------------
% Check unbraced lengths between purlin position (outer flange).
% Unneccesary to also check between brace positions as capacity not
% influenced by unbraced lengths.
% Step 1: Find any axial tension in unbraced lengths between purlins.
% Step 2: Chech against the 2 interaction formulas.
% Step 3: Check classification for correct second formula.
% ------------------------------------------------------------------------
for i=1:NumEl
    for mi=1:M(i)-1
        for k=1:3
            if CuP{i}{mi}(k)<0
                TuP{i}{mi}(k) = -CuP{i}{mi}(k);
            else
                TuP{i}{mi}(k) = 0;
            end
            if flg_ratio{i}        <= flg_class2 &&...
               web_ratio{i}{mi}(k) <= web_class2{i}{mi}(k)
                CombTP1{i}{mi}(k) = (TuP{i}{mi}(k)/...
                                     (phi*AgP{i}{mi}(k)*fy))+...
                                     (MuP{i}{mi}(k)/(phi*MplxP{i}{mi}(k)));
                CombTP2{i}{mi}(k) = -((TuP{i}{mi}(k)*ZplxP{i}{mi}(k))/...
                                      (MrP{i}{mi}(k)*AgP{i}{mi}(k)))...
                                     +(MuP{i}{mi}(k)/(MrP{i}{mi}(k)));
            else
                CombTP1{i}{mi}(k) = (TuP{i}{mi}(k)/...
                                     (phi*AgP{i}{mi}(k)*fy))...
                                     +(MuP{i}{mi}(k)/(phi*MexP{i}{mi}(k)));
                CombTP2{i}{mi}(k) = -((TuP{i}{mi}(k)*ZexP{i}{mi}(k))/...
                                      (MrP{i}{mi}(k)*AgP{i}{mi}(k)))...
                                     +(MuP{i}{mi}(k)/(MrP{i}{mi}(k)));
            end
            if CombTP1{i}{mi}(k)<0 || TuP{i}{mi}(k)==0
                CombTP1{i}{mi}(k) = 0;
            end
            if CombTP2{i}{mi}(k)<0 || TuP{i}{mi}(k)==0
                CombTP2{i}{mi}(k) = 0;
            end
        end
    end
end
COMBTP1(:,z-2) = cell2mat([CombTP1{:,:}])';
COMBTP2(:,z-2) = cell2mat([CombTP2{:,:}])';
%% COUNT VIOLATIONS
viol = viol + sum(abs(CRX_ratio(:,z-2))>=1);
viol = viol + sum(abs(CRYP_ratio(:,z-2))>=1);
viol = viol + sum(abs(CRYB_ratio(:,z-2))>=1);
viol = viol + sum(abs(MRB_ratio(:,z-2))>=1);
viol = viol + sum(abs(MRP_ratio(:,z-2))>=1);
viol = viol + sum(abs(VRP_ratio(:,z-2))>=1);
viol = viol + sum(abs(COMBPG(:,z-2))>=1);
viol = viol + sum(abs(COMBBT(:,z-2))>=1);
viol = viol + sum(abs(COMBPT(:,z-2))>=1);
viol = viol + sum(abs(COMBTP1(:,z-2))>=1);
viol = viol + sum(abs(COMBTP2(:,z-2))>=1);
% Return unity ratios.
% %% %% %% REMEMBER TO CONSIDER THE SIZE (s) ON CALCULATING THE viol
end
end
```

## PURLINfunc.m

```
%% FUNCTION-TYPE:
% Specify coords. of purlins (outside flange) and braces (inner flange)
% Herman Aucamp.
% 15045471.
% ------------------------------------------------------------------------
function[xPurl,yPurl,M,xBrace,yBrace,N,LiPurl,LiBrace] = PURLINfunc()
% ------------------------------------------------------------------------
% Call general design and physical properties.
% Check the first half of the portal frame and position purlins.
% Copy positions the second half.
% Divide each member according to max purlin spacing.
% Force algorithm to create an odd number of purlin positions per member.
% Place braces at purlin positions.

% Unhide/hide code depending on frame considered in NODEfunc.
% An automated purlin function in presented, but alternatively the...
% purlins may be place manually. The predefined positions used in the...
% study is available below to hide/unhide.
% Purlin positions should be changed according to NODEfunc to...
% realistic values for each frame-span configuration.
% ------------------------------------------------------------------------
%% Automated placement of purlins and side girts
% [NumEl,~,~,xCoord,yCoord] = NODEfunc();
% [~,~,~,~,~,~,~,~,~,~,~,~,~,~,~,~,~,~,~,~,~,~,~,~,~,~,~,~,~,~,maxsPurl,~,~,~,~,~,~] = GLOBALfunc();
% NumPurl  = 0;
% NumBrace = 0;
% for i=1:NumEl/2
%     L_(i) = sqrt((xCoord(i+1)-xCoord(i))^2+(yCoord(i+1)-yCoord(i))^2);
```

```
%% Manual placement based on Clotan purlin and brace positions
% 20m portal frame
xPurl = [0 0 0 ...
0 1.395042141 2.791079921 4.187117701 5.583155481 ...
6.979193261 8.375231041 10 ...
10 11.62476896 13.02080674 14.41684452 15.8128823 ...
17.20892008 18.60495786 20 ...
20 20 20]';
yPurl = [0 2.25 4.5 ...
    4.5 4.639504214 4.779107932 4.91871165 5.058315368 ...
    5.197919086 5.337522804 5.5 ...
    5.5 5.337522804 5.197919086 5.058315368 4.91871165  ...
    4.779107932 4.639504214 4.5 ...
    4.5 2.25 0]';
M = [3 8 8 3];
xBrace = [0 0 ...
0 1.395042141 6.979193261 10 ...
10 13.02080674 18.60495786 20 ...
20 20]';
yBrace = [0 4.5 ...
    4.5 4.639504214 5.197919086 5.5 ...
    5.5 5.197919086 4.639504214 4.5 ...
    4.5 0]';
N = [2 4 4 2];
LiPurl{1} = [0 2.25 4.5]';
LiPurl{2} = [0 1.402 2.805000599 4.208001199 5.611001798 ...
    7.014002397 8.417002996 10.04987562]';
LiPurl{3} = [0 1.402 2.805000599 4.208001199 5.611001798 ...
    7.014002397 8.417002996 10.04987562]';
LiPurl{4} = [0 2.25 4.5]';
LiBrace{1} = [0 4.5]';
LiBrace{2} = [0 1.402 7.014002397 10.04987562]';
LiBrace{3} = [0 1.402 7.014002397 10.04987562]';
LiBrace{4} = [0 4.5]';
% % 30m portal frame
% xPurl = [0 0 0 ...
% 0 1.41991807 3.086605364 4.753292658 6.419979951 8.086667245 ...
%       9.753354538 11.420041832 13.086729126 15 ...
% 15 16.91327 18.57996 20.24665 21.91333 23.58002...
%     25.24671 26.91339 28.58008 30 ...
% 30 30 30]';
% yPurl = [0 2.25 4.5 ...
%     4.5 4.6419918 4.8086605 4.975329 5.14199799 5.3086667 ...
% 5.475335 5.642004 5.8086729 6 ...
%     6 5.8086729 5.642004 5.475335 5.3086667 5.14199799 ...
% 4.975329 4.8086605 4.6419918 4.5 ...
%     4.5 2.25 0]';
% M = [3 10 10 3];
% xBrace = [0 0 ...
% 0 1.41991807 6.419979951 11.420041832 15 ...
% 15 18.57996 23.58002 28.58008 30 ...
% 30 30]';
% yBrace = [0 4.5 ...
%     4.5 4.6419918 5.14199799 5.642004 6 ...
%     6 5.642004 5.14199799 4.6419918 4.5 ...
%     4.5 0]';
% N = [2 5 5 2];
% LiPurl{1} = [0 2.25 4.5]';
% LiPurl{2} = [0 1.426999999 3.101999996 4.776999974 6.451999999 ...
%     8.126999998 9.801999954 11.47699998 13.152 15.07481343]';
% LiPurl{3} = [0 1.426999999 3.101999996 4.776999974 6.451999999 ...
%     8.126999998 9.801999954 11.47699998 13.152 15.07481343]';
% LiPurl{4} = [0 2.25 4.5]';
% LiBrace{1} = [0 4.5]';
% LiBrace{2} = [0 1.426999999 6.451999999 11.47699998 15.07481343]';
% LiBrace{3} = [0 1.426999999 6.451999999 11.47699998 15.07481343]';
% LiBrace{4} = [0 4.5]';
```

```
%     M(i)      = ceil(L_(i)/maxsPurl)+1;
%     while M(i)==0 || M(i)==1 || mod(M(i),2)==0
%         M(i) = M(i)+1;
%     end
%     xSpace    = (xCoord(i+1)-xCoord(i))/(M(i)-1);
%     ySpace    = (yCoord(i+1)-yCoord(i))/(M(i)-1);
%     sPurl(i) = sqrt(xSpace^2+ySpace^2);
%     N(i) = 0;
%     for j=1:M(i)
%         NumPurl = subs(NumPurl+1);
%         xPurl(NumPurl) = xCoord(i) + (j-1)*xSpace;
%         yPurl(NumPurl) = yCoord(i) + (j-1)*ySpace;
%         if j==1 || j==M(i) || mod(j,2)~=0 ||  (i~=1 && j==2)
%             NumBrace = subs(NumBrace+1);
%             xBrace(NumBrace) = xPurl(NumPurl);
%             yBrace(NumBrace) = yPurl(NumPurl);
%             N(i) = subs(N(i)+1);
%         end
%     end
% end
% k=1;
% for i=1:NumEl/2
%     for j=1:M(i)
%         if j==1
%             LiPurl{i}(j) = 0;
%         else
%             k=k+1;
%             LiPurl{i}(j) = LiPurl{i}(j-1)+sPurl(i);
%         end
%     end
%     k=k+1;
% end
% LiPurl = [LiPurl,fliplr(LiPurl)];
% xPurl=subs(xPurl);
% xPurl=[xPurl,2*xCoord(NumEl/2+1)-fliplr(xPurl)]';
% yPurl=subs(yPurl);
% yPurl=[yPurl,fliplr(yPurl)]';
% xBrace=subs(xBrace);
% xBrace = [xBrace,2*xCoord(NumEl/2+1)-fliplr(xBrace)]';
% yBrace=subs(yBrace);
% yBrace=[yBrace,fliplr(yBrace)]';
% k=1;
% for i=1:NumEl/2
%     for j=1:N(i)
%         if j==1
%             LiBrace{i}(j) = 0;
%         else
%             k=k+1;
%             LiBrace{i}(j) = LiBrace{i}(j-1)+...
%                 sqrt(((xBrace(k))-(xBrace(k-1)))^2+...
%                 ((yBrace(k))-(yBrace(k-1)))^2);
%         end
%     end
%     k=k+1;
% end
% LiBrace = [LiBrace,fliplr(LiBrace)];
% for i=NumEl/2+1:NumEl
%     LiBrace{i} = max(LiBrace{i})-fliplr(LiBrace{i});
% end
% M = [M,fliplr(M)]
% N = [N,fliplr(N)]
% [xPurl yPurl]
% [xBrace yBrace]
% end
```

```
% % 40m portal frame
% xPurl = [0 0 0 ...
% 0 0.804985087 1.574148835 3.392081782 5.210014729 7.027947676 ...
% 8.845880623 10.66381357 12.48174652 14.29967946 16.11761241 ...
% 17.93554536 20 ...
% 20 22.06445464 23.88238759 25.70032054 27.51825348 29.33618643 ...
% 31.15411938 32.97205232 34.78998527 36.60791822 38.42585117 ...
% 39.19501491 40 ...
% 40 40 40]';
% yPurl = [0 2.25 4.5 ...
%     4.5 4.580498509 4.657414884 4.839208179 5.021001474 5.202794769 ...
%     5.384588064 5.566381359 5.748174654 5.929967949 6.111761244 ...
%     6.293554539 6.5 ...
%     6.5 6.293554539 6.111761244 5.929967949 5.748174654 5.566381359 ...
%     5.384588064 5.202794769 5.021001474 4.839208179 4.657414884 ...
%     4.580498509 4.5 ...
%     4.5 2.25 0]';
% M = [3 13 13 3];
% xBrace = [0 0 ...
% 0 0.804985087 1.574148835 5.210014729 8.845880623 14.29967946 20 ...
% 20 25.70032054 31.15411938 34.78998527 38.42585117 39.19501491 40 ...
% 40 40]';
% yBrace = [0 4.5 ...
%     4.5 4.580498509 4.657414884 5.021001474 ...
% 5.384588064 5.929967949 6.5 ...
%     6.5 5.929967949 5.384588064 5.021001474 ...
% 4.657414884 4.580498509 4.5 ...
%     4.5 0]';
% N = [2 7 7 2];
% LiPurl{1} = [0 2.25 4.5]';
% LiPurl{2} = [0 0.809 1.582 3.409000001 5.236000001 7.063000002...
%     8.890000002 10.717 12.544 14.371 16.198 18.025 20.09975124]';
% LiPurl{3} = [0 0.809 1.582 3.409000001 5.236000001 7.063000002...
%     8.890000002 10.717 12.544 14.371 16.198 18.025 20.09975124]';
% LiPurl{4} = [0 2.25 4.5]';
% LiBrace{1} = [0 4.5]';
% LiBrace{2} = [0 0.809 1.582 5.236000001 ...
% 8.890000002 14.371 20.09975124]';
% LiBrace{3} = [0 0.809 1.582 5.236000001 ...
% 8.890000002 14.371 20.09975124]';
% LiBrace{4} = [0 4.5]';
%
% % 50m portal frame
% xPurl = [0 0 0 ...
% 0 0.836826277 1.673652554 3.597059443 5.520466332 7.443873221 ...
% 9.36728011 11.290687 13.21409389 ...
% 15.13750078 17.06090767 18.98431456 ...
% 20.90772144 22.83112833 25 ...
% 25 27.16887167 29.09227856 31.01568545 32.93909233 34.86249922 ...
% 36.78590611 38.709313 40.63271989 ...
% 42.55612678 44.47953367 46.40294056 ...
% 48.32634745 49.16317372 50 ...
% 50 50 50]';
% yPurl = [0 2.25 4.5 ...
%     4.5 4.583682628 4.667365256 4.859705945 5.052046634 5.244387323 ...
%     5.436728012 5.629068701 5.82140939 6.013750079 6.206090768 ...
%     6.398431457 6.590772146 6.783112835 7 ...
%     7 6.783112835 6.590772146 6.398431457 6.206090768 6.013750079 ...
%     5.82140939 5.629068701 5.436728012 5.244387323 5.052046634 ...
%     4.859705945 4.667365256 4.583682628 4.5 ...
%     4.5 2.25 0]';
% M = [3 15 15 3];
% xBrace = [0 0 ...
% 0 0.836826277 1.673652554 5.520466332 7.443873221 9.36728011 ...
% 13.21409389 17.06090767 20.90772144 25 ...
% 25 29.09227856 32.93909233 36.78590611 40.63271989 42.55612678 ...
% 44.47953367 48.32634745 49.16317372 50 ...
% 50 50]';
% yBrace = [0 4.5 ...
%     4.5 4.583682628 4.667365256 5.052046634 5.244387323 5.436728012 ...
%     5.82140939 6.206090768 6.590772146 7 ...
%     7 6.590772146 6.206090768 ...
%     5.82140939 5.436728012 5.244387323 5.052046634 ...
%     4.667365256 4.583682628 4.5 ...
%     4.5 0]';
% N = [2 10 10 2];
% LiPurl{1} = [0 2.25 4.5]';
% LiPurl{2} = [0 0.841 1.682 3.615 5.548000001 7.481000001 9.414000001 ...
% 11.347 13.28 15.213 17.146 19.079 21.012 22.945 25.12468905]';
% LiPurl{3} = [0 0.841 1.682 3.615 5.548000001 7.481000001 9.414000001 ...
% 11.347 13.28 15.213 17.146 19.079 21.012 22.945 25.12468905]';
% LiPurl{4} = [0 2.25 4.5]';
% LiBrace{1} = [0 4.5]';
% LiBrace{2} = [0 0.841 1.682 5.548000001 7.481000001 9.414000001 ...
%     13.28 17.146 21.012 25.12468905]';
% LiBrace{3} = [0 0.841 1.682 5.548000001 7.481000001 9.414000001 ...
%     13.28 17.146 21.012 25.12468905]';
% LiBrace{4} = [0 4.5]';
end
```

## BEAMPROPfunc.m

```
%% FUNCTION-TYPE:
% Defining the loading vectors for the FEM function.
% Herman Aucamp.
% 15045471.
% ------------------------------------------------------------------------
function[hw,Ag,Aw,Af,Ix,Zex,Mex,Zplx,Mplx,rx,Iy,Zey,Zply,ry,...
    J,Cw,Ip,rt,Ieff,Zeff] = BeamProp_func(L,Li,hw,tw,b,tf,s)
% ------------------------------------------------------------------------
% Allocate memory
% Discretize element by interpolation
% ------------------------------------------------------------------------
%% Discretised beam properties
[~,~,~,~,~,~,fy,~,~,~,~,~,~,~,~,~,~,~,~] = GLOBALfunc();
hwTemp  = zeros(s,1);
r       = zeros(s,1);
Ag      = zeros(s,1);
Aw      = zeros(s,1);
Af      = zeros(s,1);
Ix      = zeros(s,1);
Zex     = zeros(s,1);
Mex     = zeros(s,1);
Zplx    = zeros(s,1);
Mplx    = zeros(s,1);
rx      = zeros(s,1);
Iy      = zeros(s,1);
Zey     = zeros(s,1);
Zply    = zeros(s,1);
ry      = zeros(s,1);
J       = zeros(s,1);
Cw      = zeros(s,1);
Ip      = zeros(s,1);
rt      = zeros(s,1);
beff    = zeros(s,1);
Ieff    = zeros(s,1);
Zeff    = zeros(s,1);
for i=1:s
```

```
    hwTemp(i) = (Li(i)-0)*((hw(2,1)-(hw(1,1)))/(L-0))+(hw(1,1));
end
hw = hwTemp';
for i=1:s
    Li(i)   = L-(L/(s-1))*(s-i);
    r(i)    = 0;
    Ag(i)   = (tw*hw(i))+2*(b*tf);
    Aw(i)   = (tw*hw(i));
    Af(i)   = 2*(b*tf);
    Ix(i)   = (tw*hw(i)^3)/12+2*((b*tf^3)/12+(b*tf)*((hw(i)+tf)/2)^2);
    Zex(i)  = Ix(i)/((hw(i)+2*tf)/2);
    Mex(i)  = Zex(i)*fy;
    Zplx(i) = ((tw*hw(i)^2)/4)+b*tf*((hw(i)+2*tf)-tf);
    Mplx(i) = Zplx(i)*fy;
    rx(i)   = sqrt(Ix(i)/Ag(i));
    Iy(i)   = (hw(i)*tw^3)/12+2*(tf*b^3)/12;
    Zey(i)  = Iy(i)/(b/2);
    Zply(i) = (2*(tf*b^2)/4)+((hw(i)*tw^2)/4);
    ry(i)   = sqrt(Iy(i)/Ag(i));
    if (tf<=tw)
        t0 = tf;
        t1 = tw;
    else if (tf>tw)
            t0 = tw;
            t1 = tf;
        end
    end
    J(i)    = (2*(b*tf^3)+((hw(i)+tf)*tw^3))/3;
    Cw(i)   = (tf*(b^3)*(hw(i)+tf)^2)/24;
    Ip(i)   = Ix(i)+Iy(i);
    rt(i)   = sqrt((Iy(i)*(hw(i)+tf))/(2*Zex(i)));
    if b/tf>200/(2*sqrt(fy*10^(-6)))
        beff(i) = 200*tf/sqrt(fy*10^(-6));
        Ieff(i) = (tw*hw(i)^3)/12+2*((2*beff(i)*tf^3)/12+...
            (2*beff(i)*tf)*((hw(i)+tf)/2)^2);
    else
        Ieff(i) = Ix(i);
    end
    Zeff(i) = (2*Ieff(i))/(hw(i)+2*tf);
end
end
```

## SUCAPPROXfunc.m

```
%% FUNCTION-TYPE:
% Calc the elastic buckling load, using the method of successive approx.
% Herman Aucamp.
% 15045471.
% ------------------------------------------------------------------------
function[Ce] = SUCAPPROXfunc(hwt,hwb,L,B,tw,tf,Cu)
% ------------------------------------------------------------------------
% Allocate memory.
% Returns the approximate critical buckling load Ce.
% Define the maximum iteration in-case no convergence.
% Only the first time is a displacement assumed.
% for subsequent iterations the prev approx displ is used.
% ------------------------------------------------------------------------
%% Newman's method of successive approximations
[~,E,~,~,~,~,~,~,~,~,sz,conv,~,~,~,~,~,~,~] = GLOBALfunc();
syms Rk Rx_all real
Ri     = zeros([1 sz+1]);
y1     = zeros([1 sz+1]);
y_2    = zeros([1 sz+1]);
y_r    = zeros([1 sz+1]);
y2     = zeros([1 sz+1]);
hw     = zeros([1 sz+1]);
I      = zeros([1 sz+1]);
M_Fic  = zeros([1 sz+1]);
R_Fic  = zeros([1 sz+1]);
R_x    = zeros([1 sz+1]);
Theta  = zeros([1 sz+1]);
for i = 1:sz+1
    if (i == 1)
        hw(i) = hwt;
    else if(i == sz+1)
            hw(i) = hwb;
        else
            hw(i) = hwt- (i-1)*(hwt-hwb)/(sz);
        end
    end
    I(i) = ((tw*hw(i)^3)/12)+2*(((B*tf^3)/12)+(B*tf*((hw(i)+tf)/2)^2));
end
for j = 1:20
    if (j==1)
        for k = 1:sz+1
            Ri(k) = degtorad((k-1)*180/sz);
            if or((Ri(k)==0),(Ri(k)==degtorad(sz*180/sz)))
                y1(k) = 0;
            else
                y1(k) = 100*sin(Ri(k));
            end
        end;
    else
        y1 = y2;
    end
    for k = 1:sz+1
        M_Fic(k) = Cu*y1(k)/(E*I(k));
    end;
    for k = 1:sz+1
        if (y1(k)==0)
            R_Fic(k) = 0;
        else
            R_Fic(k) = ((L/sz)/12)*(M_Fic(k-1)+10*M_Fic(k)+(M_Fic(k+1)));
        end
        R_x(k) = R_Fic(k)*(L/sz)*(k-1);
    end;
    for k = 1:sz+1
        if (k==1)
            Theta(k) = sum(R_Fic)-(sum(R_x)/L);
        else
            Theta(k) = Theta(k-1)-R_Fic(k);
        end
        if (y1(k)==0)
            y_2(k) = 0;
        else if (k==2)
                y_2(k) = Theta(k-1)*(L/sz);
            else
                y_2(k) = y_2(k-1)+Theta(k-1)*(L/sz);
            end
        end
    end;
    for k = 1:sz+1
        if (y1(k)==0)
            y_r(k) = 0;
        else
            y_r(k) = y1(k)/y_2(k);
        end
        if (y1(k)==0)
```

```
            y2(k) = 0;
        else
            y2(k) = max(y1)*y_2(k)/max(y_2);
        end
    end
    y_R     = sort(y_r(:));
    Ce_Low  = y_R(3);
    Ce_Up   = y_R(sz+1);
    Ce      = sum(y1)/sum(y_2);
    x = ((Ce_Up-Ce_Low)/Ce)*100;
```

## NOMRESISTfunc.m

```
%% FUNCTION-TYPE:
% Calculate the nominal resistance for columns.
% Herman Aucamp.
% 15045471.
% ------------------------------------------------------------------------
function [fe,fr] = NOMRESISTfunc(Ce,Ag)
% ------------------------------------------------------------------------
```

## ELASBUCKfunc.m

```
%% FUNCTION-TYPE:
% Calculate the stress in the column without area reductions.
% Herman Aucamp.
% 15045471.
% ------------------------------------------------------------------------
function [gamma_e,f,f_tap] = ELASBUCKfunc(Cu,Ag,fr,s)
% ------------------------------------------------------------------------
% Allocate memory
% Find stress at several cross-sections
% Gamma_e is the factor to multiply the loads in a tapered member...
```

## EWMfunc.m

```
%% FUNCTION-TYPE:
% Calculate the stress in the column without area reductions.
% Herman Aucamp.
% 15045471.
% ------------------------------------------------------------------------
function [Qf,Qw,Q,A_,fnew,imax] = EWMfunc(Cu,hw,tw,b,tf,Ag,f,n)
% ------------------------------------------------------------------------
% Allocate memory.
% Table 3 SANS10162-1 Check Class 4 Flange.
% Table 3 SANS10162-1 Check Class 4 Web.
% Return the reduction factors, reduced Area, the new stress and
% the location of maximum stress.
% ------------------------------------------------------------------------
%% Perform effective width method in accordance with SANS10162-1:2011
[~,E,~,~,~,~,fy,~,~,~,~,~,~,~,~,~,~,~,~,~,~] = GLOBALfunc();
b_   = ones(n,1)*0.5*b;
hw_  = hw;
A_   = zeros(n,1);
Q    = zeros(n,1);
Qf    = zeros(n,1);
Qw    = zeros(n,1);
Af_    = zeros(n,1);
Af    = zeros(n,1);
Aw_    = zeros(n,1);
Aw    = zeros(n,1);
for i=1:n
    f_ = min(f(i),fy);
    W    = b/(2*tf);
    Wlim = 0.644*sqrt(0.43*E/f_);
    if (x>=conv)
        y = 0;
    else y = 1;
    end
    if (y==1)
        break
    end
end
```

```
%% Nominal reistance of a column, before any area reductions
[~,~,~,~,~,~,fy,~,~,n,~,~,~,~,~,~,~,~,~,~,~] = GLOBALfunc();
fe      = Ce/Ag;
lambda  = sqrt(fy/fe);
fr      = fy*(1+lambda^(2*n))^(-1/n);
end
```

```
% to reach the elastic buckling state of the member.
%% Find critical buckling stress at several locations
f = zeros(s,1);
for i=1:s
    f(i) = Cu/Ag(i);
end
gamma_e = fr/max(f);
for i=1:s
    f_tap(i) = gamma_e*f(i);
end
end
```

```
    if W>200/sqrt(fy*10^(-6))
        if W<=Wlim
            b_(i) = b/2;
        else
            b_(i) = 0.95*tf*sqrt((0.43*E)/f_)*...
                (1-(0.208/W)*sqrt((0.43*E)/f_));
        end
    end
    Af_(i)  = 4*(b_(i)*tf);
    Af(i)   = 2*(b*tf);
    Qf(i)   = Af_(i)/Af(i);
    W    = hw(i)/tw;
    Wlim = 0.644*sqrt(4*E/f_);
    if W>670/sqrt(fy*10^(-6))
        if W<=Wlim
            hw_(i) = hw(i);
        else
            hw_(i) = 0.95*tw*sqrt((4*E)/f_)*...
                (1-(0.208/W)*sqrt((4*E)/f_));
        end
    end
    Aw_(i)  = hw_(i)*tw;
    Aw(i)   = hw(i)*tw;
    Qw(i)   = Aw_(i)/Aw(i);
    A_(i)   = (hw_(i)*tw)+4*(b_(i)*tf);
    Q(i)    = (Qf(i)*Af(i) +Qw(i)*Aw(i))/Ag(i);
    fnew(i) = Cu/A_(i);
end
[fnewmax, imax]  = max(fnew);
end
```

## FLEXRESISTfunc.m

```
%% FUNCTION-TYPE:
% Calculate the true flexural buckling load.
% Herman Aucamp.
% 15045471.
% ------------------------------------------------------------------------
function [lambda,Cr] = FLEXRESISTfunc(Q,Ag,Ce)
% ------------------------------------------------------------------------
%% SANS10162-1 Axial capacity formula
[phi,~,~,~,~,~,fy,~,~,n,~,~,~,~,~,~,~,~,~] = GLOBALfunc();
lambda = sqrt((Ag*fy)/Ce);
Cr = phi*Q*Ag*fy*(1+lambda^(2*n))^(-1/n);
end
```

## STRESSGRADfunc.m

```
%% FUNCTION-TYPE:
% Determine the stress gradient factor in compression flange
% Herman Aucamp.
% 15045471.
% ------------------------------------------------------------------------
function [omega2] = STRESSGRADfunc(f2,fmid,f0)
% ------------------------------------------------------------------------
% Use the AASTHO method for stress gradient factor
% This replaces the equivalent moment factor
% ------------------------------------------------------------------------
%% Stress gradient factor (C_b)
if abs(fmid) < abs((f2+f0)/2)
    f1 = f0;
else
    f1 = max(2*fmid-f2,f0);
end
if (fmid/f2)>=1 || f2 == 0
    omega2 = 1;
else
    omega2 = min(1.75-1.05*(f1/f2)+0.3*(f1/f2)^2,2.3);
end
end
```

## FXfunc.m

```
%% FUNCTION-TYPE:
% Plotting of Optimal progress and FEM solution.
% Herman Aucamp.
% 15045471.
% ------------------------------------------------------------------------
function stop = FXfunc(NumGen,iGen,Gen,Opt_data,Chromosome)
%% Continuous graphical output:
% Report generation's optimum weight and number of violations...
% ...if there are no violations.
% Else report generation's maximum optimum weight and...
% number of violations if there are no violations.
% Plot the updated optimum_data vs the number of generations.
% Adjust vertical axis to 3 times the current optimal weight.
% ------------------------------------------------------------------------
grid on; hold on; clf;
subplot(1,3,1)
plot(Gen(1:iGen),Opt_data(1:iGen));
axis([0,NumGen, 0, Opt_data(iGen)*3]);
title('Optimal weight')
xlabel('No. of Generations')
ylabel('Weight (kg)')
hold on;grid on;
hold off;
%% FEM
[sNod,sEl,h,u,v,DEG,P,...
    D,axial,shear,moment,...
    ~,~,~,~,~,~] = FEMfunc(Chromosome);
[~,~,~,~,~,~,~,~,s,~,~,~,~,~,~,~,~,~,tClad,~] = GLOBALfunc();
[~,~,Nod,~,~] = NODEfunc();
[~,Var,List]=LISTfunc();
oNODE = zeros(length(Nod(:,1)),length(Nod(1,:)));
iNODE = zeros(length(Nod(:,1)),length(Nod(1,:)));
oNodx = zeros(1,s);
oNody = zeros(1,s);
for i = 1:size(Nod,1)-1
    oNodx(i,:)= linspace(Nod(i,1),Nod(i+1,1),s);
    oNody(i,:)= linspace(Nod(i,2),Nod(i+1,2),s);
end
oNodx = oNodx'; oNodx(s:s:size(oNodx,1)*size(oNodx,2)-1) = [];
if size(Nod,1) >= 3
    oNodx = oNodx';
end
oNody = oNody'; oNody(s:s:size(oNody,1)*size(oNody,2)-1) = [];
if size(Nod,1) >= 3
    oNody = oNody';
end
oNod  = [oNodx, oNody];
iNODE(1,1) = Nod(1,1) + (tClad + List{1}(Chromosome(1)));
iNODE(1,2) = Nod(1,2);
iNODE(2,1) = Nod(2,1) + (tClad + List{2}(Chromosome(2)));
iNODE(2,2) = Nod(2,2) - (tClad + List{3}(Chromosome(3)));
iNODE(3,1) = Nod(3,1);
iNODE(3,2) = Nod(3,2) - (tClad + List{7}(Chromosome(7)));
iNODE(4,1) = Nod(4,1) - (tClad + List{2}(Chromosome(2)));
iNODE(4,2) = Nod(4,2) - (tClad + List{3}(Chromosome(3)));
iNODE(5,1) = Nod(5,1) - (tClad + List{1}(Chromosome(1)));
iNODE(5,2) = Nod(5,2);
iNodx = zeros(1,s);
iNody = zeros(1,s);
for i = 1:size(iNODE,1)-1
    iNodx(i,:)= linspace(iNODE(i,1),iNODE(i+1,1),s);
    iNody(i,:)= linspace(iNODE(i,2),iNODE(i+1,2),s);
end
iNodx = iNodx'; iNodx(s:s:size(iNodx,1)*size(iNodx,2)-1) = [];
if size(iNODE,1) >= 3
    iNodx = iNodx';
end
iNody = iNody'; iNody(s:s:size(iNody,1)*size(iNody,2)-1) = [];
if size(iNODE,1) >= 3
    iNody = iNody';
end
iNod  = [iNodx, iNody];
Dof = 3;
Geom(:,1) = sNod(:,1);
Geom(:,2) = sNod(:,2);
%% Repeat for two SLS load combinations
for z = 1:1:2
%% Axis
if max(Nod(:,1)) == 0
    xAxis = 0.1;
```

```
else
    xAxis = max(Nod(:,1));
end
if max(Nod(:,2)) == 0
    yAxis = 0.1;
else
    yAxis = max(Nod(:,2));
end
%% Deformation plot
% Amplify the displacements to make them visible.
% Find the displaced horizontal coordinates and verticall coordinates.
% Then plot original and final position of element.
% Plot displ position of each member start point.
% Plot displ position of each member end point.
% Plot displ members grey.
% Plot displ members thickness as a function of the "prismatic" heights.
% Plot members black with default point marker and line width.
% Show arrows at subnodes where forces act.
% Typically 3 Dofs per subnode.
% --------------------------------------------------------------------------
subplot(2,3,2)
dispfac = (xAxis/25)/max(D(:));
%Center
DisNodPos(:,1) = sNod(:,1)+dispfac*D(u,z)*10;
DisNodPos(:,2) = sNod(:,2)+dispfac*D(v,z);
%Outer
oDisNodPos(:,1) = oNod(:,1)+dispfac*D(u,z)*10;
oDisNodPos(:,2) = oNod(:,2)+dispfac*D(v,z);
%Inner
iDisNodPos(:,1) = iNod(:,1)+dispfac*D(u,z)*10;
iDisNodPos(:,2) = iNod(:,2)+dispfac*D(v,z);
for iel = 1:size(sEl)
    %Center
    plot(   DisNodPos(sEl(iel,:),1),...
        DisNodPos(sEl(iel,:),2),...
        'color',z*0.5*[0.5 0.5 1/z],...
        'LineWidth', 1);
    hold on;grid on;
    %Outer
    plot(   oDisNodPos(sEl(iel,:),1),...
        oDisNodPos(sEl(iel,:),2),...
        'color',z*0.5*[0.5 0.5 1/z],...
        'LineWidth', 1);
    hold on;grid on;
    %Inner
    plot(   iDisNodPos(sEl(iel,:),1),...
        iDisNodPos(sEl(iel,:),2),...
        'color',z*0.5*[0.5 0.5 1/z],...
        'LineWidth', 1);
    hold on;grid on;
    plot(   (iDisNodPos(sEl(iel,:),1)+oDisNodPos(sEl(iel,:),1))/2,...
        (iDisNodPos(sEl(iel,:),2)+oDisNodPos(sEl(iel,:),2))/2,...
        'color',z*0.5*[0.5 0.5 1/z],...
        'LineWidth', 4);
    hold on;grid on;
end
title('FBD with displacment')
xlabel('Span (m)')
ylabel('Height (m)')
plot(   Geom(:,1),...
    Geom(:,2),...
    'k.-');  hold on;
axis([  -xAxis*0.25 xAxis*1.25...
    -yAxis*0.25 yAxis*1.25])
end
%% Repeat for two ULS load combinations
for z = 3:1:4
%% Axial force plot
% Again plot position of each member start point.
% Again plot position of each member end point.
% Plot the internal axial force of each member.
% Plot member axial force as red for compression.
% Plot member axial force as blue for tension.
% Plot members black with default point marker and line width.
% --------------------------------------------------------------------------
subplot(2,3,3)
axialfactor = (xAxis)/max(axial(:));
for iel = 1:size(sEl)
    if axial(iel,z)>=0
        if axial(iel,z) == 0
            axial(iel,z) = 0.001;
        end
        plot(   sNod(sEl(iel,:),1),...
            sNod(sEl(iel,:),2),...
            'r.-',...
            'LineWidth', axial(iel,z)*axialfactor);
        hold on; grid on;
    else
        plot(   sNod(sEl(iel,:),1),...
            sNod(sEl(iel,:),2),...
            'b.-',...
            'LineWidth', abs(axial(iel,z))*axialfactor);
        hold on; grid on;
    end
end
title('Axial member forces')
xlabel('Span (m)')
ylabel('Height (m)')
plot(   Geom(:,1),...
    Geom(:,2),...
    'k.-');  hold on;   grid on;
axis([  -xAxis*0.25 xAxis*1.25...
    -yAxis*0.25 yAxis*1.25])
%% Shear force plot
% Plot position of each member start point as black
% Plot position of each member end point as black
% Adds the node position as the "zero" shear postion
% Plot "shear y-position" perpendicular to member
% Plot member shear force as red for ULS1
% Plot member shear force as blue for ULS2
% --------------------------------------------------------------------------
subplot(2,3,5)
shearfactor = (xAxis*0.1)/max(shear(:));
xs = zeros(2,size(sEl,1));
ys = zeros(2,size(sEl,1));
for iel = 1:size(sEl)
    xs(:,iel) = sNod(sEl(iel,:),1) - ...
        (sind(DEG{iel})*shear(iel,z))*shearfactor;
    ys(:,iel) = sNod(sEl(iel,:),2) + ...
        (cosd(DEG{iel})*shear(iel,z))*shearfactor;
end
plot(   Geom(:,1),...
    Geom(:,2),...
    'k.-'); hold on;  grid on;
xs = subs(xs(:));
ys = subs(ys(:));
j = 1;
for i = 1:(3+2*(s-2)):(size(Nod,1)-1)*(3+2*(s-2))+1
    xs = [xs(1:i-1);Nod(j,1);xs(i:end)];
```

```
    ys = [ys(1:i-1);Nod(j,2);ys(i:end)];
    j = j+1;
end
title('Shear member forces')
xlabel('Span (m)')
ylabel('Height (m)')
if z == 3
    plot(   xs, ys,...
        'r-',...
        'LineWidth', 2.5); hold on; grid on;
else
    plot(   xs, ys,...
        'b-',...
        'LineWidth', 2.5); hold on; grid on;
end
axis([  -xAxis*0.25 xAxis*1.25...
    -yAxis*0.25 yAxis*1.25])
%% Moment force plot
% Plot "moment x-position" perpendicular to member.
% Plot "moment x-position" perpendicular to member.
% Plot "moment y-position" perpendicular to member.
% Plot "moment y-position" perpendicular to member.
% Plot position of each member start point.
% Plot position of each member end point.
% Plot member shear force as black.
% Plot "shear y-position" perpendicular to member.
% Plot member shear force as red for ULS1.
% Plot member shear force as blue for ULS2.
% --------------------------------------------------------------------------
subplot(2,3,6)
momentfactor = (xAxis*0.1)/max(moment(:));
xm = zeros(size(sEl,1),2);
ym = zeros(size(sEl,1),2);
for iel = 1:size(sEl,1)
    xm(iel,1) = sNod(sEl(iel,1),1) - ...
        (sind(DEG{iel})*moment(iel,z))*momentfactor;
    xm(iel,2) = sNod(sEl(iel,2),1) - ...
        (sind(DEG{iel})*moment(iel+1,z))*momentfactor;
    ym(iel,1) = sNod(sEl(iel,1),2) + ...
        (cosd(DEG{iel})*moment(iel,z))*momentfactor;
    ym(iel,2) = sNod(sEl(iel,2),2) + ...
        (cosd(DEG{iel})*moment(iel+1,z))*momentfactor;
end
xm = xm'; ym = ym';
xm = subs(xm(:)); ym = subs(ym(:));
j = 1;
for i = 1:(3+2*(s-2)):(size(Nod,1)-1)*(3+2*(s-2))+1
    xm = [xm(1:i-1);Nod(j,1);xm(i:end)];
    ym = [ym(1:i-1);Nod(j,2);ym(i:end)];
    j = j + 1;
end
plot(   Geom(:,1),...
    Geom(:,2),...
    'k.-'); hold on;  grid on;
title('Moment member forces')
xlabel('Span (m)')
ylabel('Height (m)')
if z == 3
    plot(   xm, ym,...
        'r-',...
        'LineWidth', 2.5); hold on; grid on;
else
    plot(   xm, ym,...
        'b-',...
        'LineWidth', 2.5); hold on; grid on;
end
axis([  -xAxis*0.25 xAxis*1.25...
    -yAxis*0.25 yAxis*1.25])
stop = false;
end
end
```